Numerical Relativity and Critical Black Holes

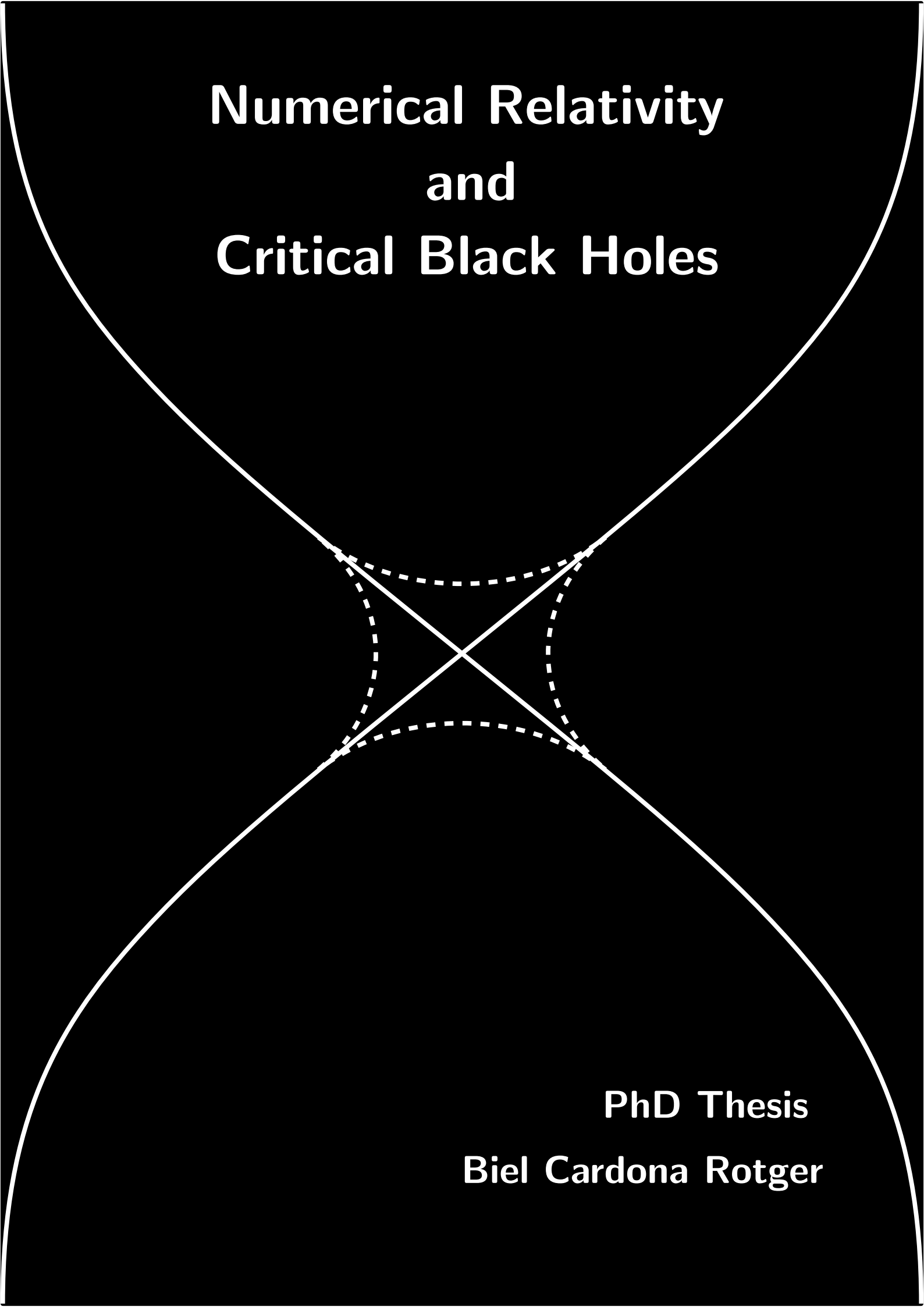

PhD Thesis

Biel Cardona Rotger

Numerical Relativity and Critical Black Holes

A dissertation submitted in fulfillment of the requirements for the degree of Doctor of Philosophy by:

Biel Cardona Rotger

October 2020

This thesis was prepared under the supervision of Prof.

Pau Figueras i Barnera

Geometry and Analysis Group

School of Mathematical Sciences

A Carmen, a mi Anucha
y a Rocco

Acknowledgements

First and foremost, I would like to thank my supervisor, Pau Figueras, for his advice, guidance, and specially, understanding, while I have been at QMUL. Clearly, this thesis would not have been possible without such decisive factors. Gràcies Pau per compartir la teva ciència amb mi!

Thanks to my tutors, Juan Valiente and Shabnam Beheshti, for being always there willing to listen, and for organizing all the group meetings and making the efforts for keeping the group alive and active. And also for making the Mondays less nasty with a pint time. Throughout my time at QMUL I have greatly enjoyed, for a shorter or longer amount of time, the company of Chenxia Gu, Lorenzo Rossi, Tiago França, Peng Zhao, Markus Kunesch, Rodrigo Panoso and Hans Bantilan. Thanks to Chenxia for letting me savor a bit of her research in time evolution, trying to find apparent horizons. It was very interesting, and a bit exasperating at some point, but it eventually worked!

I am also very grateful to José Juan for having became such a good colleague, letting me share my research with him, and for stimulating interesting discussions. We will hopefully be able to collaborate in the future! I am also very thankful to José Juan for comments on earlier drafts of this thesis. Thanks to Emilio Torrente for introducing me into the group of theoretical physics of Universidad de Murcia.

This work has been financially supported by the European Research Council grant ERC-2014-StG 639022-NewNGR. I am grateful to all the European tax-payers who have made this thesis possible, and also to the Analysis and Geometry group within the School of Mathematical Sciences at QMUL for travel funding when it has been necessary. Thanks to all the staff at QMUL who have helped me some way or another during my PhD studies. I would also like to thank Universidad de Murcia for warm hospitality during the final stages of my PhD.

També voldria dedicar unes paraules a nes meus pares, en Biel i na Joana, per haver confiat en jo tots aquests anys, i per haver-me repetit tantes vegades com fes falta que 'Tu pots!'. Aquí en teniu es resultat final, esper que la disfruteu.

Por último, quería dedicar unas palabras a Carmen, por todo el amor y apoyo recibido durante estos 4 años. En este tiempo ha habido muchos cambios, pero tu apoyo ha sido una constante y, sin duda, ha marcado una diferencia. Gracias!

Declaration of Authorship

I, Biel Cardona Rotger, confirm that the research included within this thesis, titled 'Numerical Relativity and Critical Black Holes', is my own work or that where it has been carried out in collaboration with, or supported by others, that this is duly acknowledged and my contribution indicated. I confirm that:

- This work was done wholly or mainly while in candidature for a research degree at QMUL, between September 2016 and September 2020.
- I have exercised reasonable care to ensure that the work is original, and does not to the best of my knowledge break any UK law, infringe any third party's copyright or other Intellectual Property Right, or contain any confidential material.
- I accept that the College has the right to use plagiarism detection software to check the electronic version of the thesis.
- This thesis has not been previously submitted for the award of a degree by this or any other university.
- The copyright of this thesis rests with the author and no quotation from it or information derived from it may be published without the prior written consent of the author.

The work presented in this thesis is based on material taken from the co-authored publications [1] and [2].

Biel Cardona Rotger,

London, October 2020

Abstract

In this thesis we have studied static black holes in direct product spacetimes. In this setting, there exists a universal sector describing black holes which are uniformly extended along the internal space. This sector naturally exhibits a hierarchy of length scales and dynamical instabilities of the Gregory-Laflamme type appear when one of those lengths is much larger than the other. At the onset of the instability there exists a 0-mode that hints on the existence of a new branch of black holes that are non-uniformly extended along the internal space. Typically, this new family of black holes cannot be found analytically and one has to rely on numerical methods.

In particular, we have numerically constructed these 'non-uniform black holes' in Kaluza-Klein theory and Anti-de Sitter spaces times a sphere. Moving along the space of solutions, eventually the branches of non-uniform black holes merge with another branch of black holes which have different horizon topology. These are also constructed in the Kaluza-Klein case. In this thesis we have focused on a detailed study of the extreme black holes very near the critical (or merger) point. It had been predicted that the physical properties of black holes near the critical solution are controlled by a local Ricci-flat cone that governs, locally, the singularity at the merger. We verify this prediction by extracting the critical exponents of various physical quantities in the Kaluza-Klein setting in $D = 10$. In this particular case, properties of black holes can be computed by solving a dual super Yang-Mills theory on the lattice. In another study, we consider critical non-uniform black holes in $\mathrm{AdS}_p \times S^q$ for $(p, q) = (5, 5)$ and $(p, q) = (4, 7)$, which are the relevant cases for the gauge/gravity duality, and compute, for the first time, the critical exponents. Remarkably, in these two cases our study suggests a non-Ricci-flat cone, which is consistent with the presence of non-trivial fluxes in the setting. Our results are new and non-trivial predictions of the gauge/gravity duality without supersymmetry.

Contents

List of Figures

List of Tables

Chapter 0
Introduction

The Einstein equation [3]:

$$G_{\mu\nu} = 8\pi G T_{\mu\nu}, \tag{0.0.0.1}$$

is possibly one of the most suggestive equations in physics. Roughly, it states that gravity, understood as the geometry of spacetime, is sourced by its matter content. The universality feature, first attributed to I. Newton, is now explicit. The equation (0.0.0.1) is majestic by its simplicity, and brutal due to its many (tested) predictions [4].

One of the most important tested predictions was achieved a handful of years ago at the time of writing this thesis, when in 2015 the two main worldwide experiments for the detection of gravitational waves, LIGO and VIRGO, coincided in observing the signal of a gravitational wave that matches with the imprint predicted by General Relativity (GR) [283–285] for the merger of a black hole binary system [5]. This was the first direct detection of gravitational waves, and an indirect detection of black holes: the two most fundamental solutions of GR in a single event(!) at the backyard. Since then the observations have not ceased, which now also include gravitational waves generated by neutron star binary systems. The first direct black hole observation was accomplished a bit later, with the first image reconstructed in 2019 [6]. These are undoubtedly the two major milestones in experimental GR of the last few decades, providing solid evidence of the existence of gravitational waves and black holes, and opening a new window for exploring the universe on small and large scales in the strong field regime.[1]

Despite these recent successes, there are fundamental questions that will not be able to be addressed experimentally, at least in the near (and likely far) future. This is particularly true on phenomena that occur (or have occurred) at very very small scales, where quantum gravity effects become important. These include black hole evaporation or the black hole information paradox [7] (see [8] for a review and [9] for recent developments), spacetime singularities [285] or very early cosmology [10] among others. The quantum gravity problem is perhaps one of the biggest challenges in theoretical physics today, and in this context several proposals have been made [286].

[1] Up to these two breathtaking events, most of GR tests were carried out within the Solar system, and thus in a weak field regime.

The list is led by string theories [287–289], which contain a symmetric spin-2 quantum state in their spectrum and the Einstein's equation (0.0.0.1) is recovered by taking a low-energy limit. One crucial aspect of those theories is that they live in more than $D = 4$ spacetime dimensions. For instance, $D = 10$ for superstring theories or $D = 11$ for M-theory. This clashes with our notion of 4-dimensional spacetime and one possible explanation for this lies behind a mechanism known as flux compactification.

Compactifications build up on the idea that the 4-dimensional universe we observe is just an 'effective reality', with all the spatial extra dimensions hidden in some tiny compact manifold. This assumes a direct product spacetime: $M_4 \times N^{D-4}$, where N^{D-4} would presumably be fixed by nature itself.[2] Or maybe they are not hidden but we simply can not access them due to the existence of some confining potential that sticks us to the 4-dimensional world that we experiment. In this latter case, our universe would be embedded in a higher-dimensional spacetime, or bulk [12]. The truth is that it is completely unknown if any of these possibilities is a fact of our universe. Still, research in this direction has been carried out over the last few decades, and theories of Einstein gravity have been considered in diverse spacetime dimensions, matter field content and a variety of backgrounds, some of which may have nothing to do with our reality, but in a theoretical analysis they are as valid as any other.

This connects, perhaps, with a more pragmatic point of view which is: let us accept that we can formulate theories of (Einstein) gravity in any spacetime dimension, and let us study how they differ from each other. The most appropriate way of doing this consists precisely into studying black hole type solutions. These constitute the most fundamental objects of any theory of (semi-)classical gravity[3] [290], helping to have a better control and understanding of how GR itself works.

Another motivation for doing this comes from progress within the string theory field. 'Exotic' black holes play a central role in the context of the AdS/CFT correspondence [291] which has been proved to be a successful tool for studying a wide range of quantum field theories in the regime of strong coupling, where a perturbation theory analysis fails. This has provided many new insights in disparate areas of physics such as particle physics or condensed matter, and it has been in fact the real fuel pushing for having a complete scan of black hole solutions in non-trivial spaces such as, for instance, Anti-de Sitter (AdS) space.

In this thesis we have considered GR in $D = 10$ and $D = 11$ spacetime dimensions, and we have studied static black holes that asymptote direct product spaces of the form $\text{Mink}_9 \times S^1$ (i.e. Kaluza-Klein (KK) theory), $\text{AdS}_5 \times S^5$ and $\text{AdS}_4 \times S^7$. This in turn fixes a minimal matter field content. In the former case vacuum is allowed, whereas

[2] This is essentially the 'landscape' problem of string theory. Such theories appear to describe a huge number, $\sim 10^{500}$, of 4-dimensional 'vacua' with inequivalent physics, most of which clearly do not describe our universe. The problem lies in the fact that, so far, there is no clue on which one is relevant or how to find it. See Ref. [11] for a throughout review on this subject.

[3] Gravitational waves are not that relevant since its study requires a linear approximation. Therefore they do not capture the non-linearities of the theory, which is precisely where the most interesting physics comes from.

in the other two cases there is, at least, a non-trivial (Abelian) 5-form and 4-form gauge field strength respectively. Such theories actually correspond to (truncated) low-energy type IIB superstring theory and low-energy M-theory. All three cases have relevance for GR itself and for the AdS/CFT correspondence, and in the remainder of this introductory chapter we pretend to briefly explain why, while deferring more specific details to the next chapters.

First, notice that the backgrounds we have considered have a compact manifold as internal space, a sphere essentially. This means that the disposition of a black hole in such space can be made quite precise. For instance, it can be extended along the whole internal space, or can be localized at some particular region. This naive observation is telling us that one should expect a non-trivial space of solutions.

Indeed, black holes in KK theory have a long history, but long story short, in vacuum and for any value of D there exist 3 families of one-parameter black hole solutions: uniform black strings, non-uniform black strings [13–15] and localized black holes [16–18]. The former has the largest isometry group and it is known analytically, but the latter two, with fewer isometries, are only known perturbatively or numerically. The literature in this case is vast and will be properly referenced in the research Chapter 3. On the other hand, black holes in $\mathrm{AdS}_p \times S^q$ are less known. In fact, they have only been considered for $(p, q) = (5, 5)$ [19]. The two crucial differences in this case is that the longitudinal spacetime factor has also a length scale (the AdS radius), and that the internal space is more complex. This results in an incredible richer space of solutions. In addition to the well-known Schwarzschild-$\mathrm{AdS}_p \times S^q$ black hole, now it presumably exists an infinite amount of 'lumpy' or non-uniform black holes along S^q, each one in correspondence with localized-type black holes in S^q [20]. These black hole 'pairs' also rely on numerical constructions due to the limited analytical methods currently available, and are considered in Chapter 4.

Broadly speaking, the qualitative features remain the same in all three cases. Their phase diagram are controlled by bifurcations in solution space and topology-changing phase transitions. Whereas bifurcations involve the study of 0-mode perturbations of black holes, and they thus have a well-known theory, the topology-changing phase transitions require of a more delicate analysis. This is due to the fact that topology changes put Einstein's equations at their limit, just before where it is thought that they loose their predictive power. Still, one can gain some insights in that region by considering, locally, Ricci-flat cone geometries [21]. These critical geometries were proposed long time ago to mediate the black string/black hole phase transition in KK theory, but their accurate validation just recently began hand in hand with the development of new numerical approaches and techniques.

One of the main goals of this thesis is to employ these techniques to construct the black hole phases that require a numerical treatment, and focus on the critical region where the topology-changing phase transition occurs. This was successfully accomplished in the KK setting by constructing highly non-uniform strings and large localized black holes in $D = 5, 6$ [22]. Here we extend such study to $D = 10$, which

defines a degenerate dimension for the critical cone model. Additionally, in $D = 10$ the phase diagram of these families can be mapped onto the phase diagram of their D0-charged counterparts. Kaluza-Klein black holes with D0-charge have been identified to be dual to a $(1+1)$-dimensional super Yang-Mills (SYM) theory, which, remarkably, can be solved using lattice techniques [23, 24] and therefore it provides a natural example where to test the AdS/CFT correspondence.

Regarding the black holes that arise in $\mathrm{AdS}_p \times S^q$, the case $(p, q) = (5, 5)$ has obvious relevance for being related to the duality that gave the name to 'AdS/CFT'. This is the only case studied so far, where black holes appear to be solutions to type IIB supergravity with a self-dual 5-form. To further test the cone model in a non-trivial space and with additional matter fields, we revisit the lumpy black holes in $\mathrm{AdS}_5 \times S^5$ and explore, for the first time, the critical regime of a few of its family members. The solutions clearly show the typical pinch-off that appear in black holes close enough to a merger between two branches with different topology. This allow us to conjecture about the topologic nature of the localized-type black holes that merge with. The other side of the merger is not considered in this case, though. Interestingly enough, we find that the critical geometry in this case is no longer Ricci-flat, but it is likely to be sourced by the corresponding critical flux. Furthermore, a KK holographic analysis relates the asymptotic behavior of such solutions to the vacuum expectation values (vev's) of certain scalar fields that appear in the dimensionally reduced (5-dimensional) theory. Therefore we can also test what is the imprint of the topology change in the vev's of scalar operators of the dual gauge theory.

We also construct for the first time lumpy black holes in $\mathrm{AdS}_4 \times S^7$, and examine their critical regions. In this case we deal with 11-dimensional supergravity. Remarkably, black hole families in this case do not always follow an exact parallelism with the equivalent ones in $\mathrm{AdS}_5 \times S^5$. This study constitutes the first instance where the cone model is tested beyond ten spacetime dimensions.

The structure of this thesis

The main body of this thesis can be divided in three parts. The first part consists of Chapters 1 and 2. Both are review chapters. The first chapter is devoted to introducing black holes in higher dimensions and the AdS/CFT correspondence, which are basically, the starting points of our work. In the second chapter we introduce the numerical approach and numerical methods used along this thesis. The second part is the 'research' part, and is formed by Chapters 3 and 4. These are based on Ref. [1] and [2] respectively. We close this thesis with Chapter 5, the third part, where we conclude with some final remarks and discuss possible future directions of research.

Most of the work done in this thesis is numerical, and in fact, where computations can be done analytically, a computer has also been used. To this end we have opted for using Wolfram Mathematica software. We use 'mostly plus' metric signature and for the curvature tensors we follow the conventions of Wald [284].

Chapter 1

Black Holes in Higher Dimensions and AdS/CFT Correspondence

In this chapter we review some known features and results of stationary black hole physics (mostly in vacuum) for D $>$ 4, where D is the total number of spacetime dimensions. We start in D $=$ 4, where black holes' shape and existence is pretty constrained. Then we move on to higher dimensions, where many of the theorems that hold in D $=$ 4 are violated. This results in a much richer physics. Special emphasis is put on black holes in direct product spacetimes. Most of what is presented in this first chapter part is descriptive, and precise expressions are, in general, not shown. Then we introduce the AdS/CFT correspondence. We begin with the essential ideas behind this conjecture, adding value to gravitational theories in general, and specially, to black hole type solutions. Special emphasis is put on the standard prescription of holographic renormalization, which will be needed later on in this thesis for computing the expectation values of dual gauge operators.

1.1 Black holes in D = 4

Vacuum[1] stationary black holes in four dimensions are quite simple and their main characterizing features are well-known. Their horizon has the topology of a 2-sphere, they are stable and only a very few number of conserved asymptotic charges are necessary to uniquely specify them. Moreover, for every possible configuration of the asymptotic charges only one solution exists, and most importantly, they have algebraic properties which allow them to be found analytically.

For instance, the Schwarzschild metric [25] is the unique asymptotically flat, spherically symmetric (and thus [26]) static solution of the vacuum Einstein's equations with a regular event horizon. It has one asymptotic charge, the mass M. If rotation is allowed, a second asymptotic charge is added: the angular momentum J, which satisfies the bound $J \leq M^2$, and whose saturation gives an extremal horizon (i.e. with zero surface gravity). The rotating black hole is described by the Kerr solution [27]. The

[1]Black hole solutions with (positive or) negative cosmological constant, being asymptotically (de Sitter or) Anti-de Sitter respectively, also exist in $D = 4$. Although Anti-de Sitter black holes are relevant to us, they will be discussed separately in Chapter 4.

metric is stationary and axisymmetric, and uniqueness theorems by Israel, Robinson and others (see [28] and references therein) showed that these are in fact the only vacuum asymptotically flat black hole solutions with such features for a given pair of asymptotic charges (M, J). Hawking additionally proved that their event horizon must necessarily have spherical topology, and that stationary (non-extremal) black holes are also necessarily axisymmetric [285], with the latter known as Hawking's rigidity theorem.

After uniqueness theorems were established, people began to consider gravity coupled to different kind of fields. For instance, stationary rotating black holes in Einstein-Maxwell theory are described by the Kerr-Newman metric [29, 30], which is uniquely specified by 4 asymptotic charges: M, J, plus the electric/magnetic charges, Q and P [31, 32].[2] Furthermore, when a scalar field was added to the system it was shown that in many cases this fell into the black hole or was radiated out at infinity. This fact was formally collected by a series of 'no-hair' theorems [39–42], which essentially state that black holes are only distinguished by the conserved charges, and in a gravitational collapse situation any other information of the initial matter distribution is eventually lost once the black hole is formed. This led to several studies where it was shown that beyond Einstein-Maxwell-Scalar, black holes may have 'hair'. These include Einstein-Yang-Mills and Einstein-Skyrme theory, possibly coupled to various combinations of dilaton or Higgs fields. The 'spectrum' of hairy solutions is now vast, and cannot be reviewed here. The interested reader may see Ref. [43, 44] and references therein.[3]

Another issue closely related with uniqueness of solutions is that of dynamical stability, which has implications for stellar evolution theories. The most likely outcome of realistic collapse processes of sufficiently massive stars are thought to be black holes, and therefore any good spacetime candidate to describe them must certainly be stable. Otherwise, the backreaction created by any probe particle would have catastrophic consequences and the formation process would be put in serious doubt. In GR, the non-linearity of the equations makes the stability problem a very challenging one. In fact, stability at the non-linear level has only been proved for Minkowski space [47],[4] and even for this simple solution the proof is very involved requiring a sophisticated global analysis. When a smooth event horizon is present, the analysis is much more elusive and a linear perturbation study is carried out. Then the symmetries of the spacetime are exploited to simplify the problem considerably.

First attempts in proving linear stability of Schwarzschild or Kerr black hole made Fourier decompositions with a time dependence of the form $e^{-i\omega t}$, known as mode

[2] Static solutions in this theory are given by the Reissner-Nordström [33, 34] or the multi-black hole Majumdar-Papapetrou (in the extremal case) [35] metrics; the corresponding static uniqueness theorems were extended for non-zero charge in [36] and in [37, 38] for non-connected horizons.

[3] Note that black holes with scalar-hair in more exotic spaces such as Anti-de Sitter have been found [45, 46]. Although those are not believed to play an interesting role from the astrophysical point of view, they are clearly relevant, for instance, in the context of string theory or gauge/gravity duality. See next section 1.3.

[4] And also for de Sitter space [48].

stability [49–51]. Stability implies that, when analyzing each mode separately, only those with $\mathrm{Im}[\omega] < 0$ are allowed. This, together with uniqueness theorems, numerical analysis evidence [52] and simulations of black hole collisions [53–55] or coalescence of binary systems [56–58] suggest stability, which is expected to hold even at the non-linear level. Of course, stability statements made on mode decomposition grounds are not completely rigorous and they leave a bitter flavor, specially to the mathematics community. Formally, linear stability concerns general solutions to the linearized Einstein's equations arising from smooth initial data, and not simply fixed modes. Linear stability in this broader sense was proved for Schwarzschild in recent years [59], hinting a route to prove linear stability of Kerr [60], but still, a complete proof is unavailable.

In addition to the strong constraints that black holes set on the causal structure of the spacetime, they also hide spacetime singularities which pose serious questions about the predictability of GR. More particularly, Penrose's singularity theorem [61] states that in a gravitational collapse situation, once a trapped surface is formed, curvature singularities are inevitable. However, the theorem does not say anything about where they lie, thus opening the possibility for the existence of naked singularities, i.e. those that are not hidden by an event horizon. Curvature singularities are thought to be a limitation of Einstein's theory as a classical theory, and they are expected to be resolved by quantum gravity effects. In this sense, naked singularities imply that quantum gravity would be visible to asymptotic observers, and general relativity would not be sufficient to describe all gravitational physics outside black holes. There would be a loss of the predictive power of the theory.

Weak cosmic censorship (WCC) [62–64] is a conjecture that states the opposite:

Generic initial data for asymptotically flat gravity coupled to matter (satisfying reasonable energy-conditions) does not produce naked singularities.

If the conjecture holds it implies that, at the very least, predictability outside black holes is ensured.

Since this conjecture was proposed more than fifty years ago, several studies have tried to find counter-examples to prove its feasibility. Ref. [65] first considered a model of collapsing pressureless dust, showing that it leads to naked singularities. However, those arise even with no gravity and therefore they are not related to gravitational phenomena. Several authors engineered more genuine situations using spherically symmetric scalar fields [66–70], and more recently without spherical symmetry [71,72], coupled to gravity. These studies showed that when the amplitude of the initial scalar configuration is small, the field is eventually scattered out at infinity, but for large amplitudes it collapses and forms a black hole. Precisely at the threshold of black hole formation, the evolution yields a naked singularity. Naively, one would arrive to the conclusion that WCC is violated, but this is not the case due to the fine-tuning required. In other words, the initial data is not generic.

So far, no evidence for naked singularities in $D = 4$ has been found, and actually, the conjecture has been shown to hold for a class of spacetimes with 2 Killing vectors

[73] and for time-symmetric initial data possessing a trapped surface [74, 75]. The stability of black holes also suggests that it is very likely that weak cosmic censor is true, but a formal proof seems to be a bit far away. In the mean time, people keep trying to find potential counter-examples. A first plausible scenario leading to violation has been proposed very recently in [76]. The situation, though, seems to be rather different in AdS space [77–80] where it has been reported that regions of arbitrarily large curvature are not necessarily hidden by an event horizon, and definitely also different in higher dimensions (see the upcoming section). For our purposes, the most reliable counter-examples of WCC appear in this latter context.

The 'weak' adjective hints that there exists a 'stronger' version of cosmic censor. Indeed, strong cosmic censorship (SCC) is a related, but independent, conjecture restoring the breakdown of classical determinism for all observers entering a black hole, as set by the existence of Cauchy horizons. In this sense, SCC is related to the global uniqueness of solutions since it also deals with the internal anatomy of black holes. Black hole interiors are typically excluded in numerical studies, and therefore this stronger form has less relevance here. Even so, there has been in going research in recent years from both, mathematical [81–85] and numerical [86], points of view.

End of the story?

Along this brief roadmap of stationary black hole physics in $D = 4$ we have seen how restricted they are by a series of theorems. In particular, stability, topology restriction and uniqueness theorems suggest an 'end of the story'. Not even close.

The majority of those theorems turned out to be quite dimension dependent and the natural question arises: what about if $D > 4$? Beyond the scientific desire of understanding how GR behaves as we move apart from four spacetime dimensions, the truth is that the study of higher-dimensional general relativity has been fueled over the last 3 decades by its potential applications in other areas of physics. These include: string theory [87–90, 287–289], gauge/gravity dualities (see section 1.3), brane-world scenarios or TeV-scale gravity models [12,91–97]. This manifests that Einstein's theory should nowadays be regarded more properly as a tool, rather a theory that applies only to astrophysics and cosmology. It is the goal of the next section to provide the reader with a brief overview of GR in higher dimensions, focusing on the new features that show up and stopping at the frontiers beyond which this thesis makes its insights. Some standard references covering the subject of black holes in higher dimensions are the review by Emparan and Reall [98], or [290].

1.2 'More is better': A black hole zoo

General Relativity in an arbitrary number of spacetime dimensions looks much like the 4-dimensional version. Their equations look the same but the indices range from 0 up to $D - 1$, and (the usual) Newton's constant is replaced by a D-dimensional

Newton's constant. So, why would one expect new physics? At the linearized level, the number of polarizations of a gravitational wave is already different, going from 2 to $D(D-3)/2$, which remarks the dimensional dependence of gravitational phenomena encoded in Einstein's equation. The point is that in higher D there is more room in the metric, which means more freedom for the non-linearities of theory come to play, resulting in non-uniqueness of solutions, solutions with non-spherical topologies and new gravitational instabilities, among others.

For static asymptotically flat D-dimensional vacuum gravity there is not much new. Static black holes are straightforwardly generalized and they are uniquely given by the Schwarzschild-Tangherlini black hole [99]:

$$\mathrm{d}s^2 = -f(r)\mathrm{d}t^2 + f(r)^{-1}\mathrm{d}r^2 + r^2\mathrm{d}\Omega_{D-2}^2, \qquad f(r) = 1 - \left(\frac{r_0}{r}\right)^{D-3}, \tag{1.2.0.1}$$

where the parameter r_0 locates the horizon and it is related to the asymptotic mass, M, via

$$r_0^{D-3} = \frac{16\pi G_D M}{(D-2)\Omega_{D-2}}; \tag{1.2.0.2}$$

Ω_{D-2} is the volume of the unit $(D-2)$-sphere. The fall-off of the gravitational potential has been replaced to fit in a D-dimensional space and the black hole horizon's geometry is that of a round $(D-2)$-sphere, but the essential features are still the same. In particular, it turns out that this is the unique static vacuum black hole [100]. On the other hand, notable differences occur in the presence of rotation.

The generalization of Kerr black hole for higher values of D is described by the Myers-Perry (MP) solution [101] (see also Ch. 5 of [290]), with topology S^{D-2}. Since in higher dimensions there are more planes on which simultaneous rotation may occur, now solutions with various angular momenta do exist. Notice that the fact that rotation is confined on a plane implies that the centrifugal barrier decays as r^{-2} in any spacetime dimension, but the gravitational potential is dimension dependent, $\sim r^{-(D-3)}$. The interplay between these two contributions results in ultra-spinning black holes, making the differences manifest even for single spinning higher-dimensional black holes: for $D \geq 6$, the angular momenta is not bounded by the mass and can be arbitrarily large, which has dramatic implications from the dynamical point of view (see below). Furthermore, it turns out that the MP black hole is not the only regular stationary solution that exists for asymptotically flat vacuum gravity.

In $D = 5$ (and $D > 5$) there is another family of black holes called black rings [102] (see Ch. 6 of [290] or [103] for a review), whose topology is $S^2 \times S^1$. Depending on the relative size of these two manifolds, those are referred to as 'thin' or 'fat' black rings. Note that this kind of solutions naturally need to rotate along the S^1 to compensate both: ring tension and gravitational pull, and therefore they are characterized by two asymptotic charges, M and J,[5] just as the single spinning Myers-Perry solution. Indeed, they co-exist in a certain finite range of parameter space, violating uniqueness

[5] Ultra-spinning black rings exist in the 'thin' branch [103].

of asymptotically flat stationary solutions in $D = 5$ and leaving open the possibility of having phase transitions among the different black holes.

From here onwards, the combinations seem to be endless and a whole zoo of asymptotically flat solutions has been analytically constructed in $D = 5$. For instance, rotation can be provided along the S^2 too, yielding to a doubly-rotating black ring [104]. The black ring can be even combined with the Myers-Perry black hole into a black saturn [105], with two disconnected horizon components. Other known solutions include a multi-black saturn with any number of rings rotating in the same plane, concentric multi-black rings [106, 107] or bicycling rings [108, 109] (two black rings rotating orthogonally).

It is clear that the space of stationary solutions in flat space gets more complicated [110–112] as we move apart from four dimensions, which, so far, exhibit non-uniqueness and a topology that is different from that of a sphere. The rigidity theorem has been extended to higher dimensions [113, 114], which requires (non-extremal) stationary black holes to have at least one rotational symmetry,[6] and constraints on black hole horizon's topology in $D > 4$ have been established [116] (see [117] for a comprehensive review on those theorems), but a complete classification of black holes beyond four dimensions is still an open problem. Moreover, analytic expressions describing the black objects mentioned above are only known in $D = 5$, and many solutions that are believed to exist in dimensions greater than five have only been constructed using approximate [111, 115, 118] or numerical [119–124] methods, and it is very unlikely that they actually admit a closed analytic form.

Black holes in direct product spacetimes

In addition to the solutions in flat space, in higher dimensions other possibilities arise. An important class are the so-called extended black objects. It turns out that the direct product of two Ricci-flat metrics is also Ricci-flat. Therefore, given any d-dimensional black hole solution in vacuum, call it B, one can form the metric

$$\mathrm{d}\hat{s}^2 = \mathrm{d}s^2(B) + \delta_{ij}\mathrm{d}x^i\mathrm{d}x^j, \qquad (i, j = d, \ldots, d + p - 1), \tag{1.2.0.3}$$

which is automatically a solution of the $(d + p)$-dimensional vacuum Einstein's equations. Solutions of the form (1.2.0.3) are known as black p-branes. The horizon $H \subset B$ is now extended along p flat directions, and it has topology $H \times \mathbb{R}^p$, which again, is different than a sphere. It is important to stress out that this will only work for $D > 4$, since no asymptotically flat black holes do exist in $D \leq 3$ [98].

Due to the infinite volume of the transverse space $\mathbb{R}^p$, it is common to compactify these directions, $x^i \sim x^i + L^i$, resulting in a p-torus, $\mathbb{T}^p$. The mass of the solution

[6] Interestingly enough, all the mentioned (analytic) black holes above have more than just one rotational symmetry. Solutions with less symmetry were conjectured to exist, but the complexity of the equations makes them rather difficult to find. The first example was found using the blackfold approach and consists of helical black rings [115], which have only one rotational symmetry.

is then finite. The simplest example of such black brane solutions is that of B given by the Schwarzschild-Tangherlini solution (1.2.0.1) in d dimensions and $p = 1$, i.e. a (uniform) black string with horizon topology $S^{d-2} \times S^1$.[7] Such solution is not (globally) asymptotically flat, but it is flat in the Kaluza-Klein sense. Kaluza-Klein theory [125, 126] has its own interest for the dimensional reduction procedure, but from a higher-dimensional point of view, this only involves vacuum gravity in a Minkowski times a circle background. In such theory it is where black strings naturally appear. In addition to black strings, there are also other static black holes, namely non-uniform black strings [13–15] and localized black holes [16–18],[8] as we have advanced in the introductory chapter. See also Ch. 4 of [290].

However, at this point we have not introduced these black objects to fully discuss them. This is postponed to chapter 3, where they play a first central role in this work. Instead, we wanted to illustrate how stability and weak cosmic censorship are also violated in higher D. In turn, the way in which extended objects can be molded, hints certain connections with rotating solutions in asymptotically flat space.

The Gregory-Laflamme instability

The crucial point is that the circle S^1 of a black string introduces another scale, its length L. This can be fine-tuned, relative to the horizon size r_0 (or the mass M), in such a way that unstable modes can fit into the black hole.

A key observation that suggested that black strings could be unstable, consisted into comparing the entropy of a black string and a localized black hole of the same mass [130, 290]. Localized black holes are not known analytically but, if they are small enough with respect to L, they are well approximated by a D-dimensional Schwarzschild black hole. The area theorem ensures that the horizon area never shrinks, so if an instability process is assumed and there is another configuration with larger area, and hence larger entropy, it will presumably settle down to that solution. For the system at hand, a straightforward computation reveals that

$$\frac{S_{\rm string}}{S_{\rm bh}} \sim \left(\frac{M}{L^{D-4}}\right)^{\frac{1}{(D-4)(D-3)}} . \tag{1.2.0.4}$$

Then if $L^{D-4} > M \sim r_0^{D-4}$, $S_{\rm string} < S_{\rm bh}$ and the black hole phase is preferred.

To prove the actual instability one must perform a linear analysis around the black string adding a small perturbation: $g_{MN} + \epsilon h_{MN}$, $\epsilon \ll 1$ $(M, N = 0, \ldots, D-1)$, as done for first time by Gregory and Laflamme (GL) [130] (see also [131–133]).

The key observation is that the translation invariance of the black string allows to expand any perturbation using Fourier modes with momentum k along the compact direction z: $h_{MN}(x, z) = e^{ikz} H_{MN}(x)$, where x denote collectively the coordinates transverse to the circle. Then the linearized Einstein's equations can be written as a

[7] Notice that the S^1 of a black ring is different than that of a black string, which is non-contractible.
[8] We will omit Kaluza-Klein copies [127] and bubbles [128, 129] from the discussion.

massive Klein-Gordon-type equation for the perturbation lying along the non-compact directions,

$$(\Delta_{\rm R}^{(D-1)} + k^2) H_{MN}(x) = 0. \tag{1.2.0.5}$$

The operator $\Delta_{\rm R}^{(D-1)}$ is the linearization of the Einstein's equations with respect to the $(D-1)$-dimensional Schwarzschild black hole. Additionally, it can be shown that the unstable modes lie in the scalar sector and therefore it is enough to consider the indices taking values: $M, N \to \mu, \nu = 0, \ldots, D-2$ [130, 290].

When seeking for unstable modes, an ansatz of the form $H_{\mu\nu}(x) \sim e^{\Omega t} \bar{H}_{\mu\nu}(x^i)$ (for some time and space coordinates t and x^i) is made. If regular solutions to (1.2.0.5) with $\Omega > 0$ do exist, then the perturbed D-dimensional metric $g_{MN} + \epsilon h_{MN}$ will be unstable. Originally, the instability was derived in the transverse and trace-less gauge and using Schwarzschild coordinates. After solving the gauge constraints, the linearized equations yield a single 2nd order ordinary differential equation (ODE) that can be solved numerically, for instance via Runge-Kutta integration. The major drawback of this approach is that the coordinates are singular at the horizon and the solution turns out to be very sensitive when that point is approached. Additionally, the equation needs to be discretized on a considerable amount of 'grid' points to obtain accurate results. Here instead, to illustrate, we will proceed taking a different point of view. We will make use of the methods outlined in the next chapter which, numerically speaking, are much more robust and efficient.

First, instead of using Schwarzschild coordinates, we will use ingoing Eddington-Finkelstein coordinates in $D-1$ dimensions: (v, r, Ω_{D-3}). This has the benefit that the metric is explicitly regular at the horizon, and therefore no boundary conditions need to be imposed there. And second, we will consider (the linearization of) the Einstein-DeTurck equation, introduced in §2.1.2 of the next chapter. This means that we will not fix any gauge from the beginning, but it will be fixed a posteriori once the resulting set of equations are solved. After assuming spherical symmetry, we will have four unknowns in the perturbation $\bar{H}_{\mu\nu}(r)$. We are thus interested in solving the equation:

$$(\Delta_{\rm H}^{(D-1)} + k^2)(e^{\Omega v} \bar{H}_{\mu\nu}(r)) = 0, \tag{1.2.0.6}$$

where $\Delta_{\rm H}^{(D-1)}$ is the linearized operator associated to Eq. (2.1.2.1). The equations now need to be supplemented with the choice of a reference metric, and for this particular case, the Schwarzschild metric (in ingoing Eddington-Finkelstein coordinates) in $D-1$ dimensions does the job. This ensures that solutions to the (linearized) Einstein-DeTurck equation will be in fact (linearized) Einstein solutions.

We can proceed by taking a family of metrics that contain the Schwarzschild solution in Eddington-Finkelstein coordinates and perturb it with time-dependent modes that grow in time. Inserting the ansatz into the Einstein-DeTurck equation, we can linearize to find the action of $\Delta_{\rm H}^{(D-1)}$ and the equation (1.2.0.6). We considered:

$$\mathrm{d}s^2 = -Q_1 \mathrm{d}v^2 + \frac{1}{x^2}\left(-2Q_2 \mathrm{d}v\mathrm{d}x + Q_3 \mathrm{d}\Omega^2_{(D-3)} + \frac{1}{x^2} Q_4 \mathrm{d}x^2\right), \tag{1.2.0.7}$$

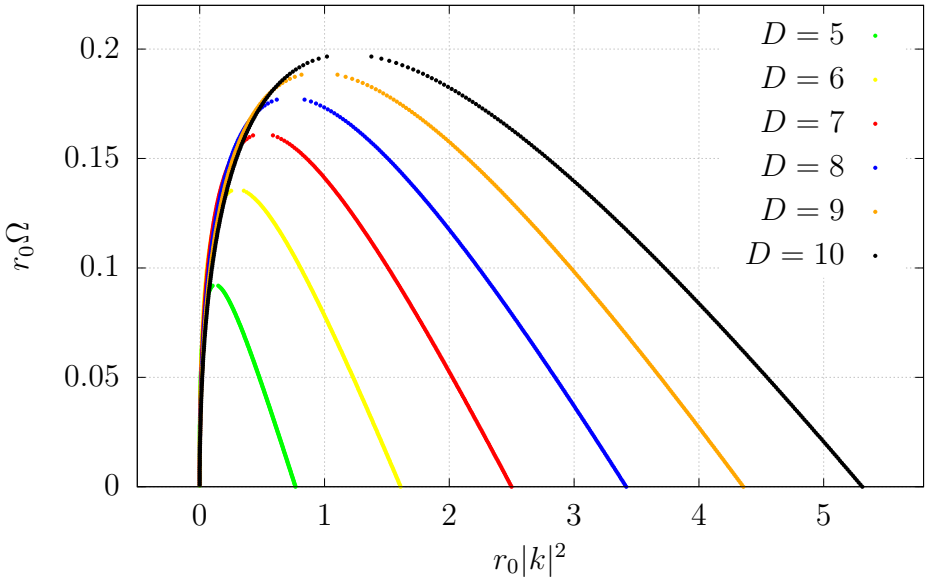

Fig. 1.1: *Dispersion relation $\Omega(k)$ for which the black string is unstable in $D = 5, \ldots, 10$ spacetime dimensions.*

D	5	6	7	8	9	10
$r_0\|k_{\mathrm{GL}}\|^2$	0.767657	1.610148	2.498791	3.417385	4.356176	5.309013

Table 1.1: *Threshold wave-number $r_0|k_{GL}|^2$ of the GL instability.*

with

$$\begin{aligned} Q_1(v,x) &= 1 - \left(\frac{x}{r_0}\right)^{D-4} + \epsilon\, e^{\Omega v} q_1(x), \\ Q_{2,3}(v,x) &= 1 + \epsilon\, e^{\Omega v} q_{2,3}(x), \\ Q_4(v,x) &= \epsilon\, e^{\Omega v} q_4(x), \end{aligned} \tag{1.2.0.8}$$

and expanded to linear order in ϵ. For $q_1 = q_2 = q_3 = q_4 = 0$, (1.2.0.7) is nothing but the Schwarzschild metric in $D-1$ dimensions written in ingoing Eddington-Finkelstein coordinates, where the original radial coordinate has been redefined in terms of x:

$$r(x) = \frac{r_0}{x}. \tag{1.2.0.9}$$

This is convenient for the numerical implementation, since x is bounded: $0 \leq x \leq r_0$, with asymptotic infinity lying at $x = 0$. At this point we must ensure that the solution is regular. A boundary analysis shows that regular linearized functions $q_{1,2,3,4}$ must vanish as $r \to \infty$ (at $x = 0$).

Having a system of 4 coupled partial differential equations for the eigenmodes $q_{1,2,3,4}$, it can be solved using the pseudo-spectral techniques discussed in Ch. 2. For any r_0 and Ω, we can determine the spectrum $\{q_{1,2,3,4}, k\}$, using for instance, the subroutine `Eigensystem` in Mathematica. In fact, scale invariance of vacuum Einstein's equations allows us to fix r_0, which we took to be one and we are left with Ω as an input. Where the uniform black string is unstable, there exists two eigenvalues of k for fixed Ω.[9] Therefore we start to scan from $\Omega = 0$, all the way up until these two eigenvalues disappear. In doing this, we produce Fig. 1.1.

This figure shows the dispersion relation that is found in 5 and up to 10 spacetime dimensions. The plots clearly intersect the k-axis at two different points: $r_0|k|^2 = 0$ and $r_0|k_{\rm GL}|^2$. The different values we have found for $|k_{\rm GL}|^2$ are tabulated in Tab. 1.1. The fact that it intersects at the origin is due to the linear stability of Schwarzschild black hole. Below the GL critical value, or in other words, for perturbations with wavelengths above $\lambda_{\rm GL} = 2\pi/k_{\rm GL}$, black strings are classically unstable. Therefore the GL instability is actually a long wavelength instability. At finite L, the perturbative mode will only fit inside the 'cylinder' if its length is larger than $\lambda_{\rm GL}$, which gives the bound:

$$L > \frac{2\pi}{k_{\rm GL}}. \tag{1.2.0.10}$$

For convenience, we have fixed r_0, and the instability condition is discussed in terms of the circle's length. For instance, in $D = 5$ all black strings with $r_0 = 1$ and length $L \gtrsim 7$ (in units of r_0) will be unstable. Since these strings have $r_0/L \sim 10^{-1}$, we talk about thin black strings. Additionally, this also shows that there exists a gap between the threshold value provided by the entropic argument and the true GL threshold value.

The GL threshold 0-mode $\Omega = 0, k = k_{\rm GL}$ is a time-independent perturbation whose net effect is to create (periodic) ripples along the string horizon. The 0-modes have physical relevance here because they suggest, at least, two things. First, they signal the onset of a dynamical instability, where modes with $k < k_{\rm GL}$ grow in time. And second, it is natural to ask whether their continuation at the non-linear level is connected to the existence of another branch of static solutions. Indeed, these are the non-uniform black strings that we construct numerically in Ch. 3.

Of course, time-dependent perturbations also create ripples along the horizon, rising a deeper question: what is the final state of the instability? The answer has been a bit controversial actually. In spite of the entropic argument, Ref. [134] showed that, according to GR, the horizon of the black string could not pinch-off to form a localized black hole in finite affine parameter along the horizon generators. The endpoint then had to be a string-like configuration. However, later numerical studies suggested precisely the opposite [135, 136]. These studies culminated in the first long-term time

[9] We want to stress out that these will correspond to physical perturbation modes, since pure gauge modes of the form $H_{\mu\nu} = 2\nabla_{(\mu}\chi_{\nu)}$ with χ^μ an arbitrary vector satisfy $\Delta_{\rm R}^{(D-1)}\nabla_{(\mu}\chi_{\nu)} = 0$. Therefore, as long as the perturbation is non-trivial, satisfies proper boundary conditions and k is different than zero, these are not gauge artifacts.

evolution in higher-dimensional GR by Lehner and Pretorius [137] (see also Ch. 3 of [290] and [138] for a large-D analysis), who simulated how the GL instability develops in $D = 5$. The output data suggested the following picture. In some regions the inhomogeneities induced by the instability grow in time, whereas the thinner regions start to develop by themselves new generations of GL instabilities in a self-similar way. The system ends up with an array of localized 'bulges' of different sizes connected by very thin necks. It was observed that the generation formation time-scale decreases geometrically, suggesting that those thin necks would eventually pinch-off and naked singularities would be produced to transition from the $S^2 \times S^1$ topology of the string to the S^3 topology of the localized black holes. Eventually, the array of localized black holes would tend to collapse into a single localized black hole.

It is important to stress out that the evolution of the black string instability is generic since it does not require any fine-tuning of the initial data, and thus it constituted the first instance where it was shown, or perhaps strongly suggested by solid numerical data, that WCC may no longer hold in higher-dimensional GR with compact spacelike extra-dimensions.

The black string (or black p-branes in general) is (are) the prototypical black hole system used to illustrate the GL instability, which also serves to infer the qualitative dynamical behavior of GL-type instabilities that occur in a variety of other black holes, even in flat space. For instance, ultra-spinning Myers-Perry black holes (for $D \geq 6$), or thin black rings, are GL unstable. In the first case, the ultra-spinning black hole flattens out with respect to the axis of rotation and resembles to a membrane (or black 2-brane) [139]. It is then expected that it will suffer from a GL (axisymmetric) instability if the relative size of directions along the membrane are much larger than those perpendicular to it. Indeed, linear stationary axisymmetric perturbations about the MP black hole were constructed in [140–142], signaling the existence of the anticipated GL instability. Additionally, another type of non-axisymmetric instabilities, known as bar-mode instabilities, have also been identified in [143,144]. These are from a different nature due to the emission of gravitational waves which, originally, lead to postulate that these would make the perturbed black hole to settle down to a more slowly spinning black hole. However, this is not the case (see below). At the end, only fully non-linear time evolution can reveal the endpoint of these instabilities.

Over the last few years, some impressive studies have followed the mentioned dynamical instabilities in time using very sophisticated numerical codes and confirming, extending and clarifying the guessed pictures. For instance, the outcome of the ultra-spinning instability turns out to be very similar to that of GL for strings. The ultra-spinning MP goes first through a multi-black ring stage with multiple inner generations connected by thin membranes which, again, become GL unstable by themselves to finally pinch-off. The endpoint is a black ring and weak cosmic censorship is violated in the process [145]. In this evolution, stationary axisymmetric solutions that serve as intermediate stages, known as bumpy black holes, were previously constructed in [146,147] using the same numerical methods that we use in this work. For $D > 5$, it

has also been shown that a certain type of non-axisymmetric (bar) modes can become dominant and develop their own GL-type instabilities leading also to violation of weak cosmic censorship [148].[10]

Similarly, a thin black ring looks, locally, much like a (boosted) black string. This motivated the GL analysis of boosted black strings, which turned out to be unstable [150]. The authors of this paper engineered an approximate model to describe the black ring based on the boosted black string, concluding that very thin black rings would be GL unstable (see also [151]). In terms of ring radii, this would happen when the length scale associated to the S^1 of the ring is much larger than that of its S^2. More recently, a linearized study of gravitational perturbations about black rings [152] found that all 'thin' rings are unstable and that even a region of the fat branch is also affected by the instability. The ultimate studies have even succeeded in simulating how it develops in time [153], identifying a new elastic-type instability that competes with the GL mode. When the elastic mode dominates, the endpoint of the instability is a spherical black hole. Otherwise, the instability unfolds similarly to that of black strings. This was in fact the first concrete evidence that weak cosmic censorship can be violated in higher-dimensional Einstein's gravity in flat space.

Mergers and conical geometries

The non-trivial family of static black holes based on uniform, non-uniform strings and localized black holes is not exclusive of KK theory. In practice, any geometry with a smooth black hole horizon, that tends asymptotically to a warped-product space $M_p \times N_q$, for some p- and q-dimensional manifolds M_p and (compact) N_q, can be disposed in different ways along the internal or transverse space. At very least, a solution that completely wraps N_q in a homogeneous way do exist. If this internal space is Ricci-flat, we have the black q-branes introduced in (1.2.0.3), but if N_q has non-zero curvature, solutions will not solve Einstein's equation in vacuum. Instead, gauge fields need to be introduced.

In view of the previous discussions, the key is to identify 0-modes (i.e. static perturbation modes with $\Omega = 0$) which hint the existence of dynamical instabilities but also the existence of inhomogeneous solutions along N_q.

For black strings, the equation for a 0-mode (1.2.0.5) can be compared with the eigenvalue equation for the $(D-1)$-dimensional Euclidean continuation of the Schwarzschild black hole, which reads $(\Delta_{\rm E}^{(D-1)} - \lambda_{\rm E})h_{\mu\nu} = 0$, and it is known to have one negative mode, $\lambda_{\rm E} < 0$ [154]. But for static perturbations, $\Delta_{\rm E}^{(D-1)} = \Delta_{\rm L}^{(D-1)}$, and both equations become the same upon the identification $\lambda_{\rm E} = -k^2$ [155]. This will occur for a certain value of the parameter labelling each black hole and will give the

[10] There was a controversy where it was suggested that bar modes could lead to unstable MP black holes even in $D = 5$ [144], whereas their spectrum of quasi-normal modes found in [149] did not reveal any exponentially growing behavior. These two results could actually be compatible with each other if the instability in $D = 5$ was non-linear. Eventually, the time evolution of non-axisymmetrically perturbed MP black holes in $D = 5$ revealed stability [148].

threshold unstable mode, which separates classically stable solutions from unstable ones.

The previous observation shows that the existence of a 0-mode in the higher-dimensional Lorentzian black hole is equivalent to the existence of a negative mode in the Euclidean black hole geometry lying along the longitudinal part M_p. Extrapolating to a generic case for a black hole in $M_p \times N_q$ space, we have the following [156]. The black hole geometry on M_p will generically have an Euclidean Lichnerowicz operator with a negative eigenvalue: $(\Delta_{\rm E}^{(p)} - \lambda_{\rm E})h_{\mu\nu} = 0$, with $\lambda_{\rm E} < 0$, as long as it is locally thermodynamically unstable, manifested by positive eigenvalues of the Hessian matrix (in the microcanonical ensemble) or negative specific heat (in the canonical ensemble). On the other hand, the 0-modes will be expanded using a complete set of eigenfunctions $\Psi_{(\mu)}$ on N_q with eigenvalues $-\mu^2$ (which can be discrete), with respect to the usual Laplacian ∇^2 on N_q. When the Euclidean mode is saturated by the momentum in the transverse space: $\lambda_{\rm E} = -\mu_*^2$, this will give a 0-mode of the higher-dimensional black hole of the form:

$$h_{MN}(x, y) = H_{MN}(x)\Psi_{(\mu_*)}(y), \tag{1.2.0.11}$$

where x and y are the coordinates along M_p and N_q respectively. For lower momentum, $0 < \mu^2 < \mu_*^2$, it is expected that the black hole will be dynamically unstable with perturbative modes growing in time, whereas at the onset of the instability a new branch of inhomogeneous solutions along N_q emerge.

Additionally, there is no reason why localized solutions on the internal space should not exist. In the simplest case, this would be a static black hole with spherical topology that feels its self-interaction along the compact space. Localized solutions and inhomogeneous ones will have different topology, but it is expected to be connected in some way. The fact that N_q is compact means that if we start with a small localized black hole and we increase its size, at some point, it will cover N_q entirely. Conversely, inhomogeneous black holes can be followed through solution space. The inhomogeneities will grow until the horizon pinches to zero thickness and localizes. At the level of static solutions, both branches should merge. The details of how this is codified by the Einstein's equations is far from trivial. The merger of the two branches seems to be continuous but this would imply that we can move from one branch with, say, topology X, to another branch with topology Y, which is not possible without forming a naked singularity. Solutions close to this merger or critical point are known as critical black holes, and they develop conifolds, i.e. a geometry containing localized cone singularities, as they approach this point more and more.

Success in describing such singular geometries has been achieved using local models based on conical manifolds, first introduced by Kol in the context of KK black holes [21] (see also [22, 157–159] for subsequent studies), and later on in asymptotically flat space [147, 160]. Conical manifolds can be understood as a local 'proxy' for the change in the topology of the black holes involved. This proxy can be smoothed in two different ways, each one leading to one of the topologic phases, X and Y, at each side of the transition. Let us be a bit more precise. A cone over a base H is described by

the self-similar metric:

$$\mathrm{d}s^2_{\text{cone}} = \mathrm{d}\rho^2 + \rho^2 \mathrm{d}s^2(H), \tag{1.2.0.12}$$

where $\forall \rho > 0$ measures the distance from the tip of the cone, and it is indeed singular at $\rho = 0$ (the tip). Relevant to us are the cone over a double or triple product of spheres,

$$H = S^l \times S^m, \quad \text{or} \quad S^l \times S^m \times S^n, \tag{1.2.0.13}$$

which are referred to as the double- and triple-cone respectively, or just critical cone. These are Ricci-flat metrics for any (positive) value of l, m and n, with a curvature singularity at the tip, and work well to model the pinch-off of black hole configurations in vacuum. However, as we show in this thesis, the pinch-off in the presence of additional matter fields may lead to a cone model that it is not necessarily Ricci-flat.

One of the spheres of the base H always comes as a fiber bundle involving the Euclidean time, $\tau = -it$, which has periodicity given by the inverse temperature of the black hole, $\beta = 1/T$. This yields a circle that has zero size at the horizon. The fiber of this S^1_β over a certain manifold, gives rise to a l-sphere. For example, in a KK setting this is a periodic line that starts and finishes on the horizon, across the compact direction (see Fig. 1.2), i.e. $l = 2$. The other sphere(s) in H is (are) inherited by the geometry of the particular solution under study. For $l = 2$, the relevant case in this thesis, the Ricci-flat double-cone metric in Lorentzian signature reads:

$$\mathrm{d}s^2_{\text{cone}} = \mathrm{d}\rho^2 + \frac{\rho^2}{D-2}\left(-\sin^2\alpha\,\mathrm{d}t^2 + \mathrm{d}\alpha^2 + (m-1)\mathrm{d}\Omega^2_{(m)}\right), \tag{1.2.0.14}$$

with $\alpha \in [0, 2\pi]$. This metric has two horizons, one at $\alpha = 0$ and the other at $\alpha = \pi$, which connect non-smoothly at the tip $\rho = 0$. Note that both spheres are contractible, and shrink to zero size at the tip. The geometry can be smoothed by resolving, for instance, for the 2-sphere, making it non-contractible. This leads to the localized black hole phase, for which the other m-sphere is contractible. Alternatively, if the m-sphere is kept non-contractible, the resulting smoothed geometry is that of the non-uniform black string (where the Euclidean 2-sphere is contractible).

Notice also that (1.2.0.14) is not asymptotically flat, nor asymptotes any of the spaces we consider in this thesis. Moreover it extends indefinitely as $\rho \to \infty$. Models based on a conical manifold are local in the sense that describe well the horizon geometry near the critical points, but the exact way of how this conical region extends to a full critical solution remains unclear. This explains why they should be good models regardless of the asymptotic boundary conditions, and in particular, regardless of the presence of a cosmological constant.

It is remarkable that such a simple model is able to describe not only solutions that, in their majority, have only been found numerically, but also in a regime where the underlying theory is less understood. Of course, the fact that (1.2.0.12) is explicitly singular gives little hope in obtaining analytical predictions for physical properties beyond of reproducing the correct local critical geometry. But it turns out that a particular perturbation mode around (1.2.0.12) describes any(!) thermodynamical

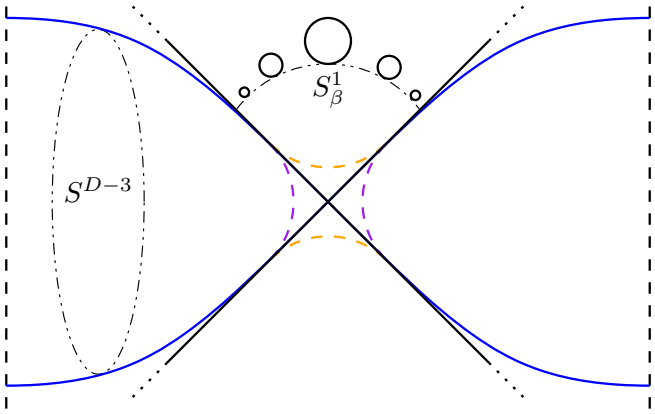

Fig. 1.2: *Pictographic representation of the conical geometry (black lines) at the critical point in the black string/black hole topology phase transition. Orange and purple dashed lines are the two different ways in which it can be smoothed leading to the non-uniform and localized phases respectively. The blue lines represent the continuation of the horizon's black hole geometry away from the pinch-off.*

quantity of solutions close enough to the merger at any side of the critical point. In this sense, the model exhibits certain universality.

More specifically, given a physical quantity Q of a critical solution, it then behaves according to [21]:

$$Q = Q_{\rm c} + C_+ \rho_0^{s_+} + C_- \rho_0^{s_-}, \tag{1.2.0.15}$$

where $Q_{\rm c}$ is the value at the critical point, ρ_0 is any black hole length that measures how it deviates from the cone, and the critical exponents s_+ and s_- are dimension dependent, which degenerate for $D = 10$. They are complex for lower dimensions and become purely real for $D \geq 10$. Most of the physical quantities of a black hole are defined on the horizon, but this is suggesting that in a topology-change phase transition, these are actually governed by the horizon regions that pinch-off.

The main task that we have carried out in this thesis consists in to check the validity of this conical model, and in particular the validity of (1.2.0.15). To this end, we have considered various one-parameter families of black holes with two different asymptotic boundary conditions, involving a topology phase transition. In the simplest case, we have considered Kaluza-Klein theory, i.e. $M_{D-1} = \text{Mink}_{D-1}$ and $N_1 = S^1$. This family was considered in $D = 10$ [161] but for a rather small range of parameter space, and in particular, far from the critical region. We revisit this particular dimension which has a 2-fold interest: first for being $D = 10$ the critical dimension of the cone, and second, for being the family dual, after a certain duality map, to thermal states of $(1 + 1)$-dimensional SYM theory on a particular background. The latter was the purpose of [161], and hence, where our data overlaps with the one shown in that paper, we checked that both results agree. However, to be able to explore the critical region some refinements need to be taken into account. This is presented in Chapter 3.

A more involved case is $M_p = \mathrm{AdS}_p$ and $N_q = S^q$. For certain values (p, q), black holes appear to be solutions of 10- and 11-dimensional supergravity theories, so we are no longer in vacuum. An infinite amount of one-parameter families of black hole solutions exist in such spaces. The reason is simple: the internal space S^q has a discrete, but infinite, set of eigenvalues, yielding an infinite number of 0-modes, each one connected to a new family of inhomogeneous, or lumpy, solutions. In this case, the values set $(p, q) = (5, 5)$ was studied in [19], but again, only slightly lumpy black holes were constructed. Our study extends and partially differs than that in [19] for $D = 10$, and also considers the case in $D = 11$. In both cases we manage to explore their critical regions and we find, for first time with Anti-de Sitter boundary conditions, the corresponding critical exponents. These coincide with those predicted by the cone model, which is no longer Ricci-flat due to the presence of non-trivial flux fields. This is the topic of study of Ch. 4. Additionally, asymptotically AdS solutions have relevance due to the AdS/CFT correspondence, which we now turn to discuss.

1.3 AdS/CFT correspondence

One of the most remarkable and counter-intuitive achievements in theoretical physics of the last 20ish years is the AdS/CFT correspondence [162–166]. The original $\mathrm{AdS}_5/\mathrm{CFT}_4$ [162] is a conjectured duality between type IIB superstring theory [287–289] on an $\mathrm{AdS}_5 \times S^5$ background and $\mathcal{N} = 4$ super Yang-Mills [167] (SYM) with gauge group $\mathrm{SU}(N)$, living in the 4-dimensional conformal boundary of AdS_5. According to this conjecture, despite both theories represent different systems and interactions, they (are supposed to) describe the exact same physics from very different perspectives. Maybe the most striking feature is that it states that a gravity-free theory is completely equivalent to, not only a theory with gravity, but a theory of quantum gravity.

In this regard, AdS/CFT is a very far-from-trivial realization of the holographic principle (see [168] for a through review), which states that in every theory of quantum gravity the degrees of freedom of a certain bulk system have a description in terms of degrees of freedom living on its boundary, and vice versa. This idea is not exclusive of AdS/CFT, but dates back to the original works by t' Hooft [169] and Susskind [170], who built on the fact that black hole temperature and entropy are given in terms of quantities defined on a surface (rather than a volume), the surface gravity and the horizon area, to infer the holographic nature of quantum gravity.

In the earlier $\mathrm{AdS}_5/\mathrm{CFT}_4$ duality, the 5-dimensional theory arising from the compactification of type IIB string theory on the S^5 is mapped to a gauge theory defined on the conformal boundary of AdS_5. Originally, the correspondence was motivated for large number of colors, $N \to \infty$, and large but fixed 't Hooft coupling, $\lambda \equiv g_{\mathrm{YM}}^2 N \gg 1$ (g_{YM} is the SYM coupling), where it was known that the gauge theory had a smooth large N limit [171] with a perturbative expansion in $1/N$. On the AdS side, this corresponded to performing a perturbative expansion in the string coupling g_{s}, with the leading contribution being (classical) type IIB supergravity. However, there is

substantial evidence that the equivalence is not only also true for generic values of the 't Hooft coupling λ, but also for non-conformal settings with less supersymmetries (see Ch. 6, 7 and 8 in [291] and references therein); with applicability ranging from heavy ion collisions [172–175] to hydrodynamics [176–181] or condensed matter systems [182–186], leading to one of the most promising and active areas of research of current times in theoretical physics. In general, one refers to the correspondences that arise in such context as gauge/gravity dualities.

One of the main incentives is that under certain limits, gauge/gravity dualities are in addition strong/weak coupling dualities. For instance, the large N, large 't Hooft coupling limits mentioned above in AdS_5/CFT_4, lead to a strongly coupled SYM gauge theory and a (free) point-particle limit of type IIB string theory, i.e. type IIB supergravity. The latter is a classical theory of gravity, and hence more clear, understood and tractable from a technical point of view than its parent stringy theory. This is quite appealing given the lack of standard and effective methods to address the non-perturbative regimes of gauge theories.[11] Now, once a dual pair is identified, one can explore such sectors using, essentially, GR coupled to other fields.

In the rest of this section we briefly introduce the subject without entering into much detail, emphasizing on the different concepts and results that will be relevant in the following chapters. There is an extensive literature where this content is explained in full detail and in turn provide different points of view. See e.g. [187–189, 289, 291].

AdS_5/CFT_4 correspondence

In [162] Juan Maldacena introduced the first example of gauge/gravity duality. On the one hand, the gauge side is $\mathcal{N} = 4$ SYM in 3+1 dimensions and it has two free parameters: the rank of the gauge group N and the dimensionless coupling $g_{\rm YM}$. On the other hand, the gravity side is type IIB string theory in $AdS_5 \times S^5$, with dimensionless string coupling $g_{\rm s}$, string length $l_{\rm s} = \sqrt{\alpha'}$ and AdS radius L (which coincides with the radius of the S^5). This is the best understood example of gauge/gravity duality, and will be the starting point of our discussion in Chapter 4, so let us elaborate a bit more in this direction. We will not give the precise references at each step of this exposition, since most the ingredients used are well-known and can be found in the literature cited above.

The duality is motivated by taking two different points of view, the closed and the open string perspectives, of type IIB string theory in the presence of a stack of N coincident D3-branes and then taking the so-called decoupling limit (which typically is a low-energy limit). Which perspective is the right one depends on the value of the string coupling which controls the interaction between the two string sectors.

In the general picture at weak coupling, $g_{\rm s}N \ll 1$, open string modes propagate

[11] Lattice gauge theory is actually non-perturbative but it only works in equilibrium situations and without fermions, and many applications of AdS/CFT correspondence are precisely concerned about far-from-equilibrium physics and/or with the presence of fermions and non-zero chemical potential.

along the world-volume of the brane, where their endpoints are attached, and closed string modes propagate in the bulk. Moreover, if one truncates the theory to the massless sector, i.e. low energies $E \ll l_{\rm s}^{-1}$, and takes the limit $l_{\rm s} \to 0$, the two sectors decouple. The dynamics of the open string excitations are described in terms of SYM gauge theory on the world-volume of the branes which is $(3+1)$-dimensional, whereas the closed string sector yields type IIB supergravity in $\mathbb{R}^{1,9}$ off the branes. In doing that, one identifies the couplings of both theories:

$$g_{\rm YM}^2 = 2\pi g_{\rm s}, \qquad 16\pi G_{10} = (2\pi)^7(\alpha')^4 g_{\rm s}^2. \tag{1.3.0.1}$$

At strong coupling, $g_{\rm s}N \gg 1$, open and closed strings interact and the backreaction on the D3-branes is significative. Then the latter can no longer be viewed as dynamic hyperplanes where open strings end. For this reason, at weak coupling one talks about the 'open string perspective'. One possible way to understand what is the effect of such backreaction is looking at the geometry sourced by the D3-branes in the effective theory. Indeed, D-branes are solitonic objects that appear in 10-dimensional supergravities. In the case of N D3's, they appear as a solution within type IIB supergravity with N units of $F_{(5)}$ flux. Its background metric is given by [190]:

$$\mathrm{d}s_{\rm D3}^2 = H(r)^{-1/2}\eta_{\mu\nu}\mathrm{d}x^\mu \mathrm{d}x^\nu + H(r)^{1/2}\Big(\mathrm{d}r^2 + r^2\mathrm{d}\Omega_5^2\Big), \tag{1.3.0.2}$$

with

$$H(r) = 1 + \frac{L^4}{r^4}, \qquad L^4 = 4\pi g_{\rm s} N(\alpha')^2 \tag{1.3.0.3}$$

and $\mu, \nu = 0, 1, 2, 3$. (There are also other non-zero fields but they are not relevant at this point.) The characteristic length L must be large compared to the string length, i.e. weak curvature, in order for the supergravity approximation to be reliable. This yields the strong coupling condition: $1 \ll L^4/l_{\rm s}^4 = 4\pi g_{\rm s} N$, valid in a 'closed string' perspective. In turn, the string coupling needs to be small, to suppress string loop effects, $g_{\rm s} \ll 1$, which implies that we are taking the large N limit, $N \to \infty$.

Now the closed strings of type IIB string theory propagate in the background (1.3.0.2). The metric has two different regions: in the asymptotic region $r \gg L$, it reduces to 10-dimensional Minkowski space, whereas in the throat, or near horizon region, $r \sim 0$, corresponds to $\mathrm{AdS}_5 \times S^5$ in the Poincaré patch:

$$\mathrm{d}s_{\rm D3}^2(r \sim 0) \to \frac{L^2}{r^2}\mathrm{d}r^2 + \frac{r^2}{L^2}\eta_{\mu\nu}\mathrm{d}x^\mu \mathrm{d}x^\nu + L^2\mathrm{d}\Omega_5. \tag{1.3.0.4}$$

This yields two sectors of closed strings, one propagating in $\mathbb{R}^{1,9}$ and another one in $\mathrm{AdS}_5 \times S^5$. In this case, the low-energy limit consists of focusing on modes that have low energy with respect to an observer in the far region $\mathbb{R}^{1,9}$. For the modes close to the horizon, this implies that one cannot throw away all the massive modes which locally have higher energies near the horizon, given that those are highly red-shifted when they climb up the gravitational wall in order to reach the asymptotically flat region. However, they do decouple from the asymptotic modes: for an asymptotic

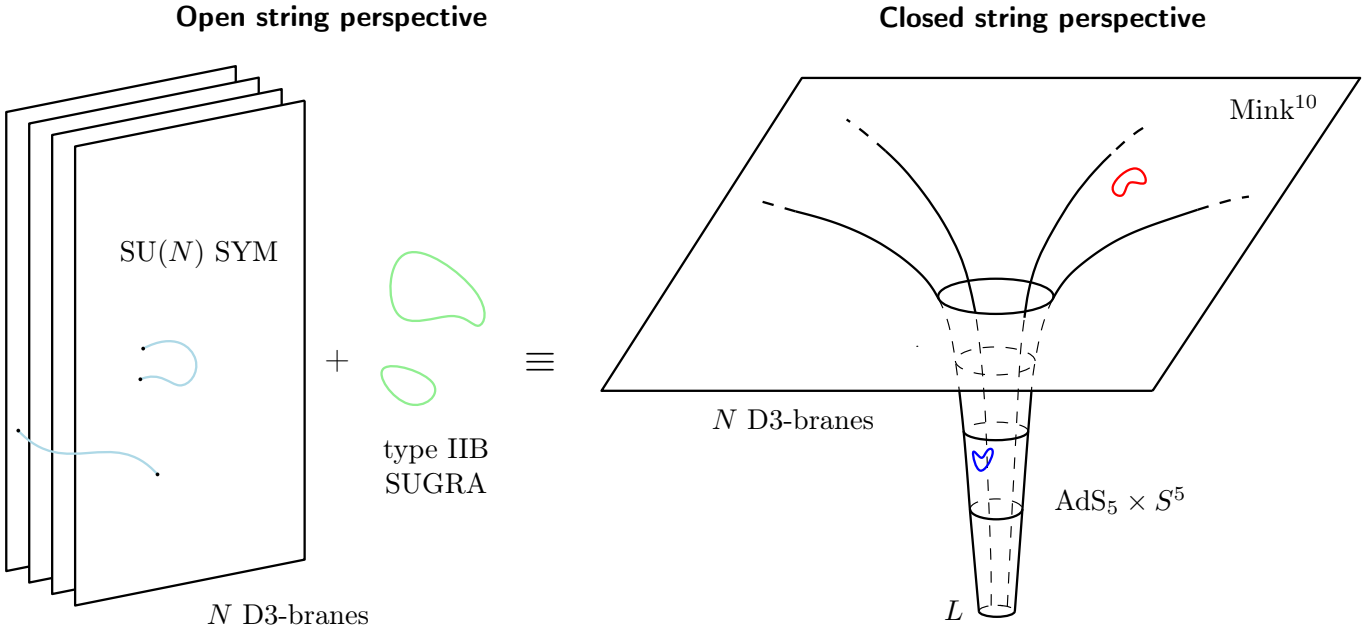

Fig. 1.3: *Pictographic representation of the AdS_5/CFT_4 correspondence.*

observer, the lower the energy that a 'throat mode' has, the deeper in the horizon is located. In the Minkowski region, though, the only modes that remain in the limit $l_s \to 0$ are those of type IIB supergravity in flat space, which decouple from any other: they do not interact among themselves because G_{10} vanishes in the limit, and their characteristic wavelength is much larger than the size of the near horizon region to resolve it and interact with the modes there. Summarizing, at low energies the 'closed string' description of the system reduces to type IIB supergravity in $\mathrm{AdS}_5 \times S^5$ plus type IIB supergravity in Minkowski space.

Putting the two perspectives together, the low-energy limit of two points of view yields two decoupled effective theories. The type IIB supergravity in $\mathbb{R}^{1,9}$ is present on both sides, and Maldacena conjectured that the other pair must agree as well, establishing that $\mathcal{N} = 4$ SYM in 3+1 dimensions with gauge group $\mathrm{SU}(N)$ is equivalent to type IIB supergravity in $\mathrm{AdS}_5 \times S^5$. This is represented in Fig. 1.3.

Once the conjecture is established, note that in the large N limit the effective coupling in the gauge side is the 't Hooft coupling, λ $(= g^2_{\mathrm{YM}} N)$, which is the only free parameter available. In the gravity side we are left with the ratio L^2/l_s^2 as free parameter, which is related to λ via: $L^4/l_s^4 = 2\lambda$. Supergravity applies provided that the curvature scale is large compared to the string length, which implies that the gauge side is actually strongly coupled, $\lambda \to \infty$. This defines the 'weak' form of the $\mathrm{AdS}_5/\mathrm{CFT}_4$ correspondence, but Maldacena went one step further and conjectured that this correspondence also holds beyond the supergravity limit, making his statement even much more profound. It relies on comparing two points of view that apply for distinct regimes of g_s, but the theories involved exist for any value of the coupling.

A simple check in support of the duality is that the global symmetries on both

sides match. $\mathcal{N}=4$ SYM in 4 dimensions is conformal and it enjoys an $\mathrm{SO}(2,4)$ symmetry, plus an $\mathrm{SO}(6)$ symmetry coming from the R-symmetry that rotates the sixteen supersymmetric charges of the theory. In the gravity side, these symmetry groups appear as the isometry group of $\mathrm{AdS}_5 \times S^5$.

The conformal boundary of the AdS factor plays an important role in the duality. In (1.3.0.2), the near horizon region yields AdS_5 (let us forget about the 5-sphere for now) in the Poincaré patch, which does not cover the AdS spacetime in full. In this patch, the conformal boundary is Minkowski space $\mathbb{R}^{1,3}$, where the dual $\mathcal{N}=4$ SYM theory is defined. It is now easy to think about extending the duality to all AdS, using for instance global coordinates. Then the conformal boundary is the Einstein static universe, $\mathbb{R}\times S^3$, and SYM theory is now defined on this compact space. This has relevance from the thermodynamic point of view, as we will discuss shortly.

Generically, the claim of the gauge/gravity duality is that the physics of some strongly coupled field theory is encapsulated in the physics of a gravitational theory on a certain background and vice versa. Holography then suggests that the boundary of such background realizes geometrically the symmetries of the dual field theory. For example, in the case at hand of $\mathrm{AdS}_5/\mathrm{CFT}_4$ on flat space, this background is (1.3.0.4), where the coordinates x^μ may be thought as the coordinates along the world-volume of the original D3-branes, and hence may be identified with the gauge theory coordinates. Furthermore, notice that the metric (1.3.0.4) realizes the invariance under dilatations of the CFT,

$$r \to \Lambda r, \qquad x^\mu \to \Lambda^{-1} x^\mu, \tag{1.3.0.5}$$

($\Lambda \in \mathbb{R}$), which in turn reveals that the AdS radial coordinate r defines an energy scale for the gauge theory (the rest of coordinates span the directions transverse to the branes). According to (1.3.0.5), small radius means large distances, or low energies, in the gauge theory, and conversely, large radius corresponds to small distances, or high energies. For this reason, the conformal boundary of AdS is, in this context, sometimes referred to as the UV boundary.

If one is interested in non-conformal theories, dilatations can no longer be an exact isometry of the dual background geometry. Then a dynamical critical or Lifshitz exponent z is introduced and one is led to consider as background [182]

$$\mathrm{d}s^2 = \frac{L^2}{r^2}\mathrm{d}r^2 + \frac{r^{2z}}{L^2}\mathrm{d}t^2 + \frac{r^2}{L^2}\delta_{ij}\mathrm{d}x^i\mathrm{d}x^j, \tag{1.3.0.6}$$

which realizes the scaling symmetry

$$r \to \Lambda r, \qquad t \to \Lambda^{-z} t, \qquad x^i \to \Lambda^{-1} x^i, \tag{1.3.0.7}$$

($i = 1, \ldots, d-1$; d being the total number of spacetime dimensions of the dual quantum field theory (QFT)). Whilst the $z=1$ case corresponds to AdS, which is dual to a relativistic CFT, for $z>1$ the gravitational theory is a possible candidate dual to some non-relativistic QFT. This is indeed the starting point for addressing certain problems in condensed matter systems using gauge/gravity duality.

With special interest for us, it is the way of computing the expectation values of composite gauge invariant operators, and explore the thermal phases of a given gauge theory at finite temperature using its gravity dual.

Holographic dictionary

The so-called 'Holographic dictionary' [163–165,291] provides the formal mapping rules between the two sides of the duality, establishing a precise one-to-one relation between operators and fields, and hence how to compute physical observables.

A first entry in this dictionary, tells us that gauge invariant operators are mapped to bulk fields, with the boundary value of the latter playing the role of sources for the dual operators. This suggests an equivalence between the generating functionals of both sides of the duality [163]:[12]

$$\left\langle e^{-S_{\rm QFT}[G_{(0)}]-\int \mathrm{d}^4x\sqrt{G_{(0)}}\mathcal{O}(x)\Psi_{(0)}(x)}\right\rangle = e^{-S_{5d}[G_{(0)},\Psi_{(0)}]}, \tag{1.3.0.8}$$

where $G_{(0)}$ and $\Psi_{(0)}$ are parametrizing the boundary values of the $(5d)$ bulk solutions $G_{\mu\nu}$ and Ψ's in AdS_5 (after dimensional reduction on the 5-sphere in the case it plays any role). Clearly, the fields $\Psi_{(0)}$ play the role of sources, whereas the classical on-shell $5d$ supergravity action is the generating functional for the Green's function of composite gauge invariant operators $\mathcal{O}$.

For simplicity, the statement in (1.3.0.8) used to be presented for scalars, but the same logic applies for other types of fields. For instance, vector and tensor fields are dual to vector currents and stress-energy tensors respectively. Note also that, formally, (1.3.0.8) would equate the string partition function and that of the dual CFT, but at the end, most of computations are done assuming the weak form of AdS/CFT, where one evaluates the string partition function from its semi-classical (on-shell) supergravity action. Of course, (1.3.0.8) is specified for AdS_5 since it is the relevant case in this thesis, but the case for a CFT defined on the d-dimensional boundary of a gravity theory in asymptotic AdS_{d+1} is straightforward to generalize.

The holographic map as given in (1.3.0.8) allows us, in principle, to compute (connected) correlators of composite gauge invariant operators. They just follow from taking the functional derivatives with respect to the sources $\Psi^i_{(0)}(x_i)$:

$$\langle \mathcal{O}_1(x_1)\dots\mathcal{O}_n(x_n)\rangle = (-1)^{n-1}\frac{\delta^n S_{5d}}{\delta\Psi^1_{(0)}(x_1)\dots\delta\Psi^n_{(0)}(x_n)}\bigg|_{\Psi^i_{(0)}=0}. \tag{1.3.0.9}$$

So far, so good, but in practice one finds some obstacles. Generically, QFTs suffer from the well-known UV divergences due to unbounded integrals in momentum space, and therefore the r.h.s. of (1.3.0.8) must also diverge. Indeed, evaluation of the on-shell supergravity action in AdS yields IR divergences due to the infinite volume of the spacetime. Then the relation between partition functionals must be understood

[12] In the semi-classical approximation and Euclidean signature.

as given in terms of 'bare' fields and to restore computation capability one must renormalize. Renormalization in QFT has been established for a long time, but now we are interested in to proceed in the gravity side. A systematic procedure exists for this and it is known as holographic renormalization. The Ward identities satisfied by symmetry-related correlators and certain quantum anomalies can also be computed with this recipe, but in the following we will only focus on correlators.

Holographic renormalization

The holographic renormalization formalism [191] applies to asymptotically AdS spacetimes, and it is conveniently developed in the Fefferman-Graham (FG) gauge where the metric reads:

$$\mathrm{d}s_D^2 = \frac{1}{Z^2}(\mathrm{d}Z^2 + G_{ij}(Z,X)\mathrm{d}X^i\mathrm{d}X^j), \tag{1.3.0.10}$$

with the $(d = D-1)$-dimensional AdS boundary B_d lying at $Z = 0$, and the additional coordinates X^k running along B_d. In this sense, FG coordinates are an analog of Gaussian normal coordinates at the conformal boundary B_d, where the metric $G_{ij}(X) = G_{ij}(0,X)$ defines a non-degenerate Riemannian metric in d dimensions. Any asymptotically AdS spacetime can be put in the FG form in the neighborhood of B_d.

Asymptotically AdS spacetimes appear in theories of classical gravity with a negative cosmological constant, possibly coupled to other fields. For our purposes, it is sufficient to consider gravity plus a scalar field. The holographic dictionary tells us that the metric G_{ij} is dual to the stress tensor T_{ij} of the d-dimensional CFT at the boundary, which has scaling dimension $\Delta = d$, and scalar fields with masses in the range $-d^2/4 \leq m^2L^2 \leq 0$ are dual to operators $\mathcal{O}_\Delta(x)$ of the CFT, with scaling dimension

$$2\Delta = d + \sqrt{d^2 + 4m^2L^2} \tag{1.3.0.11}$$

in the range $d/2 \leq \Delta \leq d$, corresponding to relevant or marginal operators. Indeed, the lower bound is the well-known unitarity bound for a scalar field in a CFT_d, now linked to the Breitenlohner-Freedman (stability) bound for scalar fields in AdS_{d+1}.

The first step in holographic renormalization consists of performing a near-boundary analysis. It turns out that the metric function $G_{ij}(Z,X)$ and the scalar field $\Psi(Z,X)$ admit a Taylor series expansion around $Z = 0$. Solving the bulk equations of motion order by order yields a schematic form of the metric $G_{ij}(Z,X)$ and scalar field $\Psi^\Delta(Z,X)$, where Δ is the dimension of the dual operator. Specifying for $D = 5$,

$$\begin{aligned} G_{ij}(Z,X) &= G_{ij}^{(0)}(X) + Z^2 G_{ij}^{(2)}(X) + Z^4\left(G_{ij}^{(4)}(X) + \log Z^2 H_{ij}^{(4)}(X)\right) \\ &\quad + \ldots, \\ \Psi^2(Z,X) &= Z^2\left(\log Z^2 \Psi_{(0)}^2(X) + \tilde{\Psi}_{(0)}^2(X) + \ldots\right), \\ \Psi^\Delta(Z,X) &= Z^{4-\Delta}\Psi_{(0)}^\Delta(X) + \cdots + Z^\Delta \Psi_{(2\Delta-4)}^\Delta + \ldots, \qquad (\Delta > 2). \end{aligned} \tag{1.3.0.12}$$

The expansion proceeds in even powers of Z due to the structure of Einstein's equations and the logarithmic terms in (1.3.0.12) are only present for d even and/or when $\Delta - d/2$

is an integer. If no deformations are added to the field theory, the equations of motion provide two constraints on $G^{(4)}_{ij}$, namely $G^{(4)}_{ij}$ is traceless and divergence-free with respect to $G^{(0)}_{ij}$. However, in the presence of sources $G^{(4)}_{ij}$ will not be divergence-free and it may or may be not traceless. In this case, the constraints on the gravity side are identical to the Ward identities in the field theory side.

The leading terms $G^{(0)}_{ij}, \Psi^2_{(0)}$ and $\Psi^{\Delta}_{(0)}$ parametrize the Dirichlet boundary conditions. In particular, the leading term $G^{(0)}_{ij}$ in the metric corresponds to the boundary metric and it thus defines the spacetime background where the dual CFT is defined on. These quantities correspond to the dual sources for the CFT stress-energy tensor, and the scalar operators of dimension 2 and Δ respectively. Together with the normalizable modes $G^{(4)}_{ij}, \tilde{\Psi}^2_{(0)}$ and $\Psi^{\Delta}_{(2\Delta-4)}$, which can be seen as Neumann data, determine the series solution completely. In fact, Neumann data contain the important information on 1-point correlators (see below).

With the asymptotic solution, one can compute the on-shell supergravity action entering in the r.h.s. of (1.3.0.9). This diverges as one approaches to the boundary and to make those terms explicit, one regularize the action defining the boundary at $Z = \epsilon$, which is eventually removed by taking the limit $\epsilon \to 0$. Defining a set of local counter-terms, the divergences can be cancelled yielding a finite result. These were determined once and for all in [191], since the precise form of $S_{\rm ct}$ is completely determined by the near boundary expansion. The renormalized action is then:

$$S_{\rm ren}\left[G_{(0)}, \Psi_{(0)}\right] = \lim_{\epsilon\to 0}\left(S_{\text{on-shell}} + S_{\rm ct}\right), \tag{1.3.0.13}$$

and now one can safely take functional derivatives of $S_{\rm ren}$ with respect to the sources $G^{(0)}_{ij}$ and $\Psi_{(0)}$, and compute the correlators.

For example, 1-point correlators show that the new piece of data $G^{(4)}_{ij}(X)$ in (1.3.0.12), is directly related to the so-called boundary stress-tensor of AdS, T_{ij}, which is dual to the expectation value of the stress-energy tensor of the dual CFT, $\langle T^{\rm CFT}_{ij}\rangle$. The result for the boundary stress-tensor for the gauged supergravity we are interested in can be written in the simple form [192, 193]:

$$\begin{aligned} T_{ij} = \frac{N^2}{2\pi^2}\Bigg(& G^{(4)}_{ij} + \frac{1}{8}\left(\mathrm{Tr}(G^{(2)})^2 - (\mathrm{Tr}(G^{(2)}))^2\right) G^{(0)}_{ij} - \frac{1}{2}(G^2_{(2)})_{ij} \\ & + \frac{1}{4}G^{(2)}_{ij}\mathrm{Tr}(G^{(2)}) + \frac{3}{2}H^{(4)}_{ij} + \frac{1}{3}(\tilde{\Psi}^2_{(0)})^2 G^{(0)}_{ij} \\ & + \left(\frac{2}{3}\Psi^2_{(0)} - \tilde{\Psi}^2_{(0)}\right)\Psi^2_{(0)} G^{(0)}_{ij}\Bigg). \end{aligned} \tag{1.3.0.14}$$

For arbitrary D, the stress-tensor can be written as $T_{ij} \sim G^{(d)}_{ij} + C_{ij}[G^{(0)}]$, where $C_{ij}\left[G^{(0)}\right]$ is a local divergence-free (then the stress-energy tensor is conserved) functional of the boundary metric and its derivatives with the property that it vanishes for Ricci-flat B_d. The details of C_{ij} are dimension-dependent and for $d = 4$ coupled to a scalar field yields (1.3.0.14). The contribution to T_{ij} given by C_{ij} comes from

the log-term in the boundary expansion, so it also vanishes in odd d dimensions, but it may not for d even. In such case, T_{ij} will not be traceless unless B_d is flat. The trace of the stress-energy tensor of any CFT vanishes at the classical level, but at the quantum level on a curved spacetime may be, precisely, non-zero in even d. This is the well-known Weyl anomaly, which is now linked to the local geometry of B_d by virtue of the AdS/CFT correspondence.

On the other hand, the 1-point correlators of the scalar field dual operator read:

$$\langle \mathcal{O}^2 \rangle = \frac{N^2}{2\pi^2}\big(2\tilde{\Psi}^2_{(0)}\big), \qquad \langle \mathcal{O}^\Delta \rangle = \frac{N^2}{2\pi^2}\big((2\Delta-4)\Psi^\Delta_{(2\Delta-4)}\big) + \text{lower}, \tag{1.3.0.15}$$

where 'lower' indicates terms with index smaller than $2\Delta - 4$, and they only appear when the weight Δ of the operator can be written as a sum of weights of other lower operators.

At this point, the expressions (1.3.0.14) and (1.3.0.15) are given in terms of completely general sources $G^{(0)}_{ij}, \Psi^2_{(0)}$ and $\Psi^\Delta_{(0)}$, whose particular form will depend upon the relevant bulk solution arising in the duality. For non-vanishing scalar field source $\Psi^{\Delta'}_{(0)}$ ($\Delta' = 2$ or Δ), the dual field theory is deformed by the corresponding relevant or marginal operator, yielding an effective Lagrangian given by

$$\mathcal{L}_{\text{QFT}} = \mathcal{L}_{\text{CFT}} + \Psi^{\Delta'}_{(0)}\mathcal{O}_{\Delta'}. \tag{1.3.0.16}$$

Even if the scalar field source vanishes, it does not necessarily imply that the corresponding 1-point function given in (1.3.0.15) is zero. In such case the result is understood as its vacuum expectation value.

In Chapter 4 we construct bulk solutions that asymptote global $\text{AdS}_5 \times S^5$, and therefore they have a well-known dual gauge theory, namely $\mathcal{N} = 4$ SYM on the 4-dimensional Einstein static universe (ESU_4). We then use holographic renormalization to find the stress-energy tensor of our solutions, and hence their energy, which allows us to study their thermodynamic phase diagram. Additionally, from the point of view of an observer in AdS_5, those solutions are accompanied by various scalar fields which are dual to certain gauge operators. Those scalar fields acquire non-trivial vev's and they are computed using the expressions presented in this section.

Gravity dual thermodynamics

The thermal structure of a given gauge theory at finite temperature can also be addressed through the AdS/CFT correspondence. The natural objects with thermodynamic properties in any (semi-)classical theory of gravity are black holes. So, if a dual pair is known and the bulk theory admits black hole solutions, then the dual gauge theory is a CFT in a thermal ensemble. More precisely, black holes in the bulk are describing thermal states of the gauge theory at finite T [163, 164].

To motivate this statement, let us turn back to the gravity dual of $\mathcal{N} = 4$ SYM at finite temperature on flat space. Being at finite temperature means that the Euclidean

time coordinate is compactified on a circle of period $\beta = 1/T$, then the theory is defined on $S^1 \times \mathbb{R}^3$. For $T = 0$, the correspondence follows from taking the decoupling limit of extremal D3-branes, which have zero temperature. The natural generalization is to consider the decoupling limit of non-extremal (black) D3-branes. Near the throat, the metric is the planar Schwarzschild-AdS$_5 \times S^5$ black hole,

$$\mathrm{d}s^2_{\text{planar}} = \frac{r^2}{L^2}\Big(- f(r)\mathrm{d}t^2 + \mathrm{d}\vec{x}^{\,2}\Big) + \frac{L^2}{r^2}\Big(f(r)^{-1}\mathrm{d}r^2 + r^2\mathrm{d}\Omega_5^2\Big), \tag{1.3.0.17}$$

with

$$f(r) = 1 - \frac{r_0^4}{r^4}. \tag{1.3.0.18}$$

This metric reduces to (1.3.0.4) at large r, but differs from it in the IR (for small values of r), where it has an horizon at $r = r_0$. This means that for large r, the duality is essentially the same as at zero temperature. This is not surprising: large r means high energies in the gauge theory and in this regime thermal excitations are not supposed to change the physics much. The black hole (1.3.0.17) has Hawking temperature

$$T_{\text{H}} = \frac{r_0}{\pi L^2} = T, \tag{1.3.0.19}$$

which is identified as the temperature of the dual CFT, i.e. $\mathcal{N} = 4$ SYM on $S^1 \times \mathbb{R}^3$ at strong coupling. The rest of the thermodynamical variables are matched as well. For instance, the Bekenstein-Hawking entropy of the black brane, S_{BH}, corresponds to the field theory entropy, S:

$$S_{\text{BH}} = \frac{\pi^2}{2} N^2 T^3 \mathrm{vol}(\mathbb{R}^3) = S, \tag{1.3.0.20}$$

where we used the dimensional reduction relation $G_5 = G_{10}/(\pi^3 L^5)$ and (1.3.0.1) to express it in terms of gauge theory variables. (1.3.0.20) gives the entropy of large N, large λ, $\mathcal{N} = 4$ SYM, and it just required a very simple area calculation. Up to now, it is not known how to compute such quantity directly in the gauge side. Naively, this would imply to sum over an infinite amount of Feynman diagrams using 'thermal' Feynman rules. However, we can compare this result with the entropy of the free theory [194], which differs with respect to (1.3.0.20) only by a factor of 4/3. In any case, a black hole quantity reproduces (at the very least) the expected form of the gauge entropy: at large N the dynamics of the theory are dominated by N^2 degrees of freedom, which is nothing but the number of gluonic states. On the other hand, the T-dependence can be justified via dimensional analysis: in a CFT the temperature is the only scale and entropy, which is dimensionless, must scale with the spatial volume (i.e. energy to the third power in $D = 4$)[13].

In practice, one usually applies AdS/CFT in one way, namely: given a CFT at finite T[14] in a certain background B_d, which is fixed, one studies the gravity dual looking for

[13] This scaling is different for a non-CFT.

[14] If the field theory is also at finite charge density or chemical potential, it will have a global U(1) symmetry. In this case one would need to include a U(1) gauge field in the bulk action.

black hole geometries that are asymptotically AdS whose conformal boundary agrees with B_d, i.e. it belongs to the same conformal class. In the gravity side B_d is then a boundary condition. For instance, another possibility for $d = 4$ is to define the gauge theory on $B_4 = S^1 \times S^3$. This introduces another parameter: the size of the 3-sphere, allowing richer physics. Precisely, Anti-de Sitter space in global coordinates has conformal boundary $B_4 = \mathbb{R} \times S^3$. Therefore, any asymptotically global AdS black hole will be mapped to a thermal state in the gauge theory, with the CFT vacuum state corresponding to the solution with lowest energy; in this case, this is global AdS itself.[15] Schwarzschild black holes in global AdS do exist, and they compete with the other spacetime configurations available, yielding the well-known Hawking-Page transition [195]. This was reinterpreted by Witten using the AdS/CFT correspondence as a confinement/deconfinement transition in the quark-gluon plasma [163]. We postpone a detailed discussion of black holes in (global) AdS space for Chapter 4.

We close this chapter with a few words on finite chemical potential and finite density. In QFT, finite density or non-zero chemical potential is introduced by means of a global U(1) gauge symmetry under which the other fields are charged. From the gravity perspective, it is then natural to add a U(1) gauge field in the bulk action with a non-trivial profile for the time-component. Then black holes will have electric charge. The near-boundary expansion of this field is:

$$A_t(z \to 0) \sim \mu + d\, z^2, \tag{1.3.0.21}$$

where μ is the chemical potential and d is proportional to the charge density. Just as for any other field, the gauge field tends to a particular value at the boundary which sources a vector current in the dual gauge theory, $J^\mu \sim \delta S_{\text{ren}}/\delta A_\mu^{(0)}$.

[15] If the time coordinate is Wick rotated, $t \to i\tau$, then the Euclidean global AdS metric is known as 'thermal' AdS. In this way we are consistent with the duality, with the conformal boundary matching the space where the gauge theory is defined. At the end, since we are dealing with static solutions, this does not make any difference.

Chapter 2
Numerical Stationary Solutions in General Relativity

In this chapter we review the basics for constructing stationary solutions (though we restrict to static ones) in numerical relativity, including both: a re-formulation of the Einstein's equations yielding to elliptic character equations, and hence a well-posed boundary value problem, and the numerical methods we implemented to solve them. We have chosen the Einstein-DeTurck approach due to its robustness and flexibility, and on the numerical side, the equations are discretized using pseudo-spectral methods.

Numerical relativity: Long-story short

In the previous chapter we have seen how wide the landscape of stationary vacuum black hole solutions is when $D > 4$. Finding those solutions means solving the non-linear coupled set of PDE's contained in Einstein's equations (0.0.0.1). However, even assuming stationarity, this task is extremely complicated. Over the years, different solution-generating techniques, such as the inverse scattering method [196, 197] or algebraic methods (see Ch. 9 of [290]) among others, have been employed successfully to find a remarkable amount of solutions, but only in $D = 5$ and under strong symmetry assumptions. The lack of effective techniques beyond five dimensions have prompted the study of approximate methods (matched asymptotic expansion [198–201], black-folds [202, 203], or more recently, the large-D expansion [204, 205] to cite a few), which are only reliable in their corresponding perturbative regimes, and by the time, the only complementary way to proceed is resorting to numerical methods [292, 293]. Originally, the field of numerical relativity was mainly concerned in dynamical situations, where initial data is evolved in time according to the Einstein's equations in $D = 4$, for making contact with the experimental side of the theory. Of course, uniqueness of vacuum black holes in $D = 4$ made not much appealing the development of numerical techniques intended for stationary (vacuum) configurations. It was with the fairly recent realization that uniqueness breaks down in $D > 4$ that this exploration path began. A throughout review can be found in [206]. See also Ch. 10 of [290].

A time-evolution or stationary numerical approach, starts requiring a system of equations with hyperbolic or elliptic character (see next section for a definition) re-

spectively, ensuring a well-posed problem. In the former case, these leads to an initial value problem with specified data on a Cauchy surface and having wave-like propagation on small scales. However, diffeomorphism invariance of GR implies that the equations are not hyperbolic (either elliptic for stationary geometries), and one needs to modify them appropriately. Some well-known and fruitful approaches yielding the desired hyperbolicity include the BBSN formalism [207, 208], the Z4 system [209] or a covariant conformal decomposition of this, known as CCZ4 [210].

Then, one possible way to construct stationary black hole solutions would be considering long-term time evolutions of an appropriate initial data, until the system reaches its final steady state. This is however clearly not convenient; at least for our purposes. Ignoring the complexity of the problem, the huge fine-tuning of initial data, and the large computational resources that this would require, many interesting stationary solutions in higher D are, or are thought to be, unstable and therefore they will never be the desired final stationary state.

Instead, stationary problems must be thought as boundary value problems where data (for example, Dirichlet, Newmann or a mix of both) is given on all boundaries. An early (non-covariant) formulation for cohomogeneity-2 boundary problems was based on the conformal gauge, which was employed successfully in a number of works, e.g. [14, 211–213]. A more recent point of view consists into solving the (fully covariant) Einstein-DeTurck equation introduced in [214] by Headrick, Kitchen and Wiseman, which works for any cohomogeneity and yields a more flexible and stable numeric scheme. This is the approach we have used in this thesis. Although originally this was intended for solving static problems, as the ones we do in this work, it was later shown that it could also be used to construct stationary solutions [215].

2.1 Einstein-DeTurck approach

To recast the Einstein's equations in a proper form to be tackled numerically, we need to see where the 'issues' come from. Either hyperbolic or elliptic equations have a well-developed theory, with formal theorems proving uniqueness of solutions.

However, an initial or boundary value problem for the Einstein's equations will not be well-posed. It cannot: general covariance implies that the differential operator associated to Einstein's equation is not invertible. In other words: a point in the space of solutions is not a point actually, it is an entire equivalence class of solutions since any other metric differing from the former by a diffeomorphism, gives an equivalent description of physics. It is the same solution. The general theory of PDE's does not allow to find the full equivalence class, but the coset by fixing a gauge. Actually, this happens in every theory with (local) gauge symmetry. In practice, to proceed we need to fix a gauge in such a way that when solving the equations in full we obtain one element in the desired class, say, the one that is consistent with our gauge choice. The point is that (0.0.0.1) codifies all the necessary information to determine the geometry, but not all the metric components. Indeed, we have $D(D+1)/2$ metric components

for $D(D-1)/2$[1] independent equations, resulting in an undetermined system. It is the price we have to pay for having a covariant formulation of the theory.

For stationary problems, the Einstein-DeTurck equation provide a way of fixing the gauge freedom, turning Einstein's equations into strongly elliptic ones, but preserving covariance. In the following sections we introduce the theoretical foundations of such re-formulation on which our studies are based on.

2.1.1 Hyperbolicity, ellipticity and DeTurck gauge fixing

Within the theory of PDE's [294, 295], the linear equations are classified depending on the value of the principal symbol $P(\zeta)$ on a given region $\Omega \subset M$ of the integration domain. This involves a combination of the functions accompanying the higher-order derivative terms, projected onto Fourier space with wave-vector ζ^μ.

In the case that the principal symbol has real, non-zero eigenvalues, with a single eigenvalue of opposite sign to the rest, the equation is said to be (weakly) hyperbolic. If it is additionally diagonalizable, the equation is strongly hyperbolic, which ensures well-posedness (at least for a certain amount of time, since many field configuration may eventually develop singularities). Hyperbolic equations may be traced back to the zeros of the principal symbol, $P(\zeta) = 0$, which defines the characteristic directions along which wave-like solutions propagate, thus providing a physical meaning.

On the other hand, if the principal symbol is invertible, which amounts to the condition $P(\zeta) \neq 0$, $\forall \zeta \neq 0$, and has real eigenvalues of the same sign, the differential operator is said to be (weakly) elliptic. The operator is strongly elliptic, and it thus yields a well-posed problem, if it is also diagonalizable. One may notice that the invertibility condition highlights the non-existence of characteristic directions, and thus the non-propagation of information. This just reflects the fact that elliptic problems cannot be thought as Cauchy problems, but as boundary value problems where data at the (spatial) boundaries of the integration domain must be prescribed.

These notions of hyperbolic and elliptic equations also hold for non-linear partial differential operators by considering the operator's linearization, which becomes a linear partial differential operator. Hence the principal symbol of the non-linear operator is the symbol of its linearization. According to this, to determine the character of the equation (0.0.0.1) we must linearize it, i.e. take $g_{\mu\nu} \to g_{\mu\nu} + \delta g_{\mu\nu}$, and expand to first order in the fluctuation. In vacuum, the result can be written as follows:

$$\Delta_{\mathrm{R}} \delta g_{\mu\nu} \equiv \Delta_{\mathrm{L}} \delta g_{\mu\nu} + \nabla_{(\mu} v_{\nu)} = 0, \tag{2.1.1.1}$$

where Δ_{L} is the quasi-linear second-order Lichnerowicz operator, defined as:

$$\Delta_{\mathrm{L}} \delta g_{\mu\nu} \equiv -\frac{1}{2}\nabla^2 \delta g_{\mu\nu} - R_{\mu\ \nu}^{\ \rho\ \sigma} \delta g_{\rho\sigma} + R_{(\mu}^{\ \ \ \sigma} \delta g_{\nu)\sigma}, \tag{2.1.1.2}$$

and

$$v_\nu \equiv \nabla_\sigma \delta g^\sigma_{\ \ \nu} - \frac{1}{2}\partial_\nu \delta g. \tag{2.1.1.3}$$

[1] Recall that the Einstein tensor must satisfy Bianchi, which provides D constraints.

The highest derivative terms appearing in $\Delta_{\rm R}$ define the principal symbol of the differential operator, P_g:

$$P_g\delta g_{\mu\nu} = \frac{1}{2}g^{\alpha\beta}\left(-\partial_\alpha\partial_\beta\delta g_{\mu\nu} + 2\partial_\alpha\partial_{(\mu}\delta g_{\nu)\beta} - \partial_\mu\partial_\nu\delta g_{\alpha\beta}\right). \tag{2.1.1.4}$$

The principal symbol of the operator is governed by short wavelength perturbations, which have large gradients and hence large second derivatives. Additionally, discarding other terms coming from the Ricci tensor, means that we only keep perturbations with wavelength much smaller than any curvature scale set by the metric $g_{\mu\nu}$, which can be taken as a fixed (constant) background.

The next step is to move on to Fourier space, replacing each derivative by a 1-form ζ_α,

$$P_g(\zeta)\delta g_{\mu\nu} = \frac{1}{2}g^{\alpha\beta}\left(-\zeta_\alpha\zeta_\beta\delta g_{\mu\nu} + 2\zeta_\alpha\zeta_{(\mu}\delta g_{\nu)\beta} - \zeta_\mu\zeta_\nu\delta g_{\alpha\beta}\right). \tag{2.1.1.5}$$

The linear operator $\Delta_{\rm R}$ (and hence the operator associated to $R_{\mu\nu} = 0$) is elliptic if and only if

$$P_g(\zeta)\delta g_{\mu\nu} \neq 0 \tag{2.1.1.6}$$

for all non-vanishing 1-forms on M and for every point $x \in \Omega$. Physically, the condition means that there is no short wavelength wave-like perturbations propagating in Ω.

From previous discussion we know that $\Delta_{\rm R}$ cannot be elliptic, which is related with gauge freedom of the equations. Indeed, recall that under an infinitesimal diffeomorphism with gauge parameter χ^μ, we have $\delta g_{\mu\nu} = 2\nabla_{(\mu}\chi_{\nu)}$, which reduces to $2\partial_{(\mu}\chi_{\nu)}$ if we assume that χ undergoes changes on very short wavelength scales. After Fourier transform it yields $P_g(\zeta)\delta g_{\mu\nu} = 0$, $\forall\zeta$. The equations can be elliptic though, on physical 'transverse' modes,

$$\partial_\nu\delta g^{\rm phy}{}^\nu{}_\mu - \frac{1}{2}\partial_\mu\delta g^{\rm phy} = 0, \tag{2.1.1.7}$$

where they are acted on by:

$$P_g\delta g^{\rm phy}_{\mu\nu} = -\frac{1}{2}g^{\alpha\beta}\partial_\alpha\partial_\beta\delta g^{\rm phy}_{\mu\nu}. \tag{2.1.1.8}$$

The latter is a manifestly elliptic/hyperbolic operator on a Riemannian/Lorentzian background. At the linear level analysis any short wavelength perturbation can be decomposed as a transverse physical part plus a longitudinal (pure gauge) part, and therefore it is now clear that the lack of strong ellipticity (or strong hyperbolicity) of the vacuum Einstein's equation is a direct consequence of gauge invariance.

It is key then to find a way to get rid of pure gauge modes. In the linear approximation, we know that the de Donder gauge does the job, so one possibility consists into de-linearize it. We have to find a one-form ξ_μ depending on the metric whose variation $\delta\xi_\mu$ about a constant background $g_{\mu\nu}$ equals to $\partial_\nu\delta g^\nu{}_\mu - \frac{1}{2}\partial_\mu\delta g$. Fixing ξ_μ will then project out the pure-gauge modes. The simplest choice is:

$$\xi_\mu = g^{\alpha\nu}\Big(\partial_\alpha g_{\nu\mu} - \frac{1}{2}\partial_\mu g_{\alpha\nu}\Big), \tag{2.1.1.9}$$

which can be rewritten as:

$$\xi^\mu = g^{\alpha\beta}\Gamma^\mu_{\alpha\beta} = -\nabla^2 x^\mu. \tag{2.1.1.10}$$

The x^μ, viewed as scalar functions on the manifold, is some coordinate chart. In particular, the gauge choice $\xi^\mu = -\nabla^2 x^\mu = 0$, is the usual harmonic gauge with harmonic coordinates x^μ, sometimes employed for time evolution in numerical GR. Indeed, in this gauge the principal symbol of the Einstein's operator becomes simply: $P_g \delta g_{\mu\nu} \sim -g^{\alpha\beta}\partial_\alpha\partial_\beta\delta g_{\mu\nu}$, which is manifestly hyperbolic and thus the system of equations can be solved as a Cauchy problem.

The main issue with this gauge choice is that, even though gauge invariance is broken (as desired), covariance is also broken since it refers to a particular coordinate system. This is aesthetically and practically not so desirable. To recast the problem in a covariant form one takes (2.1.1.9) and promotes the derivatives to covariant derivatives: $\partial \to \bar{\nabla}$, with respect to an arbitrary fixed background $\bar{g}_{\alpha\beta}$ on M. Then ξ^μ can be written as:

$$\xi^\mu = g^{\alpha\beta}\left(\Gamma^\mu_{\alpha\beta} - \bar{\Gamma}^\mu_{\alpha\beta}\right), \tag{2.1.1.11}$$

where $\bar{\Gamma}^\mu_{\alpha\beta}$ is the Levi-Civita connection for $\bar{g}_{\mu\nu}$, known as reference metric, and $\bar{\nabla}_\mu$ is the associated covariant derivative. Defined as the difference of two connections, ξ^μ is a globally covariant vector field and covariance is preserved. ξ^μ is known as the DeTurck vector [216]. A local gauge fixing of the form $\xi^\mu = 0$ accounts for the D local degrees of freedom associated to diffeomorphisms, and yields some sort of generalized harmonic coordinates, satisfying: $\nabla^2 x^\mu = -g^{\rho\sigma}\bar{\Gamma}^\mu_{\rho\sigma}$ [217, 218]. Still, the Einstein's equations are dynamical by nature and after a gauge choice is made the system is manifestly hyperbolic rather than elliptic. An elliptic system is only obtained once certain symmetries are imposed, namely staticity or stationarity.

2.1.2 Einstein-DeTurck equation

The Einstein-DeTurck approach uses the DeTurck fixing gauge term defined in (2.1.1.11) to modify the original Einstein's equations in a way that on stationary metrics the equations are elliptic. Then, instead of imposing the gauge-fixing conditions a priori, the proposition of this formulation is to solve $\xi^\mu = 0$ simultaneously with $R_{\mu\nu} = 0$. In this sense, the gauge is implemented a posteriori, once a solution to the modified equation has been found.

Following [214], this can be achieved solving the so-called Einstein-DeTurck equation:

$$R^{\mathrm{H}}_{\mu\nu} \equiv R_{\mu\nu} - \nabla_{(\mu}\xi_{\nu)} = 0, \tag{2.1.2.1}$$

with the DeTurck vector ξ^μ defined in (2.1.1.11), as the difference between the usual Levi-Civita connection of $g_{\mu\nu}$ and that one of the reference metric $\bar{g}_{\mu\nu}$. We are free to prescribe the latter up to a few restrictions that are discussed next.

In this formulation, rather than projecting out the pure-gauge modes (which would be the result of working in the space of gauge-fixed metrics), they have a kinetic term

putting them on the same footing with the physical transverse modes. This implies that instead of having the usual $D(D-1)/2$ independent Einstein's equations (with the Bianchi's supplying D gauge fixing conditions), now there are $D(D+1)/2$ equations to be solved. In turn, there are also more unknowns since no gauge conditions are imposed explicitly on the metric ansatz. The idea is to set up the boundary value problem, and this now includes a reference metric, in such a way that solutions to the Einstein-DeTurck equations are in the sector with $\xi^\mu = 0$, and hence they are Einstein. In particular, one can fine-tune the reference metric with the goal in mind of getting better numerical or/and computational efficiency.

The fundamental property of the equation (2.1.2.1) is that it has the desired principal symbol,

$$P_g^{\mathrm{H}} \delta g_{\mu\nu} = -\frac{1}{2} g^{\alpha\beta} \partial_\alpha \partial_\beta \delta g_{\mu\nu}. \tag{2.1.2.2}$$

As we mentioned earlier, this principal symbol corresponds to a strongly elliptic operator for Riemannian geometries (and thus for static black holes, since their Euclidean continuation is trivial), and to a strongly hyperbolic one in Lorentzian signature. The equations are also elliptic for Lorentzian stationary metrics whose Killing vector field is timelike everywhere asymptotically [215]. This includes the aforementioned static geometries, but also rotating ones and boosted black branes. The 'proof' relies on the rigidity theorems cited in Ch. 1, which apply to those geometries and motivate an appropriate (adapted) form for the metric. Only then it becomes clear the elliptic nature of the operator. Furthermore, the characteristic flexibility of this approach was made explicitly manifest when it was used to find solutions that lie outside of a stationary setting, where there is no guarantee that strong ellipticity applies. Ref. [219,220] found geometries with a single helical Killing vector field, and [221, 222] even succeeded in finding flowing solutions with non-Killing horizons.

A few comments more are in order. First, in Chapter 4 we consider solutions with a (negative) cosmological constant, but it enters in the equations of motion with no derivatives. Therefore the discussion presented in this chapter remains unchanged in the presence of a cosmological constant. The matter field content does not modify either the highest derivative structure of the Einstein's equations, but gauge fields in general have their own local gauge symmetry and will spoil the desired character of their equations of motion. In [223] an Einstein-DeTurck mimicking procedure for p-form gauge fields was introduced, but in practice it will be more convenient, when possible, fix the gauge of form fields algebraically, requiring for instance a vanishing gauge field at the black hole horizon if there is any.

Ricci solitons

An important issue in this re-formulation is under what circumstances solving the Einstein-DeTurck equation implies solving $R_{\mu\nu} = 0$ and $\xi^\mu = 0$ separately. Generically, solutions with $\xi^\mu \neq 0$ do exist and are called Ricci solitons, and thus we must be aware to avoid them when studying numerical solutions to Einstein's equations. Of course,

for a given problem we can always 'try and check', namely, we can solve the Einstein-DeTurck equation numerically and if ξ^μ is zero (up to numerical precision), the solution will be Einstein due to ellipticity, which guarantees local uniqueness of solutions. This means that Ricci solitons are distinguishable from Ricci-flat metrics, and therefore no confusion can arise.

Even though, it is desirable to have some knowledge about what to expect regarding the existence of Ricci solitons and luckily, there are now some established results that we now review. For simplicity, and because this is the relevant case in this thesis, we will only discuss the static case here [224], though it was recently extended to a much wider class of stationary geometries satisfying a t-ϕ symmetry in [225]. If one considers adapted coordinates (t, x^i) for the static problem, the DeTurck vector will only have non-vanishing spacelike components and therefore the norm $\phi = \xi^i \xi_i \geq 0$, and will saturate the equality only if $\xi_i = 0$, $\forall i$.

The idea is then to consider asymptotic boundary conditions compatible with $\xi_i = 0$ and to study under what circumstances this trivial DeTurck vector at the boundary remains zero as one integrates towards the interior. To this end, an equation of motion for the vector, or its norm, is needed. The contracted Bianchi identity can be combined with ∇^μ(2.1.2.1), and contracting the resulting expression with the vector ξ^μ, yields (in vacuum):

$$\nabla^2 \phi + \xi^i \partial_i \phi \geq 0. \tag{2.1.2.3}$$

Then if a Ricci-soliton exists, there must be a non-trivial solution picking up the positive sign in which case the equation admits a maximum principle. This states that if ϕ is non-constant then it must attain a maximum at the boundary of the manifold, ∂M, and additionally it has positive gradient at this maximum. Therefore, since $\phi > 0$ by construction, if $\phi = 0$ at the boundaries it must necessarily be zero everywhere.

In this sense, the prescribed data at the boundary constraints the existence of Ricci solitons. Ref. [224] found compatibility with $\xi_\mu = 0$ for Riemannian manifolds with boundaries and those that continue to static Lorentzian spacetimes which are asymptotically flat, KK, locally AdS or have extremal horizons, as long as the reference metric shares the same isometries and causal structure, and it thus approaches all the boundaries (see next section) in the same way as the desired solution. In other words, the reference metric need to be within the same metric family, but it does not need to solve the Einstein's equations. Notice that these include the two types of boundary conditions that we consider in the next chapters.

2.1.3 Boundary conditions

Strongly elliptic equations must necessarily be supplemented by boundary conditions to form a well-posed problem. The boundaries of the integration domain will include asymptotic boundaries and fictitious boundaries. See [215] for a throughout exposition.

Asymptotic boundaries lie at infinite proper distance with respect to other points, and prescribed conditions there require to preserve a certain structure set by the

problem itself. For instance, the Minkowski space, Anti-de Sitter, etc.; these use to be defined through Dirichlet-type conditions. According to previous discussion, the reference metric must be chosen in such a way that the same asymptotic behavior is also preserved, which is consistent with $\xi_\mu\big|_{\partial M} = 0$ at that boundary.

On the other hand, fictitious boundaries are at finite proper distance. Some examples include (non-extremal) Killing horizons or symmetry axis, which demand regularity of the metric. Regularity conditions depend on the precise metric ansatz that one considers, and will be discussed separately in the next chapters.

2.2 Numerics

We have seen how the DeTurck method works to re-formulate the Einstein's equations in vacuum as a (non-linear) elliptic boundary value problem to find stationary solutions, but now we need to choose a way of implementing the equations in our computer and an approach to solve them. In this thesis we have opted to discretize the equations using pseudo-spectral methods, and Newton's method[2] for integration.

We start by describing Newton-Raphson method applied to a generic system of PDE's and then we present the general scheme for solving non-linear boundary value problems. We overview the basics of pseudo-spectral methods, which involve an expansion on Chebyshev polynomials and non-uniformly distributed grid points. To better visualize the procedure, we consider a particular mathematical example in 2 spatial dimensions. Additionally, we also consider transfinite interpolation, a key tool for boundary problems with more than 4 natural boundaries as that of localized black holes studied in Chapter 3.

2.2.1 Newton-Raphson method

Newton-Raphson (NR) is a root-finding algorithm [296]. Although it was originally intended to solve equations of the form $f(x) = 0$, one can generalize it to a functional version of the method, which is suitable for solving generic systems of PDE's.

Given a set of differential equations for N functions $\{f_1(\mathbf{x}), \dots, f_N(\mathbf{x})\} \equiv [f]$ defined on $\mathbb{R}^n$ (i.e. $\mathbf{x} \in \mathbb{R}^n$), which we denote by $E_i(\mathbf{x}; [f], [\partial f], \dots) = 0$ $(i = 1, \dots, N)$, we can expand about a particular set $[f^k]$ to linear order:

$$E_i(\mathbf{x}; [f^k + \delta f], [\partial f^k + \partial \delta f], \dots) \simeq E_i(\mathbf{x}; [f^k], [\partial f^k], \dots) + \left.\frac{\delta E_i}{\delta f_j}\right|_{[f^k]} \delta f_j, \qquad (2.2.1.1)$$

where $\delta f_j = f_j - f_j^k$. The functional derivative in (2.2.1.1) is a differential operator

[2] Another integration method that has also been used successfully is based on the Ricci-flow equation [226]. This is a diffusion-type equation for evolving a one-parameter family of metrics, with the hope that the system will reach a fixed point that solves the Einstein's equations. Although this method is rather easier to implement, it is quite sensitive to the spectrum of negative modes of the desired solution, which will likely make flow the metric away from the desired fixed point.

actually, which acts on δf_j. This can be found using the standard definition,

$$\left.\frac{\delta E_i}{\delta f_j}\right|_{[f^k]} \delta f_j = \lim_{\varepsilon\to 0}\frac{1}{\varepsilon}\Big(E_i(\mathbf{x};[f^k+\varepsilon\delta f^k],[\partial f^k+\varepsilon\partial\delta f^k],\dots) - E_i(\mathbf{x};[f^k],[\partial f^k],\dots)\Big). \tag{2.2.1.2}$$

Providing a guess $[f^k]$ for the solution to the system of equations, we linearize the functionals E_i and we find a better solution $[f^{k+1}] = [f^k + \delta f]$ by setting $E_i(\mathbf{x};[f^k + \delta f],[\partial f^k + \partial\delta f],\dots) = 0$, obtaining:

$$\left.\frac{\delta E_i}{\delta f_j}\right|_{[f^k]} \delta f_j \simeq -E_i(\mathbf{x};[f^k],[\partial f^k],\dots). \tag{2.2.1.3}$$

In the most general case, we have moved from a non-linear to a linear set of equations (subject to the similarly linearized boundary conditions) which may be solved for the δf_j's using standard PDE methods. Then the corrected solution is given by $f_j^{k+1} = f_j^k + \delta f_j$. The process can be repeated by taking $[f^{k+1}]$ as the new guess to find $[f^{k+2}]$, and so on. The expression can be used iteratively until the desired accuracy ϵ is reached. In our case, the different functionals E_i are the different components of the Einstein-DeTurck equations we wish to solve, and the $[f]$ are the unknown functions appearing in the metric ansatz.

The method will converge quadratically, $\epsilon_{n+1} \sim \epsilon_n^2$, provided that the initial guess is close enough to the unknown zero. This intuitively means that the number of stable digits roughly at least doubles at each step. Such a rapid convergence makes NR a powerful method for finding roots. However, for a generic problem, there exist some difficulties. Many of them are directly related to the initial seed, after all, it sets up the point where the method starts to run.

The first one appears (almost) always in numerics: the convergence of the method. For NR we have said it is quadratic, but this depends strongly on the initial seed, which if is not chosen suitable may lead the iterations to a divergence, or on the opposite, to an infinite loop. In some cases, this can be controlled by introducing a parameter $\lambda \in \mathbb{R}$ into the iteration formula. Schematically,

$$f_{n+1} \sim f_n + \lambda\delta f, \tag{2.2.1.4}$$

with $\lambda \sim 10^{-1}$ or even smaller. The idea is to ensure that iterations keep within the basin of attraction. On the other hand, if the problem has more than one solution then exists more than one basin of attraction where the seed can be pushed. It may happen that the basin of attraction of one root dominates and then other ones may be difficult to find. Since NR only finds a single solution, one needs a separate, well-motivated guess to find other solutions. Physical intuition may be useful in this situation.

2.2.2 Pseudo-spectral methods

Pseudo-spectral methods are a collocation method [227,297–299]. The general strategy in collocation methods is to discretize the problem placing a number of points on the

domain we wish to solve it, x_i $(i = 1, \ldots, N)$, the so-called collocation points. The full set $\{x_i\}$ is referred as the grid, being N its dimension. Given the value of a function at these points $y_i = y(x_i)$, its derivatives at these points $y_i^{(n)}$ are approximated by differentiating an interpolating (usually polynomial or trigonometric) function. This operation reduces the derivative to a matrix operation

$$y_i^{(n)} \simeq D_{ij}^{(n)} y_j, \tag{2.2.2.1}$$

where $D_{ij}^{(n)}$ is the nth order differentiation $(N \times N)$ matrix, and allows us to discretize linear differential equations reducing them to standard linear algebra problems.

The various different collocation methods differ only in their choice of collocation points x_i, and the type of functions used for interpolation. For instance, kth finite differences uses a kth order degree polynomial for interpolation, on a uniform grid. This is a very local approach, where the derivative at a given grid point depends on the function value on $k + 1$ neighborhood points, allowing to evaluate k derivative at most.

For functions that are sufficiently differentiable, finite differences methods converge in a power-law fashion, with the power being equal to the order of the finite differencing. Putting the eye on computational efficiency, then the ideal would be to take the limit where the degree of the interpolating goes to infinity, which is the idea behind pseudo-spectral methods. Since one works with a finite set of collocation points, it is impossible to take this limit and the most we can opt is to use all available collocation points to form an interpolation function. This is, consider the interpolating $P(x)$ to be a single function, independent of i, such that $P(x_i) = y_i$, $\forall i$, and then approximate $y_i' = P'(x_i)$, $y_i'' = P''(x_i)$ and so on. This makes the approach non-local by nature. Now the derivative of the function at a single point depends on the values of the function at all points.

To be precise, in a pseudo-spectral approach one express the function $y(x)$ in terms of N Chebyshev functions:

$$y(x) \simeq \sum_{k=0}^{N} c_k T_k(x), \tag{2.2.2.2}$$

with $T_i(\cos(a)) = \cos(ia)$. In practice, when representing a function we do not make explicit use of this expression. We specify the function values on the grid $y_i = y(x_i)$ instead of the coefficients c_k, however, such expansion is used for computing the differentiation matrices on a given grid.

The kth Chebyshev polynomial can be written as a kth order polynomial in x, and therefore (2.2.2.2) provides an 'all-order' interpolation of the desired function. One may notice that (2.2.2.2) is nothing but a Fourier expansion in $a = \cos^{-1} x$, for which is well-known that the Fourier transforms c_k decay rapidly (provided that the function $y(x)$ is analytic, or smooth enough). This implies that the numerical error will scale as δx^{-N} as $N \to \infty$, being δx the largest grid distance, which is called exponential convergence. In comparison to finite differences, less grid points are needed to achieve

the same accuracy, which results in a better computational efficiency. One possible drawback is that it yields denser differentiation matrices since the method makes use of the function values on all grid points. It is not difficult to determine the specific form of the entries of the pseudo-spectral differentiation matrices on a Chebyshev grid of dimension N, but Mathematica has set by default a few single-line commands to define them for a bunch of well-stablished interpolation methods, pseudo-spectral among them.

Although an equidistant grid of (non-periodic) N points is appealing because its simplicity, it is not by far the best option for high order polynomials due to the Runge's phenomenon. This problem consists of the appearance of large oscillations in the interpolant (even if it is a smooth, non-oscillatory function) near the edges of an equidistant grid, and will spoil the computation. Instead, it has been shown that a pseudo-spectral approach on Chebyshev-Gauss-Lobatto (CGL, or Chebyshev for short) collocation points works extremely well in overcoming the Runge's phenomenon. If the integration domain is $x \in [x_-, x_+]$, these are given by

$$x_i = \frac{x_+ + x_-}{2} - \frac{x_+ - x_-}{2} \cos\left(\frac{i\pi}{N}\right), \tag{2.2.2.3}$$

$i = 0, \ldots, N$. This set of points has higher density towards the edges, x_- and x_+, which is precisely where the convergence problems arise in the uniform grid.

Practical example

The best way to visualize how NR works in conjunction with the pseudo-spectral methods is by considering a particular example. Let us consider the following non-linear PDE:

$$E[u, \partial_x^2 u, \partial_y^2 u; x, y] = \nabla^2 u(x, y) - e^{u(x,y)} = 0, \tag{2.2.2.4}$$

defined on the unit square $(x, y) \in [0, 1] \times [0, 1]$. We have four boundaries, and thus four boundary conditions to impose. Let us consider the Dirichlet boundary conditions $u(1, y) = 0 = u(x, 1)$, and Newman on the rest of the edges, $\partial_x u(0, y) = 0 = \partial_y u(x, 0)$. One can prove that this problem is well-posed, i.e. it has elliptic character. We will solve this boundary value problem using NR method.

Whatever the differential equation is, the main problem is to construct the matrix associated to the functional derivative of our non-linear differential operator. This calculation may be overly costly from a computational viewpoint, or numerically inaccurate. However, for boundary value problems as ours, the functional E is explicitly known and functional derivatives can be taken analytically and then implemented. For the boundary problem at hand, (2.2.1.3) is given by:

$$\left(\nabla^2 - e^u\right) \delta u = -(\nabla^2 u - e^u). \tag{2.2.2.5}$$

Now we have to discretize it. The solution data is located in a two-dimensional grid, $(x_i, y_j) \to u_{ij} = u(x_i, y_j)$, $(i = 1, \ldots, N_x$ and $j = 1, \ldots, N_y)$. We can just use the

Chebyshev grid (2.2.2.3) with $x_- = 0 = y_-$ and $x_+ = 1 = y_+$ in each direction independently, and take the cartesian product: $[0,1] \times [0,1]$.

The function u_{ij} can be though as a $N_x \times N_y$ matrix, however, it does not take long to realize that this is not the proper way to proceed. Instead of this, we consider a vector u_I derived from u_{ij}, in such a way that we deal with a partial derivative operator $\partial u_I \sim D_{IJ} u_J$. We have always considered the following convention for the ordering:

$$\begin{pmatrix} u_{11} & \dots & u_{1N_y} \\ \vdots & \ddots & \vdots \\ u_{N_x 1} & \dots & u_{N_x N_y} \end{pmatrix} \rightarrow \begin{pmatrix} u_{11} \\ \vdots \\ u_{1N_y} \\ \vdots \\ u_{N_x 1} \\ \vdots \\ u_{N_x N_y} \end{pmatrix}. \tag{2.2.2.6}$$

According to this, u_{11} is mapped to the component $I = 1$ of a vector, u_{12} to the component $I = 2$, etc. Then the first vector block corresponds to the function value at x_1, and so on. We can establish a precise relation between the pair of indices (i, j) and the index I through

$$I(i,j) = j + (i-1)N_y. \tag{2.2.2.7}$$

(This is just one possibility, the one that respects our ordering.) This index ranges from $I = 1$ to $I = N_x N_y$ and the vector u_I splits up into N_x vector blocks of length N_y. Then the corresponding differentiation matrices are found by using the Kronecker product. If $\mathbf{D}_x^{(n)}$ and $\mathbf{D}_y^{(n)}$ are the differentiation matrices on the grids x_i and y_i respectively, then the full derivatives $\mathbf{D}_X^{(n)}$ and $\mathbf{D}_Y^{(n)}$ acting on u_I are given by:

$$\mathbf{D}_X^{(n)} = \mathbf{D}_x^{(n)} \otimes \mathbf{I}_{N_y}, \qquad \mathbf{D}_Y^{(n)} = \mathbf{I}_{N_x} \otimes \mathbf{D}_y^{(n)}, \tag{2.2.2.8}$$

where $\mathbf{I}_k$ is the $k \times k$ identity matrix. Both matrices have dimension $N_x N_y \times N_x N_y$, as expected since they act on vectors with $N_x N_y$ components. Higher derivatives can be obtained as products of $\mathbf{D}_X^{(1)}$ and $\mathbf{D}_Y^{(1)}$, or by taking Kronecker products of higher derivative matrices.

Having defined how to place the function on the grid and how to take derivatives, we can proceed. (2.2.2.5) can be put in the form $M_{IJ}\delta u_J = -N_I$, with

$$\begin{aligned} M_{IJ} &= (\mathbf{D}_X^{(2)} + \mathbf{D}_Y^{(2)})_{IJ} - \mathbf{I}_{IJ} e^{u_I}, \\ N_I &= (\mathbf{D}_X^{(2)} + \mathbf{D}_Y^{(2)})_{IJ} u_J - e^{u_I}, \end{aligned} \tag{2.2.2.9}$$

at the interior points. Indeed, at the boundaries we are not interested in solving the equations. Instead we have to impose conditions that constrain the value of the solution according to the boundary values. This means that for some index values I, J, M_{IJ} need to be replaced by the linearized boundary conditions, whereas N_I need to be replaced for the boundary conditions themselves.

As an example, let us figure out how to implement $\partial_x u(0,y) = 0$, whose linearization is: $\partial_x \delta u(0,y) = -\partial_x u(0,y)$. This amounts to replace the first vector block (of length N_y) in N_I by the first vector block (of length N_y) of $(\mathbf{D}_X^{(1)} \cdot \mathbf{u})_I$. On the other hand, the matrix operator M_{IJ} splits up into N_x matrices of dimension $N_y \times N_x N_y$. Therefore we should replace the first matrix in there by the first matrix (of dimension $N_y \times N_x N_y$) in $(\mathbf{D}_X^{(1)})_{IJ}$. It is now straightforward to see what needs to be replaced to implement the boundary conditions on the other three edges.[3]

Once provided an initial seed u_I^0, we can evaluate (2.2.2.9) and solve for δu_J easily using LU decomposition, or any other standard algorithm. In our case, at each step of the iterative process the linear system is solved using the former method, implemented by subroutine `LinearSolve` in Mathematica. An improved solution will be given by: $u_I^1 = u_I^0 + \delta u_I^0$. The process can be repeated as necessary until convergence (or failure; hopefully not!) according to a defined tolerance ϵ:

$$\max_{0 \leq x_k, y_k \leq 1} |u_I^{n+1} - u_I^n| < \epsilon. \tag{2.2.2.10}$$

The construction outlined here implements the method for one single equation. If there were more equations, say, p equations for p unknowns, we should consider the discrete version of the full system. In higher dimensions everything follows as before, though in this thesis we will restrict to problems with co-dimension 2.

An important step in order to construct accurate numerical solutions is considering various subdomains, a practice that lies under the name of 'patching'. In Fig. 2.2 we display the numerical solution of the boundary problem (2.2.2.4) on a patched grid, that we have found using the techniques outlined below.

Patching

If the solution to a boundary value problem is smooth, a grid formed by one single patch to cover the whole integration domain may be enough to obtain an accurate solution, but at the moment that a solution is not that well-behaved, due to the presence of large gradients for instance, more resolution is needed to keep the accuracy in order. Typically, the singular behavior is localized in some region of the whole computational domain, and in these conditions it is convenient to use various subdomains, or patches, with different resolutions. This gives the flexibility of increasing the number of grid points just where it is necessary, instead of increasing the whole grid which would be computationally more expensive.

For example, taking the cartesian product of two 1-dimensional grids formed by two set of points that cover the domain well, results in a rectangular grid with $(2 \times 2 =)$ 4 patches. This is the most trivial example of patching. Patching implementations

[3] Notice that the grid corners belong to two boundaries. In case that both boundaries share the same condition this does not suppose any difference. But if the conditions are different, we have to make a choice and establish if the corner belongs to one or the other edge.

depend on whether the different sub-domains overlap or not. If they do, an interpolation function is used on those regions to ensure continuity. On the other hand, non-overlapping patches meet only on patch boundaries. In this thesis we only considered this second option. Then in addition to the outer boundaries, we will also have inner boundaries where continuity of the function and its normal derivative must be imposed. The full matrix M_{IJ} associated with the linear operator will have a diagonal block structure, with many blocks as subdomains, and with off-diagonal blocks adjacent to any pair used to impose the junction conditions.

Now we want to go a step further and consider grids which are covered with subdomains that have non-trivial shape. The main interest in doing that is that there exist many boundary problems that involve more than four natural boundaries, whereas rectangular grids (if the problem depends on just two coordinates) only have four. Some examples that arise in GR are the localized black holes that we find in next chapter, black rings, domain walls or plasma balls in AdS, among others. One way to tackle these problems is dividing the physical domain, i.e. where the problem is originally defined, into different non-rectangular patches. Mapping each one to a square grid, numerics are then easily carried out.

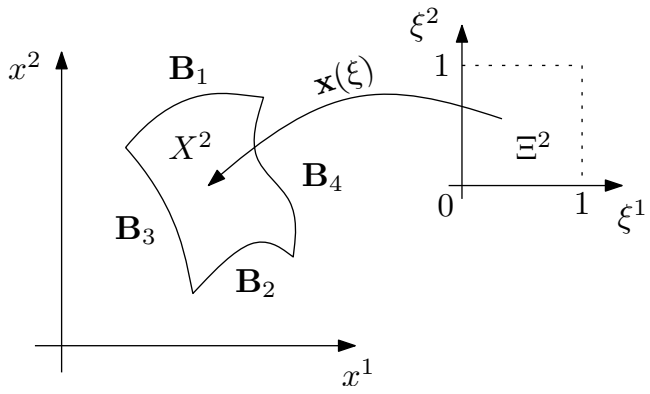

Fig. 2.1: *Transfinite interpolation.*

This lie much on the idea of a coordinate transformation. The grid points of the physical grid (or part of this) in a 2-dimensional region $X^2 \subset \mathbb{R}^2$ are defined by mapping the nodes of a rectangular reference grid Ξ^2, known as the logic or computational domain, through a certain smooth coordinate transformation: $\mathbf{x}(\xi) : \Xi^2 \to X^2$, with $\mathbf{x} = (x^1, x^2)$ and $\xi = (\xi^1, \xi^2)$. See Fig. 2.1. One way to generate such a mapping given the parametric boundaries $\mathbf{B}_1, \ldots, \mathbf{B}_4$ is by using algebraic methods. Consider a warped rectangular region in the physical space with coordinates x^1 and x^2, whose parametric equations for its four deformed boundaries in terms of the logic coordinates ξ^1 and ξ^2 (which take values in the unit interval $[0, 1]$), are

$$\begin{aligned} \mathbf{B}_1(\xi^1) &= (x_1(\xi^1), y_1(\xi^1)), \\ \mathbf{B}_2(\xi^1) &= (x_3(\xi^1), y_3(\xi^1)), \\ \mathbf{B}_3(\xi^2) &= (x_3(\xi^2), y_3(\xi^2)), \\ \mathbf{B}_4(\xi^2) &= (x_4(\xi^2), y_4(\xi^2)), \end{aligned} \tag{2.2.2.11}$$

according to Fig. 2.1. The various functions $x_i(\xi^a)$, $y_i(\xi^a)$ are any functions of our choosing such that the parametrized curves satisfy the following consistency conditions on the corners: $\mathbf{B}_1(0) = \mathbf{B}_3(1)$, $\mathbf{B}_1(1) = \mathbf{B}_4(1)$, $\mathbf{B}_2(0) = \mathbf{B}_3(0)$ and $\mathbf{B}_2(1) = \mathbf{B}_4(0)$. These conditions are all that is necessary to generate a coordinate map. The coordinate

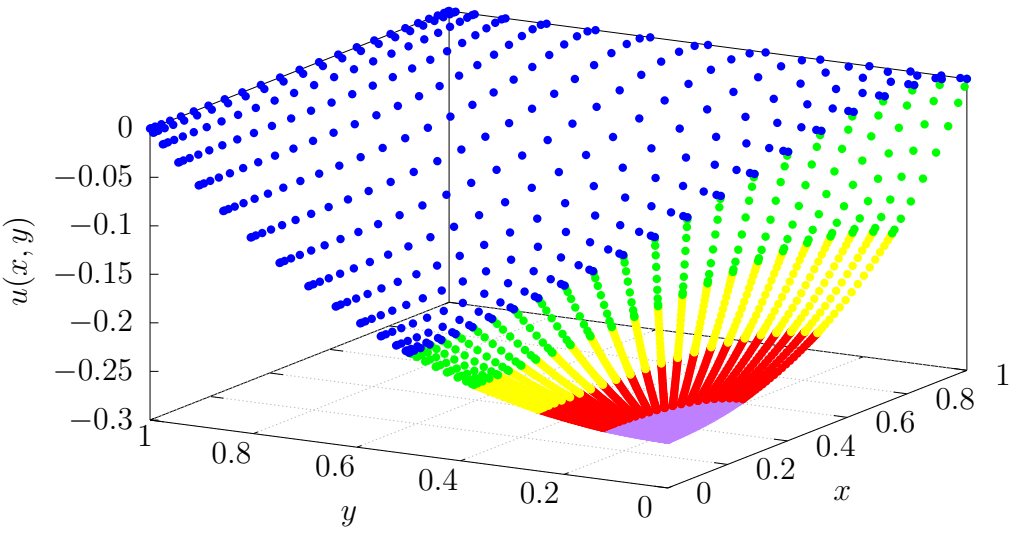

Fig. 2.2: *Numerical solution to the boundary problem (2.2.2.4) using transfinite interpolation. The physical space is divided in two different regions: one 'ellipsoidal' patch (which in turn has been divided in $n = 4$ regions) plus one 'trapezoidal' patch. The grid resolution $N_{\xi^1} \times N_{\xi^2}$ in each patch is, from the bottom up, 40×25, 30×25, 20×25, 10×25 and 25×15. We have started with trivial initial seed. Convergence is reached for $\epsilon < 10^{-12}$ after 4 iterations.*

transformation $\mathbf{x}(\xi)$ is then given by the transfinite interpolation formula [300, 301]:

$$\begin{aligned}\mathbf{x}(\xi) = {} & (1-\xi^1)\mathbf{B}_3(\xi^2) + \xi^1\mathbf{B}_4(\xi^2) + (1-\xi^2)\mathbf{B}_1(\xi^1) + \xi^2\mathbf{B}_2(\xi^1) \\ & - \Big(\xi^1\xi^2\mathbf{B}_4(1) + \xi^2(1-\xi^1)\mathbf{B}_3(1) + \xi^1(1-\xi^2)\mathbf{B}_4(0) \\ & + (1-\xi^1)(1-\xi^2)\mathbf{B}_3(0)\Big).\end{aligned} \tag{2.2.2.12}$$

The equations are written in the physical space X^2, and grid points and differentiation matrices are mapped from each logic space onto the physical space via the chain rule and the inverse function theorem applied to (2.2.2.12).

Further considerations to get more accurate numerical results include mesh-refinement techniques. These are specially necessary when the singular behavior of a given numerical function is very localized at some region of the integration domain. The critical black holes that we construct in next chapters are an example where this occurs. In particular, we consider a trivial generalization of the mesh-refinement formula presented in [228], which has enough flexibility to be adapted on the various cases that we encounter along this work. Given a set of grid points X distributed along the interval $[A, B]$, we can generate the new set $\tilde{X} = \mathrm{mesh}(X; A, B, C)$, with

$$\mathrm{mesh}(X; A, B, \chi) = A + \frac{B-A}{\sinh\chi}\sinh\left(\chi\frac{X-A}{B-A}\right), \tag{2.2.2.13}$$

which are densely distributed towards A. The parameter χ controls how densely, and typically, $1 < \chi < 10$. One does not want to be interested in using large values of χ, since the opposite region, say, the grid points close to B, will have a poor density and the final outcome may be counterproductive.

2.2.3 Convergence tests

Any numerical approach always yields errors due to the finite precision of our computers, and also because the finite size of the grid. A naive 'measure' of the error may consist into evaluate the equations on the numerical solutions, and inspect how close to zero they are. Even if this quantity is small, sometimes numerics conspire against us and we need other ways to check the validity of the solutions. Additionally, we deal with tensor equations, and it only make sense to evaluate coordinate independent quantities, which gives us the assurance that that zero is not a coordinate artifact.

In the continuum limit where the number of points is large, the error is expected to reduce to zero. How fast or low depends on the numerical scheme one uses. In the case of pseudo-spectral methods, these imply exponential convergence if the solution is smooth enough. However, if the solution only has a finite number of derivatives, the convergence rate will be a power law, which depends on the number of derivatives that the continuum solution has. Numerical solutions of a certain system of equations which represent a good approximation to the real solutions should reflect such a behavior in the error. To this end, convergence tests are usually carried out. In a converge tests one monitors the numerical error as a function of the grid resolution. Typically one choose one or two solutions that are a good representative of the whole branch of solutions that is found (in case there is a branch), and interpolates them at different resolutions. Each interpolated solution is then filtered through NR loop to obtain the actual solution at the given resolution. In any case, the behavior always flattens out for some critical N^*, precisely due to finite precision, but for $N < N^*$ one can check whether the behavior is as expected or not.

It is important to highlight that monitoring the numerical error is key to decide when more resolution is needed, or directly, when an ansatz needs to be modified to better suit the real solution. In practice, one needs to distinguish whether a bigger error occurs because of the form of the solution itself, due to the appearance of singular behavior for instance, or due to the anomalous behavior of some physical quantity. In any case, a simple plot of the solution should be enough to get us out of doubt.

The Einstein-DeTurck equation has a very valuable quantity that can be monitored and which is computationally cheaper to evaluate than the full tensor equations: the DeTurck vector ξ_M. This must vanish on the whole integration domain for Einstein solutions and therefore it provides a reasonable estimate of the numerical error. In the studies of chapters 3 and 4, we have performed convergence tests using the norm of the DeTurck vector and their non-zero components, though the latter, being coordinate dependent, are less reliable.

Chapter 3
Critical Kaluza-Klein Black Holes in D = 10

This chapter is based on [1], authored in collaboration with P. Figueras. The numerical code and posterior data analysis was written and carried out by the author of this thesis and the calculations were verified by P. Figueras.

3.1 Introduction and results

In $D = 4$ spacetime dimensions, stationary asymptotically flat black hole solutions of the Einstein equation in vacuum of a given mass have spherical topology, are presumably unique and all the evidence suggests that they are dynamically stable. However, in $D > 4$ these properties change radically. The physics of black objects turns out to be much richer, allowing for non-spherical topologies, instabilities and non-uniqueness (and thus phase transitions). Black holes are fundamental objects in general relativity. In recent years the study of such objects in non-astrophysical settings has received much attention due to the intrinsic interest in understanding fundamental aspects of gravity as described by GR (see [98] for a review), and also because of the connections to string theory and the gauge/gravity duality [162–166]. In the latter context, it is natural to consider spacetimes that are asymptotic to $M_d \times N_n$, where M_d is d-dimensional Minkowski or Anti-de Sitter space and N_n is an n-dimensional compact manifold so that the total number of spacetime dimensions is $D = d + n > 4$.

One of the most extensively studied models in this setting is that of $M_d = \text{Mink}_d$ and $N_1 = S^1$, a circle of length L. Since the compact dimension is flat, it is trivial to write down a black hole solution that is uniformly wrapped along the compact dimension: This is just given by the $(D-1)$-dimensional Schwarzschild solution times a (compact) flat direction, $\text{Schw}_{D-1} \times S^1$. Such a higher dimensional black hole is known as the uniform black string (UBS). In [130], Gregory and Laflamme (GL) famously showed that thin enough black strings are unstable under linear gravitational perturbations with a non-trivial dependence along the S^1-direction.[1] Determining the

[1] More precisely, the condition for the existence of a linear instability is $r_0/L \lesssim \mathcal{O}(1)$, where r_0 is the mass parameter of the parent Schw_{D-1} solution and L is the asymptotic length of the circle.

endpoint of such an instability has been the subject of intense studies during the past few years.

At the onset of the instability, the linear GL mode is time-independent (i.e. a zero mode) and can be continued to the non-linear regime. This indicates that there exists a new branch of black strings which are non-uniform in the compact direction and are thus known as non-uniform black strings (NUBS). NUBS were first constructed perturbatively in $D = 5$ by [13], subsequently constructed fully non-linearly in various spacetime dimensions using numerical methods [14, 157, 214, 229–232] and, more recently, using the large-D expansion [233]. It turns out that in $D < D^* = 13(.5)$, NUBS have less entropy than UBS with the same mass and hence they cannot be the endpoint of the GL instability [234, 235]. In fact, based on entropic arguments, [130] conjectured that unstable UBS would evolve into an array of localized black holes through a dynamical topology change transition; the latter can only happen through a singularity and hence the evolution of the GL instability of black strings could potentially constitute a counter-example of the weak cosmic censorship conjecture [62–64] around such spacetimes. This scenario was confirmed in Ref. [137], using numerical relativity techniques.[2] On the other hand, for $D > D^*$, NUBS can be dynamically stable and hence be the endpoint of the GL instability, as [138, 233] confirmed.

Apart from UBS and NUBS, spaces that are asymptotically $\text{Mink}_d \times S^1$ also admit static black hole solutions that are localized on the S^1. These localized black holes (LOC) have been constructed numerically [17, 18, 22, 214] and perturbatively in the limit in which the black holes are small compared to L [198–201, 236, 237].

Motivated by geometrical considerations, [21] conjectured that the NUBS and LOC branches should merge at a topology changing critical solution governed by a Ricci-flat double-cone. This conjecture was tested from the black string side in $D = 6$ [238], and later in various dimensions in [231]. However, the most non-uniform black strings in these early constructions were still too far from the critical regime to provide conclusive results (see however Ref. [230]). Only recently, Kalisch et al. [22, 157], in an impressive numerical construction, have managed to obtain NUBS and LOC in $D = 5, 6$ extremely close to the critical point, confirming the double-cone predictions to an unprecedented level of detail.

The goal of the present work is to construct NUBS and LOC in $D = 10$ very close to the critical point, where these branches of black holes merge. Critical solutions have only been previously constructed in $D = 5, 6$ [22, 157]; for higher values of D, gravity becomes more localized near the black hole horizon, which makes the numerical construction more challenging, especially very close to the critical point. Note that [161] previously constructed both NUBS and LOC in $D = 10$, but their solutions were very far from the critical regime since the aim of that paper was different (see below).

[2] Recall that this final fate is not exclusive of UBS and black holes with compact extra dimensions. Fully non-linear time evolutions of analogous instabilities in asymptotically flat black rings or ultra-spinning Myers-Perry black holes spacetimes, similarly lead to violations of the weak cosmic censorship conjecture [145, 148, 153].

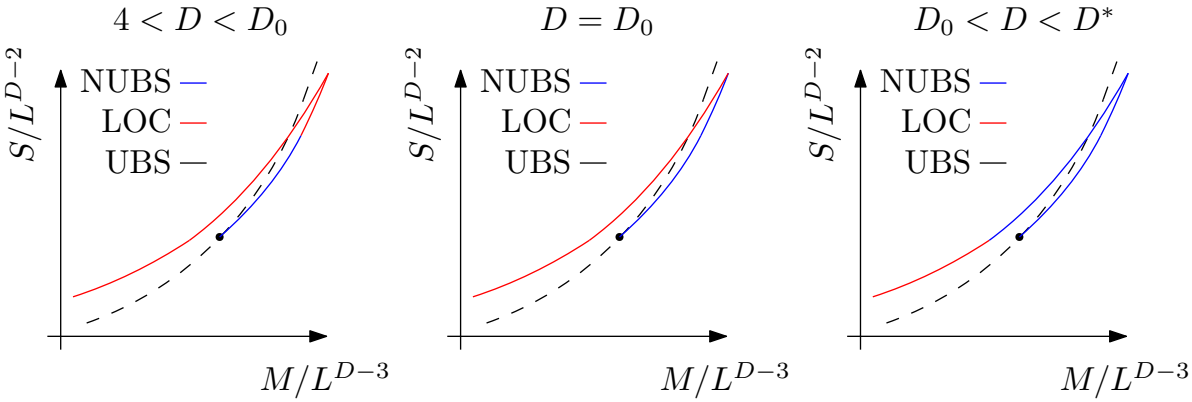

Fig. 3.1: *Schematic phase diagrams in the microcanonical ensemble for various D's. Here $D_0 = 10$ is the critical dimension of the double-cone geometry [21] and $D^* = 13(.5)$ is the critical dimension in the microcanonical ensemble [234].*

At the critical dimension D^* the dynamical stability of weakly NUBS changes from being unstable for $D < D^*$ to being stable for $D > D^*$. However, for $D = 12, 13$ [231] found that NUBS with a sufficiently large non-uniformity can also be dynamically stable.[3] This paper showed that there exists a turning point, i.e. a maximum of the mass/area, along the NUBS branch where the stability properties of the solutions change. On the other hand, in $D = 5, 6$ such a turning point is present along the LOC branch. In $D = 10$, as we move along both the LOC and the NUBS branches and approach the critical solution from both sides, we do not find any turning points on either of the branches. Therefore, the simplest picture that emerges from our work is that, sufficiently far from the critical solution, in $D < 10$ there should exist a turning point along the LOC branch, in $D > 10$ the turning point occurs along the NUBS, and in $D = 10$ there are no turning points at all. See Fig. 3.1. Recently, [233] confirmed the existence turning points in the phase diagram of NUBS in $D < 14$ using the large-D expansion, but the reliability of their approach breaks down at around $D \approx 9$. Notice, however, that the methods of [233] did not allow them to study critical solutions in detail and therefore our results complement theirs.

Our numerical data suggests that in $D = 10$ the merger happens precisely at a cusp in the phase diagram. The study of the critical geometry in [21] showed that $D = 10$ is the critical dimension of the cone geometry that governs the topology change. For $D < 10$, the approach of physical quantities to their critical values is controlled by a (dimension-dependent) power law with infinitely many oscillations (i.e. turning points); this behavior has been beautifully confirmed in [22] for $D = 5, 6$. On the other hand, for $D > 10$ the approach to the critical point should be given by two independent power laws, with no oscillations. $D = 10$ is the marginal case and the approach to the critical point should be controlled by a power law with a logarithmic correction. In

[3] It is plausible that stable NUBS also exist in $D = 11$ for larger values of the non-uniformity parameter than in [231].

this study we confirm this in $D = 10$.

In this chapter we also compute the spectrum of negative modes of the Lichnerowicz operator, Δ_L, around the LOC and NUBS branches, restricted to modes that preserve the isometries of the background. Just as in [214, 231], we find that NUBS posses two negative modes: one is continuously connected (as the non-uniformity parameter goes to zero) to the negative mode of the parent Schwarzschild black hole [154]. This mode diverges as the NUBS approach the critical solution. The other negative mode is the continuation of the GL zero mode to non-zero values of the non-uniformity parameter and our data suggests that it tends to a finite value at the critical solution. On the other hand, LOC have a single negative mode throughout the branch and it approaches the same finite value as the NUBS at the critical solution. See Fig. 3.11. Note that at an extremum of the temperature one can have zero modes corresponding to variations of the parameters of the solution that respect the boundary conditions (i.e. preserve the temperature). We do not find any evidence for new zero modes, which is consistent with the absence of extrema of the temperature along either branch of solutions.

Another motivation for the present work comes from the gauge/gravity duality. The best well-understood example of this correspondence is between maximally supersymmetric Yang-Mills (SYM) theory in $p+1$ dimensions and gauge group SU(N), and Type IIA (even p) or Type IIB (odd p) superstring theory containing N coincident Dp-branes in the decoupling limit. For $p = 1$ the duality is between 2-dimensional SU(N) SYM theory and type IIA or IIB string theory in the presence of D0- or D1-branes respectively [239]. At large N, strong coupling and finite temperature, the gauge theory is described by black hole solutions with D0- or D1-charge in the supergravity approximation, depending on the temperature (type IIA at low temperatures and type IIB at high temperatures respectively). In this chapter we are interested in vacuum black hole solutions of the Einstein equation in ten spacetime dimensions, one of which is compactified on a circle of length L. After a series of standard U-dualities [161, 240–242], these vacuum black holes can be given D0- or D1-brane charges.

According to the AdS/CFT correspondence, the black hole phase structure should be reproduced by the thermal phases of SYM on a circle at strong coupling and large N. Lattice simulations of SYM on a torus, with one of the circles being the thermal circle and with periodic boundary conditions for the fermions on the other spatial circle, have been performed. Most of the previous works in the past have focused on the $p = 0$ SYM quantum mechanics and agreement with the gravity predictions has been confirmed [243–256]. The case $p = 1$ has received less attention in the past [23], until the recent of work of [24]. This paper predicted the temperature at which a first order phase transition occurs from lattice simulations, in a regime where the latter should overlap with the supergravity calculations. The latter was only recently computed in [161] and found very good agreement with the lattice result. In this chapter, as a by-product of our calculations, we recompute the value of the phase transition temperature (or energy, in the canonical ensemble); the values that we obtain are $t_{\rm crit} = 1.09257\, t_{\rm GL}$ and $\varepsilon_{\rm crit} = 1.24181\, \varepsilon_{\rm GL}$ for the temperature and energy

at the phase transition measured with respect to the GL point. Our values differ with those found in [161] by less than a 0.25%. In addition, we have been able to locate the merger between the non-uniform and localized phases.

Organization of this chapter

The rest of this chapter is organized as follows. In §3.2.1 we start by reviewing some general aspects of black holes in Kaluza-Klein spaces. In subsections 3.2.2 and 3.2.3 we present our numerical construction of NUBS and LOC, respectively. In §3.3 we present our results. §3.3.1 contains the phase diagrams in the microcanonical and canonical ensembles, in §3.3.2 we consider the horizon geometry and in §3.3.3 we study in the detail the critical behavior of NUBS and LOC near the critical point and compare it with the predictions of the double-cone model. §3.3.4 is devoted to the computation of the spectrum of negative modes of the Lichnerowicz operator around the NUBS and LOC. §3.4 contains the results for the phase diagram of the supergravity solutions with D0-charge. We close the chapter with a discussion in §4.5.

Some technical details are relegated to the Appendices. In appendix 3.A we give more details about the integration domain that we have used to construct the localized black holes and in appendix 3.B we present some convergence tests. The mapping from neutral solutions to charged ones is presented in detail in appendix 3.C.

3.2 Black objects in Kaluza-Klein theory

Consider vacuum Einstein's gravity in $D = 10$ spacetime dimensions with Kaluza-Klein (KK) asymptotic boundary conditions, i.e. $\text{Mink}_9 \times S^1$. For static spacetimes, this theory contains three different families of static black holes, namely, UBS, NUBS and LOC. After fixing the overall scale by fixing the length of the asymptotic S^1, these three different types of black holes can be parametrized by the temperature and one may distinguish them by the topology of the horizon and the isometries. Whilst UBS are translationally invariant along the S^1 and are known explicitly, for NUBS and LOC the translation invariance along the S^1 is broken and they have to be constructed numerically (or pertubatively). In this section we explain our numerical construction of such solutions. Since we are interested in studying the thermal phases, we will be working with the Euclidean form of the solutions where the Euclidean time τ is periodic, $\tau \sim \tau + \beta$, with β being the inverse temperature.[4]

3.2.1 Generalities and uniform black strings

In this chapter we are interested in Einstein metrics that asymptote to the flat Euclidean metric, where one of the directions corresponds the Euclidean time τ, times

[4]Note that since we are considering static spacetimes, we can change to Lorentzian signature by a trivial change of coordinates $\tau \to \mathrm{i}\, t$.

a KK circle of length L. As usual, the Euclidean time τ is compact and has period β. Ultimately we will consider ten dimensional spaces but for now we shall keep the total number of spacetime dimensions D general. Moreover, we will only consider spacetimes that preserve an $\mathrm{SO}(D-2)$ subgroup of the full rotation group of the flat Euclidean metric in $D-1$ dimensions. Therefore the asymptotic isometry group of the spaces that we shall consider is $\mathrm{U}(1)_\beta\times\mathrm{SO}(D-2)\times\mathrm{U}(1)_L$, which is made explicit in the asymptotic form of the flat metric on the product space $S^1_\beta\times\mathbb{R}^{D-2}\times S^1_L$,

$$\mathrm{d}s^2=\mathrm{d}\tau^2+\mathrm{d}r^2+r^2\,\mathrm{d}\Omega^2_{D-3}+\mathrm{d}y^2\,, \tag{3.2.1.1}$$

with $\tau\sim\tau+\beta$ and $y\sim y+L$. For more general static metrics, the asymptotic behavior of the components

$$g_{\tau\tau}\simeq 1-\frac{C_\tau}{r^{D-4}}\,,\qquad g_{yy}\simeq 1+\frac{C_y}{r^{D-4}}\,, \tag{3.2.1.2}$$

is related to the asymptotic charges, the mass and tension, of the solution [257–259]:[5]

$$M=\frac{\Omega_{D-3}L}{16\pi}\big((D-3)C_\tau-C_y\big),\qquad \mathcal{T}=\frac{\Omega_{D-3}}{16\pi}\big(C_\tau-(D-3)C_y\big). \tag{3.2.1.3}$$

From these quantities one can define the relative tension $n=\mathcal{T}L/M$, which is bounded: $0\leq n\leq D-3$. Here the upper bound follows from the Strong Energy Condition which imposes that gravity is not repulsive asymptotically, while the lower bound was found in [260,261]. In addition to these charges, NUBS and LOC can be characterized using their own geometric quantities which are discussed in §3.3.2. All neutral KK solutions with a single connected horizon have temperature $T=\kappa/(2\pi)$ and entropy $S=A_{\mathrm{H}}/4$. They satisfy the 1st law of thermodynamics and the Smarr's relation,

$$\mathrm{d}M=T\mathrm{d}S+\mathcal{T}\mathrm{d}L,\qquad (D-3-n)M=(D-2)TS. \tag{3.2.1.4}$$

From the point of view of the numerics, the latter may be used as a consistency check, since the entropy and the mass are obtained from the metric. The free energy is $F=M-TS$. Note that the 1st law of thermodynamics (3.2.1.4) clarifies the physical meaning of $\mathcal{T}$: it is a force per unit of length, i.e. tension, that wants to stretch the string along the compact direction.

Uniform black strings are known explicitly for all values of D: The metric is $\mathrm{Schw}^{\mathrm{E}}_{D-1}\times S^1_L$ (E stands for Euclidean), where the Schwarzschild metric is written in (1.2.0.1) (in Lorentzian signature and in D dimensions). The parameter r_0 labels each solution and it is directly related to the physical quantities:

$$\begin{aligned}\kappa&=\frac{D-4}{2r_0}, & M&=\frac{\Omega_{D-3}L}{16\pi}(D-3)r_0^{D-4},\\ A_{\mathrm{H}}&=Lr_0^{D-3}\Omega_{D-3}, & \mathcal{T}&=\frac{\Omega_{D-3}}{16\pi}r_0^{D-4}.\end{aligned} \tag{3.2.1.5}$$

[5] Throughout, we use units of $G_D=1$, where G_D is the Newton's constant in D spacetime dimensions.

(Notice that the uniform black string has $C_\tau = r_0^{D-4}$, $C_y = 0$ and constant relative tension $n = (D-3)^{-1}$.) Finally, recall that the topology of the horizon is $S^{D-3} \times S^1$.

Gregory and Laflamme [130] famously discovered that thin enough UBS, i.e. $r_0/L \lesssim \mathcal{O}(1)$, are dynamically unstable to clumping along the compact direction. See §1.2 of Chapter 1 for a detailed exposition. More precisely, for fixed L there is a critical value $r_0^{\rm GL}$ below which there exist regular (linear) perturbations that grow exponentially with time and that break the translational invariance along the S^1; at precisely this critical value, the perturbations are time-independent thus signaling the existence of a linear solution of the Einstein equation which is not uniform along the S^1. This linear solution can be continued into the fully non-linear regime, giving rise to the NUBS. For $D = 10$, the critical value of the horizon radius at the onset of the GL instability is given by:

$$r_0^{\rm GL} = 0.36671(3)L. \tag{3.2.1.6}$$

Our aim in this work is to numerically construct vacuum NUBS and LOC solutions in $D = 10$. In practice, we will treat the different metrics as smooth Riemannian manifolds with a $\mathrm{U}(1)_\beta$ Killing vector that vanishes at the horizon and solve the Einstein vacuum equation, $R_{\mu\nu} = 0$, subject to certain regularity and asymptotic boundary conditions. As is we discussed in Ch. 2, due to the underlying gauge invariance of the theory, this equation does not yield a well-posed boundary value problem. Instead, we solve the Einstein-DeTurck equation which is manifestly elliptic.

In our numerical implementation the equations are always discretized using pseudo-spectral methods on a Chebyshev grid and we solve them by an iterative Newton-Raphson method. All this has been addressed in Ch. 2, and we refer the reader to that chapter for any clarification.

3.2.2 Numerical construction of non-uniform black strings

NUBS wrap the KK circle, and, for regular solutions, the horizon S^{D-3} is finite everywhere. This implies that with our symmetry assumptions, the integration domain has the following effective boundaries: the horizon, asymptotic infinity and the periodic boundary. Due to the symmetry of the first GL harmonic, NUBS have a $\mathbb{Z}_2$-symmetry and then one has an additional mirror boundary. Hence, a single coordinate patch is enough to cover the whole computational domain. In practice, to numerically construct highly non-uniform black strings near the critical point it is convenient to use more than one patch to get enough resolution in the regions of interest, i.e. where the metric functions behave in a singular fashion.

To find NUBS we consider the following ansatz for the metric:

$$\begin{aligned} \mathrm{d}s^2 = {} & 4\, r_0^2\, \Delta^2 \left(x^2 e^{Q_1}\, \mathrm{d}\tau^2 + \frac{e^{Q_2}}{f(x)^{2(D-3)}}\, \mathrm{d}x^2 \right) + e^{Q_3}\, \mathrm{d}y^2 \\ & + 2\, Q_4\, \mathrm{d}x\, \mathrm{d}y + \frac{r_0^2\, e^{Q_5}}{f(x)^2}\, \mathrm{d}\Omega_{D-3}^2, \end{aligned} \tag{3.2.2.1}$$

with $\Delta = (D-4)^{-1}$, $f(x) = (1-x^2)^{\Delta}$, and unknowns $Q \equiv \{Q_1, Q_2, Q_3, Q_4, Q_5\}(x, y)$. For $Q = 0$, this ansatz reduces to the UBS in D dimensions written in terms of the compact radial coordinate x,

$$x^2(r) = 1 - \left(\frac{r_0}{r}\right)^{D-4}. \tag{3.2.2.2}$$

The UBS satisfies all the relevant boundary conditions that we will impose on our solutions (see below) and we shall use it as the reference metric in the Einstein-DeTurck equation. The compact radial coordinate $x \in [0, 1)$ covers the region from the horizon ($x = 0$) to infinity ($x = 1$). Note that NUBS posses reflection symmetry along the S^1 direction. This allows us to consider only one half of the KK circle subject to mirror boundary conditions. Therefore, we take $y \in [0, 1]$, where $y = 0$ corresponds to the reflection plane and $y = 1$ the periodic boundary. This implies that the asymptotic length of the KK circle is kept fixed to be $L = 2$.

The radius of the round S^{D-3} at the horizon is a good geometric invariant that can be used to describe NUBS; with our ansatz (3.2.2.1), this is given by

$$R(y) = r_0 \sqrt{e^{Q_5}}\Big|_{x=0}. \tag{3.2.2.3}$$

Black string solutions can be characterized with the non-uniformity parameter introduced in [13],

$$\lambda = \frac{1}{2}\left(\frac{R_{\max}}{R_{\min}} - 1\right), \tag{3.2.2.4}$$

where $R_{\max} = \max[R(y)]$ and $R_{\min} = \min[R(y)]$. UBS have $\lambda = 0$, whereas NUBS have $\lambda > 0$; the limit $\lambda \to \infty$ corresponds to the merger point with the LOC branch, where $R_{\min} \to 0$ while $R_{\max}$ remains finite.

To obtain a well-posed boundary value problem that can be solved with elliptic methods we need to supplement the equations of motion with appropriate boundary conditions. These require regularity at the horizon, reflection symmetry, periodicity and KK asymptotics:

- **Horizon** at $x = 0$: smoothness of the metric at the horizon implies that all Q's must be even in x and therefore we impose Neumann boundary conditions on all Q's, except the crossed term which must be Dirichlet. The condition $Q_1(0, y) = Q_2(0, y)$ ensures that the geometry is free of conical singularities and fixes the surface gravity of the solution to be that of our reference metric.

- **Asymptotic boundary** at $x = 1$: the metric must approach the KK space. This implies the Dirichlet boundary conditions, $Q_i(1, y) = 1$, $\forall i \neq 4$, and $Q_4(1, y) = 0$.

- **Reflection plane and periodic boundary** at $y = 0$ and $y = 1$ respectively: all Q's must be even in the compact S^1 coordinate and thus we impose Neumann boundary conditions for all Q's, except for the crossed term which must be Dirichlet there.

To find NUBS, we start with the UBS close to the GL point and add a bit of the GL zero mode. This gives a good initial guess that allows us to find weakly non-uniform black strings. Once we have found a NUBS, we can move along the family varying the temperature; with our boundary conditions, the inverse temperature is given by

$$\beta = \frac{4\,\pi\, r_0}{D-4}\,. \tag{3.2.2.5}$$

We move along the branch of NUBS by using the previous solution as a seed and varying the value of the parameter r_0; we start at $r_0 = 0.73450$ which corresponds to $\lambda = 0.04$ (recall that $r_0^{\rm GL} = 0.73342(6)$ for $L = 2$) and, given our modest resources, we move up to a value of $r_0 = 0.79184$, corresponding to $\lambda = 5.05$. For $\lambda \lesssim 1$, the NUBS are relatively weakly non-uniform, not much resolution is required to construct the solutions accurately and one single patch is suffices. At this point, the solutions satisfy $\xi_a \xi^a \equiv \xi^2 < 10^{-10}$, with estimated numerical error to be less than 0.01%. The Smarr's relation is satisfied up to the order 10^{-7}.

As we move along the branch of NUBS to greater values of λ, the function Q_4 develops very pronounced peaks near the origin, corresponding to the waist of the NUBS, and some form of mesh-refinement there is needed to construct accurate solutions. We found that two conforming patches were enough to obtain good results, though the bound on the DeTurck vector goes up to $\xi^2 < 10^{-7}$ and the Smarr's relation is satisfied up to 10^{-6}.

Notice that our mesh-refinement introduces a new parameter x_0, which is the coordinate location where the two patches meet. In addition, we also considered $\tilde{y} = \text{mesh}(y; 0, 1, \chi)$, with the function mesh(...) given by (2.2.2.13). Since the steep gradients move towards the origin as λ increases, we used two different setups with appropriate grid sizes x_0 ($\sim 10^{-1}, 10^{-2}$) and values of χ ($\sim 1, 10$). It is possible that by choosing a different reference metric for highly NUBS one can achieve larger values of λ without losing accuracy.

3.2.3 Numerical construction of localized black holes

To numerically construct LOC we follow the approach of Kalisch et al. [22] with minor modifications. Essentially, we considered a different compactification of the radial coordinate so that we could extract the constants C_τ and C_y appearing in the conserved charges (3.2.1.3) by calculating 1st derivatives of our unknown functions. In this section we superficially discuss the actual numerical construction of LOC and refer the reader to [22] for further details.

We seek static axisymmetric black holes that are asymptotically KK and localized on a circle of (asymptotic) length L. We choose adapted coordinates so that symmetries of the spacetime become manifest. This implies that the actual boundaries of the computational domain are: the black hole horizon, the asymptotic infinity, the periodic boundary, the reflection plane and an axis of symmetry where the horizon S^{D-2} smoothly shrinks to zero size, which is exposed because the localization on the

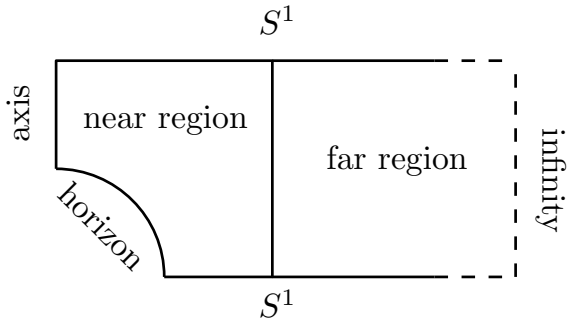

Fig. 3.2: *Sketch of the integration domain for localized black holes.*

S^1. From the point of view of finding these black holes numerically, since the integration domain has five boundaries, we naturally work with two coordinate patches: One patch adapted to a 'near' region (containing the horizon), and another one adapted to a 'far' region (containing the asymptotic infinity). See Fig. 3.2.

As in [214], one can work with cartesian coordinates (x, y) in the far patch and polar coordinates (r, a) in the near patch, and the relation between them is simply given by the polar map (see Appendix 3.A). To transfer information between the two coordinate patches one can use two overlapping domains and impose uniqueness of the solution [214]. This is simpler to implement if one uses finite differences. On the other hand, if one uses spectral methods, one can deform the two domains using some transfinite transformation and ensure that the two domains match along a curve; along this common boundary one then imposes continuity of the functions and their normal derivatives. Alternatively, in the near region [22] introduce polar-like coordinates with a modified radial coordinate which naturally matches with the Cartesian coordinates sufficiently far from the black hole. This is the approach we follow in the near region. We recall the details of the integration domain and introduce the new compactification in Appendix 3.A.

The ansatz for the metric in the far patch is:

$$\mathrm{d}s^2_{\mathrm{far}} = Q_1\,\mathrm{d}\tau^2 + x^2\,Q_2\,\mathrm{d}\Omega^2_{D-3} + Q_3\,\mathrm{d}x^2 + Q_4\,\mathrm{d}y^2 + 2\,Q_5\,\mathrm{d}x\mathrm{d}y\,, \tag{3.2.3.1}$$

where the functions $Q \equiv \{Q_1, Q_2, Q_3, Q_4, Q_5\}(x, y)$ are our unknowns. As shown in the actual integration domain, Fig. 3.13, the coordinate x ranges from $L/2$, which is the boundary between the far and near regions, to infinity; on the other hand, $y \in [0, L/2]$, where $y = 0$ is the reflection plane and $L/2$ is the periodic boundary. The boundary conditions we impose on the unknown functions Q in this patch are:

- **Asymptotic boundary** at $x = \infty$: the metric must approach the KK space. This implies the Dirichlet boundary conditions, $Q_i(\infty, y) = 1$, $\forall i \neq 5$, and $Q_5(\infty, y) = 0$.

- **Matching boundary** at $x = L/2$: we impose continuity of the metric and its normal derivative.

- **Reflection plane and periodic boundary** at $y = 0$ and $y = L/2$ respectively: all Q's must be even in the compact coordinate y and thus we impose Neumann boundary conditions on all them except the crossed term Q_5, which must be Dirichlet there.

The near horizon region ansatz covers the horizon and the symmetry axis; at the horizon, the Killing ∂_τ becomes null and at the symmetry axis the round S^{D-3} (and in fact the whole horizon S^{D-2}) smoothly shrinks to zero. The ansatz we consider is:

$$\begin{aligned} \mathrm{d}s^2_{\text{near}} = \kappa^2\,(r-r_0)^2\,Q'_1\,\mathrm{d}\tau^2 + r^2\,\cos^2 a\;Q'_2\,\mathrm{d}\Omega^2_{D-3} + Q'_3\,\mathrm{d}r^2 \\ + r^2\,Q'_4\,\mathrm{d}a^2 + 2\,r\,Q'_5\,\mathrm{d}r\mathrm{d}a, \end{aligned} \tag{3.2.3.2}$$

where $Q' \equiv \{Q'_1, Q'_2, Q'_3, Q'_4, Q'_5\}(r, a)$ are the unknowns in this patch. This metric has a Killing horizon located at $r = r_0$ with surface gravity κ, and an axis at $a = \pi/2$; $a = 0$ is the reflection plane. Although the horizon is at $r = r_0$, r_0 is simply a parameter in our ansatz and we keep it fixed throughout the calculation (we choose $r_0 = 0.8$ for convenience); the physical parameter labelling each solution is the surface gravity κ, and this the parameter that we vary to move along the branch of LOC. With the definitions given in Appendix 3.A, the boundary conditions that we impose on the unknown functions Q' in this region are:

- **Horizon** at $r = r_0$: smoothness of the metric at the horizon implies that all Q''s must be even in $r - r_0$ and therefore we impose Neumann boundary conditions for Q'_1, $r^2Q'_2$, Q'_3, $r^2Q'_4$ and Dirichlet for the crossed term Q'_5. The condition $Q'_1(r_0, a) = Q'_3(r_0, a)$ ensures that the geometry is free of conical singularities and fixes the surface gravity of the solution to be that of the reference metric (see below).

- **Axis of symmetry** at $a = \pi/2$: regularity requires that all functions Q''s are Neumann, except the crossed term which is Dirichlet there. In addition we impose $Q'_2(r, \pi/2) = Q'_4(r, \pi/2)$ to avoid conical singularities.

- **Reflection plane** at $a = 0$: all functions are Neumann except for Q'_5, that vanishes there.

- **Periodic boundary** at $r_3(L/2, a)\sin a = L/2$: using the relation between the far and near coordinates and the relation between the far and near unknown functions, one can find the boundary conditions for the near horizon functions from the boundary conditions that the far region functions satisfy there.

- **Matching boundary** at $r_2(L/2, a)\cos a = L/2$: we impose continuity of the metric and its normal derivative.

In addition to the ansatz and the boundary conditions, the DeTurck scheme requires a global reference metric as part of the gauge fixing procedure. The reference metric must satisfy the same boundary conditions as the solution we seek. For the

LOC, there is no known Einstein metric in closed analytic form that satisfies the required boundary conditions and hence one has to design it. In this study we follow [22,214], and smoothly glue together two metrics, each of which satisfy the desired boundary conditions in each region, i.e. asymptotic Kaluza-Klein space in the far region and, for instance, the asymptotically flat Schwarzschild black hole in D dimensions:

$$\mathrm{d}\bar{s}^2 = H(r)\mathrm{d}\tau^2 + \mathrm{d}r^2 + G(r)\left(\mathrm{d}a^2 + \cos^2 a\ \mathrm{d}\Omega_{D-3}^2\right) \tag{3.2.3.3}$$

with

$$\begin{aligned} H(r) &= \begin{cases} H_{\rm hor}(r) & \text{for } r < r_1 \\ 1 & \text{for } r \geq r_1 \end{cases}, \qquad G(r) = \begin{cases} G_{\rm hor}(r) & \text{for } r < r_1 \\ r^2 & \text{for } r \geq r_1 \end{cases}, \\ H_{\rm hor}(r) &= 1 - E(r), \\ G_{\rm hor}(r) &= r^2 - E(r)\left(r^2 - \frac{(D-3)^2}{4\kappa^2} - (r-r_0)^2\left[\frac{D^2}{4} - D + \frac{3}{4} - \kappa^2 r_0^2\right]\right), \end{aligned} \tag{3.2.3.4}$$

where the function $E(r)$ is given by

$$E(r) = \exp\left(-\kappa^2 \frac{(r-r_0)^2}{1-(r-r_0)^2/(r_1-r_0)^2}\right). \tag{3.2.3.5}$$

The reference metric depends on κ, r_0, and r_1, which is an additional parameter that can be adjusted (see appendix 3.A). The function $E(r)$ vanishes exponentially fast for $r \to r_1$, and the reference metric (3.2.3.3) tends to the KK space written in polar coordinates. For $r \to r_0$, $E(r) \simeq 1 - \kappa^2(r-r_0)^2$ and (3.2.3.3) takes the form of the near horizon metric of the Schwarzschild black hole in D dimensions.

To find localized black holes we start with the reference metric as a seed with $\kappa = 2.4$ and $L = 6$ (we keep this value of L for all solutions). Recall that the convergence of Newton's method strongly depends on the choice of the initial seed and finding a first solution may be difficult. To stay within the basin of attraction at each iteration, we introduce a parameter $\alpha \in \mathbb{R}^+$ in the iteration loop so that the update is $Q_k^{(n+1)} = Q_k^{(n)} + \alpha\delta Q_k$, where $\alpha \sim \mathcal{O}(10^{-2})$ or $\mathcal{O}(10^{-1})$ during the first iterations and is $\mathcal{O}(1)$ towards the end. Once we have found the first solution, we use it as the initial guess to find the next solution with a slightly different κ while keeping $\alpha = 1$. We kept the parameters of the integration domain and the coordinates fixed throughout the calculation and they are specified in Fig. 3.13.

The most critical solution we found corresponds to $\kappa = 1.262768$. In this critical regime, the functions Q'_2 and Q'_4 develop steep gradients near the axis and the horizon; to resolve them, we redefine these two functions in the pure polar patch (blue and green dots in Fig. 3.13): $Q_i^c(r,a) = 1/Q'_i(r,a)$, $i = 2,4$ [22]. The boundary conditions for these redefined functions can be easily found from the original ones for Q'_2 and Q'_4. All solutions we found satisfy $\xi^2 < 10^{-10}$ with numerical error less than 0.01% and the Smarr's relation is satisfied up to the order 10^{-6}.

3.3 Results

In this section we present our results for both NUBS and LOC. We first consider the behavior of the various thermodynamic quantities along each branch of solutions and the phase diagrams, and then we focus on the horizon geometry. We then study the critical behavior near the merger point, and provide evidence that the double-cone geometry proposed by [21] does indeed control the merger. We finally compute their spectrum of negative modes of the Lichnerowicz operator.

3.3.1 Thermodynamics

The horizon temperature labels both NUBS and LOC and is given by (3.2.2.5) for non-uniform black strings and by $\kappa/(2\pi)$ for localized solutions. The mass and the tension follow from (3.2.1.3). For the NUBS the asymptotic charges are computed as:

$$\begin{aligned} C_\tau &= \frac{r_0^{D-4}}{2}\left(\frac{L}{2}\right)^{-1}\int_0^{L/2}\mathrm{d}y\left(2+\left.\frac{\partial Q_1}{\partial x}\right|_{x=1}\right), \\ C_y &= -\frac{r_0^{D-4}}{2}\left(\frac{L}{2}\right)^{-1}\int_0^{L/2}\mathrm{d}y\left.\frac{\partial Q_3}{\partial x}\right|_{x=1}, \end{aligned} \tag{3.3.1.1}$$

where in these expressions we first interpolate the numerical data and then perform the integration. For the LOC these quantities are given in (3.A.0.3). The horizon area is found to be:

$$\begin{aligned} \text{NUBS:}\quad & A_{\mathrm{H}} = 2r_0^{D-3}\Omega_{D-3}\int_0^{L/2}\mathrm{d}y\left.\sqrt{e^{Q_3+(D-3)Q_5}}\right|_{r=r_0}, \\ \text{LOC:}\quad & A_{\mathrm{H}} = 2r_0^{D-2}\Omega_{D-3}\int_0^{\pi/2}\mathrm{d}a(\cos a)^{D-3}\left.\sqrt{{Q_2'}^{D-3}Q_4'}\right|_{r=r_0}. \end{aligned} \tag{3.3.1.2}$$

In Fig. 3.3 we display the phase diagram in the microcanonical (*top left*) and canonical (*top right*) ensembles, and the behavior of the horizon area (*middle*) and tension (*bottom*) as a function of the inverse temperature (normalized by L). The behavior of the mass and the relative tension as a function of the inverse temperature is similar to that of the area and tension and we do not display the corresponding plots here. To make the microcanonical and canonical phase diagrams easier to visualize, we plot the dimensionless entropy and free energy with respect the values of a uniform black string, $\Delta S/L^8$ and $\Delta F/L^7$.

NUBS, which exist beyond the GL point, never dominate any of these ensembles and they are presumably dynamically unstable. The LOC phase crosses the UBS branch at[6]

$$M_{\mathrm{PT}} = 0.01375(4)L^7, \quad \text{or} \quad T_{\mathrm{PT}} = 1.26682(1)L^{-1}. \tag{3.3.1.3}$$

[6]We simply used Mathematica's function `Interpolation` to interpolate our numerical data and Newton's method to find the intersection point. Our error bars are estimated from the global error of the numerical solutions, see Appendix 3.B.

For lower masses, $M < M_{\rm PT}$, or higher temperatures temperatures, $T > T_{\rm PT}$, the LOC dominate the corresponding ensemble and the UBS are unstable, whilst for $M > M_{\rm PT}$ or $T < T_{\rm PT}$, UBS dominate. At $M = M_{\rm PT}$ or $T = T_{\rm PT}$, there is first order phase transition. The phase diagrams are consistent with a merger between NUBS and LOC at

$$M_{\rm Merger} = 0.02040(4)L^7, \quad \text{or} \quad T_{\rm Merger} = 1.20585(6)L^{-1}. \tag{3.3.1.4}$$

See §3.3.3 for its derivation.

One of the remarkable features of the phase diagram in $D = 10$ is the lack of turning points away from the merger along any of the branches, either LOC or NUBS. This should be contrasted with the phase diagram in $D = 5, 6$, which exhibits a turning point along the LOC branch at some maximum mass and then there is a minimum of the temperature [22, 214]. It is reasonable to expect that such a turning point (away from the merger) exists on the LOC branch for any dimension $D < 10$. This turning point switches to the NUBS branch in $D = 12$ (and presumably in $D = 11$), as shown in [231] and more recently in the large-D expansion in [233]. As we will argue below, the lack of turning points away from the merger in the phase diagram in $D = 10$ may be related to the nature of the merger in this specific number of spacetime dimensions.

In Fig. 3.4 we plot various physical quantities, normalized by their value at the GL point, against the normalized relative tension $n/n_{\rm GL}$. Close to the merger point, our results in $D = 10$ show that the physical quantities do not approach their critical values following a spiraling behavior, with presumably infinitely many turning points, as in $D = 5, 6$ [22, 230]. Instead, the physical quantities of the NUBS and LOC branches merge at a cusp in the phase diagram, with no oscillations. As we discuss in §3.3.3, this behavior is precisely what the double-cone model of [21] for the merger predicts in $D = 10$. Notice that the physical quantities corresponding to both branches emerge from the cusp in the 'same direction'.

3.3.2 Horizon geometry

In this subsection we display the behavior of various geometric quantities defined on the horizon along the branches of solutions. Then we present the embeddings of the horizon geometry into flat space to help to visualize the geometry of NUBS and LOC.

We characterize the NUBS using the non-uniformity parameter λ defined in [13], (3.2.2.3). In addition, we consider the proper length of the horizon along the S^1:

$$L_{\rm hor} = 2\int_0^{L/2} {\rm d}y \, \sqrt{e^{Q_3}}\Big|_{x=0}. \tag{3.3.2.1}$$

Following [214], for LOC, one can define $R_{\rm eq}$ as the equatorial radius of the horizon round S^{D-3},

$$R_{\rm eq} = r_0\sqrt{Q_2'(r_0, 0)}. \tag{3.3.2.2}$$

Similarly, one defines $L_{\rm polar}$ to be the proper distance from the 'south' pole to the 'north' pole along the horizon S^{D-2}, and $L_{\rm axis}$ to be the proper distance between the

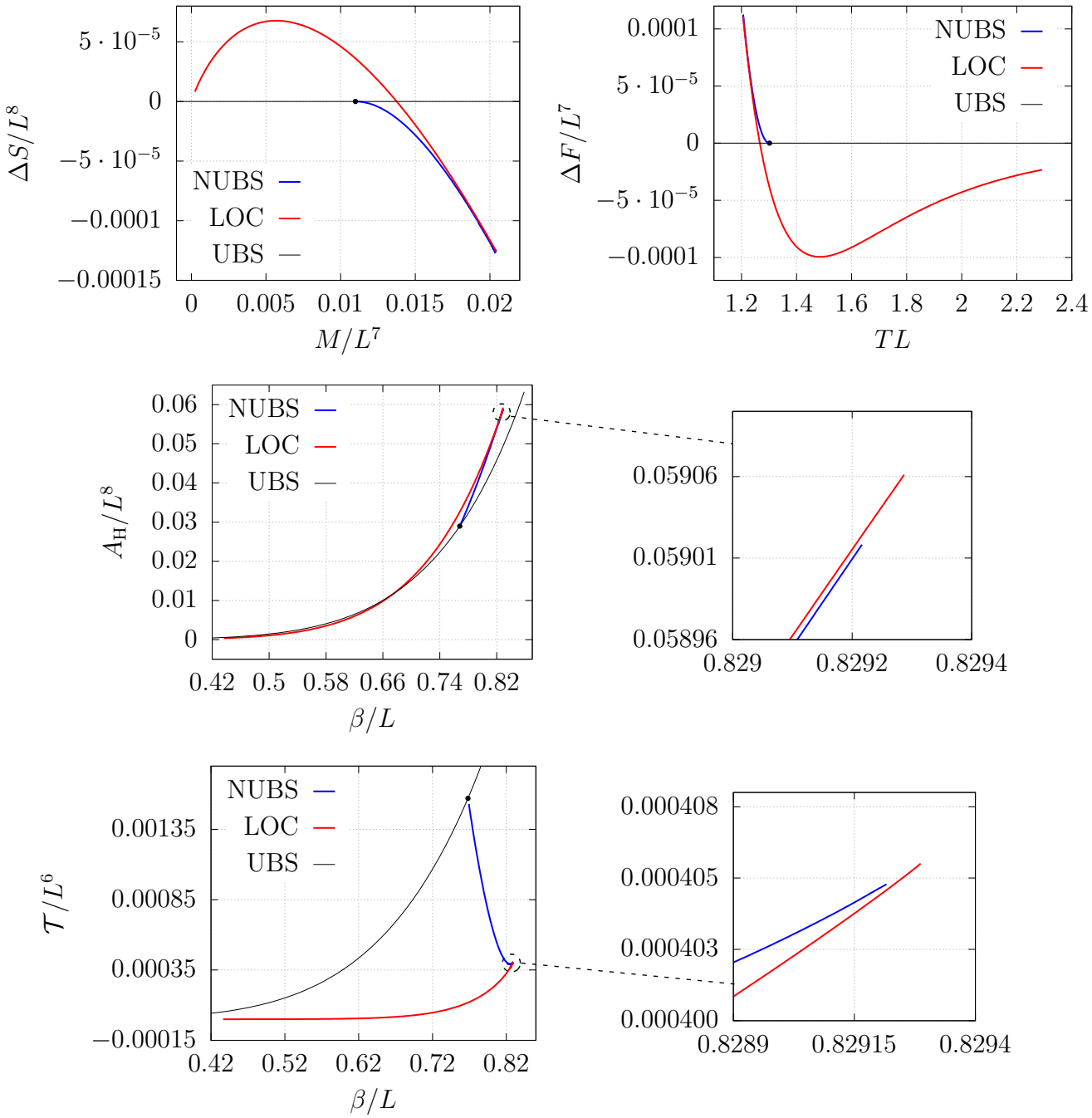

Fig. 3.3: *Phase diagram in the microcanonical (top left) and canonical (top right) ensembles respectively for the three different families of KK black objects in $D = 10$. These plots reproduce and complete those shown in the appendix of [161]. Dimensionless horizon area A_H/L^8 (middle) and tension $\mathcal{T}/L^6$ (bottom) as a function of the dimensionless ratio β/L. The GL critical point is indicated with a solid black disc. The dimensionless mass and relative tension plots are very similar to the ones shown above.*

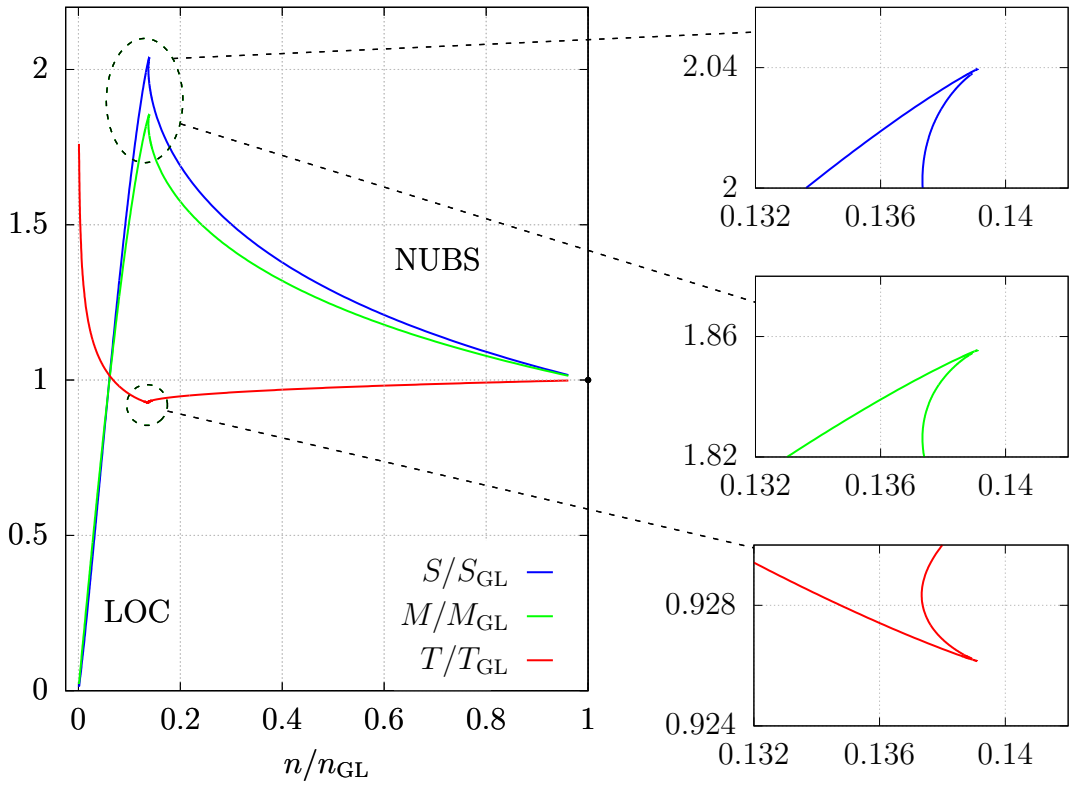

Fig. 3.4: *Entropy, mass and temperature as a function of the relative tension, normalized with respect to the values at the GL point. The mini-plots at the right hand side correspond to zooming at the merger point, as indicated by the dashed lines.*

poles along the axis:

$$L_{\rm polar} = 2r_0 \int_0^{\pi/2} {\rm d}a \sqrt{Q'_4}\Big|_{r=r_0}, \qquad L_{\rm axis} = 2\int_{r_0}^{L/2} {\rm d}r \sqrt{Q'_3}\Big|_{a=\pi/2}. \tag{3.3.2.3}$$

Recall that the asymptotically flat Schwarzschild solution in D dimensions is spherically symmetric and hence it enjoys the symmetry of the full rotation group $\mathrm{SO}(D-1)$. On the other hand, LOC break the $\mathrm{SO}(D-1)$ symmetry down to $\mathrm{SO}(D-2)$, and only for very small localized black holes, i.e. high temperatures, the full $\mathrm{SO}(D-1)$ is approximately recovered. We can characterize the deformation of the horizon geometry by comparing the area of the round equatorial horizon S^{D-3}, $A_{\rm eq} \propto R_{\rm eq}^{D-3}$, and the area of the geodesic S^{D-3} on the horizon that contains both poles, $A_{\rm pol} \propto R_{\rm pol}^{D-3}$ with

$$R_{\rm pol} = r_0 \sqrt{Q'_2(r_0, \pi/2)}. \tag{3.3.2.4}$$

We compare these two areas defining the eccentricity parameter,

$$\epsilon = \frac{A_{\rm pol}}{A_{\rm eq}} - 1\,. \tag{3.3.2.5}$$

A spherically symmetric black hole has zero eccentricity and ϵ diverges for the critical solution.

The behavior of these geometric quantities along each branch of solutions is displayed in Fig. 3.5. In the top row we display ϵ and λ as functions of β/L. At high temperatures, LOC are nearly spherically symmetric and the eccentricity is very small. In fact, ϵ remains quite small until pretty close to the merger with NUBS, where it diverges (notice that the vertical axis is in a log-scale). This explains why perturbation theory works so well for localized black holes in $D = 10$ [161], and it is another manifestation of the fact that gravity becomes more localized near the horizon as D grows. The behavior of the non-uniformity parameter λ for the NUBS is qualitatively similar. From these two plots it is clear that we managed to get closer to the merger from the LOC branch. From the behavior of ϵ and λ we can estimate that the merger occurs at $\beta_{\rm Merger} \simeq 0.829L$.

At the bottom of Fig. 3.5 we display the remaining geometric quantities as functions of the relative tension n normalized by its value at the GL point. We have added zooms of these plots to better appreciate the region where the various curves merge. In $D = 10$ the merger happens at a cusp, with the physical quantities of both the NUBS and the LOC coming out of the cusp in the same direction. This behavior should be contrasted with the $D = 5, 6$ case, in which a part from the shrinking spirals, the physical quantities for the NUBS and the LOC approach the merger from opposite sides. It would be nice to understand the side from which a given physical quantity approaches the merger point as a function of the number of spacetime dimensions D from the double-cone geometry. From the behavior of $L_{\rm axis}/L$ and $R_{\rm min}/L$ as they approach zero, we estimate the value of $n/n_{\rm GL}$ at the merger to be $n_{\rm Merger} \simeq 0.139 n_{\rm GL}$.

A useful way to visualize the geometry of $\tau =$ const. sections of the horizon is by embedding them into $(D-1)$-dimensional Euclidean space $\mathbb{E}^{D-1}$, with a flat metric

$$\mathrm{d}s^2_{\mathbb{E}^{D-1}} = \mathrm{d}X^2 + \mathrm{d}Y^2 + Y^2 \mathrm{d}\Omega^2_{D-3}\,. \tag{3.3.2.6}$$

For NUBS, the horizon geometry can be described as a surface $X = X(y)$, $Y(y) = R(y)$ in $\mathbb{E}^{D-1}$ (with $R(y)$ defined in (3.2.2.3)), whilst for LOC one has

$$X = X(a), \qquad Y(a) = r_0 \cos a \sqrt{Q_2'}\big|_{r=r_0}. \tag{3.3.2.7}$$

In each case, the embedding coordinate is given by

$$\begin{aligned} \text{NUBS:} \quad & X(y) = \int_0^y \mathrm{d}y' \sqrt{e^{Q_3} - \frac{r_0^2}{4} e^{Q_5} \left(\frac{\mathrm{d}Q_5}{\mathrm{d}y'}\right)^2}\Bigg|_{x=0}, \\ \text{LOC:} \quad & X(a) = r_0 \int_0^a \mathrm{d}a' \sqrt{Q_4' - \left(\sin a \sqrt{Q_2'} - \frac{\cos a}{2\sqrt{Q_2'}} \frac{\mathrm{d}Q_2'}{\mathrm{d}a'}\right)^2}\Bigg|_{r=r_0}. \end{aligned} \tag{3.3.2.8}$$

In Fig. 3.6 we plot Y/L vs X/L for some representative solutions, including the most critical ones. We postpone the detailed comparison with the double-cone metric to the next subsection.

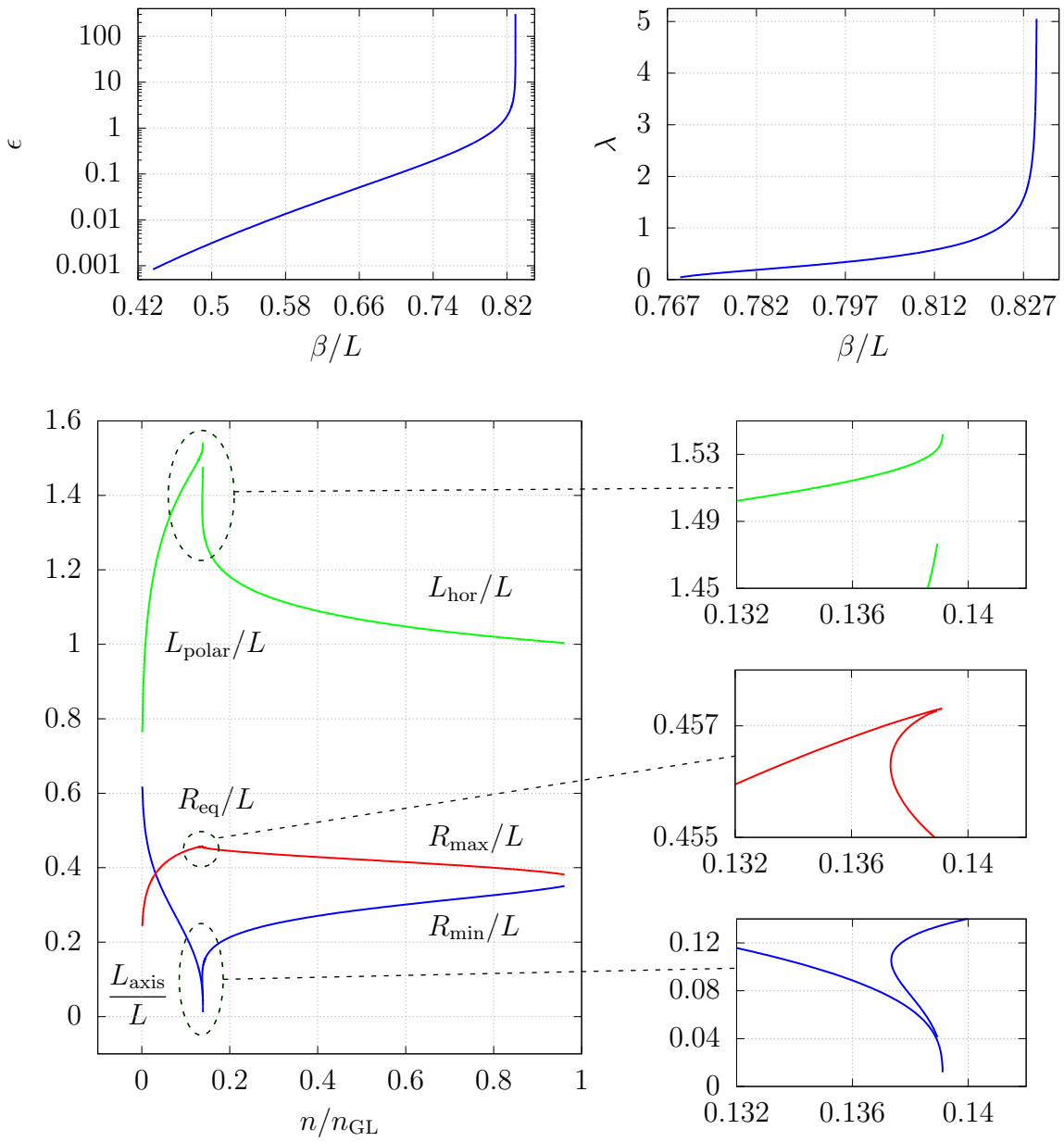

Fig. 3.5: *Eccentricity (top left) and non-uniformity parameter (top right) as a function of the dimensionless inverse temperature. These quantities give a direct measure of the deformation of LOC and NUBS respectively. Different geometrical lengths and radii for NUBS and LOC (bottom) as a function of the relative tension normalized at the GL threshold point.*

3.3.3 Critical behavior at the merger point

Kol argued that the merger between the NUBS and the LOC implies a topology change not only of the horizon geometry but in fact of the whole Euclidean manifold [21]. This is a much stronger statement than simply considering the change of the topology of

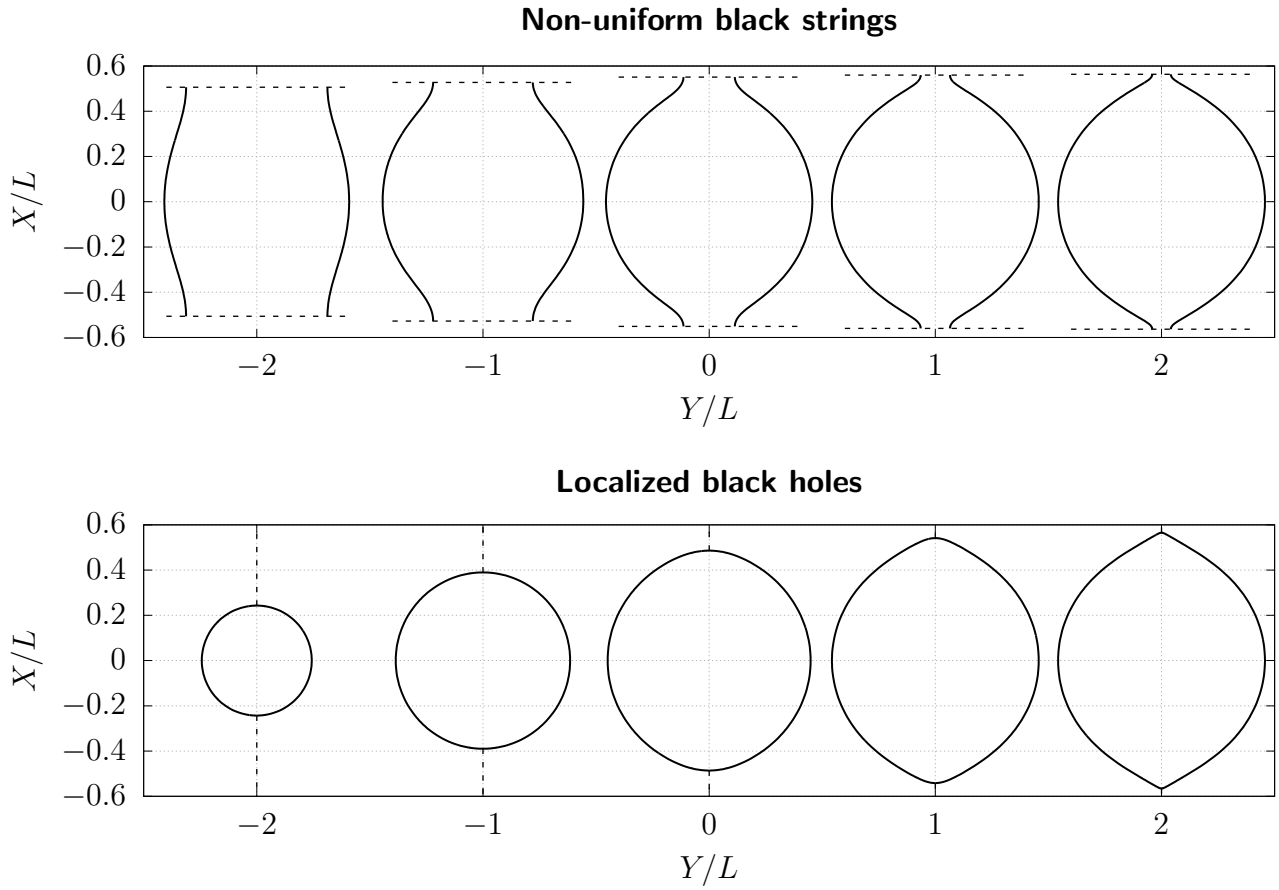

Fig. 3.6: *Embedding of the spatial cross-section of the horizon into Euclidean space for different NUBS (top) and LOC (bottom). For NUBS, from left to right,* $r_0 = 0.74328$ *(*$\lambda \sim 0.1$*),* $r_0 = 0.77216$ *(*$\lambda \sim 0.5$*),* $r_0 = 0.78950$ *(*$\lambda \sim 1.5$*),* $r_0 = 0.79156$ *(*$\lambda \sim 3$*) and* $r_0 = 0.79184$ *(*$\lambda \sim 5$*). For LOC the axis is parallel to* X/L *and represented by a dashed line starting at the poles. From left to right:* $\kappa = 2.4$ *(*$\epsilon \sim 10^{-3}$*),* $\kappa = 1.5$ *(*$\epsilon \sim 10^{-1}$*),* $\kappa = 1.29$ *(*$\epsilon \sim 10^{0}$*),* $\kappa = 1.26341$ *(*$\epsilon \sim 10$*) and* $\kappa = 1.26277$ *(*$\epsilon \sim 3 \cdot 10^{2}$*). Note that the embeddings look 'rounder' or 'fatter' compared to the ones in lower dimensions; this is just a manifestation that gravity becomes more localized as* D *increases.*

the horizon. Moreover, [21] conjectured that this topology change of the Euclidean manifold should locally be controlled by a Ricci-flat double-cone over $S^2 \times S^{D-3}$:

$$\mathrm{d}s^2 = \mathrm{d}\rho^2 + \frac{\rho^2}{D-2}\left(\mathrm{d}\Omega^2_{(2)} + (D-4)\mathrm{d}\Omega^2_{(D-3)}\right) . \tag{3.3.3.1}$$

This double-cone arises as follows. Both the NUBS and the LOC possess an explicit $\mathrm{SO}(D-2)$ spherical symmetry which must be inherited by the critical metric, i.e. it must contain a round S^{D-3}. The S^2 is less obvious and its origin is the following [21]: away from the waist, the Euclidean time, which is periodic to avoid a conical singularity

at the horizon, is fibered over an interval whose endpoints are on the horizon, thus giving rise to a two-sphere. Such an S^2 is finite everywhere on the localized phase whilst it is contractible to zero size in the black string phase (see [262] for a nice depiction). On the localized phase, one can compute the radius of this sphere on the symmetry axis at the equidistant points from the poles of the horizon S^{D-2}. By symmetry, this corresponds to the equatorial radius of the S^2 and is given by

$$R_\tau = \frac{\kappa}{2\pi}\left(\frac{L}{2} - r_0\right)\sqrt{Q_1'(L/2, \pi/2)}\,. \tag{3.3.3.2}$$

One can compare it to the radius of this S^2 along the symmetry axis,

$$R_{\text{axis}} = \frac{L_{\text{axis}}}{2\pi}, \tag{3.3.3.3}$$

along the branch of LOC. See Fig. 3.7. From this plot we see that $R_\tau \sim R_{\text{axis}}$ as the solutions approach the merger and both radii tend to zero. This shows that the S^2 becomes round as it shrinks, just as the double-cone model of [21] predicts. Also shown in this plot is the minimum radius of the horizon S^{D-3}, R_{min}, on the NUBS. This quantity also shrinks to zero at the merger.

One can further test the double-cone model of the merger by considering the embedding of the $\tau = \text{const.}$ section of (3.3.3.1) into Euclidean $\mathbb{E}^{D-1}$ space. The embedding coordinates of the double-cone metric (3.3.3.1) are simply given by

$$X(\rho) = \rho\sqrt{\frac{2}{D-2}}, \qquad Y(\rho) = \rho\sqrt{\frac{D-4}{D-2}}\,. \tag{3.3.3.4}$$

In Fig. 4.14 we compare the embedding of the double-cone in $D = 10$ dimensions with the embeddings corresponding to the most critical LOC (red) and NUBS (blue) solutions that we have found. As this plot shows, the double-cone can be smoothed in two different ways, each one leading to one of the phases at each side of the transition.

One can consider deformations of the double-cone metric of the form:

$$\mathrm{d}s^2 = \mathrm{d}\rho^2 + \frac{\rho^2}{D-2}\left(e^{\epsilon(\rho)}\mathrm{d}\Omega^2_{(2)} + (D-4)e^{-\frac{2}{D-3}\epsilon(\rho)}\mathrm{d}\Omega^2_{(D-3)}\right). \tag{3.3.3.5}$$

The linearized perturbations satisfy the following equation of motion:

$$\epsilon''(\rho) + \frac{D-1}{\rho}\epsilon'(\rho) + \frac{2(D-2)}{\rho^2}\epsilon(\rho) = 0\,, \tag{3.3.3.6}$$

and, in for any $D \neq 10$, solutions of this equation are given by

$$\epsilon(\rho) = c_+\rho^{s_+} + c_-\rho^{s_-}, \tag{3.3.3.7}$$

with

$$s_\pm = \frac{D-2}{2}\left(-1 \pm \mathrm{i}\sqrt{\frac{8}{D-2} - 1}\right). \tag{3.3.3.8}$$

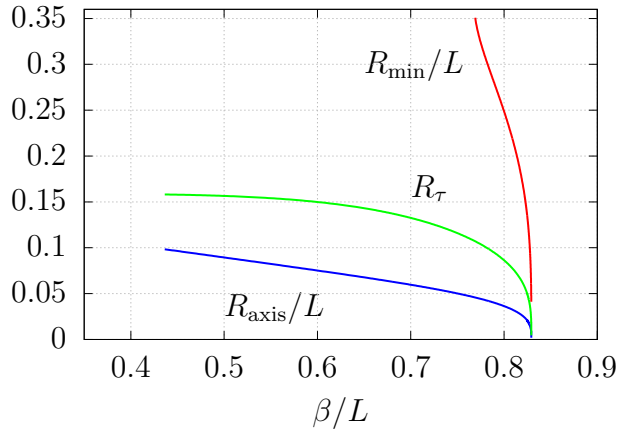

Fig. 3.7: *Euclidean time radius and axis radius as a function of the dimensionless inverse temperature. At the horizon points along the axis, i.e. at the extremes of the $S^1_{\rm axis}$, the Euclidean circle S^1_β has zero size. Then the fibration of one circle on the other gives a topological S^2. According to this figure, as we approach the merger point, $R_\tau \sim R_{\rm axis}/L$: the 2-sphere is round.*

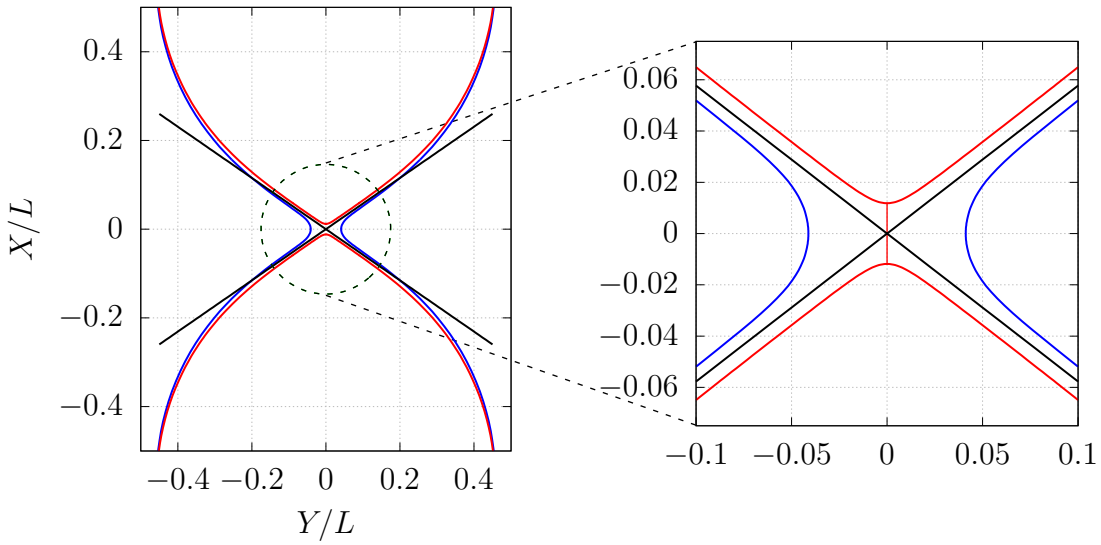

Fig. 3.8: *Comparison between the embeddings into $\mathbb{E}^9$ space of the most critical NUBS (blue line) and LOC (red line) that we have found and the Ricci-flat cone (black line). Clearly, both geometries approximate quite well the double-cone metric.*

For $D < 10$, the imaginary part of $s_\pm$ causes oscillations in $\epsilon(\rho)$, while for $D > 10$ there are two independent (real) powers. Furthermore, [263] (see also [264]) argued that the behavior of the deformations of the double-cone metric (4.4.4.6) should be reflected in the behavior of the physical quantities of NUBS and LOC sufficiently close to criticality. The argument goes as follows: if the zero mode $\epsilon(\rho)$ measures the deviation from the double-cone, then any physical quantity Q near the critical solution

should behave as

$$\delta Q = C_+ \left(\frac{\rho}{\rho_0}\right)^{s_+} + C_- \left(\frac{\rho}{\rho_0}\right)^{s_-} = \tilde{C}_+ \rho_0^{-s_+} + \tilde{C}_- \rho_0^{-s_-} \,, \tag{3.3.3.9}$$

where $\delta Q \equiv Q - Q_c$ and ρ_0 is the typical length scale associated to the smooth cone. Recently, [22] has beautifully confirmed this prediction in $D = 5, 6$.

The linearized solutions (4.4.4.6) degenerate in $D = 10$. Hence this is the critical dimension of the double-cone metric [21]. In this degenerate case, Frobenius' method gives two independent solutions of the form:

$$\epsilon^{D=10}(\rho) \sim c_1 \, \rho^4 + c_2 \, \rho^4 \ln \rho \,. \tag{3.3.3.10}$$

In the remaining of this subsection, we fit the different physical quantities of the near critical solutions that we have constructed according to the double-cone's prediction (3.3.3.10). Without loss of generality, for any physical quantity near the merger we have

$$Q(x) = Q_c + a \, x^b \, (c + d \, \ln x) \,, \tag{3.3.3.11}$$

where $\{a, b, c, d\}$ are the fitting parameters and x measures the distance to the critical solution. We consider the following dimensionless quantities that tend to zero at the merger:

$$x_{\rm NUBS} = \frac{R_{\rm min}}{r_0^{\rm GL}}, \qquad x_{\rm LOC} = \frac{L_{\rm axis}}{L}, \tag{3.3.3.12}$$

where L is the length of the KK circle and $r_0^{\rm GL}$ is the horizon radius of the black string at the GL instability point given in §3.2.1. Any other definition of x should give equivalent results up to a rescaling. We use Mathematica's `FindFit` routine to carry out the fits.

In Fig. 3.9 we present the fits for the mass (normalized with respect to the values of a UBS at the marginal GL point) for the NUBS and LOC branches. The other physical quantities behave in a qualitatively similar way and we do not present the fits here. Note that in contrast to the $D = 5, 6$ cases, in $D = 10$ the physical quantities do not present any oscillations as they approach their critical values. In fact, the fits clearly show that the approach to the critical value is governed by a power law with a logarithmic correction, in very good agreement with the double-cone prediction (3.3.3.10). In Table 3.1 we present the values of fitting parameters for the various physical quantities. To do the fits, we only have considered the solutions close enough to the merger, i.e. with small enough x; including more data points to perform the fit gives less accurate values of the critical thermodynamical values and exponent. For different physical quantities, the critical exponent coincides with the theoretical prediction of 4 with deviations of less than 0.05% in the worst case and the critical value of a given quantity coincide up to the $4^{\rm th}$ or $5^{\rm th}$ decimal number for both branches. We note that the critical values satisfy the Smarr's relation to the order 10^{-6} and 10^{-5} for NUBS and LOC respectively, which is consistent with the numerical error according to the values of ξ^2 we reached.

		Q_c	a	b	c	d
$T/T_{\rm GL}$	NUBS	**0.92615**	0.09539	**4.00001**	0.76900	−2.08080
	LOC	**0.92615**	2.41070	**3.99967**	0.21280	−3.43802
$M/M_{\rm GL}$	NUBS	**1.85551**	−1.48224	**3.99975**	0.80018	−1.68271
	LOC	**1.85551**	−9.31138	**3.99814**	2.62629	−10.83657
$S/S_{\rm GL}$	NUBS	**2.03933**	−0.76910	**4.00070**	1.88490	−4.13116
	LOC	**2.03958**	−15.75813	**4.00047**	1.27332	−8.34065
$\mathcal{T}/\mathcal{T}_{\rm GL}$	NUBS	**0.25816**	−1.49842	**3.99996**	−1.19917	−1.53764
	LOC	**0.25813**	−8.01729	**4.00188**	−12.66599	−11.94347
$n/n_{\rm GL}$	NUBS	**0.13913**	−1.50564	**4.00000**	−0.69536	−0.69743
	LOC	**0.13912**	6.72458	**4.00172**	8.18577	6.46396

Table 3.1: *Critical exponent and other parameters obtained from the fit of the non-uniform black strings (1st rows) and localized black holes (2nd rows) data points.*

		Q_c	a	b	c	d
$L_{\rm hor/polar}/L$	NUBS	**1.54505**	−0.40768	**0.99955**	1.54049	0.02272
	LOC	**1.54589**	0.41840	**1.00021**	−0.84676	−0.01620

Table 3.2: *Critical exponent and other parameters obtained from the fit of the NUBS's horizon length (1st row) and LOC's polar length (2nd row).*

Whilst the thermodynamic quantities follow the scaling law predicted by the double-cone geometry, the geometrical lengths characterizing the shape of the horizon do not follow the behavior (3.3.3.11), as it may be seen from Fig. 3.10. These are the horizon length $L_{\rm hor}$ of the black string and the polar length $L_{\rm pol}$ of the localized black holes. In lower dimensions this was also the case, and a linear term was introduced to get a proper fit [22]. In $D = 10$ the linear term appears naturally and the real critical exponent agrees to be one from both sides of the merger, just as in $D = 5, 6$. The equivalent plots to Fig. 3.9 for these lengths are shown in Fig. 3.10 and the extracted critical values and exponents are in Table 3.2. It would be interesting to better understand why these quantities do not follow the same critical behavior as the other physical quantities.

3.3.4 Spectrum of negative modes

In this subsection we present the spectrum of negative modes of the Lichnerowicz operator, Δ_L, around the NUBS and LOC solutions that we have constructed.

The negative eigenvalues of Δ_L are an invariant feature of the geometry and hence they provide another way to characterize the merger between NUBS and LOC. To com-

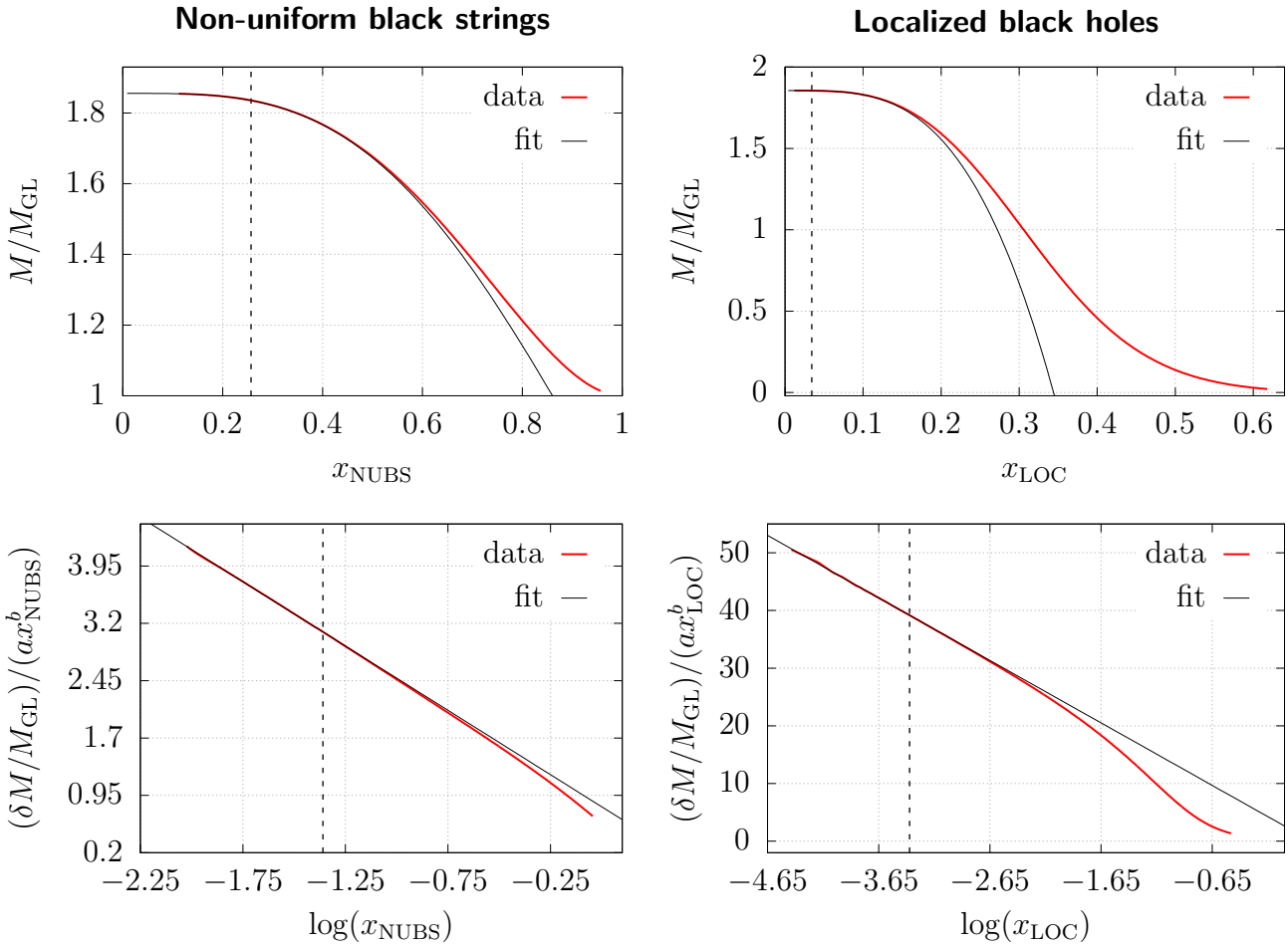

Fig. 3.9: *Normalized mass as a function of x for NUBS and LOC (top row). Data points left to the dashed vertical line are the ones used for the fit. In contrast to $D = 5, 6$ cases, in $D = 10$ our plots do not present any oscillations near the critical point, which agrees with the double-cone prediction of a real critical exponent. At the bottom row we represent $\delta M \equiv M - M_c$ normalized with respect $M_{GL} a x^b$, as a function of $\log x$. The relation is clearly lineal, in agreement with (3.3.3.10).*

pute the negative modes of Δ_L, we take advantage of the fact that, when using Newton's method to construct the solutions numerically, we have to linearize the Einstein-DeTurck operator as part of the iterative process. Around an Einstein metric, the linearized Einstein-DeTurck operator coincides with the Lichnerowicz operator [214]. It is then easy to readapt the code to find the low lying eigenvalues and eigenmodes of Δ_L, associated to (physical) metric fluctuations. Notice that with this approach we only find perturbations that are singlets under the action of $\mathrm{U}(1)_\beta \times \mathrm{SO}(D-3)$.

We display the results in Fig. 3.11. We found that NUBS have two negative modes, as in lower D [214].[7] The first one (green line in Fig. 3.11) corresponds to the

[7] In $D \geq 13$ NUBS have only one negative mode, and in $D = 12$ a mode disappears at a minimum

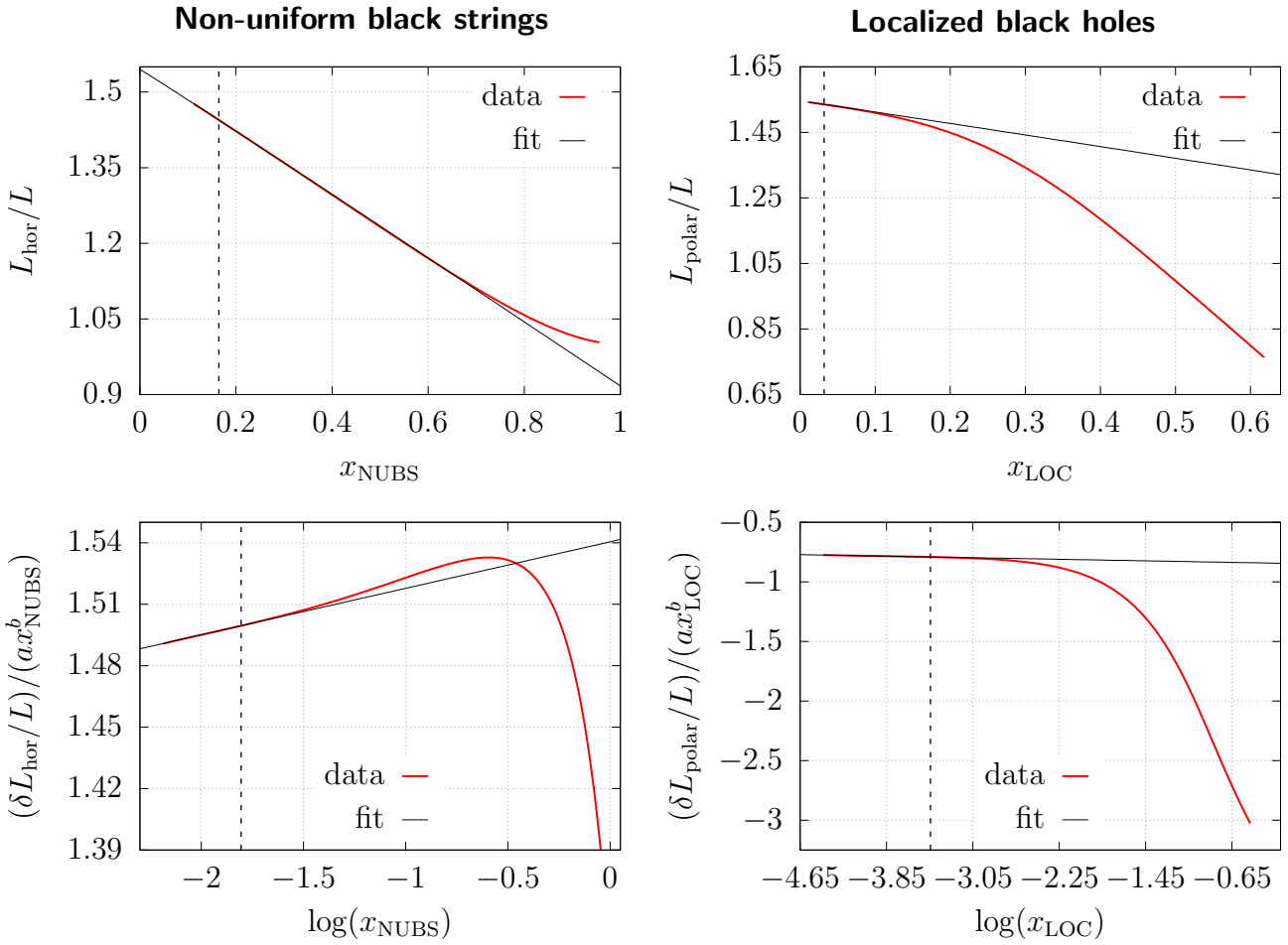

Fig. 3.10: *Normalized horizon length and polar length as a function of x for NUBS and LOC respectively (top row). Data points left to the dashed vertical line are the ones used for the fit. At the bottom row we represent $\delta L \equiv L_{hor/polar} - L_c$ normalized with respect to Lax^b, as a function of $\log x$. In both cases the relation is lineal.*

continuation of the GL zero mode to a negative mode as one moves along the branch to larger non-uniformities. The other one (blue line in Fig. 3.11) is continuously connected to the negative mode of the UBS, which arises from the negative mode of Schwarzschild [154]. For the explored range of solutions in this work, no further negative modes appear on this branch.

On the other hand, LOC have only one negative mode (red line in Fig. 3.11). For small black holes, this coincides with the negative mode of the asymptotically flat Schwarzschild solution in $D = 10$, as expected. No further negative modes appear or disappear along this branch. As we approach the critical solution from both sides, one of the modes of the NUBS diverges while the other appears to tend to a finite value;

of the temperature along the NUBS branch [231]. This is related to the fact that $D = 12$ is the critical dimension for the canonical ensemble for this system.

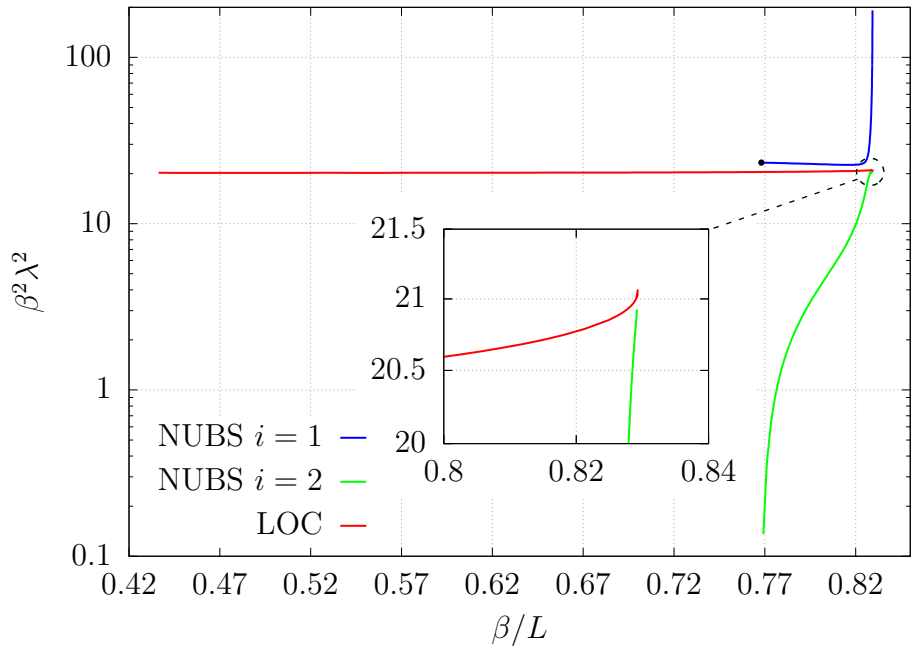

Fig. 3.11: *Absolute value of the negative modes of NUBS (green and blue lines) and LOC (red line) normalized with respect to the inverse temperature of the NUBS and LOC as a function of the dimensionless ratio β/L. The solid black discs show the zero mode and the negative mode of the UBS at the marginal GL point.*

the latter seems to match the limiting value of the negative mode on the LOC branch.

Notice that in $D = 10$, NUBS and LOC seem to have a different number of negative modes near the critical region. The reason is that there are no turning points along either branches, so modes cannot appear or disappear at a minimum of the temperature. However, modes can diverge as they approach the critical solution since it is singular. In $D = 5, 6$, there is a minimum of the temperature on the LOC branch, at which point Δ_L has a zero mode that continues to a (second) negative mode near the merger. At the merger, these two negative modes approach those of the NUBS and, in particular, a pair of them diverge at the critical solution [214].

3.4 Implications for super Yang-Mills on $\mathbb{T}^2$

In this section we derive the thermodynamics of SYM on $\mathbb{T}^2$, see also [23, 24, 161, 241, 242], using the (neutral) KK black holes. We start with a lightening review of the different limits under which string theory can be described by its supergravity sector and then we use the solutions previously found to obtain the thermodynamics of those carrying D0-brane charge. Our results extend those in [161] and allow us to find the merger point in the dual gauge theory.

3.4.1 Toroidal limits and type IIB/IIA supergravity duals

Consider (1+1)-dimensional SU(N) SYM at large N with 't Hooft coupling $\lambda = Ng^2_{\rm YM}$. If the theory is at finite temperature T so that $\beta = 1/T$ is the period of the thermal circle, and the spatial direction is also compactified on a circle of length L, then we can think of the theory as being defined on a 2-torus, $\mathbb{T}^2 = S^1_\beta \times S^1_L$. In these circumstances, one can define dimensionless quantities,

$$t = TL, \qquad \lambda' = \lambda L^2 \tag{3.4.1.1}$$

to study different regimes of the theory. From the gauge theory perspective, phase transitions can be inferred by studying the expectation values of Wilson loops, P_β and P_L, wrapping the temporal and spatial circle respectively, which serve as order parameters. For SYM on $\mathbb{T}^2$ the expectation value $\langle P_L \rangle$ changes from zero (confined phase) to non-zero values (deconfined phase) upon heating the system, whereas $\langle P_\beta \rangle$ is always non-zero at all temperatures (see [23, 24, 242] and references therein).

Now we consider the dual gravity description. This is given by the near-horizon geometry of the spacetime sourced by a stack of N coincident D1-branes of type IIB string theory [239], with a periodic identification on one spatial coordinate. In particular, one is interested in near-extremal black D1-brane configurations of the gravitational theory in the decoupling limit, which were studied in [242]. The classical type IIB supergravity description is valid provided that N is large, to suppress string quantum corrections; α'-corrections are negligible when $t \ll \sqrt{\lambda'}$, while winding modes around the circle can be ignored when $t \gg 1/\sqrt{\lambda'}$. The two conditions imply the window of validity of IIB supergravity description

$$\frac{1}{\sqrt{\lambda'}} \ll t \ll \sqrt{\lambda'}. \tag{3.4.1.2}$$

In this range one may use the type IIB supergravity solution to derive the thermodynamics of 2-dimensional SYM. In this regime, the thermal vacuum of type IIB supergravity is a black hole carrying D1-brane charge that uniformly wraps the compact circle. This solution is thought to be stable and corresponds to the uniform phase.

At temperatures $t \sim 1/\sqrt{\lambda'}$, stringy winding modes become unstable and the type IIB supergravity description is no longer valid. However, one can perform a T-duality transformation acting on the spatial circle, exchanging the theories IIB $\leftrightarrow$ IIA and hence the charges $D1 \leftrightarrow D0$, so we can use type IIA black brane solutions to describe thermal states of SYM on $\mathbb{T}^2$ on that range of temperatures. In this case, the requirement that the supergravity solution is valid gives the conditions

$$t \ll \sqrt{\lambda'}, \qquad t \ll \lambda'^{-1/6}. \tag{3.4.1.3}$$

Since D0-branes are point-like (instead of string-like, as the previous D1-branes), they can distribute the charge over the circle in various ways, either being uniformly or non-uniformly distributed, or localized on the compact circle. These three possibilities give

rise to a non-trivial phase diagram, and it is then a dynamical question which case is preferred.

Ref. [242] showed that the IIA supergravity solution with uniformly distributed D0-brane charge along the compact circle suffers a GL instability at the threshold temperature

$$t_{\rm GL} = \frac{3}{4\sqrt{\pi}} \frac{(2\pi a)^2}{\sqrt{\lambda'}}, \tag{3.4.1.4}$$

where $a \equiv r_0^{\rm GL}/\bar{L} = 0.36671(3)$, i.e.

$$t_{\rm GL} = 2.24646 \frac{1}{\sqrt{\lambda'}}, \quad \text{or} \quad \varepsilon_{\rm GL} = 78.34939 \frac{N}{\lambda'^2}, \tag{3.4.1.5}$$

in the microcanonical ensemble.

For higher temperatures (or lower energies) the charged UBS is thought to be dynamically stable. However, there exists a range of temperatures $t_{\rm GL} < t < t_{\rm PT}$ for some $t_{\rm PT}$, where it is thought (and now known) that the uniform solution becomes globally thermodynamically less favored than the localized black hole solution. Then the temperature $t_{\rm PT}$ represents a first order thermal phase transition between the uniform and localized phase. In the literature this has been termed the Gregory-Laflamme phase transition [23]. The natural interpretation of this picture on the dual gauge theory is a confinement/deconfinement phase transition.

In this section we find the temperature $t_{\rm PT}$ and also $t_{\rm Merger}$, at which the non-uniform and the localized phase merge. Note, however, that the non-uniform phase never dominates any ensemble. So far, lattice simulations on the gauge side estimated the ratio [23]

$$\frac{t_{\rm PT}}{t_{\rm GL}} \sim 1.5. \tag{3.4.1.6}$$

To determine the precise ratio from the gravity dual theory one would need to construct the near-extremal charged solutions, take the near-horizon limit and extract their thermodynamic quantities. Clearly, solving the full system of supergravity equations is a formidable numerical task. However, it is possible to generate charged solutions from uncharged ones via a process of uplifting + boosting + KK reduction [161, 240–242]. Therefore, we can consider the neutral (vacuum) solutions we have previously found and from these obtain the thermodynamics that determine the phase structure of SYM theory under consideration.

Recent construction of KK black holes in $D = 10$ determined the energy or temperature to be $\varepsilon_{\rm PT} = 97.067(N^2/\lambda'^2) = 1.245\varepsilon_{\rm GL}$ or $t_{\rm PT} = 2.451/\sqrt{\lambda'} = 1.093 t_{\rm GL}$ [161]. Since the derivation of the mapping {Black hole thermodynamics on $\mathbb{R}^{1,8} \times S^1$} $\to$ {SYM thermodynamics on $\mathbb{T}^2$} was derived in there we do not include it here; for completeness, it is rederived in detail in the appendix 3.C. Using (3.C.0.11), we have:

$$\begin{aligned} &\varepsilon = 64\pi^4 (2m_0 - s_0 t_0) \frac{N^2}{\lambda'^2}, \qquad t = 4\pi \sqrt{2 s_0 t_0^3} \frac{1}{\sqrt{\lambda'}}, \\ &s = 16\sqrt{2}\pi^3 \sqrt{\frac{s_0}{t_0}} \frac{N^2}{\lambda'^{3/2}}. \end{aligned} \tag{3.4.1.7}$$

Applying this map to the neutral UBS one gets the well-known results [242]:

$$\varepsilon_{\rm UBS}(r_0) = \frac{32\pi^7}{3}\left(\frac{r_0}{\bar{L}}\right)^6 \frac{N^2}{\lambda'^2}, \qquad t_{\rm UBS}(r_0) = 3\pi^{3/2}\left(\frac{r_0}{\bar{L}}\right)^2 \frac{1}{\sqrt{\lambda'}}. \tag{3.4.1.8}$$

At $r_0 = r_0^{\rm GL}$, these expressions correspond to the values $\varepsilon_{\rm GL}$ and $t_{\rm GL}$ previously discussed.

3.4.2 Thermodynamics

In this subsection we construct the phase diagrams in the microcanonical and the canonical ensemble describing the thermodynamics of SYM gauge theory on $\mathbb{T}^2$ using the supergravity approximation. Both diagrams are shown below in Fig. 3.12 and reproduce and complete those in [161]. In addition, we determine for first time the merger point between charged NUBS and LOC.

In Fig. 3.12 we plot dimensionless entropy or free energy difference between a given phase and the uniform one: $(s_i(\varepsilon) - s_{\rm UBS}(\varepsilon)) \times (\lambda'^{3/2}/N^2)$, $(f_i(t) - f_{\rm UBS}(t)) \times (\lambda'^2/N^2)$ with $i =$ NUBS, LOC. Then the uniform phase is represented by a simple horizontal (black) line at the origin of the vertical axis. UBS are unstable for $\varepsilon < \varepsilon_{\rm GL}$ in the microcanonical ensemble and for $t < t_{\rm GL}$ in the canonical ensemble. The non-uniform phase, which exists beyond this point, is never dominant. On the other hand, the localized phase intercepts the uniform one at

$$\varepsilon_{\rm PT} = 97.29477\frac{N^2}{\lambda'^2}, \quad \text{or} \quad t_{\rm PT} = 2.45442\frac{1}{\sqrt{\lambda'}}. \tag{3.4.2.1}$$

The ratios are: $\varepsilon_{\rm PT}/\varepsilon_{\rm GL} = 1.24181$ and $t_{\rm PT}/t_{\rm GL} = 1.09257$, and they are consistent with the predictions from the studies of SYM on the lattice. For energies or temperatures greater than this value, the uniform phase is dominant, and the LOC dominate the corresponding ensemble otherwise. The phase transition is first order, and it is thought to correspond to a confinement/deconfinement phase transition in the gauge side.

Our results allows us to determine, for first time, the merger between LOCs and NUBS with D0-brane charge. From Table 3.1 we can read off $t_0^{\rm Merger}$, $m_0^{\rm Merger}$ and $s_0^{\rm Merger}$, and using (3.4.1.7) one finds that the merger occurs at

$$\begin{aligned} \varepsilon_{\rm Meger}^{\rm NUBS} &= 143.42647\frac{N^2}{\lambda'^2}, \quad \text{or} \quad t_{\rm Merger}^{\rm NUBS} = 2.85934\frac{1}{\sqrt{\lambda'}}, \\ \varepsilon_{\rm Meger}^{\rm LOC} &= 143.41301\frac{N^2}{\lambda'^2}, \quad \text{or} \quad t_{\rm Merger}^{\rm LOC} = 2.85949\frac{1}{\sqrt{\lambda'}}. \end{aligned} \tag{3.4.2.2}$$

Since the non-uniform phase never dominates any of the ensembles (it is a genuinely unstable saddle), it may be difficult to test these numbers using lattice simulations.[8]

[8] However, in a remarkable paper, [265] managed to study a metastable state on the lattice corresponding to the field theory dual to an evaporating black hole. Furthermore, demon's methods in lattice simulations can be used to explore metastable states associated to first order phase transitions. We thank the referee for pointing this out to us.

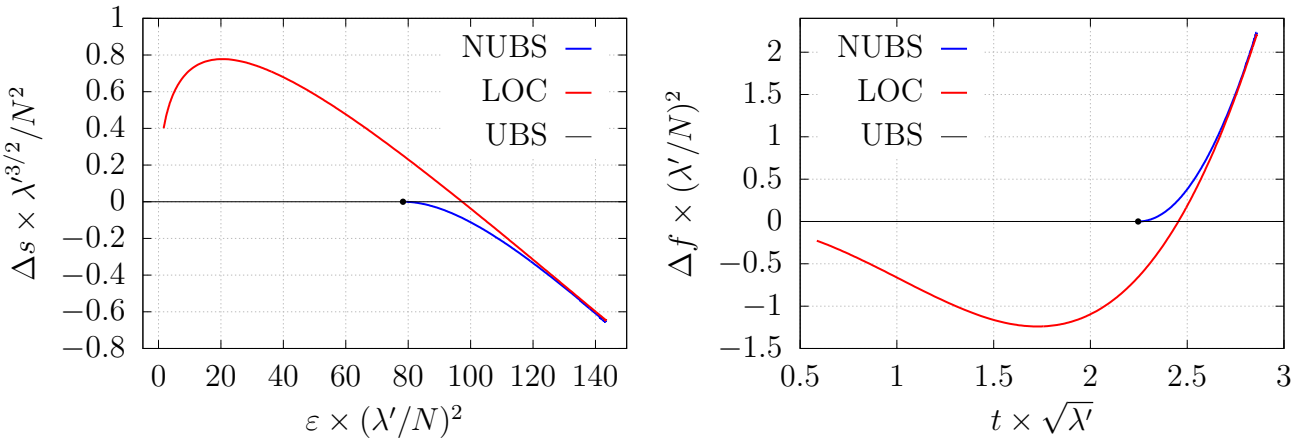

Fig. 3.12: *Phase diagram in the microcanonical ensemble (left) and canonical ensemble (right), of UBS, NUBS and LOC with D0-charge in the decoupling limit. The GL threshold point ε_{GL} or t_{GL} is indicated with a black solid disc.*

3.5 Discussion and outlook

In this chapter we have constructed NUBS and LOC in $D = 10$ and followed these two branches very close to the merger point. $D = 10$ is special from the point of view of this system since this is the critical dimension for the Ricci-flat double-cone metric that was conjectured to control the merger [21]. By fitting the physical quantities of both NUBS and LOC close to the merger point, we have shown that in $D = 10$, their approach to their critical values is governed by a power law plus a logarithmic correction, in accordance to the double-cone model. This result should be contrasted to the results in $D = 5, 6$ obtained in [22], which exhibit a spiraling behavior of the physical quantities as they approach their critical values. Moreover, we have found evidence that in $D = 10$, the merger happens at cusp in the phase diagram, and physical quantities belonging to the NUBS and the LOC emerge from the critical point in the 'same direction'. This feature should be related to the fact that $D = 10$ is the critical dimension for the double-cone metric and it would be very interesting to understand it in detail. To further confirm the double-cone model of the merger, one should construct NUBS and LOC very close to the critical point in $D > 10$ and verify that the physical quantities approach their critical values according to the predictions of the double-cone model. Work in this direction is underway.

We have not discussed the dynamical stability of NUBS and LOC. Ref. [138] considered the evolution of the GL instability of black strings in the large-D expansion and showed that they settle on a stable NUBS. More recently, [233] included corrections beyond the leading order term in the large-D expansion, and found that the endpoint depends on the thickness of the initial black string. For the cases where the black string is expected to pinch off, [138] could not follow the evolution all the way to the end. It would be very interesting to study the evolution of the instability of

uniform black strings for large yet finite D. The techniques used in [145,148,153] seem appropriate and we are currently investigating this problem.

With the methods of [22] and those used in this chapter, one can study the details of the mergers of other black hole systems of interest. In particular, for lumpy and localized black holes in $AdS_5 \times S^5$. Moreover, recently [24] obtained accurate results of the thermal phase diagram of $1+1$ SYM on a twisted torus using lattice simulations. It would be very interesting to compare their results using the supergravity approximation, but to do so one needs to consider NUBS that are electrically charged with respect to a 2-form.

3.A Generic integration domain for localized solutions

In this appendix we describe the integration domain we have used to construct the localized black holes. Due to their nature, the numerical construction involves to work in two separate coordinates systems, one adapted to the asymptotic behavior and another one adapted to the near horizon behavior.

The construction considered in [22] takes the near chart (r, a) with five boundaries and divides it into three different subdomains. This encompasses the horizon, the axis, the boundaries of the internal space and a shared boundary with the far patch. The blue and green regions in Fig. 3.13, say region 1 in the near patch, are covered by polar coordinates $r \in [r_0, r_1]$, $a \in [0, \pi/2]$ whose relation with the far patch is simply given by $x(r, a) = r \cos a$, $y(r, a) = r \sin a$. The orange and yellow regions, say regions 2 and 3, are covered by polar-like coordinates with a modified radial coordinate which is parametrized in terms of $v \in [r_1, L/2]$. In the orange region $a \in [0, \pi/4]$, whereas in the yellow one $a \in [\pi/4, \pi/2]$. The precise relation with the far coordinates is: $x(v, a) = r_k(v, a) \cos a$, $y(v, a) = r_k(v, a) \sin a$, with

$$r_k(v,a) = r_1 \frac{L/2 - v}{L/2 - r_1} + \frac{L}{2} \frac{v - r_1}{L/2 - r_1} \frac{1}{\delta_{k2} \cos a + \delta_{k3} \sin a}\,, \qquad k = 2, 3\,. \tag{3.A.0.1}$$

Here r_0 and r_1 ($< L/2$) are parameters that we are free to specify, and L is the asymptotic length of the Kaluza-Klein circle. Notice that this construction assumes that the angular coordinate in the near patch 1 is further divided into two subregions: one patch where $a \in [0, \pi/4]$, to match the density of grid points with that in the near patch 2, and another one where $a \in [\pi/4, \pi/2]$ to match the density of grid points with region 3. We also consider the mesh-refinement (2.2.2.13) near the axis, $\tilde{a} = \text{mesh}(a; \pi/2, a_*, \chi_1)$, and near the horizon, $\tilde{r} = \text{mesh}(r; r_0, r_*, \chi_2)$.

The far chart (x, y) covers the ranges $x \in [L/2, \infty)$ and $y \in [0, L/2]$. To deal with the infinity, the coordinate x is compactified introducing a new coordinate $\xi \in [-1, 1)$. Ref. [22] considers $x(\xi) = L/(1 - \xi)$, such that $\xi = -1$ corresponds to the shared boundary $x = L/2$ with the near patch and $\xi = 1$ corresponds to asymptotic infinity. The problem with this is that to find the charges C_τ and C_y, i.e. the mass and the tension, one needs to consider the asymptotic expansion of the metric components

up to $(D-4)$th order, which implies to take $D-4$ derivatives. Of course, this is problematic for $D > 5, 6$. We overcome this issue by considering the compactification

$$x(\xi) = \frac{L}{2}\left(\frac{2}{1-\xi}\right)^{\Delta}, \tag{3.A.0.2}$$

where $\Delta = (D-4)^{-1}$ has been defined in §3.2.2. This way we still have $x(-1) = L/2$ and $x(1) = \infty$, but it is sufficient to consider the metric expansion at infinity up to 1st order. In particular, the charges are given by 1st derivatives of the metric,

$$C_\tau = 2\left(\frac{L}{2}\right)^{D-5}\int_0^{L/2} \mathrm{d}y \frac{\partial Q_1}{\partial \xi}\bigg|_{\xi=1}, \qquad C_y = -2\left(\frac{L}{2}\right)^{D-5}\int_0^{L/2} \mathrm{d}y \frac{\partial Q_4}{\partial \xi}\bigg|_{\xi=1}. \tag{3.A.0.3}$$

Additionally, each patch has been further divided into other small subregions in order to be able to increase the grid resolution just where it is necessary. This is of particular interest since as we increase D gravity turns out to be more localized and the spacetime region close to the horizon needs special care. Moreover, close to the merger point with NUBS, some functions develop steep gradients. In practice, the radial coordinate in the near patch 1 is divided into two subdomains, and the compactified coordinate ξ in the far patch is divided into three subdomains. In the near patches containing the axis, the angular coordinate is also divided into two subregions. In total, this introduces four new parameters in the integration domain: r_*, ξ_*, ξ_{**} and a_*, corresponding to the values where the different patches meet. At each shared boundary, either near-near, near-far or far-far patch, one must impose continuity of the functions and their first normal derivatives.

To impose these matching conditions one may consider the same grid point densities from both sides of a given shared boundary. Alternatively, one can still require continuity of the function and its normal derivative by performing the matching on an interpolation function. Unlike [22], we have opted to work with the same grid point densities. They are naturally always the same except at the shared boundary between near and far patches. We fix this by considering the coordinate y given in terms of a coordinate σ lying in the unit interval $\sigma \in [0, 1]$:

$$y(\sigma) = \frac{L}{2}\tan\left(\frac{\pi}{4}\sigma\right). \tag{3.A.0.4}$$

Using Chebyshev grid points for σ, then the grid points along the y-direction are properly distributed.

To check whether our code with the described modifications gives rise to reasonable solutions and, in particular, accurate values for the mass, we compare the obtained results, (i) for small localized black holes, with the mass of a Schwarzschild black hole in $D = 10$, or (ii) with the perturbative results.

For small localized black holes one expects that the spacetime metric can be systematically expanded in a perturbation series with a small parameter ρ_0/L, being ρ_0 the location of the horizon. The best available perturbative approximation for the

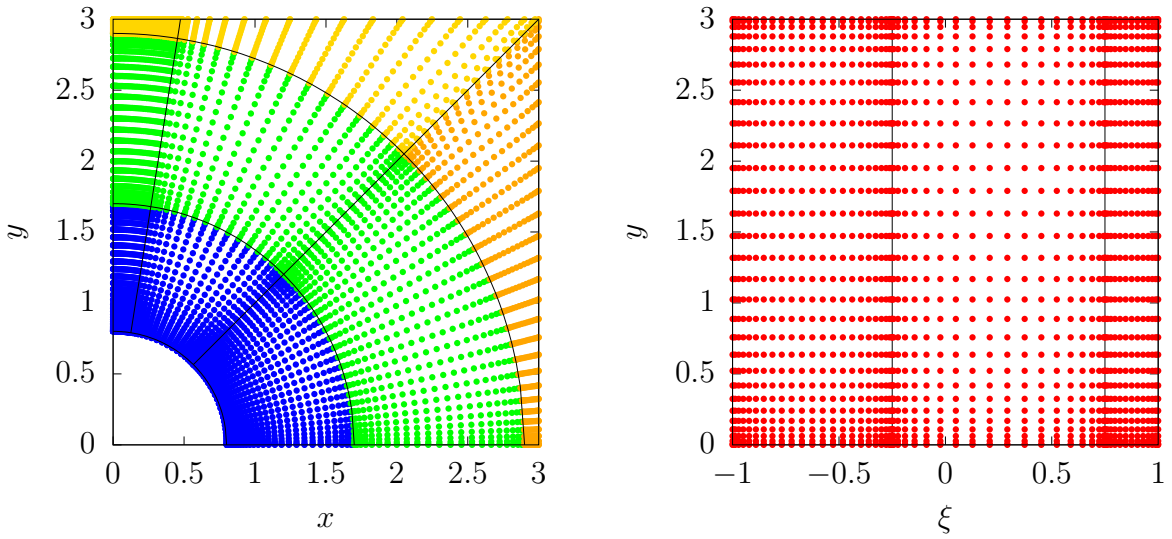

Fig. 3.13: *Physical grid with parameters:* $L = 6$, $r_0 = 0.8$, $r_* = 1.7$ *and* $r_1 = 2.9$, $a_* = 0.9 \times (\pi/2)$, $\xi_* = -0.25$, $\xi_{**} = 0.75$, $\chi_1 = 2.5$ *and* $\chi_2 = 3$. *Near patch (left) and far patch (right) in terms of the compactified* ξ*-coordinate.*

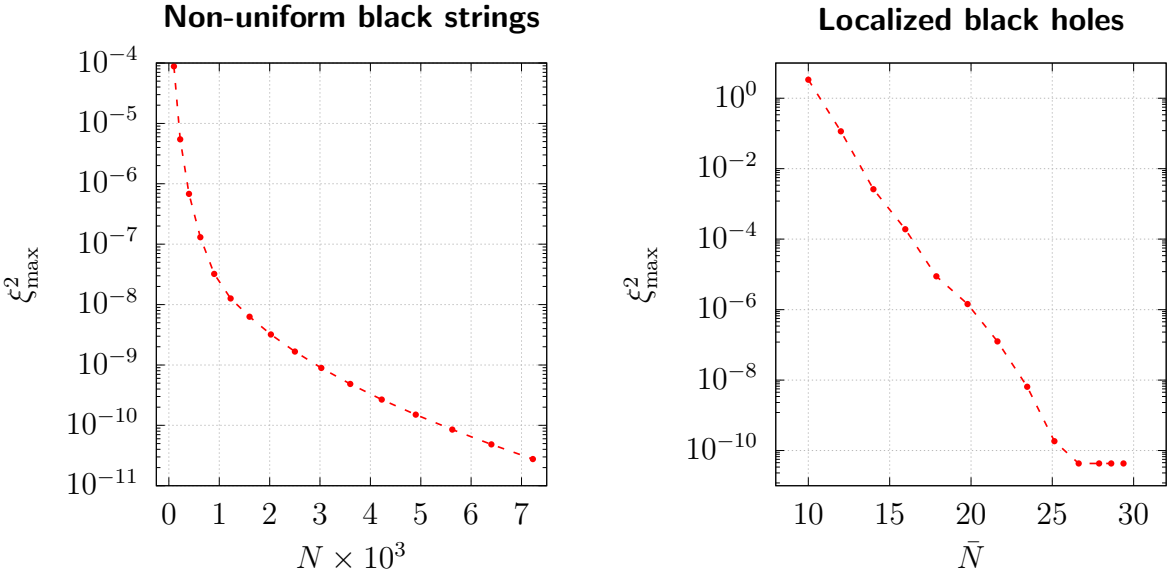

Fig. 3.14: *Logarithmic plot of* $\xi^2_{max} = max[\xi^2]$ *as a function of the grid size. In both cases, the error decays exponentially, as expected.*

thermodynamic quantities, with D arbitrary, are given in [198]. (We did not include these curves in our plots in §3.3.1 or §3.4.2 since they were not much clarifying.) For small enough black holes, i.e. with eccentricity $\epsilon < 10^{-3}$, our numerical values differ by less than a 0.05% when compared to those obtained by (i) or (ii). From the geometrical point of view, another check is to compare L_{polar} defined in (3.3.2.3), with one half

of the perimeter of a Schwarzschild black hole of the same temperature in $D = 10$. In this case the deviations are always less than 0.01%.

3.B Convergence tests

In this appendix we check that our numerical solutions converge to the continuum limit according to our discretization scheme. In the case of using pseudo-spectral methods, the error should be exponentially suppressed with increasing the grid size. To monitor it we use the squared norm of the DeTurck vector ξ^2. We expect it to become zero in the continuum limit. Indeed, Fig. 3.14 shows that our numerical implementation exhibits the expected behavior.

To produce this figure we picked up a reference solution of each branch, we interpolated it at different resolutions and then we filtered through the Newton-Raphson loop. For each output we computed the quantity of interest. For NUBS we just considered one single patch with resolution $N = N_x N_y$, being N_x and N_y the number of grid points in each direction. In the case of LOC, we considered the usual 12 patches and varied the mean resolution $\bar{N}$.

3.C D0-charge via uplifting + boosting + Kaluza-Klein reduction

In this appendix we derive the mapping between the thermodynamics of neutral Kaluza-Klein black solutions and the thermodynamics of near-extremal D0-black branes on a circle of type IIA supergravity [161,240–242]. This involves a M-theory lift-boost-reduce procedure.

Consider any static, axially symmetric metric solving $R_{\mu\nu} = 0$ in D spacetime dimensions and approaching the direct product manifold $\mathbb{R}^{1,D-2} \times \bar{S}^1$ asymptotically. The bar notation in $\bar{S}^1$ (of length $\bar{L}$) is to distinguish, in $D = 10$, the T-dual circle of type IIA supergravity from the original circle of length L of the type IIB theory. This solution can be written using isotropic coordinates:

$$\mathrm{d}s^2 = -f^2 \mathrm{d}t^2 + g^2 \left(\mathrm{d}\rho^2 + \rho^2 \mathrm{d}\Omega^2_{D-3}\right) + h^2 \mathrm{d}y^2, \tag{3.C.0.1}$$

with the generic functions f, g and h approaching 1 at $\rho \to \infty$, and $y \sim y + \bar{L}$ is the coordinate of $\bar{S}^1$. If (3.C.0.1) is a black hole with a Killing horizon located at $\rho = \rho_0$, then $f(\rho_0, y) = 0$. We can construct the dimensionless quantity $p_0 \equiv \rho_0/\bar{L}$ to label a given family of such metrics.

Now uplift the solution adding a compact coordinate z, $\mathrm{d}\hat{s}^2_{D+1} = \mathrm{d}s^2 + \mathrm{d}z^2$. Boosting along z with rapidity parameter α yields a solution to vacuum general relativity in $D + 1$ dimensions. Upon dimensional reduction with respect to z we rewrite the metric as

$$\mathrm{d}\hat{s}^2_{D+1} = e^{-2\eta\phi} \mathrm{d}s^2_D + e^{2\zeta\phi} \left(\mathrm{d}z - A_t \mathrm{d}t\right)^2, \tag{3.C.0.2}$$

with $\eta^2 = (2(D-1)(D-2))^{-1}$ and $\zeta = (D-2)\eta$. This choice of constants ensures an Einstein framed dimensionally reduced action and canonical normalization for the dilaton kinetic term. For $D = 10$, this procedure allows us to construct solutions of type IIA supergravity with only graviton, dilaton and 1-form field excitations.

The new metric, the non-trivial dilaton field and the 1-form gauge field are identified to be:

$$\begin{aligned} \mathrm{d}s_D^2 &= H^{\frac{2}{D-2}} \left(-\frac{f^2}{H^2}\mathrm{d}t^2 + g^2 \left(\mathrm{d}\rho^2 + \rho^2 \mathrm{d}\Omega_{D-3}^2 \right) + h^2 \mathrm{d}y^2 \right), \\ e^{\phi} &= H^{1/\zeta}, \\ A_{(1)} &= \left(H^{-2} - 1 \right) \coth\alpha \, \mathrm{d}t \,, \end{aligned} \tag{3.C.0.3}$$

where $H^2 = 1 + (1 - f^2)\sinh^2\alpha$. This works because momentum around the circle in the $(D+1)$th dimension is reinterpreted as D0-brane charge from the lower-dimensional viewpoint [241].

We can start with (3.C.0.1) being a neutral non-uniform black string or localized black hole, and obtain the charged solution using (3.C.0.3) (which depends on the parameter α in addition to ρ_0). Since we are interested in their thermodynamics rather than the solutions themselves, we will proceed by expressing the quantities of interest of the new charged solutions in terms of the uncharged ones. For instance, it easy to see that the temperature and the entropy of the charged solution are simply shifted by a factor of $\cosh\alpha$ with respect to the uncharged ones. To be precise,

$$T = \frac{1}{\bar{L}\cosh\alpha} t(p_0), \qquad S = \frac{1}{4G_D} \bar{L}^{D-2} \Omega_{D-3} \cosh\alpha \, s(p_0), \tag{3.C.0.4}$$

where $t(p_0)$, $s(p_0)$ encode the parametric dependence of dimensionless temperature and entropy of neutral solutions. The mass and the charge can be obtained from the asymptotic expansion of the metric and the gauge field. Because (3.C.0.1) is asymptotically KK, for large ρ we may expand

$$f(\rho, y) \simeq 1 - c_t(p_0) \frac{\bar{L}^{D-4}}{\rho^{D-4}}, \qquad h(\rho, y) \simeq 1 + c_y(p_0) \frac{\bar{L}^{D-4}}{\rho^{D-4}}. \tag{3.C.0.5}$$

Taking the square and considering the factors of H, one obtains the effective charges for the solution (3.C.0.3), $C_t(p_0)$ and $C_y(p_0)$, entering in the expression (3.2.1.3). The D0-charge may be obtained from the flux or from the asymptotic behavior of the gauge field, and the chemical potential is given by $\mu = -A_t\big|_{\rho=\rho_0} = \tanh\alpha$. The result is:

$$\begin{aligned} M &= \frac{\bar{L}^{D-3}\Omega_{D-3}}{8\pi G_D} \left((D-3)c_t(p_0) - c_y(p_0) + (D-4)c_t(p_0)\sinh^2\alpha \right), \\ Q &= \frac{\bar{L}^{D-3}\Omega_{D-3}}{8\pi G_D} (D-4) c_t(p_0) \sinh\alpha\cosh\alpha. \end{aligned} \tag{3.C.0.6}$$

Now set $D = 10$. The derived quantities so far correspond to the thermodynamic quantities of the charged solution (3.C.0.3) of type IIA supergravity with a metric,

a dilaton and a 1-form. At this point note that all physical quantities appearing in (3.C.0.4) and (3.C.0.6), reduce to those of the uncharged solution in the limit $\alpha \to 0$. The opposite limit $\alpha \to \infty$ corresponds to take the near-extremal limit. To obtain the desired mapping we have to take the decoupling limit of Ref. [239] of near-extremal configurations, which sends the string length ℓ_s to zero while keeping $g^2_{\rm YM}$ fixed. According to holography, these are dual to the decoupled field theory at finite temperature. To proceed one needs the relation between the 10-dimensional Newton's constant and the string length and coupling constant, given in (1.3.0.1) (with 'bar' string coupling), the T-dual relations [288]:

$$\bar{L} = \frac{(2\pi\ell_s)^2}{L}, \qquad \bar{g}_s = \frac{2\pi\ell_s}{L} g_s, \tag{3.C.0.7}$$

and the relation between the string coupling and SYM coupling. In the case of IIB string theory with D1-branes, this is given by

$$g^2_{\rm YM} = (2\pi)^{p-2} g_s \ell_s^{p-3}, \tag{3.C.0.8}$$

with $p = 1$ [239]. To translate back the quantities above in terms of SYM variables recall that $\lambda' = \lambda L^2 = N g^2_{\rm YM} L^2$.

The dimensionless energy above extremality, $\varepsilon = L\mathcal{E} = L(M - Q)$, in these limits corresponds to the energy density of the SYM theory. Since this becomes independent of ℓ_s, the decoupling limit is trivial. The decoupling limit of the temperature and the entropy needs to be taken with more care. At the end, one finds that the dimensionless energy, temperature and entropy associated to a stack of N-coincident near-extremal D0-branes in the decoupling limit are:

$$\begin{aligned} \varepsilon &= \frac{16}{3}\pi^7 \left(4c_t(p_0) - c_y(p_0)\right) \frac{N^2}{\lambda'^2}, \qquad t = 2\pi^{5/2}\sqrt{2c_t(p_0)}\, t(p_0) \frac{1}{\sqrt{\lambda'}}, \\ s &= \frac{16}{3}\pi^{11/2} \frac{s(p_0)}{\sqrt{2c_t(p_0)}} \frac{N^2}{\lambda'^{3/2}}. \end{aligned} \tag{3.C.0.9}$$

These expressions explicitly depend on functions that can be obtained from the KK vacuum solution (3.C.0.1). Clearly, the numerical solutions found in §3.2 are not written in isotropic coordinates which difficult the computation of such functions. It is then convenient to write (3.C.0.9) in terms of gravitational variables which are intrinsic of the solution instead of the coordinates. To this end, set $\alpha = 0$ in (3.C.0.4) and (3.C.0.6) and solve for the functions $t(p_0), s(p_0), c_t(p_0)$ and $c_y(p_0)$. The Smarr's relation closes the system of equations. The solution is:

$$\begin{aligned} t(p_0) &= t_0, & s(p_0) &= \frac{4 s_0}{\Omega_{D-3}}, \\ c_t(p_0) &= \frac{8\pi}{\Omega_{D-3}} \frac{t_0 s_0}{D-4}, & c_y(p_0) &= \frac{8\pi}{\Omega_{D-3}} \left(\frac{D-3}{D-4} t_0 s_0 - m_0 \right), \end{aligned} \tag{3.C.0.10}$$

where $t_0 = \bar{L}T$, $m_0 = M/\bar{L}^{D-3}$ and $s_0 = S/\bar{L}^{D-2}$ are the dimensionless temperature, mass and entropy of the neutral gravity solutions. Setting $D = 10$ and inserting these

expressions back into (3.C.0.9), gives the final mapping:

$$\begin{aligned} \varepsilon &= 64\pi^4 \left(2m_0 - s_0 t_0\right) \frac{N^2}{\lambda'^2}, \qquad t = 4\pi \sqrt{2 s_0 t_0^3} \frac{1}{\sqrt{\lambda'}}, \\ s &= 16\sqrt{2}\pi^3 \sqrt{\frac{s_0}{t_0}} \frac{N^2}{\lambda'^{3/2}}. \end{aligned} \tag{3.C.0.11}$$

Chapter 4
Critical Black Holes in $AdS_p \times S^q$

This chapter is based on [2], authored in collaboration with P. Figueras. The numerical code and posterior data analysis was written and carried out by the author of this thesis and the calculations were verified by P. Figueras.

4.1 Introduction and results

The gauge/gravity duality has become an important tool to unravel the physics of certain quantum field theories (QFTs) at strong coupling, where the traditional techniques of perturbation theory fail. With the current understanding of the duality, its power mostly lies on the 'gravity side' of the correspondence, which involves (semi-)classical theories of gravity that, in general, are more tractable than their respective field theory duals. The first example of the gauge/gravity duality was introduced by Maldacena in [162]. This was originally coined as the AdS/CFT correspondence, since it relates a conformal field theory (CFT) such as $\mathcal{N} = 4$ super Yang-Mills in $3+1$ spacetime dimensions and gauge group $\mathrm{SU}(N)$ to type IIB superstring theory in $\mathrm{AdS}_5 \times S^5$. Although the equivalence was conjectured to be true for generic values of N and g_{YM} (the gauge theory coupling constant), the duality is better understood in the large N and large (effective) 't Hooft coupling $\lambda = g^2_{\mathrm{YM}} N$ limit, where the dual superstring theory reduces to classical supergravity in $\mathrm{AdS}_5 \times S^5$ [166, 171]. By now, the duality has been extended to other dimensions and even to non-conformal settings. The literature on the subject is vast and we will not review it here (see the textbook [291] for a review and extensive references).

In this Chapter we are interested in equilibrium static black holes in asymptotically global $\mathrm{AdS}_p \times S^q$ spacetimes. By the gauge/gravity duality, these black holes are dual to thermal phases of certain gauge theories. The field theory is defined at the boundary, B_{p-1}, of the p-dimensional Anti-de Sitter (AdS) space, which enjoys a time-like conformal structure at infinity.[1] For instance, if B_{p-1} is taken to be Minkowski space, then the bulk spacetime is asymptotically AdS_p in Poincaré coordinates. In the Poincaré patch there exist two homogeneous solutions of the Einstein's equations,

[1] The internal manifold, S^q in our case, is reflected in the field content of the dual gauge theory.

namely pure AdS_p and the planar Schwarzschild-AdS_p black hole. However, the latter always dominates the canonical ensemble and there are no phase transitions. This is consistent with the fact that a CFT cannot have phase transitions on a scale invariant background such as Minkowski space. Considering B_{p-1} to be a space with non-zero curvature [266] can lead to new and interesting physics. In the simplest case, one can take B_{p-1} to be the Einstein static universe (ESU), $\mathbb{R} \times S^{p-2}$, which corresponds to consider asymptotically global AdS_p spacetimes in the bulk. In this case, there exists the well-known Hawking-Page phase transition [195] between global AdS_p and (large) Schwarzschild black holes in that background. This phase transition was later re-interpreted by Witten [163] (see also Ref. [164]) as a confinement/deconfinement phase transition in the dual CFT.

So far the discussion has ignored the dynamics in the internal manifold, namely the S^q in our case. There are situations where the internal geometry leads to new and interesting dynamics. This is famously the case for the Gregory-Laflamme (GL) instability of black branes [130], whose endpoint has led to counterexamples of the weak cosmic censorship conjecture in higher dimensions [137]. In fact, soon after the discovery of the GL instability, it was suggested that black holes in global AdS would undergo a similar dynamical instability that should lead to localization in the internal space [267, 268]. The instability of black holes in global AdS was addressed in [156], who found the threshold zero (i.e., time-independent) mode(s) for the Schwarzschild-$AdS_5 \times S^5$ black hole. In that paper it was shown that small (compared to the AdS radius) Schwarzschild-$AdS_5 \times S^5$ black holes had zero modes (preserving a SO(5) isometry) when the negative modes of the Schwarzschild-AdS black hole [269] coincided with the momentum along the internal space. For the latter, being a S^5, modes are expanded in terms of spherical harmonics, which are labeled by the harmonic number ℓ. Then there exists an infinite number of zero modes, one for each (discrete) value of ℓ and the corresponding specific horizon radius.

The existence of zero modes suggests two things: First, the presence of a dynamical instability and, second, the existence of new branch of static black holes. Indeed, in the case of the GL instability of black strings, [13, 14] first showed that there exists a new branch of non-uniform black strings that emanates from the uniform string branch precisely at the onset of the GL instability. Similarly, [19] constructed asymptotically global $AdS_5 \times S^5$ black holes with non-uniform horizons along the S^5 that emanate from the Schwarzschild-$AdS_5 \times S^5$ black holes at the onset of GL instability for the $\ell = 1$ and $\ell = 2$ modes respectively. These so-called lumpy black holes have the same horizon topology as their Schwarzschild-$AdS_5 \times S^5$ counterparts, but no longer preserve the full isometry group of the internal space. In the examples of [19], only a round S^4 inside the internal S^5 is preserved. The role of the lumpy black holes in the space of black hole solutions $AdS_5 \times S^5$ is analogous to that of the non-uniform black strings in the context of black holes in standard Kaluza-Klein (KK) theory. Similar to the fact that there exist localized black holes in KK theory [18], there also exist black holes in $AdS_5 \times S^5$ that are localized on the S^5. The latter were numerically

constructed in [20]. The localized black holes of [20] should presumably merge with the $\ell = 1$ lumpy black holes, but the branches of solutions in [19] and [20] are still quite far from the merger point. One of the goals of this chapter is to get close to this point from the lumpy black holes side.

Mergers in the space of static black hole solutions in general relativity have been thoroughly studied in the context of KK theory. Kol [21] proposed that the horizon topology change between the two branches is locally described by conifold-type-of transition, controlled by a (singular) self-similar double-cone geometry. This double-cone model has been confirmed for the localized black hole/non-uniform black string transition [238] (see also the recent studies [1, 22, 157–159]) and in asymptotically flat space [147, 160]. One non-trivial prediction of the double-cone model is that the behavior of any physical quantity Q near the critical point is given by

$$Q = Q_{\rm c} + C_+ \rho_0^{s_+} + C_- \rho_0^{s_-}, \tag{4.1.0.1}$$

where $Q_{\rm c}$ is the value of Q at the critical point, ρ_0 is any length that measures the deviation from the cone, and s_+ and s_- are the critical exponents that govern the perturbations away from the double-cone geometry. These critical exponents are dimension dependent, and they are complex for $D < 10$ and purely real for $D > 10$; $D = 10$ is a degenerate case that leads to a power law with a logarithmic correction. This behavior of the physical quantities near the critical point has been beautifully confirmed for $D < 10$ [157] and $D = 10$ [1, 22]. Whilst physical quantities may be defined on the whole horizon, Eq. (4.1.0.1) indicates that sufficiently close to the critical point in a topology-change transition, they are actually governed by the regions of the horizon that pinch-off.

So far no topology change transitions analogous to the localized black hole/non-uniform black string have been studied in AdS. In this chapter we fill this gap by numerically constructing critical lumpy black holes. We review, correct and extend the work of [19] by constructing lumpy black holes in AdS$_5 \times S^5$ and AdS$_4 \times S^7$ with non-uniformity parameters (see Section 4.3 for the definition) $\lambda \sim 25$ and $\lambda \sim 104$ (for $\ell = 1$) respectively.[2] Ref. [19] only considered the AdS$_5 \times S^5$ case, and from their plots we have estimated that their most critical solutions have $\lambda \sim 2$. For the $\ell = 1$ lumpy family, the phase diagrams that we obtain exhibit some differences compared to those reported in [19], with our branches being shorter (see Section 4.4.1). This may appear to be a little surprising since we have managed to construct solutions with significantly larger values of λ and hence closer to the critical point; these discrepancies can be attributed to the different quality of our numerical solutions and theirs. To get closer to the critical point, we employ the sophisticated methods that we successfully used in [1] (see also [22, 157] and Section 4.3.4). As we will show in Section 4.4.4, in the context of asymptotically AdS$_p \times S^q$ black holes, the critical geometry is controlled by a triple cone which is not Ricci-flat anymore. We have checked that to leading order

[2] Following [13], from now on we will exclusively use λ to denote the non-uniformity parameter, as is customary in the field. This should not be confused with the 't Hooft coupling.

the behavior near the critical point of physical quantities of the different families of lumpy black holes that we have constructed (more specifically $\ell = 1, 2, 3$) is given by (4.1.0.1). Furthermore, the critical exponents obtained from our numerical solutions (see Tables 4.3 and 4.4) match the prediction of the triple-cone model. Therefore, we are confident of the correctness and accuracy of our numerical solutions.

Another novelty of our work is that we use the holographic dictionary to extract how the physics of the topology change is imprinted in the dual field theory observables. Using the tools of KK holography [270], we extract the vacuum expectation values (vev's) of the boundary stress-energy tensor and certain scalar operators (see Section 4.4).[3] The latter parametrize the deformations of the internal space and, unsurprisingly, near the critical point they exhibit the behavior predicted by the triple-cone model (4.1.0.1). This result can be interpreted as a prediction from holography of how the dual field theory may detect a topology change in the bulk. We should point out that our results from KK holography differ from those of [19]. In particular, the expressions for the holographic stress-energy tensor and the scalar vev's are different, and we also find that $\langle \mathcal{O}_{\mathcal{T}^4} \rangle = 0$. To correct errors and typos in the literature, we felt the need to provide an extensive review of KK holography and the details of our calculations in Appendices 4.A and 4.B.

So far we have focused on asymptotically $\mathrm{AdS}_5 \times S^5$ lumpy black hole solutions since these are the relevant ones for type IIB supergravity in ten spacetime dimensions. In this chapter we also consider lumpy black holes in asymptotically $\mathrm{AdS}_4 \times S^7$ spacetimes, hence they are solutions to 11-dimensional supergravity/M-theory.[4] In this case, the only bosonic fields are the metric and the 4-form field strength. The equations of motion for the bosonic fields in this theory are simpler than in the IIB case (because there is no self-duality condition for the field strength), which allows us to get much closer to the merger point and test the triple-cone model with exquisite detail. Lumpy black holes in this theory should be dual to certain thermal phases of ABJM theory [271].

The gravity problem

As stated at the beginning, our problem consists of finding static black holes that are solutions to certain supergravities and are asymptotically $\mathrm{AdS}_p \times S^q$ (so $D = p + q$ is the total number of spacetime dimensions) such that the S^{p-2} inside AdS and an S^{q-1}

[3] This is only possible when the $\mathrm{SO}(q+1)$ isometry of the internal S^q is broken, as it occurs at the threshold point of the GL instability of small Schwarzschild-AdS black holes [156], and persists along the lumpy branches. Holographically, this is interpreted as a spontaneous symmetry breaking in the dual gauge theory.

[4] We could also have considered $(p, q) = (7, 4)$ within $11D$ supergravity; other possibilities are, for instance, type IIB supergravity with a 3-form field strength, corresponding to $(p, q) = (7, 3)$, or type IIA supergravity with a Ramond-Ramond (RR) 2- or 4-form. In this case one can presumably construct black hole solutions for $(p, q) = (4, 6)$, $(8, 2)$ and $(6, 4)$, respectively.

inside the S^q are round. Asymptotically, the solutions must tend to the metric:

$$\mathrm{d}s^2_{\mathrm{AdS}\times\mathrm{S}} = \mathrm{d}s^2_{(p)}(\mathrm{AdS}) + R^2\mathrm{d}\Omega^2_{(q)}, \tag{4.1.0.2}$$

where R denotes the radius of the S^q. R is fixed by supersymmetry in terms of the radius L of the AdS factor. For $(p,q) = (5,5)$ and $(4,7)$, the background metric (4.1.0.2) is a solution to the bosonic sector of type IIB SUGRA with only a RR self-dual 5-form field strength or $11D$ SUGRA respectively.

The actions for the theories considered in this study can be derived requiring local supersymmetry and we truncate them to the desired field content. We have considered the following normalizations for the field strengths:

$$\begin{aligned} S_{\mathrm{IIB}} &= \frac{1}{16\pi G_{10}}\int\left(R\star\mathbb{1} - \frac{1}{4}\star F_{(5)}\wedge F_{(5)}\right), \\ S_{11D} &= \frac{1}{16\pi G_{11}}\int\left(R\star\mathbb{1} - \frac{1}{2}\star F_{(4)}\wedge F_{(4)}\right), \end{aligned} \tag{4.1.0.3}$$

where $F_{(n)} = \mathrm{d}A_{(n-1)}$. In type IIB case, one has to additionally impose the self-duality condition $F_{(5)} = \star F_{(5)}$ after deriving the equations of motion.

A few comments are in order. First, notice that in $D = 10$, this is the minimal field content consistent with the symmetries. Since the S^3 within the AdS$_5$ factor is assumed to be round, a 3-form field strength would also be compatible with the symmetry, but it is not necessary. For simplicity, in this study we have turned it off. We leave for future work the problem of exploring for phase diagram of asymptotically AdS$_5\times S^5$ black hole solutions with an additional 3-form field strength. Second, in $D = 11$ the action contains a Chern-Simons term,

$$S^{\mathrm{SC}}_{11D} \sim \int F_{(4)}\wedge F_{(4)}\wedge A_{(3)}, \tag{4.1.0.4}$$

whose coefficient is fixed by supersymmetry. However, for static configurations and with the symmetry assumptions of this analsyis, the Chern-Simons term does not contribute and we omit it.

The equations of motion that one obtains from (4.1.0.3) can be written as follows:

$$\begin{aligned} &R_{MN} - \frac{1}{96}F_{(5)MPQRS}F_{(5)N}{}^{PQRS} = 0, \qquad \mathrm{d}F_{(5)} = 0, \qquad F_{(5)} = \star F_{(5)}, \\ &R_{MN} - \frac{1}{12}\left(F_{(4)MOPQ}F_{(4)N}{}^{OPQ} - \frac{1}{12}g_{MN}|F_{(4)}|^2\right) = 0, \qquad \mathrm{d}\star F_{(4)} = 0. \end{aligned} \tag{4.1.0.5}$$

The indices run over the whole number of spacetime dimensions. None of the equations for the metric has a 'bare' cosmological constant. Instead, this emerges from the flux of the gauge field, allowing the background (4.1.0.2) to be a solution of (4.1.0.5) with:

$$\begin{aligned} F_{(5)} &= \frac{4}{L}\left(\mathrm{vol}(\mathrm{AdS}_5) + \mathrm{vol}(S_5)\right), \qquad R = L, \\ F_{(4)} &= \frac{3}{L}\mathrm{vol}(\mathrm{AdS}_4), \qquad\qquad\qquad\quad R = 2L. \end{aligned} \tag{4.1.0.6}$$

Numerical approach

As for the numerical approach, we implement the Einstein-DeTurck equation discussed in Chapter 2. Originally, this was intended to solve static problems in vacuum Einstein's gravity [214], but it can be straightforwardly generalized to include matter. In fact, matter does not modify the principle part of Einstein's equations and therefore the non-vacuum Einstein-DeTurck equation:

$$R^H_{MN} \equiv R_{MN} - 8\pi G\left(T_{MN} - \frac{1}{D-2}g_{MN}T\right) - \nabla_{(M}\xi_{N)} = 0, \tag{4.1.0.7}$$

is manifestly elliptic on static metrics. ξ_M is the already known DeTurck vector,

$$\xi^M = g^{NO}\left(\Gamma^M_{NO} - \bar{\Gamma}^M_{NO}\right), \tag{4.1.0.8}$$

containing the usual Levi-Civita connection Γ compatible with the spacetime metric g, and a Levi-Civita connection $\bar{\Gamma}$ compatible with some reference metric $\bar{g}$ that we are free to prescribe. Additionally, there are also the matter field equations which will not be elliptic due to the underlying local gauge symmetry

$$A_{(n-1)} \to A_{(n-1)} + \mathrm{d}\Lambda_{(n-2)}, \tag{4.1.0.9}$$

where $\Lambda_{(n-2)}$ is an arbitrary $(n-2)$-form. The matter equations can also be modified by adding a DeTurck-like term, but in this case it will be easier to fix the gauge algebraically with a suitable ansatz for the gauge field.

For static spacetimes that are either asymptotically flat, KK or AdS, and whose boundary conditions are compatible with ξ_M vanishing at the boundaries of the manifold (if any exist), [224] showed that all solutions to $R^H_{MN} = 0$, are necessarily Einstein. Even though the proof of [224] is for the pure gravity case, it should be straightforward to generalize to the present case. In fact, as we shall see below, for our particular problem, the boundary conditions that we impose fall within the class considered in [224], and hence solving (4.1.0.7) is equivalent to solving the Einstein equations. In practice, we use the square of the DeTurck vector, $\xi^2 \equiv \xi_M\xi^M$, to quantify the validity of our numerical solutions and to perform convergence tests. More details about the DeTurck method can be found in §2.1 of Chapter 2 and references therein.

From the technical point of view, the equations are always discretized using pseudo-spectral methods on a Chebyshev grid and we solve them by a standard iterative Newton-Raphson method. See §2.2 of Chapter 2.

Organization of this chapter

The rest of this chapter is organized as follows. In Section 4.2 we review the simplest black hole solution with the desired asymptotics, namely the Schwarzschild-AdS$_p \times S^q$ black hole. We do so for generic values of p and q, and we present the expressions for the physical quantities. In Section 4.3 we present the metric and gauge field ansatz,

again for generic values of p and q, that we use for the numerical construction of the lumpy black holes. This section also includes a discussion about the boundary conditions that yield a well-posed boundary value problem. The one-parameter family that we use as ansatz, by construction captures the threshold GL zero mode for any ℓ. We use this mode as the initial seed to find the actual non-linear solutions. The results are presented in Section 4.4. This section constitutes the core of the chapter, where the phase diagrams are shown and discussed. Special emphasis is put on the isometric embeddings, the topology changes and the critical behavior of the solutions close enough to the merger point. In particular, we compute the critical exponents and find the critical values of various thermodynamic quantities. We close in Section 4.5 with a discussion and outlook of our results.

Finally, we include a few appendices with technical details. KK holography in $\mathrm{AdS}_5 \times S^5$ is reviewed thoroughly in Appendix 4.A, and detailed application of this procedure to our solutions can be found in Appendix 4.B. This requires a basis of spherical harmonics that preserve an SO(5) subgroup of the full SO(6) rotational group of the S^5; this is presented for generic value of q in Appendix 4.C. In Appendix 4.D we show the embedding plots in $D = 10$, which are not included in the main body of the chapter. In Appendix 4.E we include further details of the numerical construction, especially of the grids employed, and we perform some convergence tests.

4.2 Schwarzschild-AdS$_p\times$S^q black hole

The simplest black hole solution with the desired asymptotics is the Schwarzschild-$\mathrm{AdS}_p \times S^q$ black hole, which is known explicitly. In this section we review those aspects of this solution that are relevant for our analysis for generic values of p and q. Most of the material in this section is well-known and can be skipped by the expert reader.

The horizon of Schwarszchild-$\mathrm{AdS}_p \times S^q$ black hole is uniformly smeared along the internal S^q and it thus respects the full $\mathrm{SO}(q+1)$ symmetry; the horizon topology is $S^{p-2} \times S^q$. The metric reads:

$$\mathrm{d}s^2 = -f(r)\mathrm{d}t^2 + \frac{1}{f(r)}\mathrm{d}r^2 + r^2\mathrm{d}\Omega^2_{(p-2)} + R^2\mathrm{d}\Omega^2_{(q)}, \tag{4.2.0.1}$$

where $\mathrm{d}\Omega^2_{(p-2)}$ and $\mathrm{d}\Omega^2_{(q)} = \mathrm{d}\theta^2 + \sin^2\theta\,\mathrm{d}\Omega^2_{(q-1)}$ are the line elements of the round spheres appearing in the AdS_p and S^q factors respectively, and

$$f(r) = 1 + \frac{r^2}{L^2} - \left(\frac{r_+}{r}\right)^{p-3}\left(1 + \frac{r_+^2}{L^2}\right), \qquad (p > 3). \tag{4.2.0.2}$$

The field strength and radius of the S^q coincide with those for the background $\mathrm{AdS}_p \times S^q$ and are given in (4.1.0.6).

It is straightforward to compute the temperature and entropy of this black hole. The energy may be found by integrating the first law of black hole mechanics and then

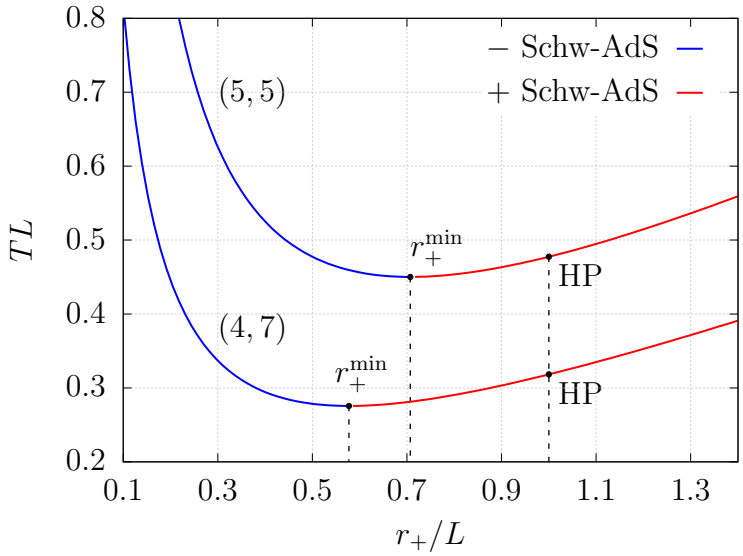

Fig. 4.1: *Dimensionless temperature vs. dimensionless control parameter for the relevant values (p, q). The value at which the HP phase transition takes place is shown.*

the free energy is given by $F = E - TS$. We find:

$$\begin{aligned} T &= \frac{p-3+(p-1)(r_+/L)^2}{4\pi r_+}, \\ S &= \frac{1}{4G_D} r_+^{p-2} \Omega_{(p-2)} R^q \Omega_{(q)}, \\ E &= E_{\mathrm{AdS}_p} + \frac{p-2}{16\pi G_D}\left(1+\frac{r_+^2}{L^2}\right) r_+^{p-3} R^q \Omega_{(p-2)} \Omega_{(q)}, \\ F &= F_{\mathrm{AdS}_p} + \frac{1}{16\pi G_D}\left(1-\frac{r_+^2}{L^2}\right) r_+^{p-3} R^q \Omega_{(p-2)} \Omega_{(q)}. \end{aligned} \tag{4.2.0.3}$$

E_{AdS_p} $(= F_{\mathrm{AdS}_p})$ is the vacuum energy of Anti-de Sitter space, which is non-vanishing for $p = 3, 5$ (it is zero for $p = 4$), and whose precise expression cannot be found from the first law, as it appears as an integration constant. One can find those 'Casimir' energies, for instance, with the prescription of [272] for defining the stress tensor of asymptotically AdS spacetimes. Here we instead use the results that follow from the KK holography analysis (see Appendix 4.B and in particular equation (4.B.0.16)).

Letting L be the AdS radius, Schwarzschild-AdS$_p \times S^q$ black holes are called small if $r_+ \lesssim L$ or large if $r_+ \gtrsim L$. We may invert the relation between the temperature T and the horizon radius r_+ in (4.2.0.3) to find the two branches of black holes at the same temperature T:

$$r_+ = \frac{L}{p-1}\left(2\pi TL \pm \sqrt{(2\pi TL)^2 - 3 - p(p-4)}\right). \tag{4.2.0.4}$$

The positive branch describes large AdS black holes, while the negative branch de-

scribes small AdS black holes. The temperature has a minimum

$$T_{\min} = \frac{\sqrt{(p-3)(p-1)}}{2\pi L}, \tag{4.2.0.5}$$

at

$$r_+^{\min} = L\sqrt{\frac{p-3}{p-1}}, \tag{4.2.0.6}$$

and diverges in the limits of either large or small r_+. This minimum temperature separates the two branches of black holes and there are no homogeneous static black holes in $\mathrm{AdS}_p \times S^q$ (for fixed values of p and q) for $T < T_{\min}$. This is summarized in Fig. 4.1.

With the expressions for the physical quantities in (4.2.0.3), we can now review the phase diagram of the homogenous asymptotically $\mathrm{AdS}_p \times S^q$ solutions. These include the background $\mathrm{AdS}_p \times S^q$ itself and the two branches of Schwarzschild-$\mathrm{AdS}_p \times S^q$ black holes. Since these spacetimes are static, we can trivially consider their Euclidean sections. There are two relevant thermodynamic ensembles: the microcanonical and the canonical ensembles. In the former, we compare solutions with the same energy and those with the largest entropy dominate; in the latter, the temperature is fixed and the solutions with the lowest free energy are preferred.

In the microcanonical ensemble the phase diagram is trivial: the background has no horizon and hence vanishing entropy; consequently, there is only one solution at a given energy, namely the corresponding Schwarzschild-$\mathrm{AdS}_p \times S^q$ black hole. On the other hand, the phase diagram in the canonical ensemble is much richer. First notice that global $\mathrm{AdS}_p \times S^q$ exists at any temperature: the period β of the Euclidean time circle can be chosen to have any value. The geometry has no horizon and therefore vanishing entropy. Consequently, $F_{\mathrm{AdS}_p} = E_{\mathrm{AdS}_p}$. From now on we subtract this contribution in (4.2.0.3), and consider the difference $\Delta F = F - F_{\mathrm{AdS}_p}$. For the Schwarzschild-$\mathrm{AdS}_p \times S^q$, regularity of the Euclidean section requires that the period of the Euclidean time circle is given by $\beta = 1/T$ with T given in (4.2.0.3). Furthermore, from (4.2.0.3) we see that $\Delta F < 0$ for $r_+ > L$, and hence large Schwarzschild-$\mathrm{AdS}_p \times S^q$ black holes above this threshold dominate the canonical ensemble. On the other hand, $\Delta F > 0$ and for $r_+ < L$, and thus thermal $\mathrm{AdS}_p \times S^q$ is preferred. At $r_+ = L$, corresponding to Hawking-Page (HP) temperature,

$$T_{\mathrm{HP}} = \frac{p-2}{2\pi L}, \tag{4.2.0.7}$$

there is a phase transition between two distinct equilibrium states: large Schwarzschild-$\mathrm{AdS}_p \times S^q$ black holes and thermal $\mathrm{AdS}_p \times S^q$. This is summarized in Fig. 4.1. The energy is discontinuous across the phase transition, $E^+_{\mathrm{HP}} \neq E^-_{\mathrm{HP}}$, with

$$E^{\pm}_{\mathrm{HP}} \equiv \lim_{T\to T^{\pm}_{\mathrm{HP}}} E(T), \tag{4.2.0.8}$$

yielding a non-vanishing latent heat ΔE, and the phase transition is of first order. For temperatures $T < T_{\min}$, there only exists thermal AdS. For $T_{\min} < T < T_{\mathrm{HP}}$,

homogenous black hole solutions do exist but do not dominate the canonical ensemble; for $T > T_{\rm HP}$, large Schwarzschild-AdS$_p \times S^q$ black holes are the preferred phase, with both phases co-existing at $T_{\rm HP}$. Small Schwarzschild-AdS$_p \times S^q$ black holes are always subdominant.[5]

So far, the physics only presents dependence on p. For the values (p, q) of interest, these quantities are shown in Table 4.1. Schwarzschild-AdS$_p \times S^q$ describes the universal sector to which Ref. [266] refers, only involving gravity in AdS and with the internal space playing no role. This is indeed the case if we only consider large black holes and the background. On the other hand, small enough Schwarzschild-AdS$_p \times S^q$ black holes are dynamically unstable under perturbations that break the isometries of the internal space [156]. Whilst the thermodynamic stability of the small black hole branch changes at

$$r_+ = r_+^{\rm min}, \tag{4.2.0.9}$$

becoming unstable for $r_+ < r_+^{\rm min}$, this does not necessarily signal the onset of a dynamical instability. Indeed, the onset of the dynamic instability occurs when the Euclidean eigenmode $\lambda_{\rm E}$ of the Schwarzschild-AdS$_p$ black hole coincides exactly with the 'momentum' in the transverse space. In the present case, where we take the internal space to be a S^q, the threshold unstable mode will occur when $\lambda_{\rm E} = -\ell(\ell + q - 1)$, where ℓ is labels the spherical harmonics on the S^q. This is how the zero mode that signals the instability was first obtained. In turn, it suggests the existence of new branches of black holes that emerge from this point and that have deformed horizons along S^q. These new branches of black holes are completely analogous to the non-uniform strings in the context of the GL instability of black strings [13, 14]. From the D-dimensional point of view, for each ℓ there is a GL zero mode that breaks the SO$(q+1)$ isometry of S^q down to SO(q). These zero modes can be uplifted to fully non-linear solutions, leading to the so-called lumpy black holes, first constructed in [19] in AdS$_5 \times S^5$. The aim of this chapter is to study in detail several branches of lumpy black holes in AdS$_5 \times S^5$ and AdS$_4 \times S^7$.

Linear perturbations about the Schwarzschild-AdS$_p \times S^q$ spacetime can be decomposed into a sum of scalar, vector and tensor perturbations, depending on how they transform under coordinate transformations on the S^q. The GL zero modes are in the scalar sector and are classified in terms of ℓ, the harmonic quantum number on the S^q. Here, instead of proceeding as in [156] and expand the AdS sector of the metric perturbations in spherical harmonics,

$$g_{\mu\nu} \to g_{\mu\nu} + h^{\ell}_{\mu\nu} Y_\ell(\theta), \tag{4.2.0.10}$$

we will linearize the full D-dimensional general ansatz for the lumpy black holes (see the next section) around Schwarzschild-AdS$_p \times S^q$. The problem of numerically finding

[5] Notice that planar-AdS$_p(\times S^q)$ black holes are infinitely extended since $B_{p-1} = \mathbb{R}^{1,p-2}$ and can be recovered in the limit $r_+ \gg L$. In this limit the free energy is always negative and therefore there are no phase transitions. As we anticipated earlier, these black holes always dominate the canonical ensemble.

(p,q)	$r_+^{\min}/L$	$T_{\min}L$	$T_{\rm HP}L$	$E^-_{\rm HP}$	$E^+_{\rm HP}$	ΔE
$(5,5)$	$\frac{1}{\sqrt{2}}$	$\frac{\sqrt{2}}{\pi}$	$\frac{3}{2\pi}$	$\frac{3N^2}{16L}$	$\frac{27N^2}{16L}$	$\frac{3N^2}{2L}$
$(4,7)$	$\frac{1}{\sqrt{3}}$	$\frac{\sqrt{3}}{2\pi}$	$\frac{1}{\pi}$	0	$\frac{128\pi^4L^8}{3}$	$\frac{128\pi^4L^8}{3}$

Table 4.1: *Relevant thermodynamic values in the phase diagram of the solutions preserving the background's isometries. In $D=10$, the G_{10} has been expressed in terms of the dual gauge theory parameter N using (4.4.1.1). In $D=11$, G_{11} is a fundamental constant and can be taken to be one.*

the lumpy black holes requires to construct the linearized Einstein-DeTurck operator,[6] and hence we can easily adapt our code to find the spectrum of time independent perturbations of Schwarzschild-AdS$_p\times S^q$ black holes. Since the latter turn out to be thermodynamically unstable for $r_+ < r_+^{\min}$, we started our search for zero modes at $r_+ = r_+^{\min}$ and gradually decreased this value until a zero mode is found. The first three zero modes, corresponding to $\ell = 1,2,3$, occur at

$$\begin{aligned}(p,q)=(5,5): &\quad y_0^{\ell=1,2,3} = \{0.44023414,\ \ 0.32388984,\ \ 0.25704192\},\\ (p,q)=(4,7): &\quad y_0^{\ell=1,2,3} = \{0.28898162,\ \ 0.24819894,\ \ 0.21751714\},\end{aligned} \tag{4.2.0.11}$$

where $y_0 = r_+/L$. In practice we use these zero modes as initial seeds for finding the corresponding non-linear families of lumpy black holes. We note that in the $D=10$ case, our values coincide with those found in [19] for $\ell = 1,2$. In the $D=11$ case, as far as we know, our results are new. The spectrum of negative modes of the Schw-AdS$_4$ black hole was computed in [269]. The threshold radii for the 0-modes that we have found agree, within numerical error, with the values of the radii where these negative modes coincide with the eigenvalues $-\ell(\ell+6)$ of the scalar harmonics on the S^7.

4.3 Lumpy black holes in AdS$_p\times$S^q

In this section we present the numerical construction of lumpy black holes in AdS$_p\times S^q$. The different cases that we explore differ by the equations of motion and by the n-form gauge field, but the ansatz for the metric is general and can be written down for any values of p and q.

Lumpy black holes in AdS$_p\times S^q$ only retain a SO(q) subgroup of the full isometry group of the internal S^q. In the space of static solutions, they emanate from the small Schwarzschild-AdS$_p\times S^q$ black hole branch at the GL threshold point, and therefore they have the same horizon topology: $S^{p-2}\times S^q$. They are classified by ℓ, which

[6] Around an Einstein metric, this operator coincides with the Lichnerowicz operator.

is the harmonic number corresponding to the scalar harmonic on the S^q that labels the corresponding zero mode. Each lumpy solution of the ℓth family depends on two coordinates: the radial coordinante r in the AdS$_p$ factor, and the polar angle θ on the S^q; using standard spherical coordinates, the polar angle ranges from 0 to π, with the 'north' pole of S^q at $\theta = 0$, the equator at $\theta = \pi/2$ and the 'south' pole at $\theta = \pi$.

Uniform horizons on S^q trivially possess a reflection symmetry $\theta \leftrightarrow \pi - \theta$ with respect to the equator of this S^q. However, under this parity transformation scalar harmonics pick up a factor of $(-1)^\ell$. Recall that the various families of lumpy black holes are non-linear solutions of the field equations that are continuously connected (in the space of solutions) to the linear deformations of the uniform black holes parametrized by the scalar harmonics. Therefore, the lumpy families labelled by the harmonic ℓ transform in the same way as the scalar harmonics under reflections about the equator of the internal S^q. Consequently, lumpy black holes labelled by an odd ℓ are not symmetric with respect to reflections about the equator, and one has to consider the whole range of the polar angle θ on the S^q to construct them. On the other hand, for even ℓ lumpy black holes enjoy a reflection symmetry about the equator and it suffices to consider $\theta \in [0, \pi/2]$.

4.3.1 Metric ansatz

Given the previous considerations, a suitable ansatz for the metric of the lumpy black holes consists of a general enough deformation of the Schwarzschild-AdS$_p$ × S^q black hole that breaks the SO$(q+1)$ symmetry down to SO(q). To solve the equations of motion numerically, it turns out to be convenient to compactify the radial coordinate and to redefine the polar angle as follows:

$$r(y) = \frac{r_+}{1-y^2}, \qquad \theta(a) = \arcsin(1-a^2). \tag{4.3.1.1}$$

In these coordinates, the horizon is located at $y = 0$ and the conformal boundary of AdS$_p$ is at $y = 1$, while the north and south poles of the S^q are at $a = \pm 1$ respectively, and the equator is at $a = 0$. Then for odd/even ℓ the integration domain is simply $[0,1] \times [-1,1]$ / $[0,1] \times [0,1]$. We will be parametrize the ansatz in terms of the dimensionless parameter $y_0 = r_+/L$. If we further rescale the time coordinate $t \to Lt$, then the AdS radius L drops out of the equations of motion, leaving y_0 as the only control parameter. This parameter effectively sets the temperature of the black hole. Therefore, for any given harmonic ℓ, the lumpy black holes form a one-parameter family of solutions specified by the temperature.

Applying these changes of coordinates and redefinitions to (4.2.0.1), the metric reads:

$$\begin{aligned} \mathrm{d}s^2 = \frac{L^2}{(1-y^2)^2}\left(-\frac{G_p(y)}{1-y^2}\mathrm{d}t^2 + \frac{4y^2(1-y^2)y_0^2}{G_p(y)}\mathrm{d}y^2 + y_0^2\mathrm{d}\Omega^2_{(p-2)}\right) \\ + R^2\left(\frac{4\mathrm{d}a^2}{2-a^2} + (1-a^2)^2\mathrm{d}\Omega^2_{(q-1)}\right), \end{aligned} \tag{4.3.1.2}$$

with

$$G_p(y) = 3y^4 - y^6 - (1+y_0^2)\left((1-y^2)^p - 1\right) - y^2\left(3+y_0^2\right). \tag{4.3.1.3}$$

This is the metric that we will use as the reference metric in the Einstein-DeTurck equations (4.1.0.7). We can now present the ansatz for the lumpy black holes. For any value of p and q, we consider:

$$\begin{aligned} \mathrm{d}s^2 = \frac{L^2}{(1-y^2)^2}\Bigg(&-\frac{G_p(y)}{1-y^2}Q_1\mathrm{d}t^2 + \frac{4y_0^2y^2(1-y^2)}{G_p(y)}Q_2\left(\mathrm{d}y - (1-y^2)^2Q_3\mathrm{d}a\right)^2 \\ &+ y_0^2Q_5\mathrm{d}\Omega^2_{(p-2)}\Bigg) + R^2\left(\frac{4Q_4}{2-a^2}\mathrm{d}a^2 + (1-a^2)^2Q_6\mathrm{d}\Omega^2_{(q-1)}\right), \end{aligned} \tag{4.3.1.4}$$

where $Q(y,a) \equiv \{Q_1,\ldots,Q_6\}(y,a)$ are the unknowns for the metric field. For $Q_i(y,a) = 1$, $\forall i \neq 3$ and $Q_3(y,a) = 0$, we recover (4.3.1.2). These are actually the Dirichlet boundary conditions imposed at $y=1$, as required by the asymptotics. The ansatz (4.3.1.4) preserves the full SO$(p-1)$ symmetry of the S^{p-2} within the AdS$_p$ factor and the unbroken SO(q) symmetry of the S^{q-1} inside the S^q.

4.3.2 Gauge field ansatz

The different theories that admit AdS$_p\times S^q$ asymptotic solutions also contain a non-trivial n-form gauge field strength; $n=5$ in $D=10$ and $n=4$ in $D=11$. In order to solve the equations of motion numerically, we need to provide a suitable ansatz for this field.

Instead of considering the form field strength $F_{(n)}$, we will work with the potential form field $A_{(n-1)}$, such that $F_{(n)} = \mathrm{d}A_{(n-1)}$. The reason is that the equations of motion for $A_{(n-1)}$ are of 2nd order and elliptic. To find a suitable ansatz, we consider a deformation of the gauge field $A_{(n-1)}$ corresponding to the Schwarzschild-AdS$_p\times S^q$ black hole (4.1.0.6) written in terms of the coordinates (y,a); see Eq. (4.3.1.1). In particular, we consider a gauge such that the $(n-1)$-form potential vanishes at the horizon, which has the benefit of simplifying the boundary conditions there. Taking these considerations into account, we have the following ansatz for $A_{(n-1)}$:

$$\begin{aligned} (p,q) = (5,5): \quad A_{(4)} &= L^4y_0^4\frac{y^2(2-y^2)(2-2y^2+y^4)}{(1-y^2)^4}Q_7\mathrm{d}t\wedge\mathrm{d}\sigma_{(3)} \\ &\quad - W\mathrm{d}\sigma_{(4)}, \\ (p,q) = (4,7): \quad A_{(3)} &= -L^3y_0^3\frac{y^2(3-3y^2+y^4)}{(1-y^2)^3}Q_7\mathrm{d}t\wedge\mathrm{d}\sigma_{(2)}, \end{aligned} \tag{4.3.2.1}$$

where $\mathrm{d}\sigma_{(r)}$ is the volume r-form of a round unit r-sphere, and $Q_7 = Q_7(y,a)$ is an unknown function that encodes the deformations away from Schwarzschild-AdS$_p\times S^q$. For $Q_7(y,a) = 1$ (and a particular function W for $(p,q)=(5,5)$), these expressions yield the field strengths given in (4.1.0.6) in the (y,a) coordinates. Having fixed the gauge *a priori*, the equation of motion for the potential is elliptic; this equation

together with the Einstein-DeTurck equations for the metric (4.1.0.7) and for suitable boundary conditions (see §4.3.3) form a well-posed boundary value problem.

There is a small caveat in the case $(p, q) = (5, 5)$. Notice that we have not specified the particular form of the function $W(y, a)$ appearing in the ansatz. The reason is that the self-duality condition $F_{(5)} = \star F_{(5)}$ allows us to eliminate the first derivatives of W in terms of the first derivatives of Q_7. Then, the equation $\mathrm{d}F_{(5)} = 0$ can be written solely in terms of Q_7 and its first and second derivatives. This is not surprising, since the self-duality condition by itself is non-dynamical.

4.3.3 Boundary conditions

The boundary value problem has to be supplemented by suitable boundary conditions to form a well-posed problem. These are obtained by requiring regularity at the horizon and at the poles (or reflection symmetry at the equator for even values of ℓ), and by requiring that the solution is asymptotically $\mathrm{AdS}_p \times S^q$. In full, the boundary conditions that we impose are:

- **Horizon** at $y = 0$: regularity at the horizon implies that all functions Q must be even in y and therefore we impose a Neumann boundary condition on all of them, except Q_3 which is Dirichlet. The condition $Q_1(0, a) = Q_2(0, a)$ ensures that the geometry is free of conical singularities and fixes the surface gravity of the lumpy black holes to be the same as that of the reference metric.

- **Asymptotic boundary** at $y = 1$: $\mathrm{AdS}_p \times S^q$ asymptotics imply Dirichlet boundary conditions $Q_i(1, a) = 1$, $\forall i \neq 3$, and $Q_3(1, a) = 0$.

- **North and south poles of S^q (for ℓ odd)** at $a = \pm 1$ respectively: all Q's must be even in $(1 \mp a)$ respectively, and thus we impose Neumann boundary conditions on all of them except the crossed term Q_3, which must satisfy a Dirichlet boundary condition, $Q_3 = 0$. In addition, to avoid conical singularities at the poles we impose: $Q_4(y, \pm 1) = Q_6(y, \pm 1)$.

- **Equator and north pole of S^q (for ℓ even)** at $a = 0$ and $a = 1$ respectively: all Q's must be even there and thus we impose Neumann boundary conditions on all of them except the crossed term Q_3 which must satisfy a Dirichlet boundary condition, $Q_3 = 0$. In this case, we only need to further impose the absence a conical singularity at the pole $(a = 1)$ by requiring $Q_4(y, 1) = Q_6(y, 1)$.

4.3.4 Further considerations

Now we are in position to construct the numerical solutions for the lumpy black holes. We start with the Schwarzschild-$\mathrm{AdS}_p \times S^q$ black hole, corresponding to $Q_i(y, a) = 1$, $\forall i \neq 3$, and $Q_3(y, a) = 0$ in (4.3.1.4) and (4.3.2.1), and we add a bit of the ℓth zero mode, depending on the lumpy family that we aim to find, to construct a good enough

initial guess of the Newton-Raphson loop. Whereas for ℓ odd, adding or subtracting the zero mode connects to the same lumpy family, this is not the case for ℓ is even. This is better understood in terms of the perturbations as written in (4.2.0.10): under a parity transformation, the perturbations transform as

$$h^{\ell}_{\mu\nu} \to (-1)^{\ell} h^{\ell}_{\mu\nu}. \tag{4.3.4.1}$$

Therefore, we see that for odd ℓ, the positive sign in the perturbation is equivalent to the negative sign by transforming $\theta \to \pi - \theta$, which is nothing but a redefinition of what we call 'north' and 'south' poles of the S^q. However, this redundancy does not apply when ℓ is even, and the choice of the sign yields physically different perturbations that connect to different families of lumpy black holes. In this chapter we have focused on finding the first four families of lumpy black holes, i.e., $\ell = 1, 2^+, 2^-$ and 3. The upper sign for $\ell = 2$ refers to the family that branches off from the Schwarzschild-AdS$_p \times S^q$ black hole by adding $(+)$ or subtracting $(-)$ the 0-mode for seeding the first solution.

Given the boundary conditions above, the temperature of our lumpy black holes is the same as the Schwarzschild-AdS$_p \times S^q$ black hole used as a reference metric and is controlled by the parameter y_0 in (4.3.1.4). We move along a given branch of lumpy black holes by varying y_0. In analogy with non-uniform black strings in KK theory [13], we define a 'lumpiness' parameter λ (see Eq. (4.4.3.3)), that measures the size of deformations away from the Schwarzschild-AdS$_p \times S^q$ black hole. Slightly non-uniform (on the S^q) lumpy black holes have $\lambda \ll 1$, while $\lambda \to \infty$ as we approach the critical regime, where lumpy black holes merge with another family of black holes with a different horizon topology. For non-critical lumpy black holes ($\lambda \lesssim 1$), one single patch of Chebyshev grid points is enough to obtain accurate numerical results. However, critical solutions need a more careful treatment.

In order to access the critical regime we employed three techniques that have been used successfully in the past [1, 22] . For critical solutions but not the most critical ones, we supplement the single domain with mesh-refinement in the region where it is necessary. As we approach the merger point, some functions develop very steep gradients near one (or both) pole(s) and mesh-refinement alone is insufficient to accurately construct such solutions; to resolve them, we simply redefine the unknowns as $Q^{\text{new}} = 1/Q^{\text{old}}$, for some functions (see below), and we split the domain into several (smaller) patches and apply mesh-refinement to increase the resolution where it is needed. The boundary conditions for the new unknowns are the same as the ones listed before, but the new functions remain bounded as we approach the critical regime.

In general, we have tracked the value of ξ^2 to determine when the resolution needs to be increased. We have always required $\xi^2 < 10^{-10}$, despite the most critical solutions we reached do not satisfy this bound. Still, the numerical error is very localized and under control. In addition, we have also monitored some physical observables (see Section 4.4) along a given family; when numerical errors are unacceptably large they are reflected in the physical quantities. With these considerations, we have managed to confidently construct families of lumpy black holes up to following maximum values

of λ:

$$\begin{aligned}(p,q)=(5,5): &\quad \lambda_{\rm max}^{\ell=1,2^+,2^-,3}=\{25,\ \ 8.1,\ \ 6.3,\ \ 26\},\\ (p,q)=(4,7): &\quad \lambda_{\rm max}^{\ell=1,2^+,2^-,3}=\{104,\ \ 109,\ \ 6.0,\ \ 100\}.\end{aligned} \tag{4.3.4.2}$$

To construct solutions in the critical regime for the various families, we generically redefine the unknowns $Q_{1,2,7}$ as described above. For the families $\ell=1,2^+$ and 3, the singular behavior appears near a pole and near the horizon. To resolve it, we increase the resolution in that corner by splitting the integration domain into several patches, with higher resolution and applying mesh-refinement in the regions where it is needed. We have considered up to 4 patches for the most critical solutions. See Appendix 4.E for more details and some examples of the types of domains that we have used to construct critical solutions.

It turns out to be much harder to construct critical solutions for the $\ell=2^-$ branch. The reason is that the singular behavior of the functions is not localized at a corner but somewhere near the horizon and in between the equator and the poles. Additionally, for the two cases that we have considered, namely $(p,q)=(5,5)$, $(4,7)$, there is a turning point along the branch in the non-critical regime. Indeed, we find that starting at $y_0=y_0^{\ell=2}$ (see equation (4.2.0.11)) and decreasing y_0, at some point we can no longer find solutions. Examining the behavior of the physical quantities near this point, it is clear that we are not at the end of the branch; in fact, we observe that the derivative of any thermodynamical variable as a function of the temperature becomes infinite. It turns out that this point corresponds to a local maximum of the temperature along the branch. To go past it and to larger values of λ, we use the trick explained in Ref. [206].

4.4 Results

4.4.1 Thermodynamics

In this section we display and discuss the phase diagrams of asymptotically global $\mathrm{AdS}_p\times S^q$ spacetimes, including the lumpy black holes solutions that we have numerically constructed. To make the microcanonical and canonical phase diagrams easier to visualize, we plot the dimensionless differences of the entropy or the free energy with respect to the small Schwarzschild-$\mathrm{AdS}_p\times S^q$ black hole with the same energy or temperature, depending on the ensemble.

In the $D=10$ case we can use the holographic relation,

$$N^2=\frac{\pi^4L^8}{2G_{10}}, \tag{4.4.1.1}$$

to express the physical quantities in terms of gauge theory units. In this way, we shall display S/N^2 versus EL/N^2 in the microcanonical ensemble and FL/N^2 versus TL for the canonical ensemble. In $D=11$, the Newton's constant is a fundamental quantity

and it is only related to Planck's length. We can safely take units where $G_{11} = 1$, and then S/L^9, E/L^8 and F/L^8 are dimensionless.

Before proceeding to display the phase diagrams, we collect the expressions for the various physical quantities of interest. Given our ansatz for the metric (4.3.1.4) and the boundary conditions that we impose, the temperature of lumpy black holes is the same as the reference Schwarzschild-AdS$_p \times S^q$ black hole and it is given by (4.2.0.3). The entropy of a black hole is proportional to its horizon area, $S = A_{\rm H}/(4G_D)$. For generic values of p and q, the area of the horizon for the lumpy black holes is given by

$$A_{\rm H} = 2(Ly_0)^{p-2} R^q \Omega_{(p-2)}\Omega_{(q-1)} \int_{-1}^{+1} {\rm d}a \, \frac{(1-a^2)^{q-1}}{\sqrt{2-a^2}} \sqrt{Q_5^{p-2} Q_4 Q_6^{q-1}}\Big|_{y=0}, \qquad (4.4.1.2)$$

for odd ℓ. For even ℓ the integral ranges from 0 to 1 and we have to multiply by a factor of 2 due to the reflection symmetry about the equator of the internal S^q. As a consistency check, note that setting $Q_4 = Q_5 = Q_6 = 1$, yields the horizon area of the Schwarzschild-AdS$_p \times S^q$ solution given in (4.2.0.3).

The most straightforward way to compute the energy of the solutions is by integrating the 1st law of thermodynamics. We can easily find the curve $S(T)$, since it only involves the computation of horizon area, and the families of lumpy black holes are parametrized by the temperature. Then the energy is given by:

$$E(T) = E_{\rm GL} + \int_{T_{\rm GL}}^{T} \frac{{\rm d}S(T')}{{\rm d}T'} {\rm d}T' \,, \qquad (4.4.1.3)$$

where $E_{\rm GL}$ and $T_{\rm GL}$ are the energy and temperature of the Schw-AdS$_p \times S^q$ black hole at the ℓth GL threshold point. This procedure, however, fails if there is a turning point along a given family, since at this point the derivative ${\rm d}S(T')/{\rm d}T'$ blows up. This is the case of the $\ell = 2^-$ branches. In this case, we can still integrate over the rest of the branch, where the first derivative is finite, and leave the contribution coming from the solutions around the turning point region as an undetermined constant. Then we can try to 'guess' such a constant using the phase diagrams: in the microcanonical ensemble the phase diagram must be smooth, whereas in the canonical ensemble the turning point must be a cusp. This trick works well as long as we have enough solutions sufficiently close to the turning from both sides. In both $D = 10$ and $D = 11$, the phase diagrams for the $\ell = 2^-$ families have been completed using this trick.

An alternative way to compute the energy E of the solutions is by performing an asymptotic expansion of the fields near the AdS boundary and apply KK holography [270] and holographic renormalization [191]. In this study we only have worked out this alternative way of finding E for $D = 10$ case. The calculation is long and tedious and the details can be found in Appendices 4.A and 4.B. The final expression is given by:

$$\frac{E\,L}{N^2} = \frac{3}{16}(1+2y_0^2)^2 + \frac{y_0^4}{512}\left(\partial_y^4 Q_5 - \partial_y^4 Q_1\right)\Big|_{y=1}. \qquad (4.4.1.4)$$

Note that for $Q_5 = 1 = Q_4$, this expression reduces to the energy in (4.2.0.3) for $(p, q) = (5, 5)$, after using (4.4.1.1) and identifying the well-known dimensionless vac-

uum energy of global AdS_5 [272]. The drawback of using (4.4.1.4) to compute E is that it implies computing four derivatives of the numerical solutions, which inevitably leads to a loss of accuracy.

(p,q) = (5,5)

In Fig. 4.2 we display the phase diagrams for both the microcanonical and canonical ensembles for the $\ell = 1$ lumpy family. The branch emanates from the GL threshold point, and it moves towards higher energies or lower temperatures. As this figure shows, the $\ell = 1$ lumpy solutions are always subdominant in both the microcanonical and canonical ensembles. Furthermore, the phase diagrams do not present any turning points for the range of temperatures that we explored. As we shall see in Section 4.4.4, the local cone model for the merger predicts that in $D = 10$ there should not be any turning points sufficiently close to the merger point, i.e. in the limit $\lambda \to \infty$. For this particular family it turns out that there are no turning points at all.

The phase diagram for the $\ell = 1$ lumpy $AdS_5 \times S^5$ black holes was previously discussed in [19]. We now compare their results with ours. In the region near the GL threshold (i.e., $\lambda \lesssim 1$), our results and theirs are in perfect agreement. However, we find some disagreement for $\lambda \sim \mathcal{O}(1)$. According to Fig. 9 in their paper, the solution with the lowest temperature (i.e., the most critical) that they managed to find has $T\,L = 0.49444$ and energy $EL/N^2 \sim 0.388$; using the data in their figure, we see that $\text{Min}[R_{S^3}] \sim 0.09$ and $\text{Max}[R_{S^3}] \sim 0.56$, which implies $\lambda \sim 2.6$. On the other hand, the most critical solution that we have found for this branch has $\lambda \simeq 25$, which corresponds to a temperature $T\,L = 0.49575$ and energy $EL/N^2 = 0.38540$. Clearly our results and theirs are not compatible. The extend of the $\ell = 1$ family in the phase diagram that we find is significantly shorter than previously reported [19]. The most reasonable explanation for this discrepancy is that the resolution used in [19] is insufficient to accurately construct the lumpy black holes with large λ. Indeed, we had to use various tricks (see Section 4.3.4) to be able to numerically construct critical lumpy black holes, whilst [19] used a single patch with moderate resolution. According to our estimates, the grid setup used in [19] rapidly becomes insufficient to accurately resolve the lumpy black holes with $\lambda \sim \mathcal{O}(1)$. Therefore, it seems reasonable to conclude that part of the phase diagram reported in [19] is unphysical.

The phase diagrams for the branches $\ell = 2^+, 3$ are qualitatively the same as those for the $\ell = 1$ family and we do not discuss them any further. We simply stress that these other families of lumpy black holes are also always subdominant in both the microcanonical and canonical ensembles. In order to 'locate' in the phase diagram the various families of lumpy black holes that we have studied, in Fig. 4.4 we display the phase diagram in the canonical ensemble with all solutions that we have found. In this case we compare the free energy with respect to that of global $AdS_5 \times S^5$. As this figure illustrates, lumpy black holes occupy a very small portion of the entire phase diagram.

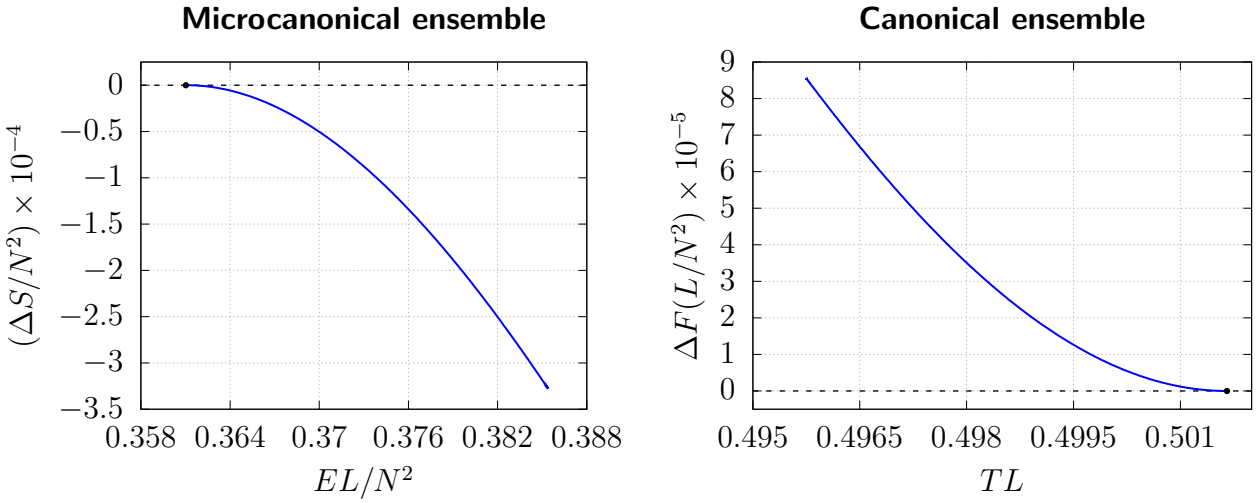

Fig. 4.2: *Phase diagram in the microcanonical ensemble (left) and the canonical ensemble (right), for $\ell = 1$ lumpy black holes. The GL threshold point is indicated with a black solid disc. The zero is taken to be the Schwarzschild-$AdS_5 \times S^5$ black hole phase. Lumpy black holes are always subdominant in both ensembles. The phase diagrams of the other families of lumpy black holes that we have constructed are qualitatively similar, except for $\ell = 2^-$.*

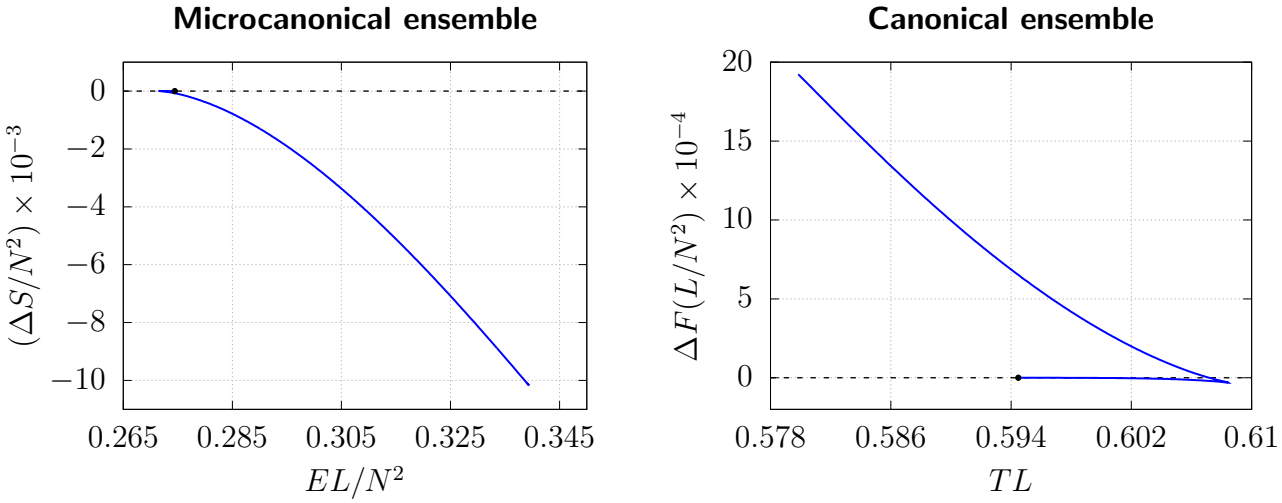

Fig. 4.3: *Phase diagram in the microcanonical ensemble (left) and canonical ensemble (right), of $\ell = 2^-$ lumpy black holes. The GL threshold point is indicated with a black solid disc. The zero is taken to be the Schwarzschild-$AdS_5 \times S^5$ black hole phase. The $\ell = 2^-$ lumpy black holes dominate the microcanonical ensemble near the GL threshold. In the canonical ensemble, the $\ell = 2^-$ lumpy black holes are also dominant with respect to the small Schwarzschild-$AdS_5 \times S^5$ black hole for temperatures near the GL point, but thermal $AdS_5 \times S^5$ is always the preferred phase in this range of temperatures.*

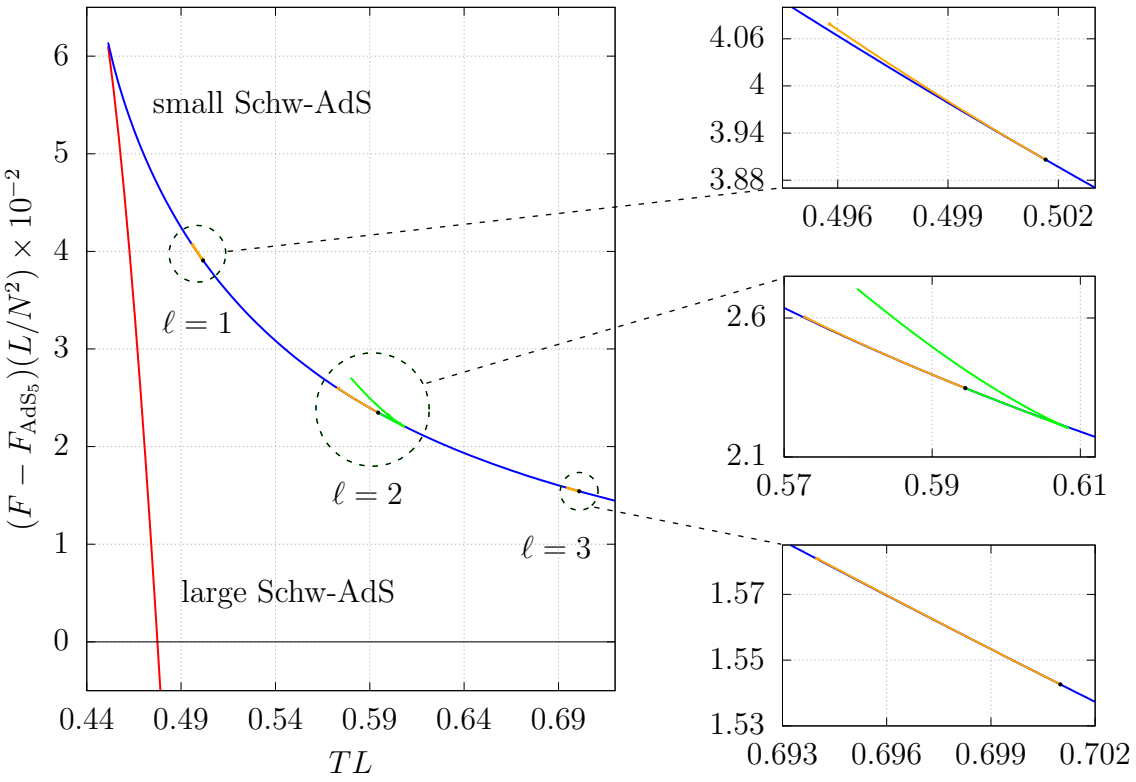

Fig. 4.4: *Phase diagram in the canonical ensemble containing all asymptotically $AdS_5 \times S^5$ spacetimes that we consider in this chapter. The GL threshold point for the various modes is indicated with a solid black disk. The zero of the free energy is taken to be the background thermal $AdS_5 \times S^5$, which has free energy $F_{AdS} = 3N^2/(16L)$. All lumpy black holes are subdominant, even though the $\ell = 2^-$ family has lower free energy than the small Schwarzschild-$AdS_5 \times S^5$ black hole for some temperatures.*

Before we move on to discuss the phase diagrams for the $\ell = 2^-$ branch, we briefly comment on the previous results by [19] on the $\ell = 2^+$ and $\ell = 2^-$ branches. In particular, their most critical solution has temperature $T\,L = 0.57278$. We infer from their Fig. 11 (right panel) that this solution has $\lambda \sim 3.1$. On the other hand, the left panel of their Fig. 11 indicates that their most critical solution for the $\ell = 2^-$ branch has temperature $T\,L = 0.60849$ and $\lambda \sim 0.5$. In both cases, this agrees with our results and up to these solutions, our phase diagrams and theirs match very well. With our more accurate numerics, we have been able extend both the $\ell = 2^+$ and $\ell = 2^-$ families to larger values of λ, closer to the critical point.

It turns out that for the $\ell = 2^-$ branch, the solution with $TL = 0.60849$ is very close to a turning point, and more specifically to a local maximum of the temperature. This solution has $\lambda \sim 0.54$, and hence it is still very far (in solution space) from the critical regime. We have managed to continue beyond this turning point, and the full phase diagram for the $\ell = 2^-$ family is displayed in Fig. 4.3. Note that whilst

the $\ell = 2^+$ branch never dominates any ensemble, the $\ell = 2^-$ lumpy black holes can be favored with respect to the small Schwarzschild-AdS$_5 \times S^5$ black hole. In the microcanonical ensemble, the $\ell = 2^-$ phase has larger entropy than the Schwarzschild-AdS$_5 \times S^5$ black hole (for the same energy) in the region near the GL point. Likewise, in the canonical ensemble the $\ell = 2^-$ lumpy black holes dominate over the small Schwarzschild-AdS$_5 \times S^5$ black hole near the GL threshold point and until slightly beyond the turning point. However, in this range of temperatures, thermal AdS is always the preferred phase in the canonical ensemble. It is interesting to note that for this particular branch of lumpy black holes, the microcanonical and the canonical ensembles seem to give slightly different results. This minor observation adds to the puzzles raised in [273] related to the apparent differences between the two ensembles in the thermodynamic limit.

(p,q) = (4,7)

The phase diagrams in the microcanonical and canonical ensembles for $\ell = 1$ lumpy black holes in AdS$_4 \times S^7$ are depicted in Fig. 4.5. According to this figure, the $\ell = 1$ lumpy phase exists beyond the corresponding GL threshold point towards larger energies or lower temperatures, depending on the ensemble under consideration. Just as in the $(p, q) = (5, 5)$ case, this phase is always subdominant with respect to the small Schwarzschild-AdS$_4 \times S^7$ black hole (and of course with respect to thermal AdS$_4 \times S^7$, which is the dominant phase in the canonical ensemble in this range of temperatures). It is interesting to note that even though we have managed to follow this branch up until $\lambda = 104$, and hence very close to the merger point, we did not find any turning points along the family. In the critical regime (i.e., large values of λ) the local cone model predicts the absence of turning points and our numerical construction confirms this model beautifully (see Section 4.4.4 for more details). The phase diagrams for the $\ell = 2^+$, 3 lumpy AdS$_4 \times S^7$ black hole families are qualitatively similar to those of the $\ell = 1$ black holes and we do not present them here.

On the other hand, the phase diagrams for the $\ell = 2^-$ family exhibit some notable differences. In Fig. 4.6 we display the microcanonical and canonical phase diagrams for the $\ell = 2^-$ lumpy AdS$_4 \times S^7$ black holes. Using the trick explained in the discussion after equation (4.4.1.3), we can find the complete phase diagram beyond the turning point and up to the most critical solution that we have been able to construct, even if we are integrating the 1st law. Fig. 4.6 includes the whole $\ell = 2^-$ family, up to $\lambda = 6.00374$ corresponding to $TL = 0.37907$.

In the microcanonical ensemble (left panel in Fig. 4.6), the $\ell = 2^-$ black holes dominate for energies near the GL point. This suggests that this family of black holes could be dynamically stable in some region of parameter space, and a certain (perhaps fine-tuned) class of perturbations of the Schwarzschild-AdS$_4 \times S^7$ black holes could evolve into them at the non-linear level. There is a minimum energy along this branch at $E_{\rm min}/L^8 = 519.30461$; presumably, at this point the stability properties of these

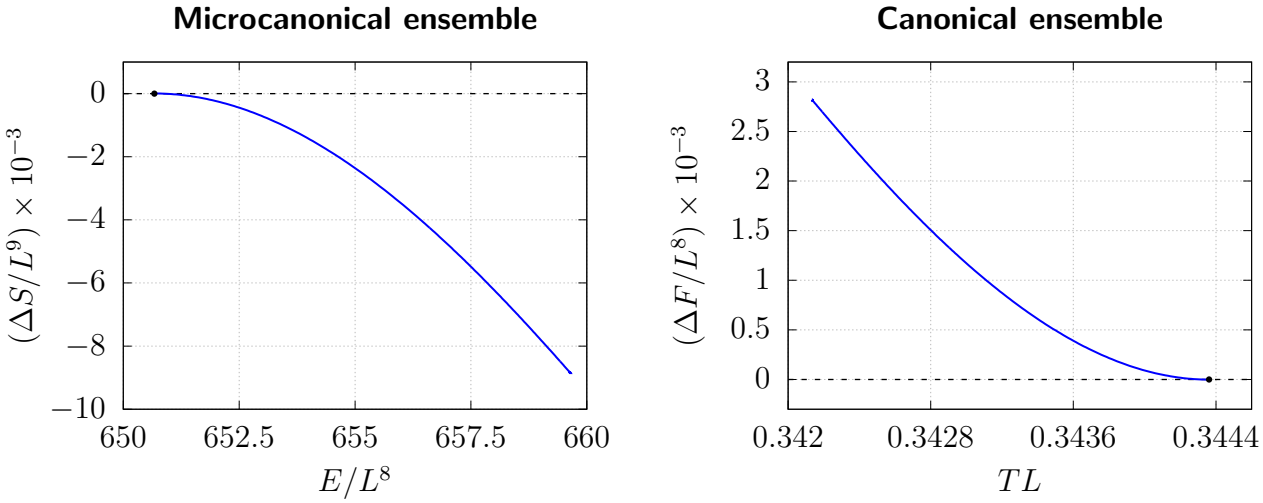

Fig. 4.5: *Phase diagram in the microcanonical ensemble (left) and canonical ensemble (right), of $\ell = 1$ lumpy black holes. The GL threshold point is indicated with a black solid disc. The zero is taken to be the Schwarzschild-$AdS_4 \times S^7$ black hole phase. The lumpy black holes are subdominant in both ensembles. The phase diagrams of the other families of lumpy black holes that we have constructed are qualitatively similar, except for the $\ell = 2^-$ family.*

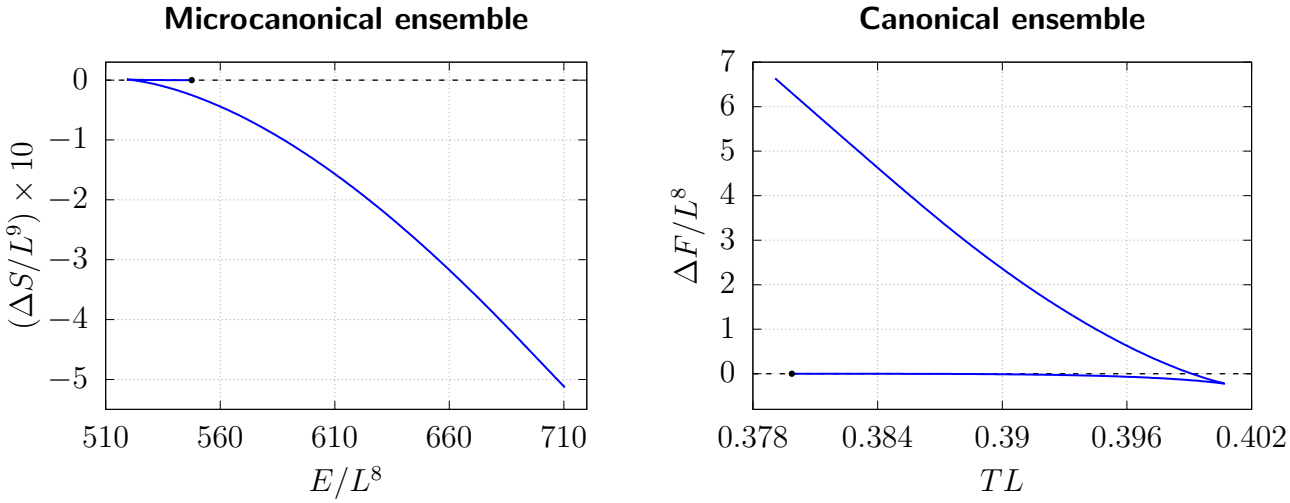

Fig. 4.6: *Phase diagram in the microcanonical ensemble (left) and canonical ensemble (right), of $\ell = 2^-$ lumpy black holes. The GL threshold point is indicated with a black solid disk. The zero is taken to be the Schwarzschild-$AdS_4 \times S^7$ black hole phase. The $\ell = 2^-$ dominate over the small Schwarzschild-$AdS_4 \times S^7$ black hole near the GL threshold point in both ensembles. In the canonical ensemble, thermal $AdS_4 \times S^7$ is the dominant phase in this range of temperatures.*

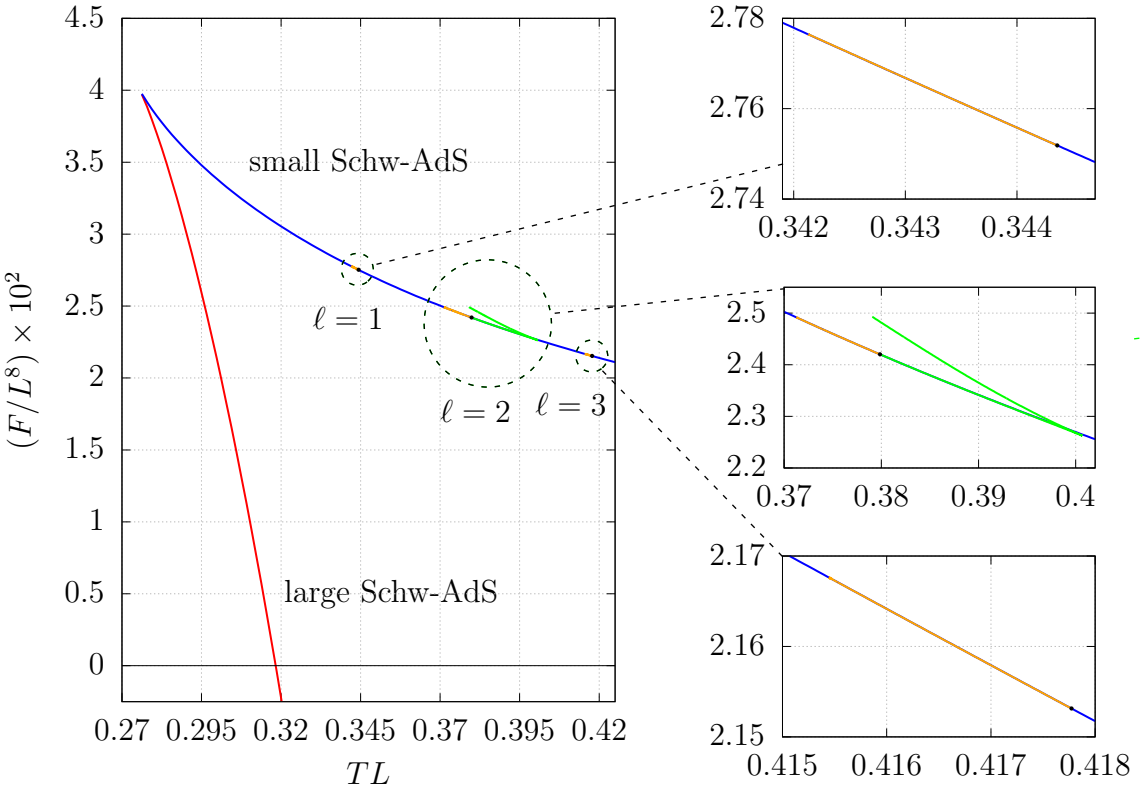

Fig. 4.7: *Phase diagram in the canonical ensemble of all lumpy black holes we have found in $D = 11$. The GL threshold points for the various modes are indicated with black solid disks. The zero of the free energy is taken to be the background $AdS_4 \times S^7$. As this figure shows, all lumpy black holes are subdominant with respect to thermal $AdS_4 \times S^7$ for the range of temperatures that they exist.*

black holes change [274]. The branch continues to higher energies again while the entropy decreases until it reaches $E^*/L^8 = 521.80046$. At this energy, the lumpy black holes and the Schwarzschild-AdS$_4 \times S^7$ black holes have the same entropy. Continuing along the $\ell = 2^-$ branch, for energies higher than E^*, the Schwarzschild-AdS$_4 \times S^7$ black hole is the phase with the highest entropy. The last solution we have found has energy $710.39314 \times L^8$, corresponding to $\lambda = 6$, but the phase diagram extends way beyond this value.

In the canonical ensemble, right panel in Fig. 4.6, the $\ell = 2^-$ black holes dominate over the small Schwarzschild-AdS$_4 \times S^7$ near the GL threshold. There is a turning point along this branch at $T_{\rm turn}L = 0.400824$ ($\lambda_{\rm turn} = 1.37424$) corresponding to a local maximum of the temperature. The difference of free energies increases at lower temperatures beyond the turning point and it becomes zero at $TL = 0.399124$. At even lower temperatures, the small Schwarzschild-AdS$_4 \times S^7$ dominates over the lumpy black hole phase. However, in the range of temperatures that the $\ell = 2^-$ black holes exist, thermal AdS$_4 \times S^7$ is always the dominant phase in the canonical ensemble.

The phase diagram in the canonical ensemble showing all the black hole phases that we have considered in this study is displayed in Fig. 4.7. As this figure shows, all families of lumpy black holes that we have studied are subdominant with respect to thermal $AdS_4 \times S^7$ in the range of temperatures that they exist. However, the $\ell = 2^-$ branch locally dominates over the small Schwarzschild-$AdS_4 \times S^7$ black holes for a small range of temperatures. It is clear from Fig. 4.7 that the families of lumpy black holes occupy a very small portion of the phase diagram.

4.4.2 Kaluza-Klein holography

An important class of observables that characterize the lumpy black holes are the vev's of the dual scalar operators of different conformal dimensions. These essentially parametrize the deformations of the internal space and they can be obtained using KK holography [270]. In this subsection we will focus on the $(p, q) = (5, 5)$, i.e. type IIB supergravity in $AdS_5 \times S^5$, since in this case the details of this procedure have been fully worked out in [270]. We provide the details of our calculation in the Appendices 4.A and 4.B to correct some typos in the literature and because the calculation of [19] seems to have some mistakes. The generalization to the $(p, q) = (4, 7)$ is beyond the scope of this study, even though there are some partial results in the literature [275, 276].

The lumpy black holes in $AdS_5 \times S^5$ have horizons that are non-uniformly smeared over the S^5, breaking the SO(6) symmetry of the latter down to SO(5). Holographically, this corresponds to the spontaneous breaking of the R-symmetry in the dual $\mathcal{N} = 4$ SYM theory and is reflected in the condensation of an infinite tower of scalar operators. The vev's of these operators encode the deformations of the internal S^5 and they can be computed, using KK holography, from the asymptotic expansion of the unknown functions $Q_1, \ldots, Q_7$ near the boundary of AdS_5 (see Appendix 4.B). We find that the operators with the lowest conformal dimension that develop a non-trivial vev are $\mathcal{S}^2$, $\mathcal{S}^3$ and $\mathcal{S}^4$. From (4.B.0.18), the vev's of these operators are given by:

$$\begin{aligned}
\langle \mathcal{O}_{\mathcal{S}^2} \rangle &= \frac{N^2}{2\pi^2} \frac{\sqrt{2}}{15} y_0^2 \beta_2, \\
\langle \mathcal{O}_{\mathcal{S}^3} \rangle &= \frac{N^2}{2\pi^2} \frac{1}{\sqrt{3}} y_0^3 \gamma_3, \\
\langle \mathcal{O}_{\mathcal{S}^4} \rangle &= \frac{N^2}{2\pi^2} \frac{1}{\sqrt{3}} y_0^4 \Big(\frac{19\sqrt{7}}{1500} \beta_2^2 - \delta_4 \Big),
\end{aligned} \tag{4.4.2.1}$$

where β_2, γ_3 and δ_4 are constants that can be obtained from the numerical solutions that we find. On the other hand, the other family of scalar operators of low dimension that could have contributed, namely $\{\mathcal{T}^0, \mathcal{T}^1, \mathcal{T}^2, \mathcal{T}^3, \mathcal{T}^4\}$, all have vanishing vev's.[7]

[7] From the expressions in equation (A.42) of [19], it would seem that $\langle \mathcal{O}_{\mathcal{T}^4} \rangle \neq 0$. We believe that this is incorrect. In fact, we have checked from the near boundary expansions in equation (A.10) of [19] that the equations of motion for some of the gauge invariant scalar fields at linear and quadratic order are not satisfied. Therefore, it may be that some of the expressions for the vev's given in [19] may not be correct.

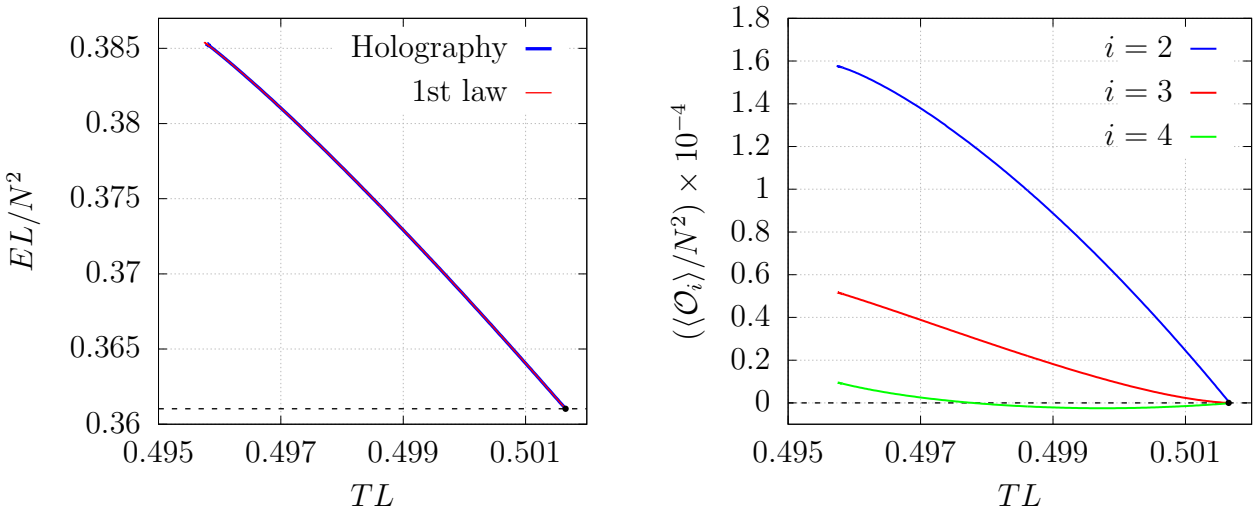

Fig. 4.8: *$\ell = 1$ bumpy black hole energy comparison (left) when it is computed by integrating the 1st law of thermodynamics (red line) and when it is computed using the holographic expression (4.4.1.4) (blue line). Dimensionless vev of the dual lower-dimensional scalar field $\mathcal{S}^{2,3,4}$ (right), as a function of the dimensionless temperature.*

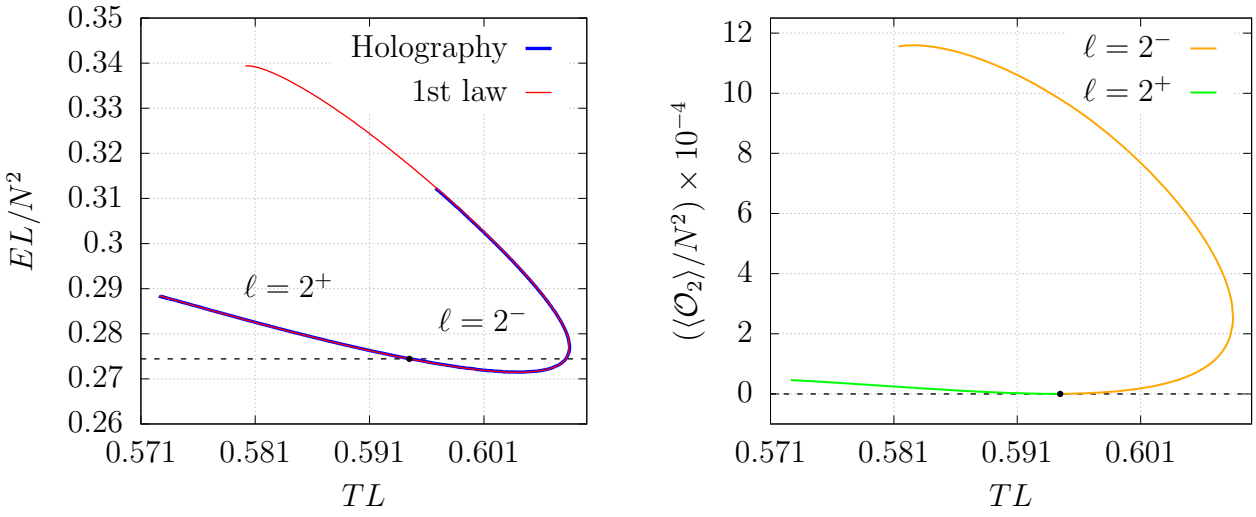

Fig. 4.9: *$\ell = 2$ bumpy black hole energy comparison (left) when it is computed by integrating the 1st law of thermodynamics (red line) and when it is computed using the holographic expression (4.4.1.4) (blue line). Dimensionless vev of the dual lower-dimensional scalar field $\mathcal{S}^2$ (right), as a function of the dimensionless temperature.*

There are various ways to extract the coefficients β_2, γ_3 and δ_4 (and δ_0) appearing in (4.4.2.1) from our numerical solutions. One possibility consists of taking derivatives of the Q's at the boundary and then project on to the harmonic basis. For instance,

from (4.B.0.5) the constant β_2 is given by:

$$\beta_2 \sim \int_{-1}^{+1} \partial_y^2 Q_{1,2,4,5,6,7}\big|_{y=1} Y_2(x)\mathrm{d}x \qquad (\text{for } \ell \text{ odd}), \tag{4.4.2.2}$$

where $Y_2(x)$ is the $\ell = 2$ SO(5) scalar harmonic (see Appendix 4.C) and the precise coefficient in front of the integral depends on the function Q that one uses to do the extraction. Another possibility to find the undetermined constants is to fit our numerical data according to the asymptotic expansion (4.B.0.5). This latter option has been shown to be more accurate and stable towards the end of the branches, specially for the coefficients that appear at 3rd and 4th order. The reason is that too close to the merger, the accuracy of the numerical solution deteriorates and we could not reliably compute the numerical derivatives needed to calculate the coefficients. In practice, we compute β_2 using both: (4.4.2.2) for all Q_i's, $i = 1, 2, 4, 5, 6, 7$ and performing data fits to check the consistency of the results and estimate the error in this quantity. The other coefficients, γ_3 and δ_4 (and δ_0), have generically been found fitting our numerical data.

The temperature dependence of $\langle \mathcal{O}_i \rangle \equiv \langle \mathcal{O}_{\mathcal{S}^i} \rangle$, $i = 2, 3, 4$, along the $\ell = 1$ lumpy black hole family is shown in Fig. 4.8 (right). The vev's vanishes at the GL threshold point, which lies on the Schwarzschild-AdS$_5 \times S^5$ solution, and attains a finite value at the merger. The behavior of $\langle \mathcal{O}_1 \rangle$ is consistent with the plot shown in Ref. [19], but $\langle \mathcal{O}_3 \rangle$ differ in sign and value. The corresponding behavior of the vev's along the $\ell = 3$ is qualitatively the same as that for the $\ell = 1$ family. As we show in Section 4.4.4, the approach of all three vev's to the merger is controlled by the local (singular) cone geometry in the bulk; in particular, it follows the same power law (with a logarithmic correction) and the same critical exponents as the other physical observables.

For the families with even ℓ we have only been able to compute accurately the vev $\langle \mathcal{O}_2 \rangle$ and the result is shown in Fig. 4.9 (right). Again, it vanishes at the GL threshold point and becomes positive along the extend of our branch. Unfortunately, in this case we could not find enough critical solutions to recover the critical exponents predicted by the local cone model.

We have also included an energy comparison when it is computed via integration of the 1st law and using the expression (4.4.1.4). In Fig. 4.8 (left) and 4.9 (left) we present the energy as a function of the temperature for $\ell = 1, 2^+$ and 2^- lumpy black holes. For the $\ell = 1$ and 2^+ families we check the consistency of the energy values almost for the whole branch. For the $\ell = 2^-$ family we could only do it partially, but far enough to cover the turning point, which is the main interest in this case. Clearly, the turning point is well-resolved by the energy computed using the 1st law. In all cases, the deviations for the values shown in these figures were less than a 0.03%.

4.4.3 Horizon geometry

In this subsection we study in detail the geometry of the horizon of the lumpy AdS$_p \times S^q$ black holes. We construct embedding diagrams of the horizon geometry into Euclidean

space to visualize how the shapes of the various spheres change as one moves along a given family of solutions. This allows us to get a better understanding of the possible topology changes at the critical points, where the lumpy black holes merge with new families of black holes.

The induced metric on the spatial cross-sections of the horizon of the lumpy AdS$_p\times$ S^q black holes is:

$$\begin{aligned} \mathrm{d}s^2\Big|_{\mathrm{H}} &= L^2 y_0^2 Q_5(0,a)\mathrm{d}\Omega^2_{(p-2)} \\ &\quad + R^2\left(\frac{4Q_4(0,a)}{2-a^2}\mathrm{d}a^2 + (1-a^2)^2 Q_6(0,a)\mathrm{d}\Omega^2_{(q-1)}\right). \end{aligned} \tag{4.4.3.1}$$

At the horizon, the radii of the S^{p-2} within the Anti-de Sitter factor and the radii of the S^{q-1} within the internal S^q are given by:

$$R_{p-2}(a) = L y_0\sqrt{Q_5(0,a)}, \qquad R_{q-1}(a) = R(1-a^2)\sqrt{Q_6(0,a)}, \tag{4.4.3.2}$$

respectively. These are gauge invariant quantities within the symmetry class of space-times that we consider. The behavior of these two quantities (and in particular their zeroes) as functions of the polar angle a dictate the topology of the horizon. Indeed, the geometry (4.4.3.1) can be understood as a fibration of an S^{p-2} and an S^{q-1} over an interval parametrized by the coordinate a with $a\in[-1,1]$. For all lumpy black holes, we see from (4.4.3.2) that $R_{q-1}(a)$ smoothly shrinks to zero size at both ends of the interval whilst R_{p-2} is always finite there. This results in the familiar horizon topology $S^{p-2}\times S^q$, as the Schwarzschild-AdS$_p\times S^q$ black hole. In the latter case, both radii $R_{p-2}(a)$ and $R_{q-1}(a)$ are constant everywhere. As we shall see momentarily, for the lumpy black holes these radii develop a non-trivial profile as we move along a given family, away from the GL threshold. In particular, $R_{p-2}(a)$ approaches zero at a point (or several points, depending on the harmonic ℓ labelling the family) on the horizon, becoming precisely zero at the merger. At the zero(s) of $R_{p-2}(a)$, the horizon becomes singular and the branch of lumpy black holes presumably merges with a new branch of topologically distinct black holes in a conifold-type-of transition. In analogy with the non-uniform black strings [13], we may define the 'lumpiness' parameter in terms of $R_{p-2}(a)$ as a measure of the 'distance' to the merger:

$$\lambda = \frac{1}{2}\left(\frac{\max[R_{p-2}(a)]}{\min[R_{p-2}(a)]} - 1\right). \tag{4.4.3.3}$$

For solutions close to the threshold of the GL ℓth zero mode, $R_{p-2}(a)$ is approximately constant on the horizon and consequently $\lambda\sim 0$, with $\lambda = 0$ precisely at the GL threshold point. Conversely, as we move along the family of lumpy black holes and towards the merger point, $\max[R_{p-2}(a)]$ remains finite whilst $\min[R_{p-2}(a)]\to 0$ and hence $\lambda\to\infty$, just as in the standard KK setting. The vanishing of R_{p-2} at a certain point $a = a_*$ happens in a singular way at the merger. We should expect that at the other side of the transition, the vanishing of R_{p-2} occurs in a smooth manner,

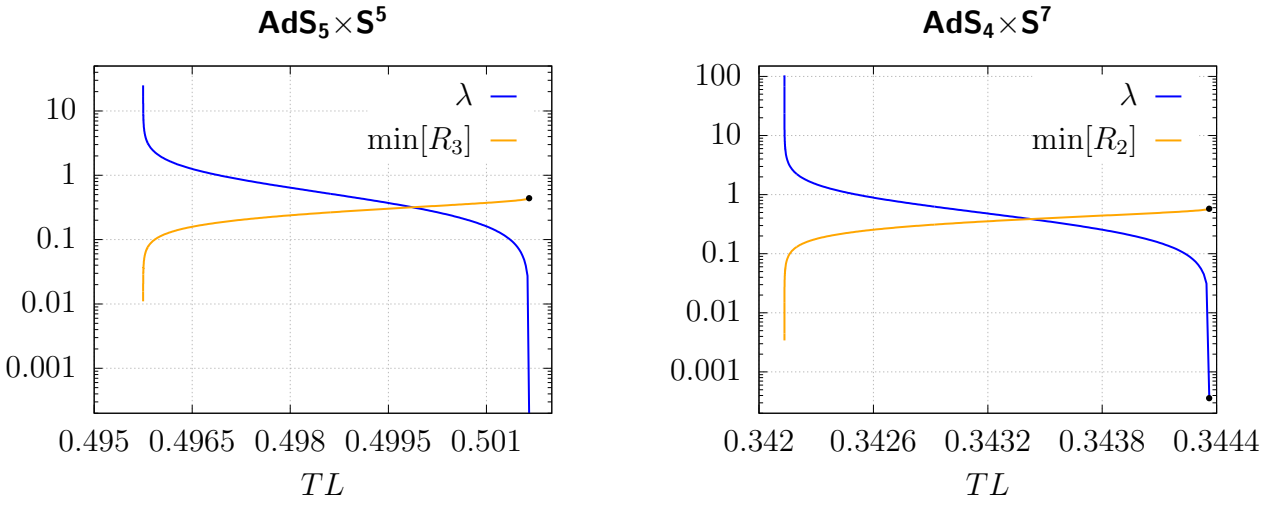

Fig. 4.10: *Lumpiness parameter λ and minimum radius of the S^{p-2}, $min[R_{p-2}(a)]$, for the $\ell = 1$ family of lumpy black holes as a function of the dimensionless temperature for the $(p, q) = (5, 5)$ (left) and $(p, q) = (4, 7)$ (right) cases. These plots show that λ diverges as we approach the merger point. Lumpy black hole families labelled by other harmonics ℓ exhibit a qualitatively similar behavior.*

	ℓ	1	2^+	3
$L_{\rm hor}/L$	$D = 10$	3.26912	–	3.21607
	$D = 11$	6.34959	6.39356	6.33214

Table 4.2: *Dimensionless horizon's length values of the most critical solutions that we have found for the families $\ell = 1, 3$ in $D = 10$ and $\ell = 1, 2^+, 3$ in $D = 11$. We did not construct critical enough solutions for $\ell = 2^+$ in $D = 10$.*

as it should if there exists a smooth family of black holes with a different horizon topology. We point out that even though the radius $R_{q-1}(a)$ of the horizon S^{q-1} vanishes smoothly at the endpoints of the interval parametrized by a for all lumpy black holes, for some families (but not all) the horizon S^{q-1} can also become singular at the merger. However, for all cases that we have considered, the horizon S^{p-2} shrinks to zero size in a singular manner somewhere on the horizon precisely at the merger, and hence the lumpiness parameter defined in (4.4.3.3) is a good measure of the degree of deformation of the horizon geometry.

In Fig. 4.10 we plot λ and the minimum of R_{p-2} on the horizon, as functions of the temperature. This figure shows that λ defined in (4.4.3.3) behaves in the same way as the analogous quantity for the non-uniform black strings: λ increases monotonically

along the family and diverges at the merger point. The behavior of λ for the other families of lumpy black holes labelled by different harmonics ℓ is qualitatively similar to Fig. 4.10 and we will not display them here. Note that for the $\ell = 2^-$ family, λ (and $\min[R_{p-2}(a)]$) are not uni-valued functions of the temperature because there is a turning point at some temperature. However, the corresponding λ still increases monotonically along the family and it diverges in a qualitatively similar manner as in the other families as we approach the merger point.

One may also define the horizon length along the S^q:

$$L_{\rm hor} = 2R\int_{-1}^{+1} {\rm d}a \sqrt{\frac{Q_4(0,a)}{2-a^2}}. \tag{4.4.3.4}$$

Again, for $\ell = 2$ solutions the integral is from 0 to 1 and there is an extra factor of 2. The Schwarzschild-AdS$_p \times S^q$ black hole has $L_{\rm hor} = \pi R$, which is nothing but the geodesic distance between the poles of the S^q of radius R. The behavior of this physical quantity along the family of lumpy black holes is quite generic. For a given ℓ, the curve starts at the GL point where $L_{\rm hor}/L = \pi$ or $L_{\rm hor}/L = 2\pi$ in $D = 10$ or 11 respectively, and it is a monotonically increasing function until it attains a finite value at the merger point. In Table 4.2 we list the different values at the merger for the families for which we have constructed critical enough solutions. As this table shows, the value of $L_{\rm hor}/L$ at the merger point is unique to each family. Critical localized-type black holes that merge with the various family of lumpy solutions studied here should give the same values of $L_{\rm hor}/L$.

Ref. [19] considered the possible topologies of the localized black hole solutions that would merge with a given family ℓ of lumpy black holes in $D = 10$. This reference based their analysis on the behavior of the induced Ricci scalar at the poles of the S^q, and concluded that the divergence of the Ricci scalar there indicated localization. In this study we follow a different route and instead we consider embedding diagrams into Euclidean space, as they are more intuitive and the topology changes become apparent.

One may consider two possible embeddings: at fixed coordinates of the S^{p-2} or fixed coordinates of the S^{q-1}. For fixed S^{q-1} coordinates, the horizon geometry may be embedded into $\mathbb{E}^p$, whereas for fixed S^{p-2} coordinates the horizon geometry may be visualized as an embedded surface in $\mathbb{E}^{q+1}$. Generically, the metric of $\mathbb{E}^n$ reads

$${\rm d}s^2_{\mathbb{E}^n} = {\rm d}X^2 + {\rm d}Y^2 + Y^2 {\rm d}\Omega^2_{(n-2)}. \tag{4.4.3.5}$$

The embedded surface has the form: $X = X(a)$ and $Y = R_{p-2}(a)$ or $Y = R_{q-1}(a)$ for fixed S^{q-1} or S^{p-2} coordinates respectively. Then, matching (4.4.3.5) with (4.4.3.1), we obtain $X(a)$:

$$X(a) = R\int_{-1}^{+1} {\rm d}a \sqrt{\frac{4Q_4(0,a)}{2-a^2} - y_0^2 \frac{(L/R)^2}{4Q_5(0,a)}\left(\frac{{\rm d}Q_5(0,a)}{{\rm d}a}\right)^2}, \tag{4.4.3.6}$$

for fixed S^{q-1} or

$$X(a) = R\int_{-1}^{+1} \mathrm{d}a \sqrt{\frac{4Q_4(0,a)}{2-a^2} - 4Q_6(0,a)\left(a - \frac{1-a^2}{4}\frac{\mathrm{d}\ln Q_6(0,a)}{\mathrm{d}a}\right)^2}, \qquad (4.4.3.7)$$

for fixed S^{p-2}. Recall that for $\ell = 2$ lumpy black holes the range of the integral is from 0 to 1, and to represent the full embedding we just add the mirror image with respect to the equator ($a = 0$). In our plots we present X/L versus Y/L for the three families $\ell = 1, 2^+$ and 2^-. For each of these families, we show together the embedding plots for fixed S^{p-2} and fixed S^{q-1} coordinates respectively, to make the topology of the horizon apparent. The qualitative behavior of the $\ell = 3$ family is essentially the same as that of $\ell = 1$; we comment on it below but we do not display any embedding plots for this case.

In Figs. 4.11, 4.12 and 4.13 we show the embeddings for different families of the $\mathrm{AdS}_4 \times S^7$ lumpy black holes. The analogous embeddings for the $\mathrm{AdS}_5 \times S^5$ lumpy black holes are qualitatively similar and we display them in Appendix 4.D. The only exception is the $\ell = 2^-$ family, which we comment on below.

In Fig. 4.11 we show representative embeddings for the $\ell = 1$ $\mathrm{AdS}_4 \times S^7$ lumpy black holes for fixed S^2 coordinates (top) and fixed S^6 coordinates (bottom). This figure shows that whilst the S^6 smoothly shrinks to zero size at both poles of the S^7, as λ increases it develops a conical singularity at the south pole. Similarly, the horizon S^2 has finite size everywhere on the S^7 for all lumpy black holes, but as λ increases it also develops a conical singularity at the south pole, suggesting that it pinches off there. At the other side of the transition, both of these singularities will be resolved, resulting on a S^6 that smoothly shrinks to zero size at the north pole of the S^7, whilst it has finite size on the south pole; conversely, the S^2 will continue to have finite size at the north pole but it shrinks smoothly at the south pole. The induced geometry at the other side of the merger can hence be modeled by the line element,

$$\sim f_1(a)\mathrm{d}a^2 + \cos^2 a f_2(a)\mathrm{d}\Omega^2_{(p-2)} + \sin^2 a f_3(a)\mathrm{d}\Omega^2_{(q-1)}, \qquad (4.4.3.8)$$

with the poles located at $a = 0$ and $a = \pi/2$, and non-trivial smooth and finite functions $f_i(a)$, $i = 1, 2, 3$, such that $f_3(0) = f_1(0)$ and $f_2(\pi/2) = f_1(\pi/2)$. Indeed, this geometry has the topology of S^{D-2} and hence it corresponds to a single localized black hole, as expected.

In Fig. 4.12 we consider the embeddings for different values of λ for the $\ell = 2^+$ family of $\mathrm{AdS}_4 \times S^7$ lumpy black holes. From the top panel in this figure, (i.e. fixed S^2 coordinates,) we see that the S^6 will develop conical singularities at the merger point at both the north and the south pole of the S^7. Likewise, the bottom panel (i.e. fixed S^6 coordinates) shows that the S^2 will also develop conical singularities at both poles for $\lambda \to \infty$. Then, we expect that the resolved geometry at the other side of the merger will have an S^6 that is finite in the whole a-interval, whilst the S^2 will smoothly shrink to zero size at both endpoints, giving an S^3. Therefore, we conclude

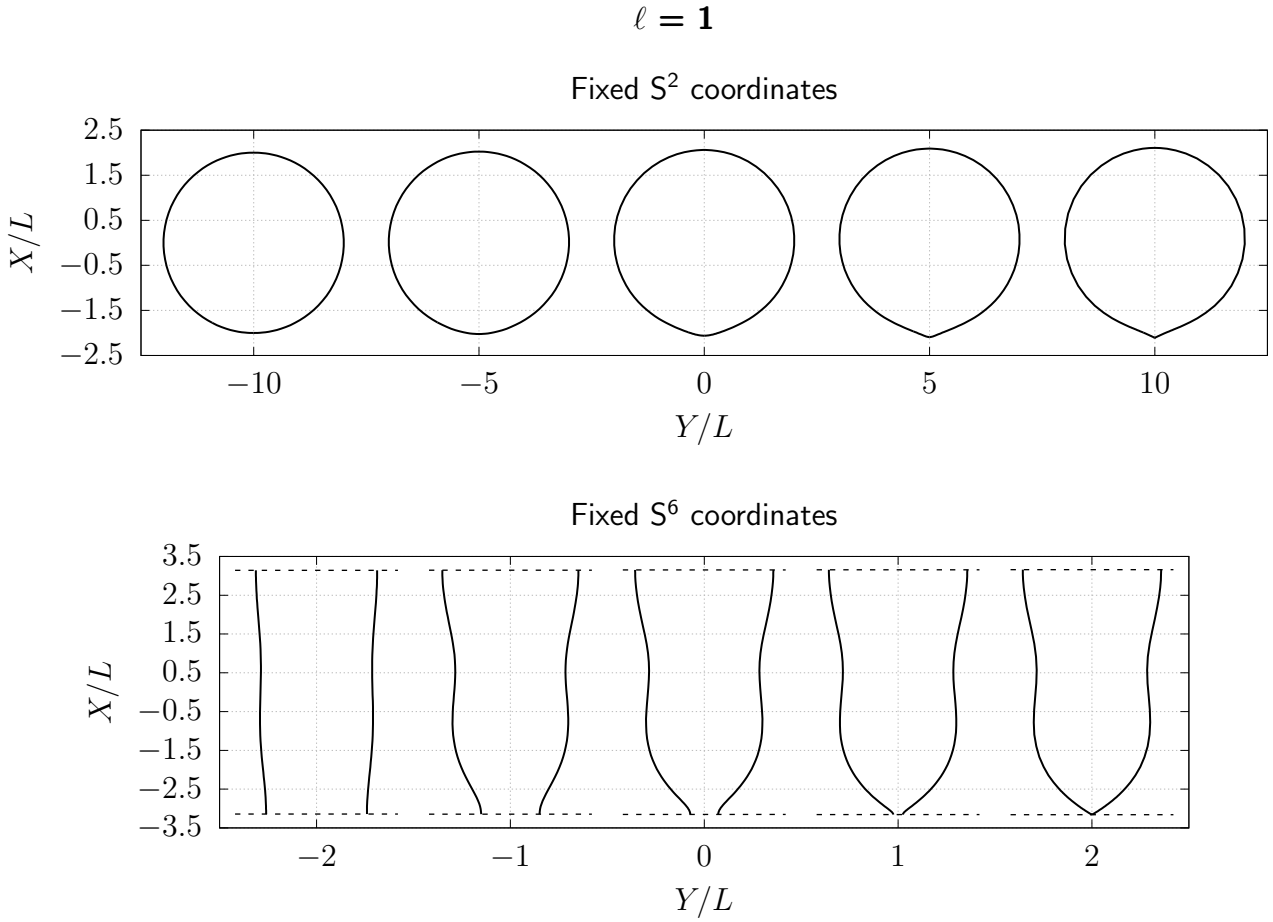

Fig. 4.11: *Embedding plots for fixed S^2/S^6 coordinates of lumpy black holes in $AdS_4 \times S^7$ with $\ell = 1$. This family merges with a localized black hole with S^9 horizon topology. The corresponding plots for $\ell = 3$ are similar to those for $\ell = 1$, but the pinch-off appears at the opposite pole.*

that the topology of the horizon of the family of black holes sitting at the other side of the merger is $S^3 \times S^6$, corresponding to a black belt.

The sequence of embeddings for the $\ell = 2^-$ family are shown in Fig. 4.13. For fixed S^2 coordinates (top panel), we see that see that the S^6 becomes more deformed, but it continues to shrink to zero size smoothly at the endpoints of the a-interval, even in the $\lambda \to \infty$ limit. On the other hand, for fixed S^6 coordinates (bottom panel), we see that for $\lambda \to \infty$ the S^2 will pinch off at two different points $a_*^{N/S}$ near the north and the south poles of the S^7. Therefore, in the resolved geometry at the other side of the merger, we expect that the a-interval will be divided in three subintervals, $-1 < a_*^S < a_*^N < 1$, such that: For $-1 \leq a \leq a_*^S$, the S^6 shrinks to zero size smoothly at $a = -1$, whilst it remains finite at $a = a_*^S$; on the other hand, the S^2 is finite at $a = -1$ and smoothly shrinks to zero at $a = a_*^S$. Therefore, the horizon topology in this region is S^9. Likewise, a similar reasoning shows that the horizon topology in the $a_*^N \leq a \leq 1$ interval is also that of an S^9. On the other hand, in the middle interval, $a_*^S \leq a \leq a_*^N$, we have that the S^6 is finite everywhere, whilst the S^2 smoothly

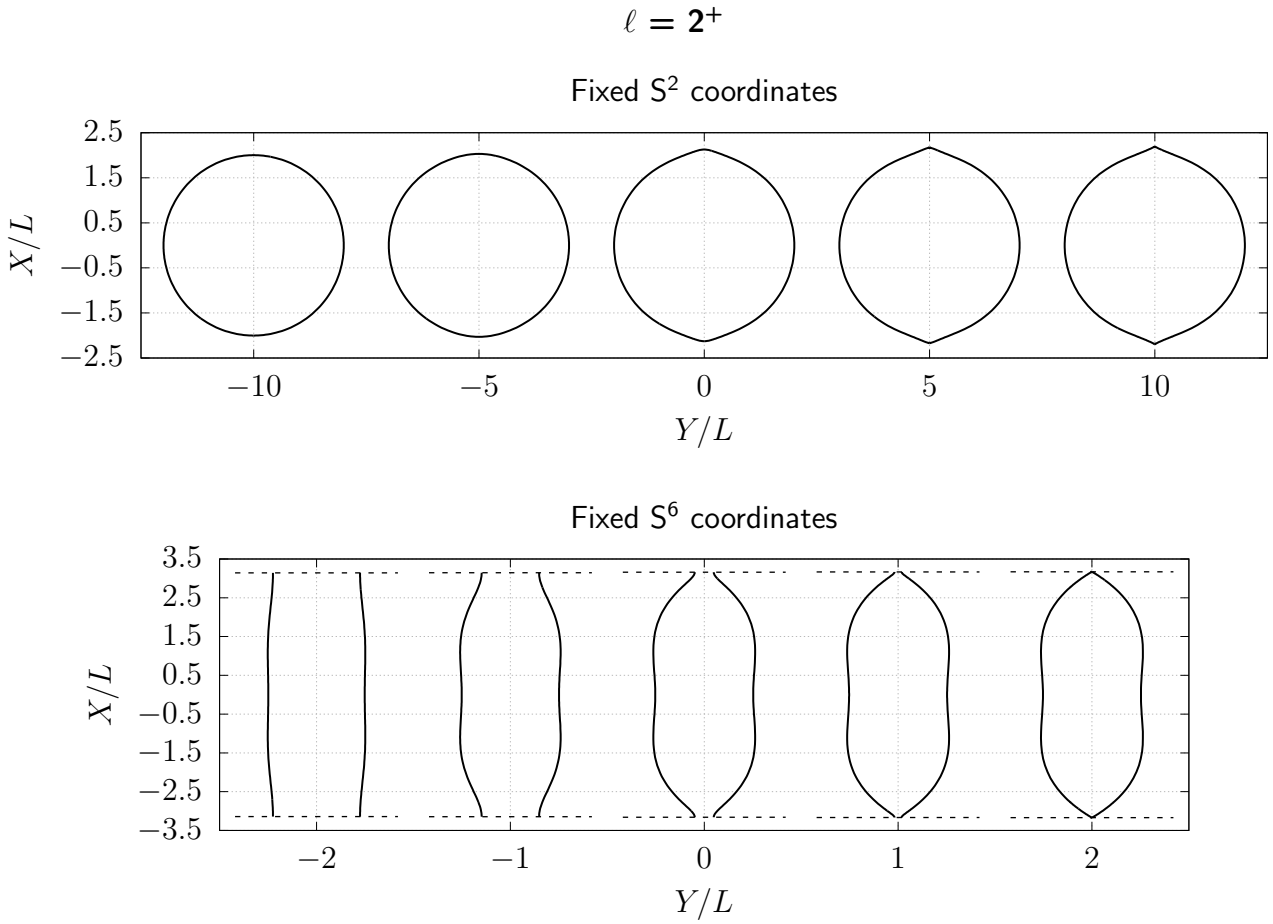

Fig. 4.12: *Embedding plots for fixed S^2/S^6 coordinates of lumpy black holes in $AdS_4 \times S^7$ with $\ell = 2^+$. This family merges with a black belt with horizon topology $S^3 \times S^6$.*

shrinks at the endpoints, giving a horizon topology of $S^3 \times S^6$. Putting everything together, we conclude that the $\ell = 2^-$ family of lumpy black holes merges with a family of black holes whose horizon topology is a connected sum $S^9\#(S^3 \times S^6)\#S^9$, that is, two localized black holes with a black belt joining them. Interestingly, the $\ell = 2^-$ family in the $AdS_5 \times S^5$ seems to merge with a different family of black holes. Indeed, as [19] pointed out and our embedding diagrams confirm (see Fig. 4.16), in this case the lumpy black holes merge with a double localized black hole, and hence the horizon topology of the latter is $S^8\#S^8$. It would seem that it should also be possible to connect the two localized black holes with a black belt, giving a topology $S^8\#(S^4 \times S^4)\#S^8$. However, if such a family of black holes exists, it does not merge with the $\ell = 2^-$ lumpy $AdS_5 \times S^5$ black holes.

The $\ell = 3$ solutions do not differ much with respect to the $\ell = 1$ ones in terms of the topology change across the transition. Although the profile of the embeddings presents more oscillations (since it belongs to a higher harmonic family), our data seems to indicate that the branch merges with another localized black hole with S^9

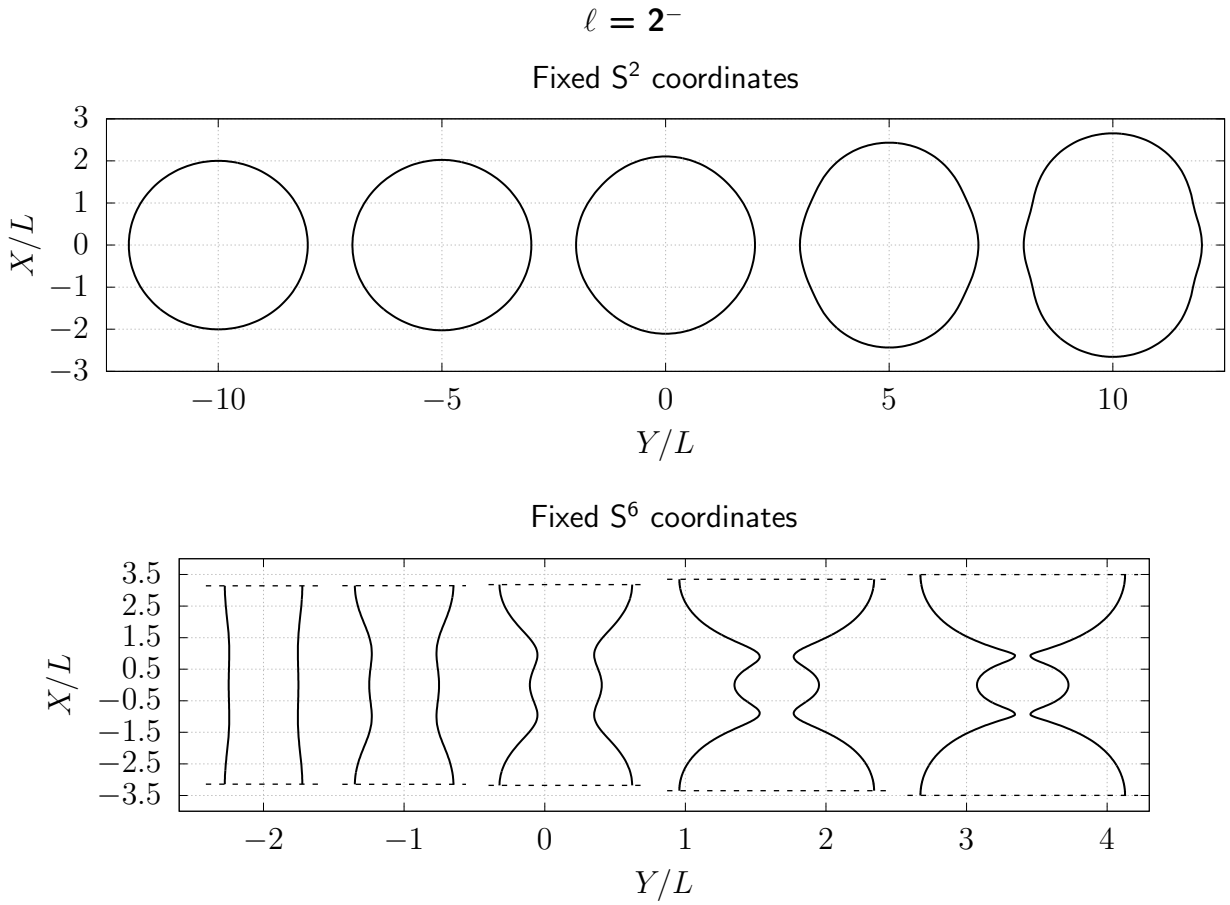

Fig. 4.13: *Embedding plots for fixed S^2/S^6 coordinates of lumpy black holes in $AdS_4 \times S^7$ with $\ell = 2^-$. This family merges with a black hole whose horizon topology is the connected sum $S^9\#(S^3 \times S^6)\#S^9$.*

horizon topology, but potentially having lumpiness along its horizon and hence distinct from the localized black hole family that merges with the $\ell = 1$ lumpy branch. Presumably, this new family of deformed localized black holes would merge with new families of multiple localized black holes and black belts. This is quite analogous to the situation in higher dimensional asymptotically flat singly spinning black holes, where different families of topologically spherical bumpy black holes, corresponding to different harmonics, merge with different families of black rings and bumpy black rings [147].

Summarizing, we have the following topology-change phase transitions for the different families of lumpy black holes considered in this chapter:

$$\begin{aligned}
\ell = 1: &\quad S^{p-2} \times S^q &\to &\quad S^{p+q-2}\,, \\
\ell = 2^+: &\quad S^{p-2} \times S^q &\to &\quad S^{p-1} \times S^{q-1}\,, \\
\ell = 2^-: &\quad S^{p-2} \times S^q &\to &\quad \begin{array}{l} S^{p+q-2}\#(S^{p-1} \times S^{q-1})\#S^{p+q-2} \\ S^{p+q-2}\#S^{p+q-2} \end{array}\,, \\
\ell = 3: &\quad S^{p-2} \times S^q &\to &\quad S^{p+q-2}\,.
\end{aligned} \tag{4.4.3.9}$$

Given the richness of the various topology changes that we have uncovered, it is not inconceivable that other topology changes are possible for values of (p, q) not considered in this analysis.

We see that except for the $\ell = 2^-$ family, the topology-changing transitions depend in a trivial way on the number of spacetime dimensions. The details of the underlying theory in each of the cases that we have considered, either type IIB supergravity or $11D$ supergravity, do seem not play a significant role. However, the particular way in which physical quantities approach the critical point does depend on the spacetime dimension, and is predicted by the local cone model governing the change of topology.

4.4.4 Critical behavior at the merger point

Topology-changing transitions in the space of equilibrium solutions have been previously studied in higher-dimensional general relativity. The first and most studied system is the transition between non-uniform black strings and localized black holes in standard KK theory. Kol [21] proposed that, in this case, the transition is governed by a Ricci-flat double cone over $S^2 \times S^{D-3}$. The S^{D-3} appears explicitly in both the non-uniform black strings and in the localized black holes; the S^2 on the other hand comes from the fact that the Euclidean time is fibered over an interval whose endpoints are on the horizon. The S^{D-3} is non-contractible in the black string phase, while it is contractible in the localized black hole phase; the opposite happens with the S^2, which is contractible in the black string phase and non-contractible in the black hole phase. There is now detailed numerical evidence that this model is correct in $D = 5, 6$ [22,157] and in $D = 10$ [1,158] (see [159] for an analytical approach in the large-D limit of general relativity). Beyond KK theory, Ref. [147, 160] considered mergers of singly spinning black hole solutions in asymptotically flat space and described local Lorentzian double cone models for the critical geometries controlling them. These papers considered mergers between rotating black holes, black rings, di-rings and black saturns in $D \geq 6$, providing strong evidence that such double-cone models do indeed describe the topology-changing phase transitions for asymptotically flat stationary black holes as well.

The topology-changing transitions that have been considered so far involve black hole spacetimes in pure Einstein gravity, and hence it is natural to consider local Ricci-flat cones to model the local singularity at the merger point. However, in this chapter we consider Einstein gravity in asymptotically $\mathrm{AdS}_p \times S^q$ coupled to a certain form field strength so it is not obvious that local Ricci-flat cones should still control the topology-change transitions in this case. In this section we will show that even though the topology change is still controlled by a conical geometry, the latter is no longer Ricci-flat due to the presence of fluxes in the internal S^q.

We will focus on the local merger between the $\ell = 1$ lumpy black holes with horizon topology $S^{p-2} \times S^q$ and a localized black hole with horizon topology S^{p+q-2}, but the discussion also applies to the other ℓ's. Based on previous studies, the double-cone

inherits a huge amount of spherical symmetry from the full solution: the S^{p-2} and S^{q-1} that appear explicitly in the metric, plus an additional S^r that comes from the fibration, in the Wick rotated geometry, of the Euclidean time circle over some base manifold that depends on the particular merger. In the canonical non-uniform black string/localized black hole merger, the base is an interval with the two endpoints on the horizon; this, together with the fibered Euclidean time circle, gives $r = 2$; in the black ring/black hole merger the base is a 2-disk giving $r = 3$. In the case under consideration the base is also an interval. This consists of any path that connects two points on the horizon along the polar direction and thus $r = 2$, just as in non-uniform black string/localized black hole transition. Similarly, this S^2 is contractible in the lumpy black hole phase, but it is not contractible in the localized phase.

By symmetry, the merger should be described by a cone over a triple direct product of spheres, $S^2 \times S^{p-2} \times S^{q-1}$:

$$\mathrm{d}s^2 = \mathrm{d}\rho^2 + \frac{\rho^2}{D-2}\left(\mathrm{d}\Omega^2_{(2)} + (p-3)\mathrm{d}\Omega^2_{(p-2)} + \alpha\,\mathrm{d}\Omega^2_{(q-1)}\right). \tag{4.4.4.1}$$

With the presence of a non-trivial fluxes, it is not obvious that the cone that controls the merger should be Ricci-flat and, as we shall see shortly, our data indicates that it is not. We will leave to future work the first principles understanding of the types of cones that control the topology changing transitions in the presence of fluxes. The numerical factors in (4.4.4.1) have been chosen so that the embeddings agree with our numerical solutions in the critical regime. The factors in front of the S^2 and the S^{p-2} in (4.4.4.1) ensure that the components in these directions of the associated Ricci tensor vanish; on the other hand, our data suggests that

$$\alpha = \alpha_0 + \frac{D}{4}, \tag{4.4.4.2}$$

where $\alpha_0 = q - 2$ corresponds to the coefficient for which (4.4.4.1) is Ricci-flat. This implies that the components of the Ricci tensor along the S^q do not vanish.

To test the validity of the local model (4.4.4.1), we compare the embeddings of the cone:

$$\begin{aligned}
&\text{Fixed } \Omega_{(q-1)}: \quad X(\rho) = \rho\sqrt{\frac{q+1}{D-2}}, \qquad Y(\rho) = \rho\sqrt{\frac{p-3}{D-2}},\\
&\text{Fixed } \Omega_{(p-2)}: \quad X(\rho) = \rho\sqrt{\frac{D-2-\alpha}{D-2}}, \qquad Y(\rho) = \rho\sqrt{\frac{\alpha}{D-2}},
\end{aligned} \tag{4.4.4.3}$$

with the embeddings of the horizon geometry of the critical lumpy black holes described in Section 4.4.3. The results are shown in Fig. 4.14 for the $AdS_4 \times S^7$ case and in Fig. 4.17 for the $AdS_5 \times S^5$ one. For fixed S^6 coordinates, Fig. 4.14 shows that there is a very good agreement between the local cone model and the actual geometry of the horizon. On the other hand, for fixed S^2 coordinates along the AdS factor, we can demand that the local geometry of the horizon near the pinch off region is well described by (4.4.4.1) and thereby fix the constant α. By doing this, we find

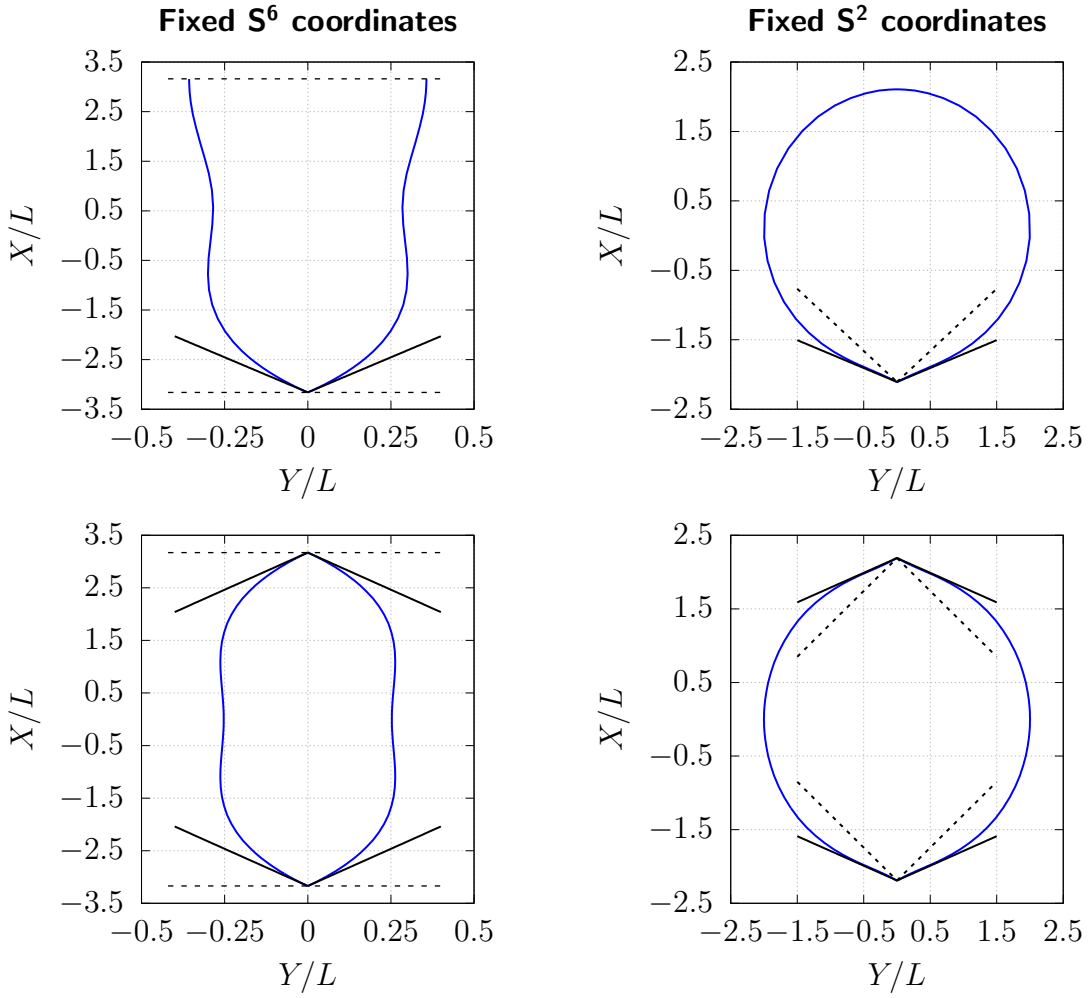

Fig. 4.14: *Embedding diagrams of the horizon for the $\ell = 1$ (top) and $\ell = 2^+$ (bottom) lumpy black holes (blue line) in $AdS_4 \times S^7$ for the largest lumpiness parameter that we have reached. The plots on the left correspond to fixed S^6 coordinates while the plots on the right correspond to fixed S^2 coordinates. The black lines correspond to the embeddings of the local cone that mediates the topology change transition. For fixed S^6 coordinates, the agreement between the cone model and the local horizon geometry is very good. For fixed S^2 coordinates, demanding that the cone model agrees with the local geometry suggests $\alpha = q - 2 + \frac{D}{4} = \frac{31}{4}$. In these two plots, the embeddings dictated by the Ricci-flat cone are indicated with dashed lines. Clearly, the latter do not agree with our data.*

that (4.4.4.2) is preferred. The dashed line in this figure shows the embedding of a Ricci-flat cone. Clearly, our numerical data is incompatible with a Ricci-flat cone.

The local cone model not only captures the shape of the horizon near the pinch off, but it also predicts the behavior of the physical quantities near the merger [263].

The latter follows from considering perturbations of (4.4.4.1) that preserve the various spheres while they change their relative sizes:

$$ds^2 = d\rho^2 + \frac{\rho^2}{D-2}\left(e^{\epsilon(\rho)}d\Omega^2_{(2)} + (p-3)e^{-\xi\epsilon(\rho)}d\Omega^2_{(p-2)} + \alpha\, e^{-\eta\epsilon(\rho)}d\Omega^2_{(q-1)}\right), \quad (4.4.4.4)$$

where ξ and η are free parameters. Imposing that the $\rho\rho$, S^2 and S^{p-2} components of the Ricci tensor of the perturbed cone (4.4.4.4) vanish implies that

$$\xi = \frac{2}{p-2}, \qquad \eta = 0, \qquad \text{or} \qquad \xi = 0, \qquad \eta = \frac{2}{q-1}. \quad (4.4.4.5)$$

Either choice leads to the same linear equation of motion for $\epsilon(\rho)$ and, unsurprisingly, it coincides with the equation of motion for the perturbation mode of the double-cone of [21]. Note that in our case, the first solution is the relevant one since it implies that the metric on the internal S^q is not modified at linear order; this is consistent with the vanishing of the components of the Ricci tensor along the S^2 and the S^{p-2} directions. On the other hand, the components along the S^q are affected by the leftover fluxes on this internal sphere, and hence they should be sourced at second order in perturbation theory. The general solution is given by:

$$\epsilon(\rho) = c_+\rho^{s_+} + c_-\rho^{s_-}, \quad (4.4.4.6)$$

with critical exponents

$$s_\pm = \frac{D-2}{2}\left(-1 \pm i\sqrt{\frac{8}{D-2}-1}\right). \quad (4.4.4.7)$$

For $D < 10$, the solutions have a non-zero imaginary part, which implies that they will spiral infinitely many times as they approach the origin $\rho = 0$; $D = 10$ is a marginal dimension for this model, where the imaginary part vanishes and the solution has a quartic power-law with an additional logarithmic term. For $D > 10$, the critical exponents become purely real and the approach to the origin is govern by two powers. In $D = 11$, we have $s_+ = 6$ and $s_- = 3$.

The prediction of [21] is that the deformations of the cone metric (4.4.4.6) should be reflected in the behavior of the physical quantities of the black holes sufficiently close to criticality, with the zero mode $\epsilon(\rho)$ measuring the deviation from the cone. According to this prediction, any physical quantity Q near the critical solution should behave as

$$\begin{aligned} (p,q) &= (5,5): \qquad \delta Q = \rho_0^4(C_1 + C_2\log\rho_0), \\ (p,q) &= (4,7): \qquad \delta Q = C_+\rho_0^6 + C_-\rho_0^3, \end{aligned} \quad (4.4.4.8)$$

where $\delta Q \equiv Q - Q_c$ and ρ_0 is any typical length scale that measures the deviation from the actual cone. In principle, sufficiently close to the merger, the topology change develops in the same manner independently of the boundary data that one considers.

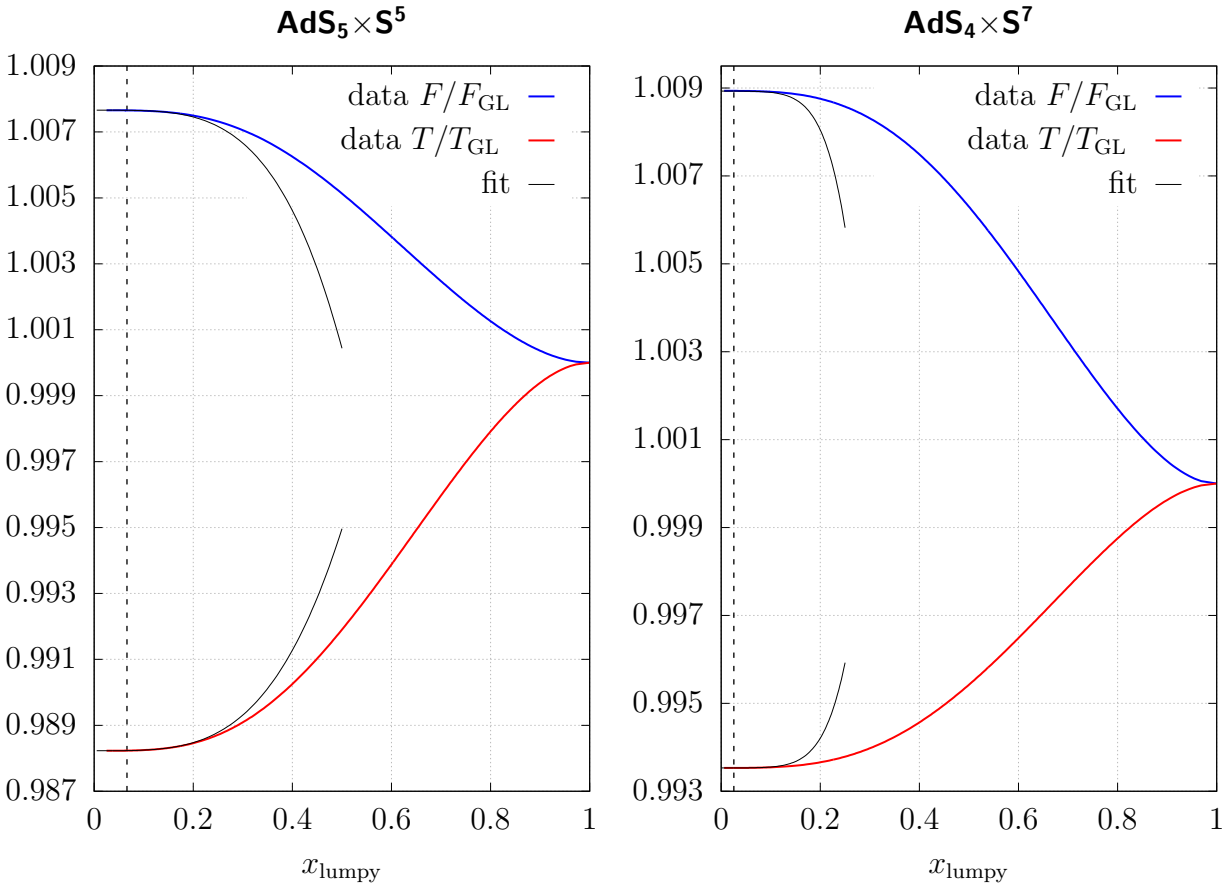

Fig. 4.15: *Normalized free energy (blue) and temperature (red) as a functions of x_{lumpy} for $\ell = 1$ lumpy black holes in $AdS_p \times S^q$. Data points to the left of the dashed vertical line are the ones used for the fit (in black). The other thermodynamic quantities exhibit a similar behavior.*

To compute the critical exponents from our numerical data and compare them with the predictions of the cone model (4.4.4.8), we have fitted the temperature, energy, entropy and free energy of critical enough solutions according to

$$\begin{aligned} (p,q) &= (5,5): \qquad f(x) = f_c + x^A(B + C\log x), \\ (p,q) &= (4,7): \qquad f(x) = f_c + x^A(B + Cx^3), \end{aligned} \tag{4.4.4.9}$$

with

$$x_{\text{lumpy}} = \frac{\min[R_{p-2}(a)]}{R y_0^\ell}\,, \tag{4.4.4.10}$$

measuring the deviation from the cone. Notice that at this point in $D = 11$ we have already assumed that one of the exponents is $A + 3$. This exponent corresponds precisely to the smallest contribution to $f(x)$. In this case one would ideally want to fit the near critical data to a function of the form $f(x) = f_c + Ax^B + Cx^D$, so that both exponents can be independently extracted and tested. However, in practice this turns out to be quite hard. The reason is that to carry out the fits, we only consider

	ℓ	Q_c	A	B	C
$T/T_{\rm GL}$	1	**0.98823**	**4.00002**	0.07251	−0.05082
	3	**0.98996**	**4.00017**	−0.01765	−0.08789
$E/E_{\rm GL}$	1	**1.06752**	**4.00005**	−0.75232	−0.00001
	3	**1.00739**	**3.99931**	−0.02129	0.04625
$S/S_{\rm GL}$	1	**1.18230**	**4.00004**	−2.04392	−0.00002
	3	**1.04771**	**3.99951**	−0.38000	0.21411
$\langle\mathcal{O}_2\rangle/N^2$	1	$\mathbf{1.571 \times 10^{-4}}$	**3.99997**	−0.13485	−0.05648
	3	$\mathbf{9.464 \times 10^{-6}}$	**3.99996**	0.00029	0.00016
$\langle\mathcal{O}_3\rangle/N^2$	1	$\mathbf{5.168 \times 10^{-5}}$	**3.99949**	−0.00052	0.00018
	3	$\mathbf{1.090 \times 10^{-6}}$	**4.00060**	-6×10^{-6}	9×10^{-6}
$\langle\mathcal{O}_4\rangle/N^2$	1	$\mathbf{9.499 \times 10^{-6}}$	**3.99994**	−0.00039	0.00015
	3	$\mathbf{7.882 \times 10^{-6}}$	**4.00028**	−0.00001	0.00003

Table 4.3: *Critical exponents and other parameters obtained from the fit of the temperature, energy, entropy and scalar vev's of the different lumpy solutions in $AdS_5 \times S^5$.*

	ℓ	Q_c	A	B	C
$T/T_{\rm GL}$	1	**0.99353**	**3.00005**	0.01318	8.97006
	2^+	**0.97730**	**2.99940**	0.02580	9.55439
	3	**0.99443**	**3.00003**	0.01290	8.68568
$E/E_{\rm GL}$	1	**1.01374**	**3.00000**	−0.02690	−16.87280
	2^+	**1.03911**	**2.99982**	−0.04605	−35.34570
	3	**1.00826**	**2.99996**	−0.01918	−12.96730
$S/S_{\rm GL}$	1	**1.02389**	**3.00000**	−0.04691	−29.42860
	2^+	**1.07090**	**2.99982**	−0.08444	−64.81000
	3	**1.01520**	**2.99996**	−0.03538	−23.91850

Table 4.4: *Critical exponents and other parameters obtained from the fits of the temperature, energy and entropy of the different lumpy solutions in $AdS_4 \times S^7$. Note that for a given ℓ, the critical exponents for the energy and the entropy are exactly the same. This is not surprising, since they are not independent: recall that in $D = 11$ the energy is found by integrating the 1st law of black hole mechanics.*

the solutions that are close to the merger and for those we have $x \sim 10^{-3}$. Therefore, the behavior of $f(x)$ near the critical point is completely dominated by the smallest exponent, 3 in this case, and the corrections introduced by the other exponent (6 in $D = 11$) are too small to be reliably detected.

In Figure 4.15 we present the fits for the free energy and the temperature (normalized with respect to the values at the marginal GL point) for the $\ell = 1$ lumpy family in $D = 10$ and $D = 11$. The other physical quantities behave in a qualitatively similar way and we do not present the fits here. We have critical enough solutions for the families $\ell = 1, 3$ in $D = 10$ and $\ell = 1, 2^+, 3$ in $D = 11$. The fit parameters that we have extracted from the various physical quantities are shown in Tables 4.3 and 4.4 respectively. As these tables show, the values of the exponents obtained from fitting different physical quantities are perfectly compatible with each other and match the predictions of the cone model. With our fitting procedure we also extract the values of the different thermodynamic quantities (normalized with respect to the values of the ℓth family at the marginal GL point) at the merger point. In the different cases studied in this chapter, the agreement with the cone model is very good, with deviations of 0.1% in the worst case. Working with a denser grid and/or including more data points, i.e. more solutions near the merger region, may improve the accuracy of the critical exponents. It should be clear from our studies that (4.4.4.1) does indeed capture both the local geometry of the horizon and the behavior of the physical quantities.

In $D = 10$ we have also explicitly checked that the vev's of the dual scalar field $\mathcal{S}^2$, $\mathcal{S}^3$ and $\mathcal{S}^4$, follow the same power law behavior near the merger as the other physical quantities. From the point of view of the cone model, this should not be surprising since any observable should exhibit the same behavior near the merger. However, from the point of view of holography, this is quite interesting. Firstly, the fact that the field theory observables, such as the vev's of the scalar operators, exhibit this scaling behavior indicates how the field theory knows about the topology change in the bulk: none of the field theory observables seem to become singular at the merger point; they simply develop a scaling behavior with exponents determined by the local cone model in the bulk. Secondly, one might naively expect that the vev's, being associated to scalar fields that are coupled to 5-dimensional gravity in AdS, develop a spiraling behavior since in $D = 5$ the critical exponents have a non-zero imaginary part. However, our result shows that this is not the case; the behavior near criticality is inherited from the full higher-dimensional solution.

4.5 Discussion and outlook

In this Chapter we have numerically constructed various families of asymptotically $\mathrm{AdS}_p \times S^q$ black holes with a non-trivial field strength; we have considered the specific cases of $(p, q) = (5, 5)$ corresponding to IIB supergravity in $\mathrm{AdS}_5 \times S^5$, and $(p, q) = (4, 7)$ corresponding to $11D$ supergravity in $\mathrm{AdS}_4 \times S^7$. These black holes have horizon topology $S^{p-2} \times S^q$ and were called 'lumpy' black holes in [19]. Each family is specified by an integer ℓ that labels the harmonic on the internal S^q in the decomposition of the linear perturbations around the Schwarzschild-$\mathrm{AdS}_p \times S^q$ black hole. For each harmonic, at a specific value of the horizon radius of the Schwarzschild-$\mathrm{AdS}_p \times S^q$ black hole given in (4.2.0.11), there exists a time-independent linear solu-

tion (i.e. a zero mode) of the Einstein's equations corresponding to a black hole with a slightly deformed horizon on the S^q. These linear modes can be uplifted to full non-linear solutions of the Einstein's equations, corresponding to the lumpy black holes. These zero modes signal the onset of the corresponding GL instability of the small Schwarzschild-$AdS_p \times S^q$ black hole.

Ref. [19] was the first one to construct lumpy black holes in $AdS_5 \times S^5$; on the other hand, our solutions in the $AdS_4 \times S^7$ case are new. Arguably, the solutions of [19] are only slightly non-uniform on the S^5, with their non-uniformity parameter (4.4.3.3) being $\lambda \sim \mathcal{O}(1)$ at most. In this study we have used similar numerical techniques as in the previous chapter of this thesis to extend the various families of lumpy black holes to very large values of λ, all the way to near the critical regime where they are expected to merge with other families of black holes with different horizon topology. While our results and those of [19] agree very well near the GL threshold point ($\lambda \ll 1$), we found some inconsistencies further along the branch towards more non-uniform lumpy black holes. We attribute this disagreement to the fact that the resolutions used in [19] were insufficient to accurately describe their most non-uniform black holes.

We have constructed the phase diagrams in both the microcanonical and the canonical ensembles all the way to the critical regime. In the microcanonical ensemble, we find that the lumpy black holes are always subdominant with respect to the Schwarzschild-$AdS_p \times S^q$ black hole with the same energy, except for the $\ell = 2^-$ family, which dominates in the region near the GL threshold point. In the canonical ensemble, for the range of temperatures that the lumpy black holes exist, thermal $AdS_p \times S^q$ is always the dominant phase whilst the lumpy black holes are always subdominant, even though the $\ell = 2^-$ family dominates over the small Schwarzschild-$AdS_p \times S^q$ black hole. This apparent disagreement between these two thermodynamic ensembles in $AdS_5 \times S^5$ was highlighted in [273].

The main goal of this chapter was to explore the topology-changing transitions that presumably connect, in the space of static solutions, $AdS_p \times S^q$ lumpy black holes with other families of black holes with different horizon topologies. This transitions have been well-studied in the past in the context of black holes in KK theory. Kol [21] predicted that such transitions were of the conifold-type and were governed by a local Ricci-flat cone. According to this model, the local cone not only controls the change of topology, but it also determines the near-merger behavior of the physical quantities of the black holes on both sides of the transition. These predictions have been recently numerically verified [1,22,157]. In this study we have extended these local cone models to black holes in $AdS_5 \times S^5$ and $AdS_4 \times S^7$ coupled to a (self-dual) five-form and a four-form field strength respectively. By constructing lumpy black holes with very large 'lumpiness' parameters (see (4.3.4.2)), we have verified, for the first time, that such local cone models also accurately describe the topology-changing transitions in $AdS_p \times S^q$ with the presence of non-trivial fluxes. Interestingly, we have found that the local cones (4.4.4.1) are no longer Ricci-flat because of the presence of fluxes in the internal S^{q-1} in this limit. Work towards understanding the new class of conical

geometries that arise when there are fluxes in the internal spheres is in progress.

For the asymptotically $AdS_5 \times S^5$ lumpy black holes, we have extracted the dual field theory observables using the procedure of KK holography [270]. Our computation fixes some typos and inconsistencies in [19]. We give the expressions for the vev's of the scalar operators $\mathcal{S}^2$, $\mathcal{S}^3$ and $\mathcal{S}^4$ in (4.B.0.18); on the other hand, the vev's of $\mathcal{T}^\ell$, $\ell = 0, 1, 2, 3, 4$, vanish identically in these backgrounds (and in the localized $AdS_5 \times S^5$ black holes). The vev's of the dual scalar operators exhibit the same scaling behavior near the merger as the other physical quantities, thus showing how these topology changes are 'detected' by the dual CFT. It is important to note that the behavior of the scalar operators near the merger is dictated by the full $10D$ geometry. The $11D$ solutions can also be dimensionally reduced on the S^7. The KK map in this case, to leading and quadratic order, was worked out in [275], and [276] respectively. We will leave the computation of the holographic data for this case for future work.

The most natural extension of this work is to consider localized black holes in $AdS_5 \times S^5$ and in $AdS_4 \times S^7$. Localized black holes in $AdS_5 \times S^5$ have been previously constructed in [20], but their solutions are still quite far from the merger with the lumpy black holes considered in this study. Using the same numerical techniques as in [1], we should be able to construct localized black holes in the critical regime and verify the predictions of the local cone model from the other 'side' of the transition. Work in this direction is in progress.

4.A Kaluza-Klein holography

In this appendix we review the procedure of holographic renormalization for solutions of IIB supergravity that are asymptotically $AdS_5 \times S^5$. This procedure was worked out in [270] (see also [277, 278] for related work) and named, for obvious reasons, Kaluza-Klein holography, or KK holography for short. We review it here to set up our conventions and fix the numerical factors. In Appendix 4.B we apply it to the specific class of solutions considered in this chapter. These calculations were previously reported in [19]. However, since we found some disagreements with their results, we decided to write down our calculations in full detail so that they can be straightforwardly and independently checked, should anyone wish to do so. That said, we have verified that our calculations pass all consistency checks and hence we are certain of their correctness.

Let us begin recalling that in the context of gauge/gravity duality one can compute vev's of the dual gauge invariant fields in the bulk by differentiating the (renormalized) on-shell supergravity action once with respect to the sources, a procedure known as holographic renormalization [191] (see also [192, 193]). In this way, one obtains the vev's of gauge invariant operators of the dual field theory in terms of certain coefficients in the asymptotic expansion of the bulk fields. Originally, this procedure was worked out for solutions that are asymptotically AdS. The extension to generic solutions that asymptote to the direct product $AdS \times X$, where X is some internal

(compact) manifold, requires to first carry out the dimensional reduction on X. In general, this dimensional reduction will involve an infinite tower of massive KK fields that come from the deformations of X, and which are dual to an infinite number of gauge invariant operators in the CFT. Here we will concentrate on the $\mathrm{AdS}_5 \times S^5$ case, which is the relevant one for this study.

Given that the information needed is encoded in the asymptotic behavior of the solution near the AdS boundary, one may work out the dimensional reduction analysis as a linear perturbation about the $\mathrm{AdS}_5 \times S^5$ background and then apply holographic renormalization. This is what the authors of [270] did in the most general way, using gauge invariant variables. This paper finds the effective 5-dimensional field equations and an explicit non-linear map between the higher-dimensional fields (which is the numerical data we have) and the solutions to these 5-dimensional equations. Integrating the latter equations one obtains a 5-dimensional (super)gravity action, which involves certain scalar fields; from here one can compute the 1-point correlation functions of the dual field theory applying holographic renormalization, introduced in Chapter 1.

At this point the idea is clear and [270] provides an algorithm to implement it in practice. However, the expressions that arise are quite lengthly and involved. This is essentially because the dimensional reduction cannot be truncated to the massless sector when the isometries of the internal space are broken. In other words, the mapping between higher- and lower-dimensional fields, ψ^k and Ψ^k respectively, in general is going to be highly non-linear:

$$\Psi^i = \psi^i - \sum_{j,k} \left(A^i_{jk} \psi^j \psi^k + B^i_{jk} D_\mu \psi^j D^\mu \psi^k + \mathcal{O}[\psi^3] \right), \tag{4.A.0.1}$$

where A^i_{jk} and B^i_{jk} are numerical coefficients. Luckily, it turns out that to find the vev of an operator of a given dimension, one only needs the map truncated at certain order in the number of fields [270]. Let us elaborate a bit more on this. If Ψ^i is dual to an operator of dimension i, one would need to expand the field up to order Z^i in the standard Fefferman-Graham (FG) coordinate to extract the operator's vev:

$$\Psi^i = \Psi^i_{(0)} + \Psi^i_{(1)} Z + \Psi^i_{(2)} Z^2 + \cdots + \Psi^i_{(i)} Z^i + \text{irrelevant terms}. \tag{4.A.0.2}$$

If only a finite number of terms in the near boundary expansion are needed to compute the vev of (4.A.0.1), then the r.h.s. of this expression can only involve a finite number of fields. Recall that after all, the outcome of this mapping is directly related to a physical observable which must be finite. As we will see in the following sections and in Appendix 4.B, the scalar operators whose vev's we shall compute have at most conformal dimension 4. Hence we will need to compute the near boundary expansion of the corresponding bulk fields up to order Z^4 in the FG radial coordinate. This truncates the mapping (4.A.0.1) to quadratic order in the number of fields.

In the rest of this appendix we will provide the details of this procedure in the context of this chapter. This has been done before in [270] and in [19]. Here we repeat the analysis in these references because we use slightly different conventions and we take this opportunity to fix typos.

4.A.1 Kaluza-Klein dimensional reduction on S^5

The first step consists of dimensionally reducing the higher-dimensional solutions on the S^5. To this end, we need to expand a general perturbation of $AdS_5 \times S^5$ into a complete set of scalar, vector and tensor harmonics. Due to the symmetries of the spacetimes that we consider, we only have to consider scalar harmonics on the S^5; from these we can obtain the corresponding scalar derived vector and tensor harmonics. The details of the basis of harmonics that we use in this chapter are summarized in the Appendix 4.C.

We consider solutions that are fluctuations about the $AdS_5 \times S^5$ background (denoted by the superscript "(0)"),

$$g_{MN} = g^{(0)}_{MN} + h_{MN}, \qquad F_{(5)} = F^{(0)}_{(5)} + f_{(5)}. \tag{4.A.1.1}$$

The indices are split up into $M = (\mu, a)$, with $\mu \in AdS_5$ and $a \in S^5$. From the point of view of transformations on the S^5, the perturbations of the metric components with two legs along the AdS factor behave as scalars, and the ones with one/two leg/s along the S^5, behave as vectors/tensors. Then we may expand the metric as follows:

$$\begin{aligned} h_{\mu\nu}(z,x) &= \sum_\ell h^\ell_{\mu\nu}(z) Y_\ell(x), & h_{\mu a}(z,x) &= \sum_\ell A^\ell_\mu(z) D_a Y_\ell(x), \\ h_{(ab)}(z,x) &= \sum_\ell B^\ell(z) D_{(a} D_{b)} Y_\ell(x), & h^a_a(z,x) &= \sum_\ell C^\ell(z) Y_\ell(x). \end{aligned} \tag{4.A.1.2}$$

Notice that the internal metric perturbation is split into the trace, which behaves as a scalar, and a traceless symmetric part which behaves as a tensor. Here we use the notation $T_{(ab)}$ to denote the symmetric and traceless part of a given 2-tensor T_{ab}: $T_{(ab)} = (T_{ab} + T_{ba})/2 - g_{ab} T^a_a/5$.

The 5-form field strength is expanded in the following way:[8]

$$\begin{aligned} f_{\mu\nu\rho\sigma\tau}(z,x) &= \sum_\ell 5 D_{[\mu} b^\ell_{\nu\rho\sigma\tau]}(z) Y_\ell(x), \\ f_{a\nu\rho\sigma\tau}(z,x) &= \sum_\ell b^\ell_{\nu\rho\sigma\tau}(z) D_a Y_\ell(x), \\ f_{abcd\mu}(z,x) &= \sum_\ell D_\mu b^\ell(z) \omega_{abcd}{}^e D_e Y_\ell(x), \\ f_{abcde}(z,x) &= \sum_\ell \omega_{abcde} b^\ell(z) \Lambda_\ell Y_\ell(x). \end{aligned} \tag{4.A.1.3}$$

where ω_{abcde} denotes the volume 5-form of the S^5 and $\Lambda_\ell = -\ell(\ell+4)$ is the harmonic eigenvalue with respect to the scalar Laplacian on the S^5. Given the self-duality condition of the 5-form, it turns out that the perturbation functions $b_{\nu\rho\sigma\tau}(z)$ and $b(z)$ are algebraically related,

$$b_{\nu\rho\sigma\tau} = \omega_{\mu\nu\rho\sigma}{}^\gamma (A^\ell_\gamma - D_\gamma b^\ell), \tag{4.A.1.4}$$

[8] The numerical constants here are introduced to match with the conventions of [279].

so we may just focus on one of them; $b(z)$ for instance.

A few comments are in order. First, in the expansions (4.A.1.3) we have only included fields that couple to scalar-derived vector and tensor harmonics. Although the analysis can be carried out in full generality, including transverse vector and tensor harmonics, the additional terms would break the SO(5) isometry that the class of spacetimes that we consider have. In addition, not all the expansions in (4.A.1.2) and (4.A.1.3) start with the lowest harmonic, $\ell = 0$; there are a few exceptions. Given that $\Lambda_0 = D_a Y_0(x) = D_{(a}D_{b)}Y_{0,1}(x) = 0$, then $A^0_\mu(z)$, $B^0(z)$, $B^1(z)$ and $b^0(z)$ are not defined, and the expansion for the perturbation fields $h_{\mu a}(z,x)$, $h_{(ab)}(z,x)$ and $f_{abcde}(z,x)$ starts at $\ell = 1$, $\ell = 2$ and $\ell = 1$, respectively.

The next step consists of inserting the expansions (4.A.1.2) and (4.A.1.3) into the linearized field equations, work out the mapping between the higher and the lower-dimensional fields, and obtain the 5-dimensional equations of motion for the dimensionally reduced fields. Before that, let us count the number of fields that we have. From the lower-dimensional perspective we have, for each value of ℓ, a graviton, $h^\ell_{\mu\nu}$, a vector, A^ℓ_μ, and three scalars: B^ℓ, C^ℓ and b^ℓ. However, some of these fields are pure gauge modes. By finding the gauge transformation rules, we can determine which ones are pure gauge and which ones correspond to the physical modes; a straightforward way to do this is to explicitly fix the gauge. For instance, Refs. [279–282] performed the actual dimensional reduction in the de Donder gauge, which can be shown to be equivalent to setting to zero the fields A^ℓ_μ and B^ℓ. In the analysis we do here we follow [270], and these are not set to zero but instead they are used to define gauge invariant physical fields. This is much more convenient in practice since, in general, solutions to 10-dimensional supergravity equations will not be in the de Donder gauge.

Consider a gauge transformation: $\delta x^M = -\xi^M$. The shift up to linear terms in the perturbation fields is given by[9]

$$\begin{aligned}\delta h_{MN} &= (D_M\xi_N + D_N\xi_M) + (D_M\xi^P h_{PN} + D_N\xi^P h_{PM} + \xi^P D_P h_{MN}),\\ \delta f_{MNPQR} &= -5D_{[M}\xi^S F^{(0)}_{NPQR]S} - (5D_{[M}\xi^S f_{NPQR]S} - \xi^S D_S f_{MNPQR}).\end{aligned} \tag{4.A.1.5}$$

Here the gauge parameter $\xi_M(z,x)$ is also expanded in harmonics,

$$\xi_\mu(z,x) = \sum_\ell \xi^\ell_\mu(z)Y_\ell(x)\,, \quad \xi_a(z,x) = \sum_\ell \xi^\ell(z)D_a Y_\ell(x)\,. \tag{4.A.1.6}$$

Plugging (4.A.1.2), (4.A.1.3) and (4.A.1.6) into (4.A.1.5), we obtain the gauge transformations of the perturbations at linear order, and from these we can identify the gauge invariant combinations. At linear order these transformations can be directly read off by looking at the coefficients of each harmonic. At quadratic order, one needs to project onto the basis of spherical harmonics to identify the transformation rules.

[9] Notice that the background is kept fixed: $\delta g^{(0)}_{MN} = 0 = \delta F^{(0)}$.

	Fields	Gauge inv. fields
$\ell = 0$	$h^0_{\mu\nu}$ C^0	$\bar{C}^0 \equiv C^0$
$\ell = 1$	$h^1_{\mu\nu}$ C^1 A^1_μ b^1	$\bar{h}^1_{\mu\nu} \equiv h^1_{\mu\nu} - D_\mu \tilde{A}^1_\nu - D_\nu \tilde{A}^1_\mu$ $\bar{b}^1 \equiv \frac{1}{4} b^1 - \frac{1}{2\Lambda_1} C^1$
$\ell \geq 2$	$h^\ell_{\mu\nu}$ C^ℓ A^ℓ_μ b^ℓ B^ℓ	$\bar{h}^\ell_{\mu\nu} \equiv h^\ell_{\mu\nu} - D_\mu \tilde{A}^\ell_\nu - D_\nu \tilde{A}^\ell_\mu$ $\bar{C}^\ell \equiv C^\ell - \Lambda_\ell B^\ell$ $\bar{b}^\ell \equiv \frac{1}{4} b^\ell - \frac{1}{2} B^\ell$

Table 4.5: *Fields and gauge invariant combinations at linear order. For $\ell = 0$ there is only one gauge invariant field and $h^0_{\mu\nu}$ is a deformation of the AdS part of the background metric (since it carries trivial harmonic index). To construct gauge invariant combinations for $\ell > 0$, one needs to introduce the auxiliary field: $\tilde{A}^1_\mu \equiv A^1_\mu - D_\mu C^1/(2\Lambda_1)$, such that $\delta \tilde{A}^1_\mu = \xi^1_\mu$, and for $\ell > 1$, $\tilde{A}^\ell_\mu \equiv A^\ell_\mu - D_\mu B^\ell/2$ (then $\delta \tilde{A}^\ell_\mu = \xi^\ell_\mu$).*

Gauge invariance and equations at leading order

At leading order one obtains the following gauge transformations of the perturbations:

$$\begin{aligned} \delta h^\ell_{\mu\nu} &= D_\mu \xi^\ell_\nu + D_\nu \xi^\ell_\mu, & \ell \geq 0, \\ \delta A^\ell_\mu &= D_\mu \xi^\ell + \xi^\ell_\mu, & \ell \geq 1, \\ \delta B^\ell &= 2\xi^\ell, & \ell \geq 2, \\ \delta C^\ell &= 2\Lambda_\ell \xi^\ell, & \ell \geq 0, \\ \delta b^\ell &= \xi^\ell, & \ell \geq 1. \end{aligned} \tag{4.A.1.7}$$

Given that the different harmonics ℓ are decoupled at linear order, we analyze the cases $\ell = 0, 1$ and $\ell \geq 2$, separately. From (4.A.1.7) one can easily identify the gauge invariant combinations, which we summarize in the following table:

Notice that the definition of the field $\bar{b}^\ell$ in Table 4.5 includes a factor $1/4$ which is not present in [270]. This simply corresponds to a different normalization of the field strength: in our equations of motion (4.1.0.5) the coupling in front of the field strength is $1/96$, whereas [270, 279–282] considered $1/6$. To be consistent with the mapping, we need to rescale our field strength which amounts to the $1/4$ factor in the dimensionally reduced b^ℓ field.

To obtain the equations of motion for the gauge invariant fields, we plug the expansions (4.A.1.2) and (4.A.1.3) into the linearized type IIB supergravity equations

of motion and project onto a given spherical harmonic. The equations for the fields $\bar{h}^\ell_{\mu\nu}$, $\bar{C}^\ell$ nor $\bar{b}^\ell$ are of the Klein-Gordon type, but these fields are not mass eigenstates. Diagonalizing, one finds the following gauge invariant combinations [279, 280]:

$$\begin{aligned}
\hat{s}^\ell &= \frac{1}{20(\ell+2)}\left(\bar{C}^\ell - 10(\ell+4)\bar{b}^\ell\right), && \ell \geq 2,\\
\hat{t}^\ell &= \frac{1}{20(\ell+2)}\left(\bar{C}^\ell + 10\ell\bar{b}^\ell\right), && \ell \geq 0,\\
\hat{\phi}^\ell_{(\mu\nu)} &= \bar{h}^\ell_{(\mu\nu)} - \frac{1}{(\ell+1)(\ell+3)} D_{(\mu}D_{\nu)}\left(\frac{2}{5}\bar{C}^\ell - 12\bar{b}^\ell\right), && \ell \geq 1,
\end{aligned} \tag{4.A.1.8}$$

satisfying:

$$\begin{aligned}
\Box\hat{s}^\ell &= \ell(\ell-4)\hat{s}^\ell, && \ell \geq 2,\\
\Box\hat{t}^\ell &= (\ell+4)(\ell+8)\hat{t}^\ell, && \ell \geq 0,\\
\Box\hat{\phi}^\ell_{(\mu\nu)} &= \left(\ell(\ell+4)-2\right)\hat{\phi}^\ell_{(\mu\nu)}, && \ell \geq 1,
\end{aligned} \tag{4.A.1.9}$$

where the 'box' operator is the D'Alembertian in AdS$_5$. Now one can easily identify the mass of the different modes (in units of AdS radius $L = 1$); the scalar fields $\hat{s}^\ell$, $\hat{t}^\ell$ and the graviton $\hat{\phi}^\ell_{(\mu\nu)}$ are dual to operators of conformal dimensions:[10] $\{\Delta_+, \Delta_-\} = \{\ell, 4-\ell\}$, $\{\Delta_+, \Delta_-\} = \{\ell+8, -\ell-4\}$ and $\{\Delta_+, \Delta_-\} = \{\ell+4, -\ell\}$ respectively.

Gauge invariance and equations at quadratic order

At quadratic order the expressions are much more involved; for this reason we first discuss the scalar sector (B^ℓ, C^ℓ and b^ℓ) and then the tensor sector ($h^\ell_{\mu\nu}$ and A^ℓ_μ).

As mentioned earlier, at quadratic order the gauge transformations are obtained by projecting onto the basis of spherical harmonics. For instance, the transformation rule for the scalar field B^ℓ is given by:

$$\delta B^\ell(z) = \frac{1}{z(\ell)q(\ell)}\int D^{(a}D^{b)}Y_\ell\,\delta h_{(ab)}\,\mathrm{d}\omega_5, \tag{4.A.1.10}$$

with $\delta h_{(ab)} = 2D_{(a}\xi^P h_{b)P} + \xi^P D_P h_{(ab)}$; $z(\ell)$ and $q(\ell)$ are defined in Appendix 4.C. Let us discuss again different values of ℓ separately. For $\ell = 1$ we have two scalars, C^1 and b^1, whose gauge transformations are the same as those at linear order, equation (4.A.1.7), and hence the gauge invariant quantities at quadratic order are the same as those in Table 4.5. For $\ell = 0$ we only have one scalar: C^0; its gauge transformation is:

$$\begin{aligned}
\delta C^0 = \sum_{\ell\geq 1}\frac{z(\ell)}{\Omega_5}\Bigg(&2\xi^\ell B^\ell q(\ell) + \frac{2}{5}\Lambda_\ell\xi^\ell C^\ell + \xi^\mu_\ell D_\mu\bar{C}^\ell\\
&- \Lambda_\ell\left(\xi^\ell C^\ell + 2\xi^\mu_\ell\tilde{A}^\ell_\mu\right)\Bigg),
\end{aligned} \tag{4.A.1.11}$$

[10] Recall that $\Delta_- = 4 - \Delta_+$.

and the corresponding gauge invariant combination is given by:

$$\bar{\bar{C}}^0 = \bar{C}^0 + \sum_{\ell\geq 1}\frac{z(\ell)}{\Omega_5}\Big(\frac{3}{10}\Lambda_\ell B^\ell \bar{C}^\ell - \frac{1}{4}\Lambda_\ell\left(\Lambda_\ell+8\right)(B^\ell)^2 - \tilde{A}^\mu_\ell D_\mu \bar{C}^\ell + \Lambda_\ell \tilde{A}^\mu_\ell \tilde{A}^\ell_\mu\Big), \tag{4.A.1.12}$$

where $\bar{C}^\ell$ and $\tilde{A}^\ell_\mu$ are defined in Table 4.5. Notice that the sum above starts at $\ell = 1$, but B^1 is not defined. We have written it this way just for notational compactness, and from this section onwards whenever we have B^1 we actually mean C^1/Λ_1. Here Ω_5 denotes the surface area of the unit round S^5.

For $\ell \geq 2$ we have the whole scalar sector, B^ℓ, C^ℓ and b^ℓ. At quadratic order the gauge transformations are given by

$$\begin{aligned}
\delta B^{\ell_1} &= 2\xi^{\ell_1} + \frac{1}{z_{\ell_1}q_{\ell_1}}\sum_{\ell_2,\ell_3\geq 1}\Big(2\xi^\mu_{\ell_2}A^{\ell_3}_\mu c_{\ell_1\ell_2\ell_3} + \frac{2}{5}\xi^{\ell_2}C^{\ell_3}d_{\ell_3\ell_1\ell_2} \\
&\qquad + \xi^\mu_{\ell_2}D_\mu B^{\ell_3}d_{\ell_2\ell_1\ell_3} + \xi^{\ell_2}B^{\ell_3}e_{\ell_1\ell_2\ell_3}\Big), \\
\delta C^{\ell_1} &= 2\Lambda_{\ell_1}\xi^{\ell_1} + \frac{1}{z_{\ell_1}}\sum_{\ell_2,\ell_3\geq 1}\Big(2B^{\ell_2}\xi^{\ell_3}d_{\ell_1\ell_2\ell_3} + \left(\xi^{\ell_2}C^{\ell_3} + 2\xi^\mu_{\ell_2}A^{\ell_3}_\mu\right)b_{\ell_1\ell_2\ell_3} \\
&\qquad + \Big(\frac{2}{5}\Lambda_{\ell_2}\xi^{\ell_2}C^{\ell_3} + \xi^\mu_{\ell_2}D_\mu C^{\ell_3}\Big)a_{\ell_1\ell_2\ell_3}\Big), \\
\delta b^{\ell_1} &= \xi^{\ell_1} + \frac{1}{\Lambda_{\ell_1}z_{\ell_1}}\sum_{\ell_2,\ell_3\geq 1}\left(\xi^\mu_{\ell_2}D_\mu b^{\ell_3} + \Lambda_{\ell_2}b^{\ell_2}\xi^{\ell_3}\right)\left(b_{\ell_1\ell_2\ell_3} + \Lambda_{\ell_3}a_{\ell_1\ell_2\ell_3}\right),
\end{aligned} \tag{4.A.1.13}$$

with the notation for normalization factors and triple integrals defined in Appendix 4.C: $z_{\ell_1} \equiv z(\ell_1)$, $a_{\ell_1\ell_2\ell_3} \equiv a(\ell_1,\ell_2,\ell_3)$, etc. From these transformations one infers the following gauge invariant fields:[11]

$$\begin{aligned}
\bar{\bar{C}}^{\ell_1} &= \bar{C}^{\ell_1} - \frac{1}{2z_{\ell_1}}\sum_{\ell_2,\ell_3\geq 1}\Big(\frac{2}{5}\Big(\Lambda_{\ell_2}a_{\ell_1\ell_2\ell_3} + \frac{5}{2}b_{\ell_1\ell_2\ell_3} - \frac{\Lambda_{\ell_1}}{q_{\ell_1}}d_{\ell_3\ell_1\ell_2}\Big)B^{\ell_2}\bar{C}^{\ell_3} \\
&\quad + \Big(d_{\ell_1\ell_2\ell_3} - \frac{\Lambda_{\ell_1}}{2q_{\ell_1}}e_{\ell_1\ell_2\ell_3} \\
&\qquad + \frac{\Lambda_{\ell_3}}{5}\Big[\Lambda_{\ell_2}a_{\ell_1\ell_2\ell_3} + \frac{5}{2}b_{\ell_1\ell_2\ell_3} - \frac{\Lambda_{\ell_1}}{q_{\ell_1}}d_{\ell_2\ell_1\ell_3}\Big]\Big)B^{\ell_2}B^{\ell_3} \\
&\quad + 2\tilde{A}^{\ell_2}_\mu\Big(D^\mu\bar{C}^{\ell_3}a_{\ell_1\ell_2\ell_3} + \tilde{A}^\mu_{\ell_3}\Big[b_{\ell_1\ell_2\ell_3} - \frac{\Lambda_{\ell_1}}{q_{\ell_1}}c_{\ell_1\ell_2\ell_3}\Big]\Big)\Big), \\
\bar{\bar{b}}^{\ell_1} &= \bar{b}^{\ell_1} + \frac{1}{z_{\ell_1}}\sum_{\ell_2,\ell_3\geq 1}\Big(\frac{\Lambda_{\ell_3}}{2\Lambda_{\ell_1}}B^{\ell_2}\bar{b}^{\ell_3}b_{\ell_3\ell_1\ell_2} + \frac{1}{10q_{\ell_1}}d_{\ell_3\ell_1\ell_2}B^{\ell_2}\bar{C}^{\ell_3} \\
&\quad + \frac{1}{8}\Big(\frac{\Lambda_{\ell_3}}{\Lambda_{\ell_1}}b_{\ell_3\ell_1\ell_2} + \frac{2}{5}\frac{\Lambda_{\ell_3}}{q_{\ell_1}}d_{\ell_2\ell_1\ell_3} + \frac{1}{q_{\ell_1}}e_{\ell_1\ell_2\ell_3}\Big)B^{\ell_2}B^{\ell_3} \\
&\quad + \tilde{A}^{\ell_2}_\mu\Big(\frac{1}{2q_{\ell_1}}\tilde{A}^\mu_{\ell_3}c_{\ell_1\ell_2\ell_3} + \frac{1}{\Lambda_{\ell_1}}D^\mu\bar{b}^{\ell_3}b_{\ell_2\ell_1\ell_3}\Big)\Big).
\end{aligned} \tag{4.A.1.14}$$

[11] A few typos have been corrected with respect to the expressions given in [19, 270].

In the tensor sector we are only interested in the massless KK graviton, i.e., $h^0_{\mu\nu}$ (see [270] for the analysis of massive gravitons). At quadratic order, this field transforms according to:

$$\begin{aligned}\delta h^0_{\mu\nu} = D_\mu\xi^0_\nu + D_\nu\xi^0_\mu + \Big(& D_\mu\xi^\alpha_0 h^0_{\alpha\nu} + D_\nu\xi^\alpha_0 h^0_{\alpha\mu} + \xi^\alpha_0 D_\alpha h^0_{\mu\nu} \\ &+ \sum_{\ell\geq 1}\frac{z_\ell}{\Omega_5}\Big(D_\mu\xi^\alpha_\ell h^\ell_{\alpha\nu} + D_\nu\xi^\alpha_\ell h^\ell_{\alpha\mu} + \xi^\alpha_\ell D_\alpha h^\ell_{\mu\nu} \\ &- \Lambda_\ell(\xi^\ell h^\ell_{\mu\nu} + 2D_{(\mu}\xi^\ell A^\ell_{\nu)})\Big)\Big).\end{aligned} \tag{4.A.1.15}$$

Then the combination

$$\begin{aligned}\bar{\bar{h}}^0_{\mu\nu} = h^0_{\mu\nu} + \frac{1}{3}\bar{\bar{C}}^0 g^{(0)}_{\mu\nu} - \sum_{\ell\geq 1}\frac{z_\ell}{\Omega_5}\Big(& -\frac{1}{2}\Lambda^\ell\Big(B^\ell\bar{h}^\ell_{\mu\nu} + \frac{1}{2}D_\mu B^\ell D_\nu B^\ell\Big) \\ &+ D_\mu\tilde{A}^\alpha_\ell\bar{h}^\ell_{\nu\alpha} + D_\nu\tilde{A}^\alpha_\ell\bar{h}^\ell_{\mu\alpha} + \tilde{A}^\alpha_\ell D_\alpha\bar{h}^\ell_{\mu\nu} \\ &+ D_\mu\tilde{A}^\alpha_\ell D_\nu\tilde{A}^\ell_\alpha + \tilde{A}^\alpha_\ell\tilde{A}^\ell_\alpha g^{(0)}_{\mu\nu} - \tilde{A}^\ell_\mu\tilde{A}^\ell_\nu\Big),\end{aligned} \tag{4.A.1.16}$$

where $g^{(0)}_{\mu\nu}$ denotes the AdS$_5$ background metric, is not gauge invariant but provides a correction to the spacetime metric that transforms nicely. Notice that what plays the role of 'gauge invariant' field at linear order here is the combination:

$$\bar{h}^{(0)}_{\mu\nu} \equiv h^0_{\mu\nu} + \frac{1}{3}\bar{C}^0 g^{(0)}_{\mu\nu}, \tag{4.A.1.17}$$

although it is not gauge invariant either (recall that $\delta\bar{C}^0 = 0$ but $\delta h^0_{\mu\nu} = D_\mu\xi^0_\nu + D_\nu\xi^0_\mu$). The shift in $\bar{C}^0$ can be understood as a Weyl transformation that brings the 5-dimensional action to the Einstein frame. Then $\bar{h}^{(0)}_{\mu\nu}$ satisfies the proper linearized Einstein equation [270].

From the gauge invariant scalar fields, one can define the same combinations as in (4.A.1.8), now replacing the 'bar' fields by the double 'bar' ones, which satisfy the modified equations of motion [280]:

$$\begin{aligned}(\Box - \ell(\ell-4))\,\hat{\hat{s}}^\ell &= \frac{1}{2(\ell+2)}\Big((\ell+4)(\ell+5)Q^\ell_1 + Q^\ell_2 \\ &\qquad + (\ell+4)(D_\mu Q^{\mu\ell}_3 + Q^\ell_4)\Big), \\ (\Box - (\ell+4)(\ell+8))\,\hat{\hat{t}}^\ell &= \frac{1}{2(\ell+2)}\Big(\ell(\ell-1)Q^\ell_1 + Q^\ell_2 - \ell(D_\mu Q^{\mu\ell}_3 + Q^\ell_4)\Big),\end{aligned} \tag{4.A.1.18}$$

where the double 'hat' notation is to emphasize that these are defined in terms of gauge invariant fields at quadratic order (i.e., they are built up from double 'bar' fields). Note that the masses are the same as those of the linear fields $\hat{s}$ and $\hat{t}$, equation (4.A.1.9). The box operator is again the D'Alembertian in AdS$_5$ and the Q's that appear in the

r.h.s. of the equations are given by:

$$\begin{aligned}
Q_1^{\ell_1} &= \frac{1}{20 z_{\ell_1} q_{\ell_1}} \sum_{\ell_2,\ell_3} \Big((c_{\ell_1\ell_2\ell_3} + d_{\ell_2\ell_3\ell_1} + d_{\ell_3\ell_2\ell_1}) T_{\ell_2\ell_3} \\
&\qquad + 32 c_{\ell_1\ell_2\ell_3} D_\mu \hat{s}^{\ell_2} D^\mu \hat{s}^{\ell_3} \Big), \\
Q_2^{\ell_1} &= \frac{1}{20 z_{\ell_1}} \sum_{\ell_2,\ell_3} \Big(10 S_{\ell_1\ell_2\ell_3} + (b_{\ell_1\ell_2\ell_3} - 2 f_{\ell_3} a_{\ell_1\ell_2\ell_3}) T_{\ell_2\ell_3} \\
&\qquad + 32 b_{\ell_1\ell_2\ell_3} D_\mu \hat{s}^{\ell_2} D^\mu \hat{s}^{\ell_3} \Big), \\
Q_3^{\mu\ell_1} &= \frac{1}{z_{\ell_1} f_{\ell_1}} \sum_{\ell_2,\ell_3} \Big((U_{\ell_2} + 3V_{\ell_2}) \hat{s}^{\ell_2} D^\mu \hat{s}^{\ell_3} + W_{\ell_2} D^{(\mu} D^{\nu)} \hat{s}^{\ell_2} D_\nu \hat{s}^{\ell_3} \Big) b_{\ell_2\ell_1\ell_3}, \\
Q_4^{\ell_1} &= -\frac{1}{4 z_{\ell_1}} \sum_{\ell_2,\ell_3} \Big(T_{\ell_2\ell_3} + V_{\ell_2} (16 f_{\ell_3} - 40 V_{\ell_3}) \hat{s}^{\ell_2} \hat{s}^{\ell_3} \Big) a_{\ell_1\ell_2\ell_3},
\end{aligned} \tag{4.A.1.19}$$

with

$$\begin{aligned}
T_{\ell_2\ell_3} &= (3 V_{\ell_2} V_{\ell_3} + 5 U_{\ell_2} U_{\ell_3}) \hat{s}^{\ell_2} \hat{s}^{\ell_3} + W_{\ell_2} W_{\ell_3} D^{(\mu} D^{\nu)} \hat{s}^{\ell_2} D_{(\mu} D_{\nu)} \hat{s}^{\ell_3}, \\
S_{\ell_1\ell_2\ell_3} &= -V_{\ell_2} V_{\ell_3} b_{\ell_2\ell_1\ell_3} \hat{s}^{\ell_2} \hat{s}^{\ell_3} - 8 (a_{\ell_1\ell_2\ell_3} f_{\ell_2} f_{\ell_3} \hat{s}^{\ell_2} \hat{s}^{\ell_3} + b_{\ell_1\ell_2\ell_3} D^\mu \hat{s}^{\ell_2} D_\mu \hat{s}^{\ell_3}) \\
&\quad + V_{\ell_3} U_{\ell_2} a_{\ell_1\ell_2\ell_3} D^\mu (\hat{s}^{\ell_2} D_\mu \hat{s}^{\ell_3}) + W_{\ell_2} V_{\ell_3} a_{\ell_1\ell_2\ell_3} D_\mu (D^{(\mu} D^{\nu)} \hat{s}^{\ell_2} D_\nu \hat{s}^{\ell_3}) \\
&\quad + a_{\ell_1\ell_2\ell_3} V_{\ell_2} (64 f_{\ell_3} - 80 V_{\ell_3}) \hat{s}^{\ell_2} \hat{s}^{\ell_3},
\end{aligned} \tag{4.A.1.20}$$

and

$$V_\ell = -\frac{5}{3} U_\ell = 2\ell, \qquad W_\ell = \frac{4}{\ell + 1}. \tag{4.A.1.21}$$

4.A.2 Non-linear mapping: 5d action

If we pack together fields and masses: $\hat{\hat{\psi}}^I_\ell = \{\hat{\hat{s}}^\ell, \hat{\hat{t}}^\ell\}$, $m^2_{I,\ell} = \{\ell(\ell-4), (\ell+4)(\ell+8)\}$ $(I = 1, 2)$, the scalar field equations at quadratic order (4.A.1.18) may be written as:

$$\begin{aligned}
(\Box - m^2_{I,\ell_1}) \hat{\hat{\psi}}^I_{\ell_1} = \sum_{\ell_2,\ell_3 \geq 1} \Big(& D^I_{\ell_1\ell_2\ell_3} \hat{s}^{\ell_2} \hat{s}^{\ell_3} + E^I_{\ell_1\ell_2\ell_3} D_\mu \hat{s}^{\ell_2} D^\mu \hat{s}^{\ell_3} \\
& + F^I_{\ell_1\ell_2\ell_3} D_{(\mu} D_{\nu)} \hat{s}^{\ell_2} D^{(\mu} D^{\nu)} \hat{s}^{\ell_3} \Big),
\end{aligned} \tag{4.A.2.1}$$

for some coefficients $D^I_{\ell_1\ell_2\ell_3}$, $E^I_{\ell_1\ell_2\ell_3}$ and $F^I_{\ell_1\ell_2\ell_3}$ that are easily identified using the expressions in (4.A.1.19) (see Table 4.6). Notice that the scalar fields in the l.h.s. are the gauge invariant combinations at second order whilst the fields in the r.h.s. are the gauge invariant fields at linear order (given that the r.h.s. side is quadratic in the fields). In the case where $\hat{s}^2$ is the only non-zero field at linear order (as it is for our solutions), the gauge invariant combinations can be written in the form:

$$\hat{\hat{\psi}}^I_\ell = \hat{\psi}^I_\ell + A^I_{\ell sB} \hat{s}^2 B^2 + A^I_{\ell BB} (B^2)^2 + A^I_{\ell sA} D^\mu \hat{s}^2 \tilde{A}^2_\mu + A^I_{\ell AA} (\tilde{A}^2_\mu)^2 \tag{4.A.2.2}$$

with $\hat{\psi}^I_\ell = \{\hat{s}^\ell, \hat{t}^\ell\}$. The four coefficients $A^I_{\ell XX}$ are also given in Table 4.6.

The higher derivative terms on the r.h.s. of equation (4.A.2.1) can be removed via a field redefinition $\hat{\bar{\psi}}^I_\ell \to \Psi^I_\ell = \{\mathcal{S}^\ell, \mathcal{T}^\ell\}$ of the form:

$$\Psi^I_{\ell_1} = w^I_{\ell_1}\left(\hat{\bar{\psi}}^I_{\ell_1} - \sum_{\ell_2,\ell_3\geq 1}\left(J^I_{\ell_1\ell_2\ell_3}\hat{s}^{\ell_2}\hat{s}^{\ell_3} + K^I_{\ell_1\ell_2\ell_3}D_\mu\hat{s}^{\ell_2}D^\mu\hat{s}^{\ell_3}\right)\right), \tag{4.A.2.3}$$

with

$$\begin{aligned} w^I_\ell &= \left\{\sqrt{\frac{8\ell(\ell-1)(\ell+2)}{\ell+1}\frac{z_\ell}{\Omega_5}}, \sqrt{\frac{8(\ell+2)(\ell+4)(\ell+5)}{\ell+3}\frac{z_\ell}{\Omega_5}}\right\}, \\ J^I_{\ell_1\ell_2\ell_3} &= \frac{1}{2}E^I_{\ell_1\ell_2\ell_3} + \frac{1}{4}F^I_{\ell_1\ell_2\ell_3}\left(m^2_{I,\ell_1} - m^2_{1,\ell_2} - m^2_{1,\ell_3} + 8\right), \\ K^I_{\ell_1\ell_2\ell_3} &= \frac{1}{2}F^I_{\ell_1\ell_2\ell_3}. \end{aligned} \tag{4.A.2.4}$$

Then the field equations for the fields Ψ^I_ℓ read

$$(\Box - m^2_{I,\ell_1})\Psi^I_{\ell_1} = \sum_{\ell_2,\ell_3\geq 1}\lambda^I_{\ell_1\ell_2\ell_3}\mathcal{S}^{\ell_2}\mathcal{S}^{\ell_3}, \tag{4.A.2.5}$$

where

$$\begin{aligned} \lambda^I_{\ell_1\ell_2\ell_3} = \frac{w^I_{\ell_1}}{w^1_{\ell_2}w^1_{\ell_3}}\Big(&D^I_{\ell_1\ell_2\ell_3} + (m^2_{I,\ell_1} - m^2_{1,\ell_2} - m^2_{1,\ell_3})J^I_{\ell_1\ell_2\ell_3} \\ &- \frac{2}{5}K^I_{\ell_1\ell_2\ell_3}m^2_{1,\ell_2}m^2_{1,\ell_3}\Big). \end{aligned} \tag{4.A.2.6}$$

All quadratic and cubic scalar couplings have been determined and can be found in the literature [279–282], but in our case it is sufficient to retain only the quadratic coupling to the field $\hat{s}^2$ (or $\mathcal{S}^2$). The numerical factors up to this quadratic coupling can be found in Table 4.6.

A very similar approach can be carried out for the massless KK graviton; the equation of motion for $\bar{\bar{h}}^0_{\mu\nu}$ at quadratic order is sourced by higher derivative interactions [270] which, just as in the case of the scalars, can be removed through the field redefinition:

$$\begin{aligned} G_{\mu\nu} = \bar{\bar{h}}^0_{\mu\nu} - \frac{1}{12}\Big(&\frac{2}{9}D_\mu D^\rho\hat{s}^2 D_\nu D_\rho\hat{s}^2 - \frac{10}{3}\hat{s}^2 D_\mu D_\nu\hat{s}^2 \\ &+ \Big(\frac{10}{9}D_\mu\hat{s}^2 D^\mu\hat{s}^2 - \frac{32}{9}(\hat{s}^2)^2\Big)g^{(0)}_{\mu\nu}\Big). \end{aligned} \tag{4.A.2.7}$$

The equations of motion for the scalar fields and the massless graviton after the field redefinitions, (4.A.2.3) and (4.A.2.7), can be obtained by varying a 5-dimensional action with a negative cosmological constant. Therefore these mappings define the desired non-linear KK map from solutions of the 10-dimensional equations $\{\hat{s}^\ell, \hat{t}^\ell, \bar{\bar{h}}^0_{\mu\nu}\}$ to solutions of the 5-dimensional equations $\{\mathcal{S}^\ell, \mathcal{T}^\ell, G_{\mu\nu}\}$. More precisely, given the

	$\hat{\hat{s}}^\ell$ $(I=1)$		$\hat{\hat{t}}^\ell$ $(I=2)$		
ℓ	2	4	0	2	4
$D^I_{\ell 22}$	$-16\sqrt{\frac{2}{15}}$	$-\frac{172\sqrt{7}}{25}$	$\frac{229}{75}$	$\frac{304}{25}\sqrt{\frac{6}{5}}$	$\frac{52\sqrt{7}}{5}$
$E^I_{\ell 22}$	$\frac{2}{5}\sqrt{\frac{6}{5}}$	$\frac{3\sqrt{7}}{5}$	$-\frac{11}{20}$	$-\frac{6}{5}\sqrt{\frac{6}{5}}$	$-\frac{\sqrt{7}}{5}$
$F^I_{\ell 22}$	$\frac{1}{3}\sqrt{\frac{2}{15}}$	$\frac{7\sqrt{7}}{45}$	$\frac{1}{60}$	$\frac{1}{15}\sqrt{\frac{2}{15}}$	0
$A^I_{\ell sB}$	$\frac{7}{5}\sqrt{\frac{3}{10}}$	$\frac{7\sqrt{7}}{10}$	$-\frac{3}{40}$	$-\frac{7}{5\sqrt{30}}$	$-\frac{\sqrt{7}}{10}$
$A^I_{\ell BB}$	$-\frac{17}{20}\sqrt{\frac{3}{10}}$	$-\frac{\sqrt{7}}{10}$	$-\frac{1}{80}$	$\frac{3}{20}\sqrt{\frac{3}{10}}$	$\frac{\sqrt{7}}{40}$
$A^I_{\ell sA}$	$-\frac{1}{\sqrt{30}}$	$-\frac{3\sqrt{7}}{20}$	$-\frac{1}{48}$	$-\frac{1}{5\sqrt{30}}$	0
$A^I_{\ell AA}$	$-\frac{1}{4}\sqrt{\frac{3}{10}}$	$-\frac{\sqrt{7}}{20}$	$-\frac{1}{80}$	$-\frac{1}{20}\sqrt{\frac{3}{10}}$	0
$J^I_{\ell 22}$	$\frac{8}{5}\sqrt{\frac{2}{15}}$	$\frac{83\sqrt{7}}{90}$	$-\frac{3}{40}$	$-\frac{8}{15}\sqrt{\frac{2}{15}}$	$-\frac{\sqrt{7}}{10}$
$K^I_{\ell 22}$	$\frac{1}{3\sqrt{30}}$	$\frac{7\sqrt{7}}{90}$	$\frac{1}{120}$	$\frac{1}{15\sqrt{30}}$	0
$\lambda^I_{\ell 22}$	$-\frac{16}{\sqrt{15}}$	0	0	0	0

Table 4.6: *Numerical coefficients in equations (4.A.2.1)-(4.A.2.6). Notice that our numerical coefficients differ with respect to those given in [270]. More precisely, all the non-zero coefficients for $\ell = 2$ or $\ell = 4$ differ by the same factor, $4\sqrt{2/5}$ and $\sqrt{7/5}$ respectively, compared to the corresponding coefficients in that paper. This is due to the fact that we use a different harmonic representation, which also includes odd values of ℓ. The coefficients are the same for $\ell = 0$. For ℓ odd all coefficients vanish.*

normalization factors $w(\psi^I_\ell)$ in (4.A.2.4), the 5-dimensional theory corresponds to the bosonic sector of $D = 5$, $\mathcal{N} = 8$ gauged supergravity, whose action is given by:

$$S_{5D} = \frac{N^2}{2\pi^2}\int \mathrm{d}^5x\sqrt{-G}\left[\frac{1}{4}R + 3 - \sum_{I,\ell}\left(\frac{1}{2}(\partial\Psi^I_\ell)^2 + V(\Psi^I_\ell)\right)\right]. \tag{4.A.2.8}$$

This yields the equation of motion for $G_{\mu\nu}$:

$$R_{\mu\nu}[G] = 2\left(-2G_{\mu\nu} + T_{\mu\nu} - \frac{1}{3}G_{\mu\nu}T\right), \tag{4.A.2.9}$$

with

$$T_{\mu\nu}=\sum_{I,\ell}\left(\partial_\mu\Psi^I_\ell\partial_\nu\Psi^I_\ell-G_{\mu\nu}\Big(\frac{1}{2}(\partial\Psi^I_\ell)^2+V(\Psi^I_\ell)\Big)\right), \tag{4.A.2.10}$$

and the non-homogeneous Klein-Gordon equations (4.A.2.5) for the scalar fields.

Let us remark again that if one considered the problem in full generality, the resulting action would involve an infinite tower of KK fields. However, to find 1-point correlation functions we only need to expand the 5-dimensional fields near the AdS boundary up to a certain order. This truncates the infinite KK tower to a finite number of fields. When applying this procedure to our solutions we will see that the only field that contributes to the dual scalar vev's and the dual stress tensor is the field $\mathcal{S}^2$. This amounts to having the following non-zero potential in the action (4.A.2.8):

$$V(\mathcal{S}^2)=\frac{1}{2}m^2_{1,2}(\mathcal{S}^2)^2-\frac{16}{3\sqrt{15}}(\mathcal{S}^2)^3. \tag{4.A.2.11}$$

Having a five-dimensional theory of gravity coupled to scalars in AdS allows us to apply the standard holographic renormalization prescription introduced §1.3 of Chapter 1 to calculate the dual field theory observables: the dual stress-energy tensor and thus the energy of the gravittational solutions, and the scalar vev's.

4.B Harmonic expansion, stress-energy tensor and scalar vev's

In this section we perform the near boundary dimensional reduction for the class of spacetimes that we consider. We first expand our solutions near the AdS boundary in spherical harmonics on the S^5 according to (4.A.1.2) and (4.A.1.3). We work with the compactified radial coordinate y in our ansatz (4.3.1.4), and then transform to the FG gauge.

Our ansatz for the metric (4.3.1.4) involves products of the variables Q_2, Q_3 and Q_4, which are not convenient to perform the decomposition in spherical harmonics. For instance, the (aa)-component is not just the polar component of the S^5 times the unknown function Q_4, but it also includes a shift proportional to the product $Q_2Q_3^2$, coming from the crossed $y-a$ term. The Q_3^2 factor in this term would introduce scalar-derived vector harmonic modes into the component $h_{aa}(y,a)$, which is not compatible with the decompositions in (4.A.1.2). We overcome this issue through a simple redefinition of variables:

$$\begin{aligned}
Q_2&=Q_2',\\
Q_3&=\frac{G_p(y)}{4y^2y_0^2(1-y^2)}\frac{Q_3'}{Q_2'},\\
Q_4&=Q_4'-\frac{(1-y^2)(2-a^2)G_p(y)}{16y^2y_0^2}\frac{{Q_3'}^2}{Q_2'},
\end{aligned} \tag{4.B.0.1}$$

so that the new variables Q_2', Q_3' and Q_4' have a transparent decomposition in spherical harmonics. Then the spacetime metric reads

$$\begin{aligned} \mathrm{d}s^2 = \frac{L^2}{(1-y^2)^2}\Bigg(&-\frac{G_p(y)}{1-y^2}Q_1\mathrm{d}t^2 + \frac{4y_0^2y^2(1-y^2)}{G_p(y)}Q_2'\mathrm{d}y^2 \\ &- 2(1-y^2)^2Q_3'\mathrm{d}y\mathrm{d}a + y_0^2Q_5\mathrm{d}\Omega_{(p-2)}^2\Bigg) \\ &+ R^2\left(\frac{4Q_4'}{2-a^2}\mathrm{d}a^2 + (1-a^2)^2Q_6\mathrm{d}\Omega_{(q-1)}^2\right). \end{aligned} \tag{4.B.0.2}$$

Given the asymptotic boundary conditions that our solutions satisfy, the unknown functions appearing in the metric (4.B.0.2) have the following near boundary expansion:

$$\begin{aligned} Q_k(y,a) &= 1 + \sum_{i=1}^{\infty}(1-y^2)^i\sum_{\ell=0}^{i} q_k(i)^\ell Y_\ell(a), \qquad (k=1,2,5,7), \\ Q_3'(y,a) &= \sum_{i=1}^{\infty}(1-y^2)^i\sum_{\ell=1}^{i+1} q_3(i)^\ell S_1^\ell(a), \\ Q_4'(y,a) &= 1 + \frac{2-a^2}{4}\sum_{i=2}^{\infty}(1-y^2)^i\sum_{\ell=2}^{i} q_S(i)^\ell S_{aa}^\ell(a) \\ &\quad + \frac{1}{5}\sum_{i=1}^{\infty}(1-y^2)^i\sum_{\ell=0}^{i} q_T(i)^\ell Y_\ell(a), \\ Q_6(y,a) &= 1 + \frac{1}{(1-a^2)^2}\sum_{i=2}^{\infty}(1-y^2)^i\sum_{\ell=2}^{i} q_S(i)^\ell S_{\Omega\Omega}^\ell(a) \\ &\quad + \frac{1}{5}\sum_{i=1}^{\infty}(1-y^2)^i\sum_{\ell=0}^{i} q_T(i)^\ell Y_\ell(a), \end{aligned} \tag{4.B.0.3}$$

The various q's are constants that can be determined by solving the equations of motion order by order near the AdS boundary, at $y=1$. The factors in the expansions for Q_4' and Q_6 have been chosen such that the internal part of the metric can be written as

$$\mathrm{d}s_{\mathrm{int}}^2 = g_{ab}^{(0)}\mathrm{d}x^a\mathrm{d}x^b + h_{(ab)}(y,a)\mathrm{d}x^a\mathrm{d}x^b + \frac{1}{5}g_{ab}^{(0)}h(y,a)\,\mathrm{d}x^a\mathrm{d}x^b + \mathcal{O}(h^2), \tag{4.B.0.4}$$

where $h_{(ab)}$ and h are the symmetric-traceless and trace parts respectively. They have an expansion in harmonics as in (4.A.1.2), where now the coefficients of the harmonics are functions of the compact radial coordinate y.

At each order in the near boundary expansion only a finite number of harmonics are necessary to solve the equations of motion. This has already been taken into account in the form of the expansions: notice that at ith order in the near boundary expansion, the sum in (4.B.0.3) over the harmonics only runs up to the $\ell = i$ harmonic.[12] Plugging

[12] For Q_3' this sum runs up to $i+1$; the reason for this is that in the metric ansatz this term appears multiplied by an extra factor of $1-y^2$.

the expansions (4.B.0.3) into the equations of motion yields, at each order and after projecting them into the spherical harmonics, algebraic relations between the different $q(i)^\ell$'s; at the end, only a few q's remain undetermined. Up to order $(1-y)^4$ we obtain:

$$
\begin{aligned}
Q_1(y,a) \simeq\ & 1-\frac{4}{15}\beta_2 Y_2(y-1)^2-\frac{4}{15}\big(\beta_2 Y_2+30\gamma_3 Y_3\big)(y-1)^3\\
&+\left(16\delta_0 Y_0-\frac{1}{15}\Big(1-\frac{32}{5}\sqrt{\frac{2}{15}}\beta_2\Big)\beta_2 Y_2-4\left(3\gamma_3 Y_3-4\delta_4 Y_4\right)\right)(y-1)^4\\
Q_2(y,a) \simeq\ & 1-\frac{4}{15}\beta_2 Y_2(y-1)^2-\frac{4}{15}\big(\beta_2 Y_2+30\gamma_3 Y_3\big)(y-1)^3\\
&+\left(\frac{1}{9}\beta_2^2 Y_0-\frac{1}{15}\Big(1-\frac{96}{25}\sqrt{\frac{6}{5}}\beta_2\Big)\beta_2 Y_2-12\gamma_3 Y_3-16\Big(\frac{2\sqrt{7}}{375}\beta_2^2-\delta_4\Big)Y_4\right)(y-1)^4,\\
Q_3(y,a) \simeq\ & \frac{1}{15}\beta_2 (S_a)^2(y-1)+\Big(\gamma_1(S_a)^1-\frac{1}{30}\beta_2(S_a)^2+\gamma_3(S_a)^3\Big)(y-1)^2\\
&+\left(\Big(\frac{1}{30}+\frac{4}{15}\frac{1}{y_0^2}+\frac{4}{225}\beta_2 Y_2-\frac{56}{1125}\sqrt{\frac{2}{15}}\beta_2\Big)\beta_2(S_a)^2+\frac{4}{3}\Big(\frac{\sqrt{7}}{375}\beta_2^2-\delta_4\Big)(S_a)^4\right)(y-1)^3,\\
Q_4(y,a) \simeq\ & 1+\frac{4}{5}\beta_2 Y_2(y-1)^2+4\Big(\frac{2}{3}\gamma_1 Y_1+\frac{1}{5}\beta_2 Y_2+4\gamma_3 Y_3\Big)(y-1)^3\\
&+\Big(-\frac{3}{125}\beta_2^2 Y_0+4\gamma_1 Y_1+\frac{1}{5}\Big(1-\frac{992}{375}\sqrt{\frac{2}{15}}\beta_2\Big)\beta_2 Y_2+24\gamma_3 Y_3+\Big(\frac{544}{5625}\beta_2^2-\frac{80}{3}\delta_4\Big)Y_4\\
&\quad+\frac{16}{375}\sqrt{\frac{2}{15}}\beta_2^2(S^\Omega{}_\Omega)^2+\frac{8\sqrt{7}}{1125}\beta_2^2(S^\Omega{}_\Omega)^4-\frac{16}{225}\beta_2^2(S^a)^2(S^a)^2\Big)(y-1)^4,\\
Q_5(y,a) \simeq\ & 1-\frac{4}{15}\beta_2 Y_2(y-1)^2-\frac{4}{15}\big(\beta_2 Y_2+30\gamma_3 Y_3\big)(y-1)^3\\
&+\left(\frac{16}{3}\Big(\frac{1}{900}\beta_2^2-\delta_0\Big)Y_0-\frac{1}{15}\Big(1-\frac{32}{5}\sqrt{\frac{2}{15}}\beta_2\Big)\beta_2 Y_2-4\left(3\gamma_3 Y_3-4\delta_4 Y_4\right)\right)(y-1)^4,\\
Q_6(y,a) \simeq\ & 1+\frac{4}{5}\beta_2 Y_2(y-1)^2+4\Big(\frac{2}{3}\gamma_1 Y_1+\frac{1}{5}\beta_2 Y_2+4\gamma_3 Y_3\Big)(y-1)^3\\
&+\Big(-\frac{3}{125}\beta_2^2 Y_0+4\gamma_1 Y_1+\frac{1}{5}\Big(1-\frac{992}{375}\sqrt{\frac{2}{15}}\beta_2\Big)\beta_2 Y_2+24\gamma_3 Y_3\\
&\quad+\Big(\frac{544\sqrt{7}}{5625}\beta_2^2-\frac{80}{3}\delta_4\Big)Y_4+\frac{16}{375}\sqrt{\frac{2}{15}}\beta_2^2(S^\Omega{}_\Omega)^2+\frac{8\sqrt{7}}{1125}\beta_2^2(S^\Omega{}_\Omega)^4\Big)(y-1)^4,\\
Q_7(y,a) \simeq\ & 1-\frac{8}{15}\beta_2 Y_2(y-1)^2-\frac{8}{15}\big(\beta_2 Y_2+30\gamma_3 Y_3\big)(y-1)^3\\
&+\left(16\alpha_0 Y_0-\frac{2}{15}\Big(1+\frac{16}{y_0^2}-\frac{512}{75}\sqrt{\frac{2}{15}}\beta_2\Big)\beta_2 Y_2-24\gamma_3 Y_3+32\Big(\frac{\sqrt{7}}{1500}\beta_2^2+\delta_4\Big)Y_4\right)(y-1)^4.
\end{aligned}
\tag{4.B.0.5}
$$

The harmonic expansion near the AdS boundary depends on six undetermined constants: β_2, γ_1, γ_3, δ_0, δ_4 and α_0. Gauge freedom of both the metric and gauge field allows us to set γ_1 and α_0 to any value and we choose to set them to zero. Note that even if they are not set to zero, observables are gauge invariant and therefore, at the end, they cannot depend on these two constants. The rest of coefficients,

$\{\beta_2, \gamma_3, \delta_0, \delta_4\}$, correspond to data that can only be determined from the full bulk solution.

To bring the metric into the FG gauge (z, θ) in $10D$ we perform the coordinate transformation $y = y(z, \theta)$, $a = a(z, \theta)$ in a series expansion near the AdS boundary $z = 0$. At each order in the FG coordinate z^i, we have two functions to solve for and the only requirement is that the AdS part of the metric takes the FG form, i.e. $g_{zz} = 1/z^2$ (recall that $L = 1$) and $g_{zi} = 0$. This completely determines the form of the coordinate transformation. The first terms are given by:

$$\begin{aligned} y(z,\theta) &= 1 + \frac{y_0}{2} z - \frac{y_0^2}{8} z^2 + \frac{1}{8} y_0 \left(1 + \frac{1}{2} y_0^2 \left(1 + \frac{2}{15} \beta_2 Y_2(\theta)\right)\right) z^3 + \dots \\ a(z,\theta) &= \theta + \frac{1}{20} \sqrt{\frac{3}{10}} y_0^2 \beta_2 \, \theta (2 - 3\theta^2 + \theta^4) z^2 \\ &\quad + \frac{1}{12} y_0^3 \sqrt{2 - \theta^2} (1 - \theta^2) \left(\gamma_1 - \frac{1}{\sqrt{10}} \gamma_3 \left(1 - 8\theta^2 (2 - \theta^2)\right)\right) z^3 + \dots \end{aligned} \tag{4.B.0.6}$$

To obtain the metric up to order z^4 we need this change of coordinates up to order z^7 for $y(z, \theta)$ and up to order z^5 for $a(z, \theta)$.

Now we can identify the different fields appearing in (4.A.1.2) and (4.A.1.3).[13] To this end, it is useful to write the background $\mathrm{AdS}_5 \times S^5$ in FG coordinates since we have to subtract it:

$$\begin{aligned} \mathrm{d}s^2_{(0)} = \frac{L^2}{z^2} \Bigg(\mathrm{d}z^2 - \left(1 + \frac{z^2}{2L^2} + \frac{z^4}{16L^4}\right) \mathrm{d}t^2 + \left(1 - \frac{z^2}{2L^2} + \frac{z^4}{16L^4}\right) L^2 \mathrm{d}\Omega_{(3)} \Bigg) \\ + L^2 \mathrm{d}\Omega_{(5)}, \end{aligned} \tag{4.B.0.7}$$

and $F^{(0)}_{(5)}$ is given in (4.1.0.6) in a coordinate invariant form. We are now in a position to find the various harmonic contributions to the near boundary expansions of the fields h_{MN} and f_{MNPQR}. For the components of the metric along the AdS_5 factor we find:

$$\begin{aligned} h^0_{\mu\nu}(z) &= -y_0^2 \left(\frac{3h_0}{4}(1 + y_0^2) - y_0^2 \left(\frac{h_1}{7200} \beta_2^2 + h_0 \delta_0\right)\right) z^2 \eta_{\mu\nu}, \\ h^2_{\mu\nu}(z) &= -\frac{1}{10} y_0^2 \beta_2 \left(1 + \frac{3}{4}\left(h_2 - \frac{23}{75}\sqrt{\frac{2}{15}} y_0^2 \beta_2\right) z^2\right) \eta_{\mu\nu}, \\ h^3_{\mu\nu}(z) &= -\frac{4}{3} y_0^3 \gamma_3 z \eta_{\mu\nu}, \\ h^4_{\mu\nu}(z) &= \frac{1}{4} y_0^4 \left(\frac{13\sqrt{7}}{1500} \beta_2^2 + 5\delta_4\right) z^2 \eta_{\mu\nu}, \end{aligned} \tag{4.B.0.8}$$

with $\{h_0, h_1, h_2\} = \{-1/3, 11/3, 1/9\}$ when the indices are along the S^3 within the AdS_5 space, otherwise these constants are all equal to one; $\eta_{\mu\nu} = \mathrm{diag}(0, -1, \sigma_{\hat{\imath}\hat{\jmath}})$, where $\sigma_{\hat{\imath}\hat{\jmath}}$ is the standard metric on the unit round S^3. Since, by construction, in

[13] Note that because we work with gauge invariant variables, strictly speaking we should not need to put the $10D$ solution in the FG gauge.

the FG gauge there are no crossed terms between the AdS$_5$ and S^5 factors, we have $A^\ell_\mu(z)=0$. The scalar fields (from the point of view of AdS$_5$) that come from the components of the $10D$ metric along the S^5 are given by:

$$\begin{aligned}
B^2(z)&=\frac{1}{20}y_0^2\beta_2\left(1+\frac{5}{8}\left(1-\frac{1}{25}\sqrt{\frac{2}{15}}y_0^2\beta_2\right)z^2\right)z^2, \qquad B^3(z)=\frac{2}{9}y_0^3\gamma_3 z^3,\\
B^4(z)&=\frac{1}{48}y_0^4\left(\frac{\sqrt{7}}{300}\beta_2^2-5\delta_4\right)z^4,\\
C^0(z)&=\frac{1}{600}y_0^4\beta_2^2z^4, \qquad C^2(z)=\frac{2}{5}y_0^2\beta_2\left(1+\frac{5}{16}\left(1-\frac{17}{25}\sqrt{\frac{2}{15}}y_0^2\beta_2\right)z^2\right)z^2,\\
C^3(z)&=\frac{16}{3}y_0^3\gamma_3z^3, \qquad C^4(z)=\frac{1}{300}y_0^4\left(\sqrt{7}\beta_2^2-5\delta_4\right)z^4.
\end{aligned} \tag{4.B.0.9}$$

Finally, the 5-dimensional scalar fields arising from the 5-form are:

$$\begin{aligned}
b^2&=-\frac{1}{10}y_0^2\beta_2\left(1+\frac{3}{8}\left(1-\frac{31}{75}\sqrt{\frac{2}{15}}y_0^2\beta_2\right)z^2\right)z^2, \qquad b^3=-\frac{8}{9}y_0^3\gamma_3z^3,\\
b^4&=-\frac{1}{8}y_0^4\left(\frac{7\sqrt{7}}{750}\beta_2^2-5\delta_4\right)z^4.
\end{aligned} \tag{4.B.0.10}$$

From these expressions we can find the gauge invariant combinations at linear order from Table 4.5, and then the corresponding gauge invariant mass eigenfields defined in (4.A.1.8). To leading order in the number of fields, the equations of motion are satisfied up to order z^2, since higher order terms in z can (and will!) receive contributions from the non-linear interactions. The leading order field $\hat{s}^2$ is given by

$$\hat{s}^2=\frac{1}{20}y_0^2\beta_2z^2+\mathcal{O}(z^4). \tag{4.B.0.11}$$

The rest of the fields fields $\hat{s}^\ell$, $\ell=3,4$ are at least $\mathcal{O}(z^3)$ and $\hat{t}^\ell$, $\ell=0,1,2,3,4$, are $\mathcal{O}(z^4)$. We do not present the explicit expressions for them in this appendix, but they can be non-trivial at this order and they are needed to find the dimensionally reduced scalar fields $\mathcal{S}^\ell$ and $\mathcal{T}^\ell$.

The relevant fields to the second order are $\hat{\bar{s}}^2$ and $\bar{\bar{h}}^0_{\mu\nu}$. Using (4.A.2.2) and (4.A.1.16) we find:

$$\begin{aligned}
\hat{\bar{s}}^2&=\frac{1}{20}y_0^2\beta_2z^2+\frac{1}{40}y_0^2\beta_2\left(1-\frac{1}{25}\sqrt{\frac{2}{15}}y_0^2\beta_2\right)z^4,\\
\bar{\bar{h}}^0_{zz}&=-\frac{11}{3600}y_0^4\beta_2^2z^2\,,\\
\bar{\bar{h}}^0_{ij}&=\left(\frac{3}{4}h_0'y_0^2\left(1+y_0^2\right)-\frac{1}{960}h_1'y_0^4\beta_2^2-h_0'y_0^4\delta_0\right)z^2\delta_{ij}\,,
\end{aligned} \tag{4.B.0.12}$$

where $\delta_{ij}=\mathrm{diag}(1,\sigma_{\hat{\imath}\hat{\jmath}})$, and $\{h_0',h_1'\}=\{1/3,-61/45\}$ for indices along the S^3 and one otherwise. We are interested in the scalar fields $\mathcal{S}^\ell$, $\mathcal{T}^\ell$ given in (4.A.2.3) and the massless KK graviton $G_{\mu\nu}$ (4.A.2.7). These are $5D$ fields involving only quadratic

contributions in $\hat{s}^2$ and its derivatives. After adding the background in the case of the metric, we find:

$$\begin{aligned}
\mathcal{S}^2 &= \frac{1}{15\sqrt{2}}y_0^2\beta_2 z^2 + \frac{1}{30\sqrt{2}}y_0^2\beta_2\left(1-\frac{4}{15}\sqrt{\frac{2}{15}}y_0^2\beta_2\right)z^4,\\
G_{zz} &= \frac{1}{z^2} - \frac{13}{10800}y_0^4\beta_2^2 z^2,\\
G_{ij} &= \left(\frac{1}{z^2}+\frac{G_0}{2}+\left(\frac{1}{16}-\frac{3G_0}{4}y_0^2(1+y_0^2)\right)z^2\right.\\
&\quad \left. - y_0^4\left(\frac{31G_1}{43200}\beta_2^2 - G_2\delta_0\right)z^2\right)\eta_{ij},
\end{aligned} \tag{4.B.0.13}$$

with $\eta_{ij} = \mathrm{diag}(-1,\sigma_{\hat{\imath}\hat{\jmath}})$, $(G_0,G_1,G_2) = (-1,15/31,-1/3)$ for the components along the S^3 and one otherwise. The fields $\mathcal{T}^\ell$, $\ell = 0,1,2,3,4$ are $\mathcal{O}(z^5)$. Therefore, up to order z^4, there are only two other scalars which can acquire non-trivial vev's:

$$\begin{aligned}
\mathcal{S}^3 &= \frac{1}{2\sqrt{3}}y_0^3\gamma_3 z^3,\\
\mathcal{S}^4 &= -\frac{1}{1200\sqrt{3}}y_0^4(\sqrt{7}\beta_2^2+300\delta_4)z^4.
\end{aligned} \tag{4.B.0.14}$$

Having the $5D$ fields, we are now in a position to apply the standard holographic renormalization prescription (see §1.3 of Chapter 1). Clearly, the metric in (4.B.0.13) is not in FG gauge; introducing the $5D$ FG coordinate Z through

$$z(Z) = Z + \frac{13}{86400}y_0^4\beta_2^2 Z^5 + \mathcal{O}(Z^6), \tag{4.B.0.15}$$

we can bring it to the canonical FG form. Finally, identifying the different terms that appear in the FG expansion, we obtain the stress-energy tensor from (1.3.0.14):

$$\langle T_{ij}\rangle = \frac{N^2}{2\pi^2}\left(\frac{3}{16}(1+2y_0^2)^2 + y_0^4\left(\frac{\beta_2^2}{3600}-\delta_0\right)\right)(1,\sigma_{\hat{\imath}\hat{\jmath}}/3). \tag{4.B.0.16}$$

The boundary geometry B_4 is conformally flat and therefore there is no conformal anomaly: the stress-energy tensor is traceless $\langle T_i^i\rangle = 0$. It is also trivially conserved, $D^i_{(0)}\langle T_{ij}\rangle = 0$, and in the limit $\beta_2,\delta_0 \to 0$, it reduces to the stress-energy tensor of the Schwarzschild-AdS black hole, as expected. The energy of the spacetime is simply given by $E = \Omega_3\langle T_{00}\rangle$, which includes the well-known Casimir energy of the dual $\mathcal{N}=4$ SYM on the ESU_4. Using the expressions in (4.B.0.5) one has the relation

$$\frac{\beta_2^2}{3600} - \delta_0 = \frac{1}{512}\left(\partial_y^4 Q_5 - \partial_y^4 Q_1\right)\Big|_{y=1}, \tag{4.B.0.17}$$

which is very useful in order to check the numerics.

The non-vanishing scalar vev's associated to $\mathcal{S}^2,\mathcal{S}^3$ and $\mathcal{S}^4$ follow from (1.3.0.15). Recall that the conformal dimension of operators dual to $\mathcal{S}^\ell$ is $\Delta_+ = \ell$ ($\Delta_- = 4-\ell$). Notice that in our case the dual operator with smallest conformal dimension is 2

and therefore the non-linear terms that appear for operators with higher conformal dimension vanishes for $\Delta = 3$ and it is proportional to $\langle\mathcal{O}^2\rangle^2$ for $\Delta = 4$. In the latter case, the proportionality factor can be computed for our harmonic representation using the expressions in Ref. [270].

The expressions for the vev's are given by:

$$\begin{aligned}
\langle\mathcal{O}_{\mathcal{S}^2}\rangle &= \frac{N^2}{2\pi^2}(2\tilde{S}^2_{(0)}) = \frac{N^2}{2\pi^2}\frac{\sqrt{2}}{15}y_0^2\beta_2,\\
\langle\mathcal{O}_{\mathcal{S}^3}\rangle &= \frac{N^2}{2\pi^2}(2S^3_{(2)}) = \frac{N^2}{2\pi^2}\frac{1}{\sqrt{3}}y_0^3\gamma_3,\\
\langle\mathcal{O}_{\mathcal{S}^4}\rangle &= \frac{N^2}{2\pi^2}\Big(4S^4_{(4)} + \frac{3\sqrt{21}}{5}(2\tilde{S}^2_{(0)})^2\Big) = \frac{N^2}{2\pi^2}\frac{1}{\sqrt{3}}y_0^4\Big(\frac{19\sqrt{7}}{1500}\beta_2^2 - \delta_4\Big).
\end{aligned} \tag{4.B.0.18}$$

4.C Scalar harmonics of S^q with SO(q) symmetry

In this appendix we construct the scalar spherical harmonics on S^q that preserve an S^{q-1}. These are necessary to perform the dimensional reduction of our solutions and compute the vev's of the dual operators.

The metric of S^q in the standard spherical coordinates can be found recursively through:

$$\begin{aligned}
\mathrm{d}\Omega_1^2 &= \mathrm{d}\theta_1^2,\\
\mathrm{d}\Omega_q^2 &= \mathrm{d}\theta_q + \sin^2\theta_q \mathrm{d}\Omega_{q-1}^2,
\end{aligned} \tag{4.C.0.1}$$

with $\theta_1 \in [0, 2\pi)$ and $\theta_k \in [0, \pi)$, $\forall k = 2, \ldots, q$. The corresponding volume forms are:

$$\begin{aligned}
\mathrm{d}\omega_1 &= \mathrm{d}\theta_1,\\
\mathrm{d}\omega_q &= \sin^{q-1}\theta_q \mathrm{d}\theta_q \wedge \mathrm{d}\omega_{q-1},
\end{aligned} \tag{4.C.0.2}$$

and the Laplace operators are:

$$\begin{aligned}
\Delta_1 &= \frac{\partial^2}{\partial\theta_1^2},\\
\Delta_q &= \frac{1}{\sin^{q-1}\theta_q}\frac{\partial}{\partial\theta_q}\left(\sin^{q-1}\theta_q\frac{\partial}{\partial\theta_q}\right) + \frac{1}{\sin^2\theta_q}\Delta_{q-1}.
\end{aligned} \tag{4.C.0.3}$$

The defining equations for the scalar spherical harmonics are:

$$\begin{aligned}
\left(\Delta_1 + \ell_1^2\right) Y_{\ell_1}(\theta_1) &= 0,\\
\left(\Delta_q - \Lambda_{\ell_q}\right) Y_{\ell_1\ldots\ell_q}(\theta_1, \ldots, \theta_q) &= 0,
\end{aligned} \tag{4.C.0.4}$$

with $\Lambda_{\ell_n} = -\ell_n(\ell_n + n - 1)$, $n = 1, \ldots, q$ and $\ell_i = 0, 1, 2, \ldots$. Scalar harmonics in one dimension (on a circle), are given by the Fourier modes: $Y_{\ell_1}(\theta_1) \propto e^{i\ell_1\theta_1}$ (up to a normalization constant). Requiring univaluedness implies that $\ell_1 \in \mathbb{Z}$.

We focus on harmonics that preserve an SO(q) subgroup out of the full SO($q+1$) isometry group of the S^q. Imposing SO(q) symmetry implies that these spherical

harmonics can only depend on the polar angle $\theta_q \equiv \theta$, and thus they are labeled by a single quantum number $\ell_q \equiv \ell$. Therefore, the scalar harmonics that we are interested in satisfy:

$$\left(\frac{1}{\sin^{q-1}\theta}\frac{\partial}{\partial\theta}\left(\sin^{q-1}\theta\frac{\partial}{\partial\theta}\right)-\Lambda_\ell\right)Y_\ell(\theta)=0. \tag{4.C.0.5}$$

Let $Y_\ell(\theta) = y(\cos\theta)$ and consider the change of variables $\theta = \arccos(x)$. Defining $2\mu = q-1$ and $\nu = \ell$, equation (4.C.0.5) becomes the Gegenbauer differential equation:

$$(1-x^2)y''(x)-(2\mu+1)xy'(x)+\nu(\nu+2\mu)y(x)=0. \tag{4.C.0.6}$$

The general solution to this equation is

$$y(x)=(x^2-1)^{(1-2\mu)/4}\left(C_1\,P^{1/2-\mu}_{\mu+\nu-1/2}(x)+C_2\,Q^{1/2-\mu}_{\mu+\nu-1/2}(x)\right), \tag{4.C.0.7}$$

where C_1 and C_2 are integration constants, and $P^a_b(x)$ and $Q^a_b(x)$ are the Legendre's polynomials of first and second kind respectively. Finiteness at the poles, $x = \pm1$, requires that $C_2 = 0$, and ν to be a non-negative integer, i.e., $\ell \geq 0$.

The solution may be written in terms of hypergeometric functions. Redefining the integration constant by absorbing the numerical factors that arise, we write the regular solution as:

$$y(x)=\bar{C}_1\cdot{}_2F_1\left(-\nu,2\mu+\nu;\mu+\frac{1}{2};\frac{1-x}{2}\right) \tag{4.C.0.8}$$

where $\bar{C}_1$ is determined by requiring a proper normalization. To be consistent, we use the same normalization as in the previous literature [279–282]. The desired scalar harmonics are then given by:

$$Y_\ell(\theta)=\sqrt{\frac{2^{-\ell-q+2}\pi^{1/2}\Gamma(\ell+q-1)}{\Gamma(\ell+\frac{q-1}{2})\Gamma(q/2)}}\;{}_2F_1\left(-\ell,\ell+q-1;\frac{q}{2};\frac{1-\cos\theta}{2}\right), \tag{4.C.0.9}$$

satisfying

$$\int Y_{\ell_1}Y_{\ell_2}\mathrm{d}\omega_q=z(\ell_1)\delta_{\ell_1\ell_2},\qquad z(\ell_1)=\frac{\ell_1!(\frac{q-1}{2})!}{2^{\ell_1}(\ell_1+\frac{q-1}{2})!}\Omega_q, \tag{4.C.0.10}$$

where Ω_q is the surface area of the unit q-sphere. This normalization ensures that totally symmetric traceless rank k tensors of $\mathrm{SO}(q+1)$, which can be used to represent the scalar harmonics, are normalized to a delta function.

From the scalar harmonics one may define scalar-derived quantities such as vector and tensor harmonics by taking covariant derivatives on the S^q. Letting the metric on the S^q be σ_{ab}, with compatible covariant derivative D_a, the scalar-derived vector and tensor harmonics are given by

$$\begin{aligned}S^\ell_a(\theta)&=D_aY_\ell,\\ S^\ell_{ab}(\theta)&\equiv D_{(a}D_{b)}Y_\ell=D_aD_bY_\ell-\frac{\Lambda_\ell}{q}\sigma_{ab}Y_\ell.\end{aligned} \tag{4.C.0.11}$$

With these definitions, these harmonics satisfy:

$$\begin{aligned} D^a S^\ell_a &= \Lambda_\ell Y_\ell, & D^a S^\ell_{ab} &= (q-1)\left(1+\frac{\Lambda_\ell}{q}\right) S^\ell_a, \\ D^b D_b S^\ell_a &= (\Lambda_\ell + q - 1)\, S^\ell_a, & D^c D_c S^\ell_{ab} &= (\Lambda_\ell + 2q)\, S^\ell_{ab}, \\ \int S^{\ell_1}_a S^a_{\ell_2}\, \mathrm{d}\omega_q &= z(\ell_1) f(\ell_1) \delta^{\ell_1}_{\ell_2}, & \int S^{\ell_1}_{ab} S^{ab}_{\ell_2}\, \mathrm{d}\omega_q &= z(\ell_1) q(\ell_1) \delta^{\ell_1}_{\ell_2}, \end{aligned} \tag{4.C.0.12}$$

where $z(\ell)$ has been defined in (4.C.0.10) and

$$f(\ell) = -\Lambda_\ell, \qquad q(\ell) = \Lambda_\ell (q-1)\left(1+\frac{1}{q}\Lambda_\ell\right). \tag{4.C.0.13}$$

In order to find the gauge transformations of the lower-dimensional fields in Appendix 4.A, one also needs the following triple integrals of spherical harmonics:

$$\begin{aligned} a(\ell_1,\ell_2,\ell_3) &= \int Y_{\ell_1} Y_{\ell_2} Y_{\ell_3}\, \mathrm{d}\omega_q & b(\ell_1,\ell_2,\ell_3) &= \int Y_{\ell_1} S^{\ell_2}_a S^a_{\ell_3}\, \mathrm{d}\omega_q, \\ c(\ell_1,\ell_2,\ell_3) &= \int S^{ab}_{\ell_1} S^{\ell_2}_a S^{\ell_3}_b\, \mathrm{d}\omega_q, & d(\ell_1,\ell_2,\ell_3) &= \int Y_{\ell_1} S^{ab}_{\ell_2} D_a S^{\ell_3}_b\, \mathrm{d}\omega_q, \\ e(\ell_1,\ell_2,\ell_3) &= \int S^{ab}_{\ell_1}\left(2 D_a S^c_{\ell_2} S^{\ell_3}_{cb} + S^c_{\ell_2} D_c S^{\ell_3}_{ab}\right)\, \mathrm{d}\omega_q. \end{aligned} \tag{4.C.0.14}$$

The expressions for $b(\ell_1,\ell_2,\ell_3), c(\ell_1,\ell_2,\ell_3), d(\ell_1,\ell_2,\ell_3)$ and $e(\ell_1,\ell_2,\ell_3)$ can be written in terms of $a(\ell_1,\ell_2,\ell_3)$ by partial integrating, e.g.

$$b(\ell_1,\ell_2,\ell_3) = \frac{1}{2}\Big(f(\ell_2) + f(\ell_3) - f(\ell_1)\Big) a(\ell_1,\ell_2,\ell_3). \tag{4.C.0.15}$$

Useful identities among them also include:

$$\begin{aligned} d(\ell_2,\ell_1,\ell_3) + c(\ell_1,\ell_2,\ell_3) + \frac{q(\ell_1)}{\Lambda_{\ell_1}} b(\ell_2,\ell_1,\ell_3) &= 0, \\ b(\ell_2,\ell_1,\ell_3) + b(\ell_1,\ell_2,\ell_3) + \Lambda_{\ell_3} a(\ell_1,\ell_2,\ell_3) &= 0. \end{aligned} \tag{4.C.0.16}$$

4.D Embedding plots in AdS$_5\times$S^5

In Fig. 4.16 of this Appendix we include the embedding diagrams for the lumpy black hole families $\ell = 1, 2^+$ and 2^- in AdS$_5\times S^5$. These figures help to visualize the topology changing transition, in which the lumpy black holes merge with another family of black holes with a different horizon topology. In the AdS$_5 \times S^5$ case, the values of lumpiness parameter λ that we were able to confidently achieve are smaller than in the AdS$_4 \times S^7$ case, but yet significantly larger than in [19]. The topology changes are qualitatively similar to the corresponding ones in AdS$_4 \times S^7$, except for the $\ell = 2^-$ case; in the AdS$_5 \times S^5$ case, the lumpy black holes merge with a black hole family whose horizon topology is $S^8 \# S^8$, i.e. a double localized black hole.

$\ell = 1$

Fixed S^3 coordinates

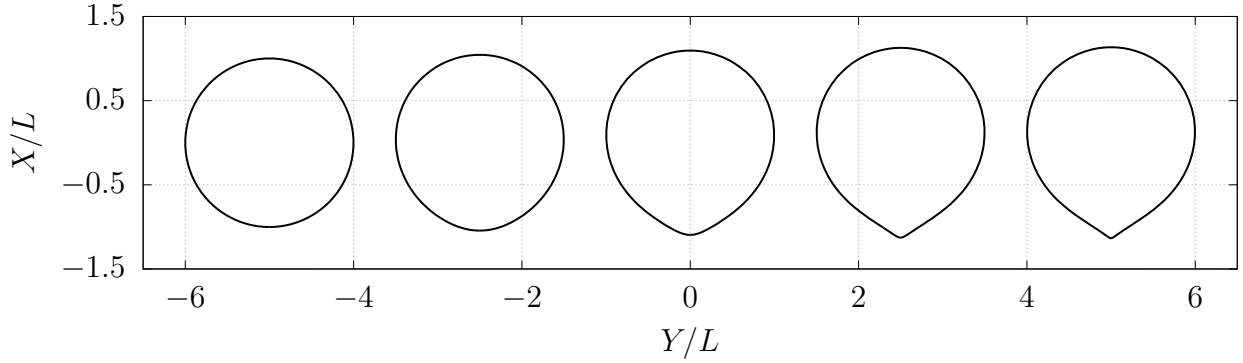

Fixed S^4 coordinates

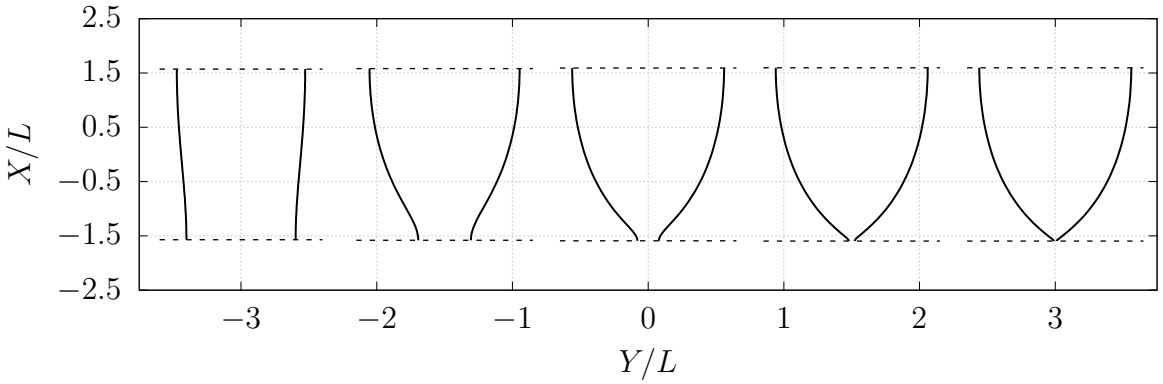

$\ell = \mathbf{2}^+$

Fixed S^3 coordinates

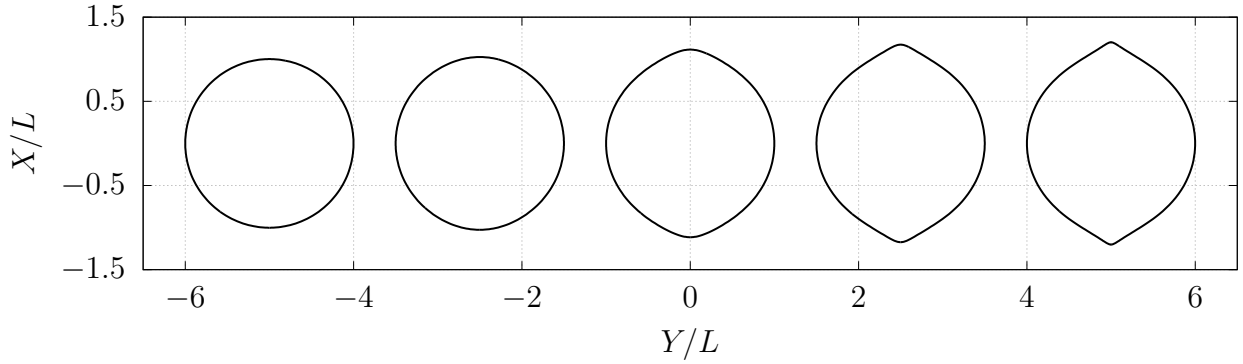

Fixed S^4 coordinates

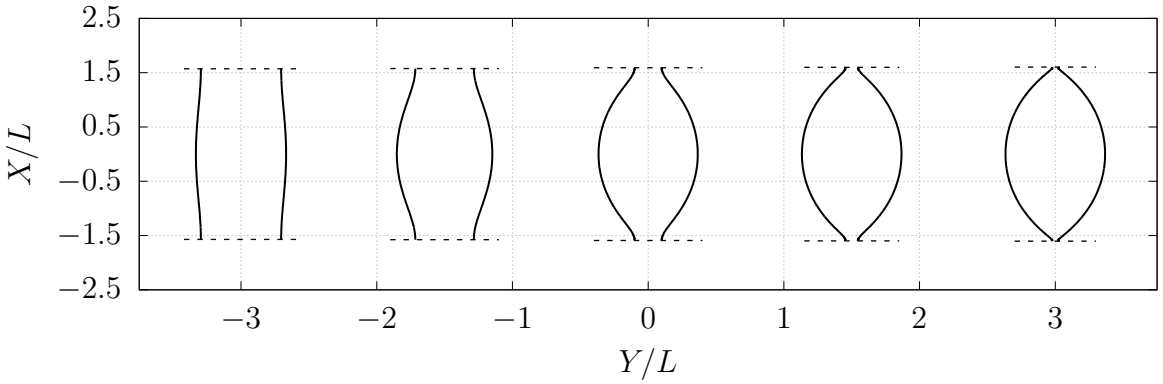

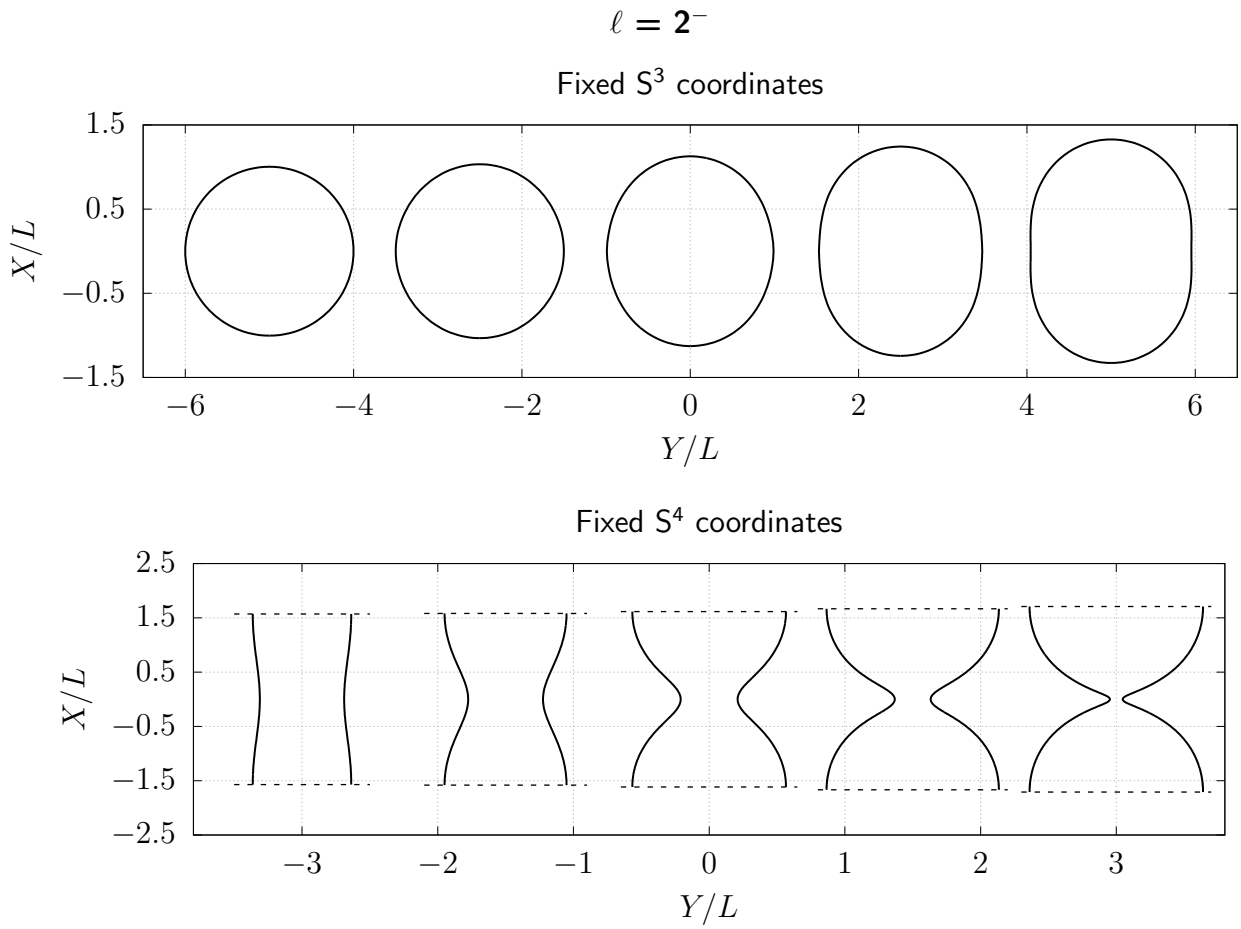

Fig. 4.16: *Embeddings plots for fixed S^3/S^4 coordinates of lumpy black holes in $AdS_5 \times S^5$ with $\ell = 1, 2^+$ and 2^-. The corresponding plots for $\ell = 3$ are similar to those for $\ell = 1$, but the pinch-off appears at the opposite pole.*

In Fig. 4.17 we show the embedding plots of the most critical solution we have found along the $\ell = 1$ branch, and compare them with the embeddings of the local cone. The embedding along the internal S^4 indicates that the local cone must be sourced by some flux field along the internal directions, and it is consistent with (4.4.4.2).

4.E Numerics and convergence tests

In this appendix we provide further details of our numerical construction of the lumpy black hole solutions and present some convergence tests.

Our numerical approach to construct critical solutions relies on the re-definition of certain unknown functions to ensure that the new functions have bounded values at the merger. However, steep gradients are unavoidable and therefore, very close to critical limit, these re-definitions are useless if they are not accompanied by a numerical grid that can properly resolve these gradients. To this end, it is convenient to divide the original grid into other small subregions in order to be able to increase the grid resolution just where it is necessary. Of course, it is not desirable to consider

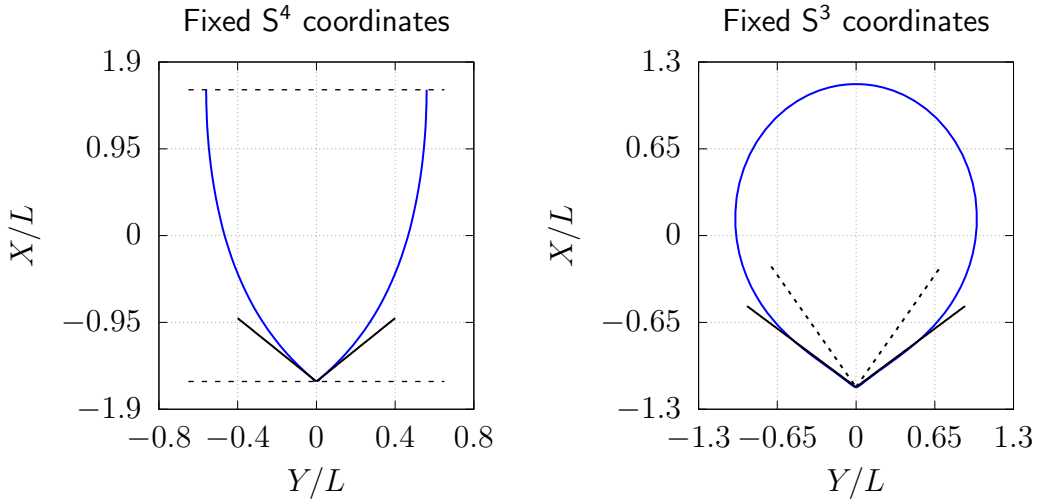

Fig. 4.17: *Embedding diagrams of $\ell = 1$ lumpy black hole (blue line) in $AdS_5 \times S^5$, for the largest lumpiness parameter we have reached with fixed S^4 coordinates (left) and fixed S^3 coordinates (right). The black lines correspond to the cone embeddings proposed to mediate the topology change transition. For fixed S^3 coordinates, the embedding dictated by the Ricci-flat cone is indicated with dashed lines.*

many subdomains as it may result in a loss of computational efficiency. A moderate number of patches together with mesh-refinement overcomes the efficiency issue while redistributing the density of points in a useful manner.

In this study we have used up to 4 subdomains and the mesh-refinement function (2.2.2.13) in the patch where the singular behavior appears, which is typically at a pole in the near horizon region. Therefore, where needed, we redefine the coordinates as $\tilde{x} = \text{mesh}(x; 0, x^*, \chi_x)$ and $\tilde{y} = \text{mesh}(y; 0, y^*, \chi_y)$. In total, this introduces four new parameters: x^* and y^*, corresponding to the coordinate values where the different patches meet, and χ_x and χ_y, which control the 'strength' of the density of the new grid points along each coordinate direction. Typical values that we used are $\chi_x, \chi_y = 4$. At each shared boundary one must impose continuity of the functions and their first normal derivatives. An example of such grids is shown in Fig. 4.18. As for the resolution used, for all families we began with a single patch with 60×60 grid points, and then we increased the number of patches up to four as we moved along the branch of solutions towards the critical regime. The smallest patch where the peaks of the functions typically appear has 50×50 resolution, whereas for the other patches lower resolutions suffice, e.g. $\sim 30 \times 50$ or 30×30.

To check whether the solution on a given grid is good enough, we monitor the numerical error. If this is greater than a few percent, then the resolution needs to be increased. To this end, we use the squared norm of the DeTurck vector ξ^2 and its non-zero components ξ_x and ξ_y since they should all vanish in the continuum limit

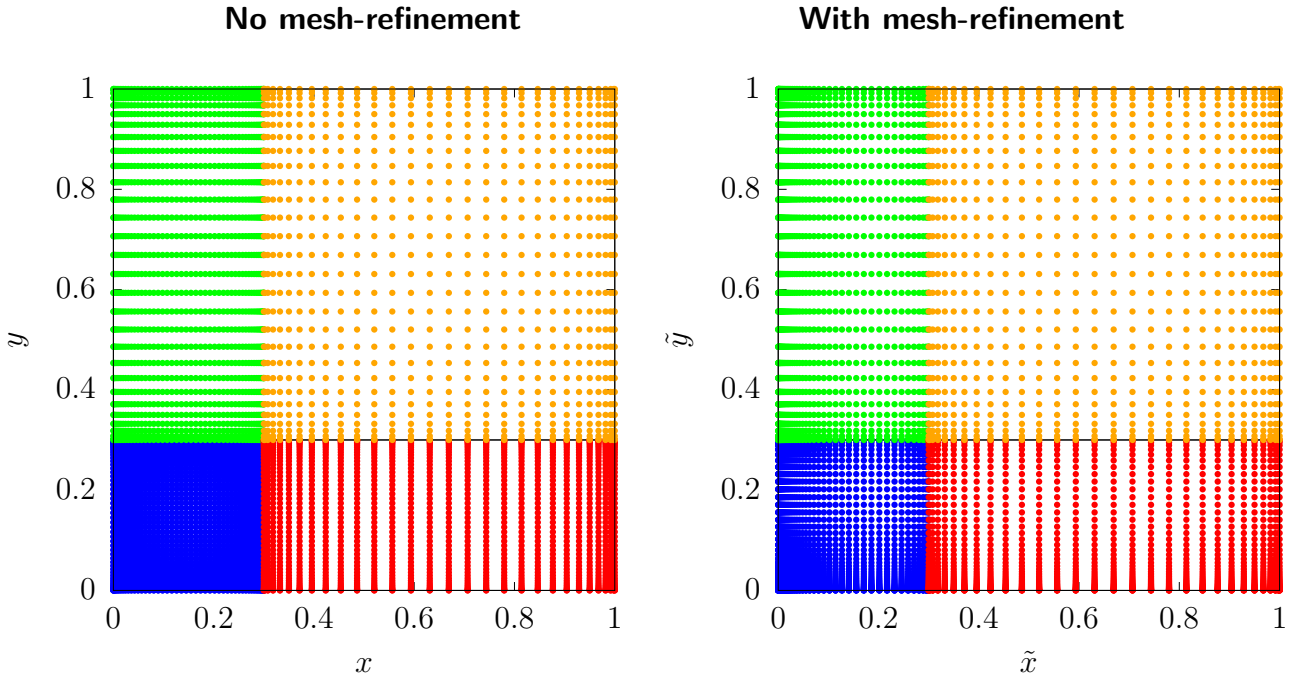

Fig. 4.18: *Physical grid to construct solutions with ℓ even, with grid parameters $x^* = 0.3 = y^*$. Left: simple Chebyshev grid points for the various patches. Right: mesh-refined grid points $\tilde{x} = mesh(x; 0, x^*, \chi_x)$, $\tilde{y} = mesh(y; 0, y^*, \chi_y)$, with $\chi_{x,y} = 4$, in the blue patch. In the green and red patches only x- and y-directions need to be refined respectively.*

and hence they are good measures of the error. In the case of using a pseudo-spectral numerical approach, as in this chapter, the error should be exponentially suppressed in the continuum limit, i.e. with increasing the grid size. Insufficient resolution can also reflect itself in some unphysical behavior of the physical parameters in the phase diagram of the family of black holes under consideration. For this reason, we also monitor the physical quantities along the branch.

In Fig. 4.19 we compare the maximum values of ξ^2 and ξ_y for a reference solution (with $\lambda \sim 0.2$) at different resolutions in each of the branch of solutions we have constructed. To produce this figure we picked up a reference solution of each branch, we interpolated it at different resolutions and then we filtered through the Newton-Raphson loop. Solutions with other values of λ behave in a qualitatively similar manner. Of course, the larger the λ is the larger the error is with the same grid structure and resolution.

Indeed, in all cases shown we observe that those quantities vanish in the continuum limit. This ensures that our numerical solutions provide a good approximation to the actual solution of the continuous problem. Notice that for the component ξ_y, the values themselves, being coordinate dependent, are not physical. However, the fact that they become zero for large N confirms that we are finding an Einstein metric

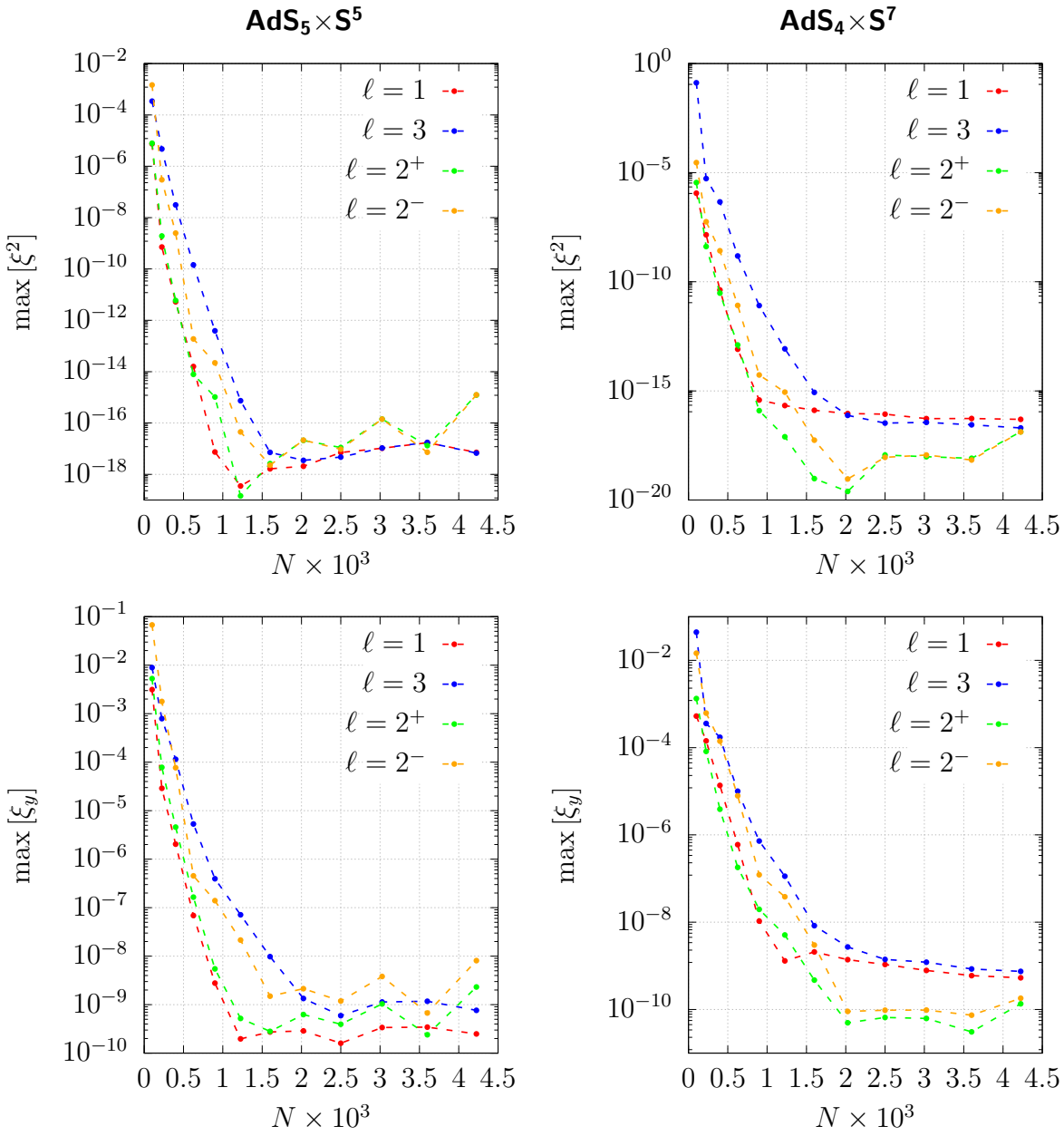

Fig. 4.19: *Logarithmic plot of the maximum values of ξ^2 and ξ_y on the whole integration domain, as a function of the grid size. In both cases the error decays exponentially, as expected. The plot for the DeTurck vector component along the x-direction is very similar to that for the y-component, so we do not include it here.*

rather than a Ricci soliton.

Chapter 5
Summary and Outlook

In this thesis we have used numerical methods to solve Einstein's equations and construct static black hole solutions in spacetimes with compact spaces. These are physically motivated due to the appearance of conifold geometries which, so far, have been barely studied in General Relativity. We have considered $D = 10$ and 11 spacetime dimensions, which are the relevant cases for the AdS/CFT correspondence. We have investigated various thermodynamic and geometric aspects of these solutions, and the possible relation between these two aspects on a specific region of solution space, namely close to the merger or critical point. At this point the solutions become singular and some numerical refined techniques need to be used to approach it. Additionally, using holography we have been able to make some novel predictions regarding the thermal phase diagrams of certain dual gauge theories, and how the critical behavior of the gravitational solutions is imprinted in the gauge side. The results are presented in the research Chapters 3 and 4, which are based on Ref. [1] and [2] respectively.

More precisely, we have first considered static black hole solutions in 10-dimensional Kaluza-Klein theory, which means that they are asymptotically $\text{Mink}_9 \times S^1$ vacuum solutions of Einstein's equations. We have numerically constructed black holes whose horizons are localized or non-uniformly distributed along the Kaluza-Klein circle S^1. Utilizing some well-motivated numerical techniques we have been able to reach solutions with critical (or conical) horizon deformations, just where both solutions are about to merge at the level of solution space. Remarkably, we find that the merger happens at a cusp in the phase diagram, in contrast to what occurs in lower spacetime dimensions. This can be linked to the cone geometry that reproduces the horizon regions that presumably pinch-off, as previously predicted, and now verified. Indeed, we show that the critical geometry is locally controlled by a Ricci-flat double-cone, which explains how the different physical quantities approach to their critical values. In $D = 10$, the double-cone predicts a quartic power law plus a logarithmic correction and using our solutions we have checked that this is indeed the case.

According to holography, D0-charged 10-dimensional localized black holes and black strings are dual to thermal states of $(1 + 1)$-dimensional SU(N) maximal super Yang Mills theory compactified on a circle. The corresponding phase diagrams for this particular point-like charge can be obtained from our neutral solutions. The

phase diagrams show a 1st order phase transition between these two phases, which is consistent with the available lattice simulations carried out in the gauge side. At this point, though, lattice results are insufficient to talk about an holographic test, since they just put a bound on the temperature. In this sense, our results comprise new holographic predictions that will surely be used in the future to test AdS/CFT.

Having numerical codes available for the construction of these Kaluza-Klein solutions, it would be easy to find them in dimensions greater than ten, specially for examining the stability properties of such families which are believed to change around the critical spacetime dimension $D^* = 13.5$. Large-D analysis have considered approximate solutions around this particular dimension, which may not be high enough for the results be completely reliable. Thus, it would be interesting to check if there is any substantial deviation with respect to the 'exact' (but numerical) results.

Then we have moved on to Anti-de Sitter space. Fomented by AdS/CFT, solutions with a negative cosmological constant are now a very active area of research. Here we have considered static black holes with non-uniform horizons along a q-sphere, also known as lumpy black holes in the literature. The solutions are asymptotically $\mathrm{AdS}_p \times S^q$, which require of the presence of a form field strength. For the values examined, $(p, q) = (5, 5)$ and $(4, 7)$, the theories that we solve are type IIB supergravity (with a self-dual 5-form) and low-energy M-theory. The solutions we are interested in are labeled by the harmonic number ℓ of scalar harmonics that respect their isometries. We constructed four families corresponding to $\ell = 1, 2^+, 2^-$ and 3. Using the same techniques as those for the Kaluza-Klein setting, we were able to reach unprecedented values of lumpiness parameter, which characterize the deformations along the internal space S^q. With the solutions in our power, we study their thermodynamics and geometry. In particular, our data allows us to infer the horizon topology of the solutions that are supposed to merge with the lumpy black holes at the merger or critical point. We show that the geometry of the horizon near the merger is well-described by a cone over a triple product of spheres, thus extending the original local cone model to the present asymptotics. Interestingly enough, our data is not compatible with a Ricci-flat cone, specially for the components along the internal sphere, which is consistent with the presence of a non-trivial flux. The pinch-off occurs at the horizon, and therefore we do not expect that this can be direct consequence of the presence of the AdS boundary. A perturbation analysis around the critical cone accounts for the behavior of the physical quantities of the actual solutions sufficiently close to the critical point. To leading order, this perturbation mode coincides with that of the Ricci-flat double-cone. We compute with an exceptional accuracy the critical exponents predicted by the cone model, which coincide as well.

Dimensionally reducing our solutions on the sphere, yields asymptotically AdS_p solutions coupled to additional scalar fields coming from the compactification. These fields acquire non-zero vacuum expectation values that can be computed using our numerical data. We examined these expectation values only in $D = 10$. Although they lie in a 4-dimensional gauge theory (or 5-dimensional AdS gravity theory), the

imprint from the 10-dimensional bulk solutions is reflected in the critical behavior of such quantities: they follow a quartic power law with a logarithmic correction, just as dictates the leading order perturbation analysis of the cone in the bulk. These comprise new further non-trivial predictions for the dual gauge theory on which to test AdS/CFT.

There are some natural extensions of this work. The black hole solutions that merge with the lumpy ones are only known in $D = 10$ and for the family with $\ell = 1$, which corresponds to a spherical black hole localized on the 5-sphere. Still, the available results are very far away from the merger point. The phase diagram of these localized solutions indicate the existence of a 1st order phase transition between these solutions and (small) Schwarzschild-$\mathrm{AdS}_5 \times S^5$ black holes, which is interpreted as spontaneous symmetry breaking in the dual gauge theory. However, the little numerical data available required of extrapolation to deduce its temperature. The techniques developed and used in this thesis would definitely help to resolve towards more critical black holes, allowing to obtain the precise value at which the phase transition occurs. Likewise, their different quantities should match with the ones that we have found from the lumpy side, towards the end of the branch. Of course, it would also be interesting to construct localized black holes in $\mathrm{AdS}_4 \times S^7$, or localized black holes that merge with higher harmonic lumpy solutions. Further work is currently being carried out in this direction. So far we have been able to design a proper reference metric resembling a spherical black hole near the horizon and being asymptotically $\mathrm{AdS}_p \times S^q$. Although this is the hard or creative part in this problem, the code we have still fails to find the desired solution. To fix this we need to fine tune the parameters that enter in the numerical problem and/or finding a more refined ansatz for the fields.

Another thing to consider would be to extend the Kaluza-Klein holography analysis to $D = 11$ spacetime dimensions. This case has received less attention and a fully generic gauge invariant mapping to 4-dimensional AdS gravity beyond linear order in the number of fields is not yet available. There are some results applied to the so-called LLM geometries which are clearly useful in our context, but the complete analysis requires some further work.

Bibliography

[1] B. Cardona and P. Figueras, *Critical Kaluza-Klein black holes and black strings in $D = 10$*, *JHEP* **11** (2018) 120 [hep-th/1806.11129].

[2] B. Cardona and P. Figueras, *Critical lumpy black holes in $AdS_p \times S^q$* (2020). To Appear.

[3] A. Einstein, *Die Feldgleichungen der Gravitation*, *Sitz. Preuß. Akad. Wiss.* (1915) 844.

[4] C. M. Will, *The Confrontation between General Relativity and Experiment*, *Living Rev. Rel.* **17** (2014) 4 [gr-qc/1403.7377].

[5] B. P. Abbott et al., *Observation of Gravitational Waves from a Binary Black Hole Merger*, *Phys. Rev. Lett.* **116** (2016) 061102 [gr-qc/1602.03837].

[6] The Event Horizon Telescope Collaboration, *First M87 Event Horizon Telescope Results. I. The Shadow of the Supermassive Black Hole*, *ApJ* **875** (2019) L1 [astro-ph.GA/1906.11238].

[7] S. W. Hawking, *Breakdown of Predictability in Gravitational Collapse*, *Phys. Rev. D* **14** (1976) 2460.

[8] J. Polchinski, *The Black Hole Information Problem*, *at 2015 TASI Summer School* (2016) [hep-th/1609.04036].

[9] A. Almheiri, T. Hartman, J. Maldacena, E. Shaghoulian and A. Tajdini, *The entropy of Hawking radiation*, (2020) [hep-th/2006.06872].

[10] M. Bojowald, *Quantum cosmology: a review*, *Rep. Prog. Phys.* **78** (2015) 023901 [gr-qc/1501.04899].

[11] M. R. Douglas and S. Kachru, *Flux compactification*, *Rev. Mod. Phys.* **79** (2007) 733 [hep-th/0610102].

[12] L. Randall and R. Sundrum, *An alternative to compactification*, *Phys. Rev. Lett.* **83** (1999) 4690 [hep-th/9906064].

[13] S. S. Gubser, *On nonuniform black branes*, *Class. Quant. Grav.* **19** (2002) 4825 [hep-th/0110193].

[14] T. Wiseman, *Static Axisymmetric Vacuum Solutions and Non-Uniform Black Strings*, *Class. Quant. Grav.* **20** (2003) 1137 [hep-th/0209051].

[15] T. ,Wiseman, *From Black Strings to Black Holes*, *Class. Quant. Grav.* **20** (2003) 1177 [hep-th/0211028].

[16] R. C. Myers, *Higher Dimensional Black Holes in Compactified Space-times*, *Phys. Rev. D* **35** (1987) 455.

[17] H. Kudoh and T. Wiseman, *Properties of Kaluza-Klein black holes*, *Prog. Theor. Phys.* **111** (2004) 475 [hep-th/0310104].

[18] E. Sorkin, B. Kol and T. Piran, *Caged Black Holes: Black Holes in Compactified Spacetimes I – Theory*, *Phys. Rev. D* **69** (2004) 064031 [hep-th/0309190]; *Caged Black Holes: Black Holes in Compactified Spacetimes II – 5d numerical implementation*, *Phys. Rev. D* **69** (2004) 064032 [hep-th/0310096].

[19] Ó. J. C. Dias, J. E. Santos and B. Way, *Lumpy $AdS_5 \times S^5$ black holes and black belts*, *JHEP* **04** (2015) 060 [hep-th/1501.06574].

[20] Ó. J. C. Dias, J. E. Santos and B. Way, *Localised $AdS_5 \times S^5$ Black Holes*, *Phys. Rev. Lett.* **117** (2016) 151101 [hep-th/1605.04911].

[21] B. Kol, *Topology change in General Relativity and the black-hole black-string transition*, *JHEP* **0510** (2005) 049 [hep-th/0206220].

[22] M. Kalisch, S. Mckel and M. Ammon, *Critical behavior of the black hole/black string transition*, *JHEP* **08** (2017) 049 [gr-qc/1706.02323].

[23] S. Catterall, A. Joseph and T. Wiseman, *Thermal phases of D1-branes on a circle from lattice super Yang-Mills*, *JHEP* **12** (2010) 022 [hep-th/1008.4964].

[24] S. Catterall, R. G. Jha, D. Schaich and T. Wiseman, *Testing holography using lattice super-Yang-Mills theory on a 2-torus*, *Phys. Rev. D* **97** (2018) 086020 [hep-th/1709.07025].

[25] K. Schwarzschild, *Über das Gravitationsfeld eines Massenpunktes nach der Einsteinschen Theorie*, *Sitzungsberichte der Kniglich Preussischen Akademie der Wissenschaften* **7** (1916) 189.

[26] G. D. Birkhoff, *Relativity and Modern Physics*, *Harvard University Press, Cambridge, MA* (1923).

[27] R. P. Kerr, *Gravitational field of a spinning mass as an example of algebraically special metrics*, *Phys. Rev. Lett.* **11** (1963) 237.

[28] P. O. Mazur, *Black Hole Uniqueness Theorems*, (2000) [hep-th/0101012].

[29] E. T. Newman and A. I. Janis, *Note on the Kerr Spinning-Particle Metric*, *J. Math. Phys.* **6** (1965) 915.

[30] E. T. Newman, R. Couch, K. Chinnapared, A. Exton, A. Prakash and R. Torrence, *Metric of a Rotating, Charged Mass*, *J. Math. Phys.* **6** (1965) 918.

[31] D. C. Robinson, *Classification of black holes with electromagnetic fields*, *Phys. Rev. D* **10** (1974) 458.

[32] P. Mazur, *Proof of uniqueness of the Kerr-Newman black hole solution*, *J. Phys. A* **15** (1982) 3173.

[33] H. Reissner, *Über die Eigengravitation des elektrischen Feldes nach der Einsteinschen Theorie*, *Annalen der Physik* **50** (1916) 106.

[34] G. Nordström, *On the Energy of the Gravitational Field in Einstein's Theory*, *Verhandl. Koninkl. Ned. Akad. Wetenschap., Afdel. Natuurk.* **26** (1918) 1201.

[35] J. B. Hartle and S. W. Hawking, *Solutions of the Einstein-Maxwell equations with many black holes*, *Comm. Math. Phys.* **26** (1972) 87.

[36] W. Israel, *Event horizons in static electrovac space-times*, *Comm. Math. Phy.* **8** (1968) 245.

[37] P. T. Chrusciel and N. S. Nadirashvili, *All electro-vacuum Majumdar-Papapetrou space-times with nonsingular black holes*, *Class. Quant. Grav.* **12** (1995) L17 [gr-qc/9412044].

[38] M. Heusler, *On the Uniqueness of the Papapetrou-Majumdar Metric*, *Class. Quant. Grav.* **14** (1997) L129 [gr-qc/9607001].

[39] R. Ruffini and J. A. Wheeler, *Introducing the Black Hole*, *Physics Today* **24** (1971) 30.

[40] J. E. Chase, *Event Horizons in Static Scalar-Vacuum Spacetimes*, *Commun. Math. Phys.* **19** (1970) 276.

[41] J. Hartle, *Long-Range Neutrino Forces Exerted by Kerr Black Holes*, *Phys. Rev. D* **3** (1971) 2938; C. Teitelboim, *Nonmeasurability of the Quantum Numbers of a Black Hole*, *Phys. Rev. D* **5** (1972) 2941.

[42] J. D. Bekenstein, *Nonexistence of Baryon Number for Static Black Holes*, *Phys. Rev. Lett.* **28** (1972) 452; *Nonexistence of Baryon Number for Static Black Holes*, *Phys. Rev. D* **5** (1972) 1239; *Nonexistence of Baryon Number for Black Holes II*, *Phys. Rev. D* **5** (1972) 2403.

[43] M. S. Volkov and D. V. Gal'tsov, *Gravitating nonAbelian solitons and black holes with Yang-Mills fields*, *Phys. Rept.* **319** (1999) 1 [hep-th/9810070].

[44] P. T. Chrusciel, J. L. Costa and M. Heusler, *Stationary Black Holes: Uniqueness and Beyond*, *Liv. Rev. Rel.* **15** (2012) 7 [gr-qc/1205.6112].

[45] T. Torii, K. Meeda, M. Narita, *Toward the no-scalar-hair conjecture in asymptotically de Sitter spacetime*, *Phys. Rev. D* **59** (1999) 064027 [gr-qc/9809036].

[46] T. Torii, K. Meeda, M. Narita, *Scalar hair on the black hole in asymptotically anti-de Sitter spacetime*, *Phys. Rev. D* **64** (2001) 044007.

[47] D. Christodoulou and S. Klainerman, *The nonlinear stability of the Minkowski metric in general relativity*, in C. Carasso, P. Charrier, B. Hanouzet and JL. Joly (eds), "Nonlinear Hyperbolic Problems. Lecture Notes in Mathematics", vol. 1402. Springer, Berlin (1989).

[48] H. Friedrich, *On the existence of n-geodesically complete or future complete solutions of Einstein's field equations with smooth asymptotic structure*, *Comm. Math. Phys.* **107** (1986) 587.

[49] C. V. Vishveshwara, *Stability of the Schwarzschild Metric*, *Phys. Rev. D* **1** (1970) 2870.

[50] R. H. Price, *Nonspherical Perturbations of Relativistic Gravitational Collapse. I. Scalar and Gravitational Perturbations*, *Phys. Rev. D* **5** (1972) 2419.

[51] B. F. Whiting, *Mode Stability of the Kerr Black Hole*, *J. Math. Phys.* **30** (1989) 1301.

[52] M. Zilhão, V. Cardoso, C. Herdeiro, L. Lehner and U. Sperhake, *Testing the nonlinear stability of Kerr-Newman black holes*, *Phys. Rev. D* **90** (2014) 045 [hep-th/1410.0694].

[53] P. Anninos, D. Hobill, E. Seidel, L. Smarr and W. M. Suen, *Collision of Two Black Holes*, *Phys. Rev. Lett.* **71** (1993) 2851 [gr-qc/9309016]; *Head-on collision of two equal mass black holes*, *Phys. Rev. D* **52** (1995) 2044 [gr-qc/9408041].

[54] U. Sperhake, V. Cardoso, F. Pretorius, E. Berti, and J. A. González, *The high-energy collision of two black holes*, *Phys. Rev. Lett.* **101** (2008) 161101 [gr-qc/0806.1738].

[55] M. Shibata, H. Okawa, and T. Yamamoto, *High-velocity collisions of two black holes*, *Phys. Rev. D* **78** (2008) 101501 [gr-qc/0810.4735].

[56] F. Pretorius, *Evolution of Binary Black Hole Spacetimes*, *Phys. Rev. Lett.* **95** (2005) 121101 [gr-qc/0507014].

[57] M. Campanelli, C. O. Lousto, P. Marronetti and Y. Zlochower, *Accurate Evolutions of Orbiting Black-Hole Binaries Without Excision*, *Phys. Rev. Lett.* **96** (2006) 111101 [gr-qc/0511048].

[58] J. G. Baker, J. Centrella, D-I. Choi, M. Koppitz and J. van Meter, *Gravitational wave extraction from an inspiraling configuration of merging black holes*, *Phys. Rev. Lett.* **96** (2006) 111102 [gr-qc/0511103].

[59] M. Dafermos, G. Holzegel and I. Rodnianski, *The linear stability of the Schwarzschild solution to gravitational perturbations*, *Acta Math.* **222** (2019) 1 [gr-qc/1601.06467].

[60] M. Dafermos, G. Holzegel and I. Rodnianski, *Boundedness and decay for the Teukolsky equation on Kerr spacetimes I: the case* $|a| \ll M$ (2017) [gr-qc/1711.07944].

[61] R. Penrose, *Gravitational Collapse and Space-Time Singularities*, *Phys. Rev. Lett.* **14** (1965) 57.

[62] R. Penrose, *Gravitational collapse: The role of general relativity*, *Riv. Nuovo Cim.* **1** (1969) 252. Republished in *General Relativity and Gravitation* **34** (2002) 1141.

[63] R. Wald, *Gravitational Collapse and Cosmic Censorship*, in B.R. Iyer, B. Bhawal (eds), "Black Holes, Gravitational Radiation and the Universe", vol. 100. Springer, Dordrecht (1999) [gr-qc/9710068].

[64] D. Christodoulou, *On the global initial value problem and the issue of singularities*, *Class. Quant. Grav.* **16** (1999) A23.

[65] D. Christodoulou, *Violation of cosmic censorship in the gravitational collapse of a dust cloud*, *Comm. Math. Phys.* **93** (1984) 171.

[66] D. Christodoulou, *A mathematical theory of gravitational collapse*, *Comm. Math. Phys.* **109** (1987) 613.

[67] D. Christodoulou, *The formation of black holes and singularities in spherically symmetric gravitational collapse*, *Comm. Pure Appl. Math.* **44** (1991) 339.

[68] D. Christodoulou, *Examples of Naked Singularity Formation in the Gravitational Collapse of a Scalar Field*, *Annals Math.* **140** (1994) 607.

[69] M. W. Choptuik, *Universality and scaling in gravitational collapse of a massless scalar field*, *Phys. Rev. Lett.* **70** (1993) 9.

[70] E. Sorkin and Y. Oren, *On Choptuik's scaling in higher dimensions*, *Phys. Rev. D* **71** (2005) 124005 [hep-th/0502034].

[71] K. Clough, E. A. Lim, *Critical Phenomena in Non-spherically Symmetric Scalar Bubble Collapse*, (2016) [gr-qc/1602.02568].

[72] N. Deppe, L. E. Kidder, M. A. Scheel, and S. A. Teukolsky, *Critical behavior in 3-d gravitational collapse of massless scalar fields*, *Phys. Rev. D* **99** (2019) 024018 [gr-qc/1802.08682].

[73] H. Ringström, *Cosmic Censorship for Gowdy Spacetimes*, *Liv. Rev. Rel.* **13** (2010) 2.

[74] G. Huisken and T. Ilmanen, *The Inverse Mean Curvature Flow and the Riemannian Penrose Inequality*, *J. Diff. Geom.* **59** (2001) 353.

[75] H. L. Bray, *Proof of the Riemannian Penrose Conjecture Using the Positive Mass Theorem*, *J. Diff. Geom.* **59** (2001) 177.

[76] F. C. Eperon, B. Ganchev and J. E. Santos, *Plausible scenario for a generic violation of the weak cosmic censorship conjecture in asymptotically flat four dimensions*, *Phys. Rev. D* **101** (2020) 041502 [gr-qc/1906.11257].

[77] B. E. Niehoff, J. E. Santos and B. Way, *Towards a violation of cosmic censorship*, *Class. Quant. Grav.* **33** (2016) 185012 [hep-th/1510.00709].

[78] G. T. Horowitz, J. E. Santos and B. Way, *Evidence for an Electrifying Violation of Cosmic Censorship*, *Class. Quant. Grav.* **33** (2016) 195007 [hep-th/1604.06465].

[79] T. Crisford and J. E. Santos, *Violating weak cosmic censorship in AdS_4*, *Phys. Rev. Lett.* **118** (2017) 181101 [hep-th/1702.05490].

[80] T. Crisford, G. T. Horowitz and J. E. Santos, *Attempts at vacuum counterexamples to cosmic censorship in AdS* , *JHEP* **02** (2019) 092 [hep-th/1805.06469].

[81] J. Luk and J. Sbierski, *Instability results for the wave equation in the interior of Kerr black holes*, (2015) [gr-qc/1512.08259].

[82] J. Luk and S.-J. Oh, *Proof of linear instability of the Reissner-Nordström Cauchy horizon under scalar perturbations*, *Duke Math. J.* **166** (2017) 437 [gr-qc/1501.04598].

[83] Y. Angelopoulos, S. Aretakis, and D. Gajic, *Late-time asymptotics for the wave equation on spherically symmetric, stationary spacetimes*, *Adv. Math.* **323** (2018) 529 [math.AP/1612.01566].

[84] J. Luk and S.-J. Oh, *Strong cosmic censorship in spherical symmetry for two-ended asymptotically flat initial data I. The interior of the black hole region* (2017) [gr-qc/1702.05715]; *Strong cosmic censorship in spherical symmetry for two-ended asymptotically flat initial data II. The exterior of the black hole region* (2017) [gr-qc/1702.05716].

[85] M. Dafermos and J. Luk, *The interior of dynamical vacuum black holes I: The C_0-stability of the Kerr Cauchy horizon*, (2017) [gr-qc/1710.01722].

[86] V. Cardoso, J. L. Costa, K. Destounis, P. Hintz and A. Jansen, *Quasinormal Modes and Strong Cosmic Censorship*, *Phys. Rev. Lett.* **120** (2018) 031103 [gr-qc/1711.10502].

[87] D. Youm, *Black Holes and Solitons in String Theory*, *Phys. Rept.* **316** (1999) 1 [hep-th/9710046].

[88] K. Maeda and M. Nozawa, *Black hole solutions in string theory*, *Prog. Theor. Phys. Supp.* **1899** (2011) 310 [hep-th/1104.1849].

[89] A. Strominger and C. Vafa, *Microscopic origin of the Bekenstein-Hawking entropy*, *Phys. Lett. B* **379** (1996) 99 [hep-th/9601029].

[90] I. Bena, N. P. Warner, *Black Holes, Black Rings and their Microstates*, *Lect. Notes in Phys.* **755** (2008) 1 [hep-th/0701216].

[91] I. Antoniadis, *A Possible new dimension at a few TeV*, *Phys. Lett. B* **246** (1990) 377.

[92] N. Arkani-Hamed, S. Dimopoulos, and G. R. Dvali, *The hierarchy problem and new dimensions at a millimeter*, *Phys. Lett. B* **429** (1998) 263 [hep-ph/9803315].

[93] N. Arkani-Hamed, S. Dimopoulos, and G. R. Dvali, *Phenomenology, Astrophysics and Cosmology of Theories with Sub-Millimeter Dimensions and TeV Scale Quantum Gravity*, *Phys. Rev. D* **59** (1999) 086004 [hep-ph/9807344].

[94] L. Randall and R. Sundrum, *A large mass hierarchy from a small extra dimension*, *Phys. Rev. Lett.* **83** (1999) 3370 [hep-th/9905221].

[95] I. Antoniadis, N. Arkani-Hamed, S. Dimopoulos, and G. R. Dvali, *New dimensions at a millimeter to a Fermi and superstrings at a TeV*, *Phys. Lett. B* **436** (1998) 257 [hep-ph/9804398].

[96] G. R. Dvali, G. Gabadadze and M. Porrati, *4D Gravity on a Brane in 5D Minkowski Space*, *Phys. Lett. B* **485** (2000) 208 [hep-th/0005016].

[97] M. Cavaglia, *Black hole and brane production in TeV gravity: A review*, *Int. J. Mod. Phys. A* **18** (2003) 1843 [hep-ph/0210296].

[98] R. Emparan and H. S. Reall, *Black Holes in Higher Dimensions*, *Living Rev. Rel.* **11** (2008) 6 [hep-th/0801.3471].

[99] F. Tangherlini, *Schwarzschild field in n dimensions and the dimensionality of space problem*, *Nuovo Cim.* **27** (1963) 636.

[100] G. W. Gibbons, D. Ida, and T. Shiromizu, *Uniqueness and non-uniqueness of static vacuum black holes in higher dimensions*, *Prog. Theor. Phys. Suppl.* **148** (2003) 284 [gr-qc/0203004].

[101] R. C. Myers and M. Perry, *Black Holes in Higher Dimensional Space-Times*, *Annals of Physics* **172** (1986) 304.

[102] R. Emparan and H. S. Reall, *A rotating black ring in five dimensions*, *Phys. Rev. Lett.* **88** (2002) 101101 [hep-th/0110260].

[103] R. Emparan and H. S. Reall, *Black Rings*, *Class. Quant. Grav.* **23** (2006) R169 [hep-th/0608012].

[104] A. A. Pomeransky, R. A. Sen'kov, *Black ring with two angular momenta*, (2006) [hep-th/0612005].

[105] H. Elvang and P. Figueras, *Black Saturn*, *JHEP* **0705** (2007) 050 [hep-th/0701035].

[106] H. Iguchi and T. Mishima, *Black diring and infinite nonuniqueness*, *Phys. Rev. D* **75** (2008) 064018 [hep-th/0701043].

[107] J. Evslin and C. Krishnan, *The Black Di-Ring: An Inverse Scattering Construction*, *Class. Quant. Grav.* **26** (2009) 125018 [hep-th/0706.1231].

[108] H. Elvang and M. J. Rodriguez, *Bicycling Black Rings*, *JHEP* **04** (2008) 045 [hep-th/0712.2425].

[109] K. Izumi, *Orthogonal black di-ring solution*, *Prog. Theor. Phys.* **119** (2008) 757 [hep-th/0712.0902].

[110] H. Elvang, R. Emparan and P. Figueras, *Phases of Five-Dimensional Black Holes*, *JHEP* **0705** (2007) 056 [hep-th/0702111].

[111] R. Emparan, T. Harmark, V. Niarchos, N. A. Obers and M. J. Rodriguez, *The Phase Structure of Higher-Dimensional Black Rings and Black Holes*, *JHEP* **0710** (2007) 110 [hep-th/0708.2181].

[112] R. Emparan and P. Figueras, *Multi-black rings and the phase diagram of higher-dimensional black holes*, *JHEP* **11** (2010) 022 [hep-th/1008.3243].

[113] S. Hollands, A. Ishibashi and R. M. Wald, *A Higher Dimensional Stationary Rotating Black Hole Must be Axisymmetric*, *Comm. Math. Phys.* **271** (2007) 699 [gr-qc/0605106].

[114] V. Moncrief and J. Isenberg, *Symmetries of Higher Dimensional Black Holes*, *Class. Quant. Grav.* **25** (2008) 195015 [gr-qc/0805.1451].

[115] R. Emparan, T. Harmark, V. Niarchos and N. A. Obers, *New Horizons for Black Holes and Branes*, *JHEP* **1004** (2010) 046 [hep-th/0912.2352].

[116] G. J. Galloway and R. Schoen, *A Generalization of Hawking's black hole topology theorem to higher dimensions*, *Comm. Math. Phys.* **266** (2006) 571 [gr-qc/0509107].

[117] S. Hollands and A. Ishibashi, *Black hole uniqueness theorems in higher dimensional spacetimes*, *Class. Quant. Grav.* **29** (2012) 163001 [gr-qc/1206.1164].

[118] K. Tanabe, *Black rings at large D*, *JHEP* **02** (2016) 151 [hep-th/1510.02200].

[119] H. Kudoh, *Doubly Spinning Black Rings*, *Phys. Rev. D* **75** (2007) 064006 [gr-qc/0611136].

[120] B. Kleihaus, J. Kunz and E. Radu, $d \geq 5$ *static black holes with* $S^2 \times S^{d-4}$ *event horizon topology*, *Phys. Lett. B* **678** (2009) 301 [hep-th/0904.2723].

[121] B. Kleihaus, J. Kunz, E. Radu and M. J. Rodriguez, *New generalized nonspherical black hole solutions*, *JHEP* **02** (2011) 058 [gr-qc/1010.2898].

[122] B. Kleihaus, J. Kunz and E. Radu, *Black rings in six dimensions*, *Phys. Lett. B* **718** (2013) 1073.

[123] B. Kleihaus, J. Kunz and E. Radu, *Black Rings in More Than Five Dimensions*, *Proceedings of The Thirteenth Marcel Grossmann Meeting (MG13): Stockholm, Sweden, July 1-7, 2012* (2015) 1321 [hep-th/1205.5437].

[124] B. Kleihaus, J. Kunz, and E. Radu, *Black ringoids: spinning balanced black objects in* $d \geq 5$ *dimensions – the codimension-two case*, *JHEP* **01** (2015) 117 [gr-qc/1410.0581].

[125] Th. Kaluza, *Zum Unitätsproblem der Physik*, *Sitzungsber. Preuss. Akad. Wiss. Berlin (Math. Phys.)* (1921) 966 [hist-ph/1803.08616].

[126] O. Klein, *Quantentheorie und fünfdimensionale Relativitätstheorie*, *Zeitschrift für Physik* **37** (1926) 895.

[127] G. T. Horowitz, *Playing with black strings*, (2002) [hep-th/0205069].

[128] E. Witten, *Instability of the Kaluza-Klein vacuum*, *Nucl. Phys. B* **195** (1982) 481.

[129] H. Elvang, T. Harmark, and N. A. Obers, *Sequences of Bubbles and Holes: New Phases of Kaluza-Klein Black Holes*, *JHEP* **01** (2005) 003 [hep-th/0407050].

[130] R. Gregory and R. Laflamme, *Black strings and p-branes are unstable*, *Phys. Rev. Lett.* **70** (1993) 2837 [hep-th/9301052].

[131] R. Gregory and R. Laflamme, *The Instability of charged black strings and p-branes*, *Nucl. Phys. B* **428** (1994) 339 [hep-th/9404071].

[132] B. Kol and E. Sorkin, *On Black-Brane Instability in an Arbitrary Dimension*, *Class. Quant. Grav.* **21** (2004) 4793 [gr-qc/0407058].

[133] T. Harmark, V. Niarchos, and N. A. Obers, *Instabilities of black strings and branes*, *Class. Quant. Grav.* **24** (2007) R1 [hep-th/0701022].

[134] G. T. Horowitz and K. Maeda, *Fate of the Black String Instability*, *Phys. Rev. Lett.* **87** (2001) 131301 [hep-th/0105111].

[135] M. W. Choptuik, L. Lehner, I. Olabarrieta, R. Petryk, F. Pretorius and H. Villegas, *Towards the Final Fate of an Unstable Black String*, *Phys. Rev. D* **68** (2003) 044001 [gr-qc/0304085].

[136] D. Garfinkle, L. Lehner, and F. Pretorius, *Numerical examination of an evolving black string horizon*, *Phys. Rev. D* **71** (2005) 064009 [gr-qc/0412014].

[137] L. Lehner and F. Pretorius, *Black Strings, Low Viscosity Fluids, and Violation of Cosmic Censorship*, *Phys. Rev. Lett.* **105** (2010) 101102 [hep-th/1006.5960].

[138] R. Emparan, R. Suzuki and K. Tanabe, *Evolution and End Point of the Black String Instability: Large D Solution*, *Phys. Rev. Lett.* **115** (2015) 091102 [hep-th/1506.06772].

[139] R. Emparan and R. C. Myers, *Instability of ultra-spinning black holes*, *JHEP* **0309** (2003) 025 [hep-th/0308056].

[140] Ó. J. C. Dias, P. Figueras, R. Monteiro, J. E. Santos and R. Emparan, *Instability and new phases of higher-dimensional rotating black holes*, *Phys. Rev. D* **80** (2009) 111701 [hep-th/0907.2248].

[141] Ó. J. C. Dias, P. Figueras, R. Monteiro, H. S. Reall, and J. E. Santos, *An instability of higher-dimensional rotating black holes*, *JHEP* **05** (2010) 076 [hep-th/1001.4527].

[142] Ó. J. C. Dias, P. Figueras, R. Monteiro and J. E. Santos, *Ultraspinning instability of rotating black holes*, *Phys. Rev. D* **82** (2010) 104025 [hep-th/1006.1904].

[143] M. Shibata and H. Yoshino, *Bar-mode instability of rapidly spinning black hole in higher dimensions: Numerical simulation in general relativity*, *Phys. Rev. D* **81** (2010) 104035 [gr-qc/1004.4970].

[144] M. Shibata and H. Yoshino, *Nonaxisymmetric instability of rapidly rotating black hole in five dimensions*, *Phys. Rev. D* **81** (2010) 021501 [gr-qc/0912.3606].

[145] P. Figueras, M. Kunesch, L. Lehner and S. Tunyasuvunakool, *End Point of the Ultraspinning Instability and Violation of Cosmic Censorship*, *Phys. Rev. Lett.* **118** (2017) 151103 [hep-th/1702.01755].

[146] Ó. J. C. Dias, J. E. Santos and B. Way, *Rings, Ripples, and Rotation: Connecting Black Holes to Black Rings*, *JHEP* **07** (2014) 045 [hep-th/1402.6345].

[147] R. Emparan, P. Figueras, M. Martinez, *Bumpy black holes*, *JHEP* **12** (2014) 072 [hep-th/1410.4764].

[148] H. Bantilan, P. Figueras, M. Kunesch and R. Panoso, *End point of nonaxisymmetric black hole instabilities in higher dimensions*, *Phys. Rev. D* **100** (2019) 086014 [hep-th/1906.10696].

[149] Ó. J. C. Dias, G. S. Hartnett and J. E. Santos, *Quasinormal modes of asymptotically flat rotating black holes*, *Class. Quant. Grav.* **31** (2014) 245011 [hep-th/1402.7047].

[150] J. L. Hovdebo and R. C. Myers, *Black Rings, Boosted Strings and Gregory-Laflamme*, *Phys. Rev. D* **73** (2006) 084013 [hep-th/0601079].

[151] H. Elvang, R. Emparan and A. Virmani, *Dynamics and stability of black rings*, *JHEP* **0612** (2006) 074 [hep-th/0608076].

[152] J. E. Santos and B. Way, *Neutral Black Rings in Five Dimensions are Unstable*, *Phys. Rev. Lett.* **114** (2015) 221101 [hep-th/1503.00721].

[153] P. Figueras, M. Kunesch, and S. Tunyasuvunakool, *End Point of Black Ring Instabilities and the Weak Cosmic Censorship Conjecture*, *Phys. Rev. Lett.* **116** (2016) 071102 [hep-th/1512.04532].

[154] D. J. Gross, M. J. Perry and L. G. Yaffe, *Instability of flat space at finite temperature*, *Phys. Rev. D* **25** (1982) 330.

[155] H. S. Reall, *Classical and Thermodynamic Stability of Black Branes*, *Phys. Rev. D* **64** (2001) 044005 [hep-th/0104071].

[156] V. E. Hubeny and M. Rangamani, *Unstable Horizons*, *JHEP* **0205** (2002) 027 [hep-th/0202189].

[157] M. Kalisch and M. Ansorg, *Pseudo-spectral construction of non-uniform black string solutions in five and six spacetime dimensions*, *Class. Quant. Grav.* **33** (2016) 215005 [gr-qc/1607.03099].

[158] M. Ammon, M. Kalisch and S. Moeckel, *Notes on ten-dimensional localized black holes and deconfined states in two-dimensional SYM*, *JHEP* **11** (2018) 090 [hep-th/1806.11174].

[159] R. Emparan and R. Suzuki, *Topology-changing horizons at large D as Ricci flows*, *JHEP* **07** (2019) 094 [hep-th/1905.01062].

[160] R. Emparan and N. Haddad, *Self-similar critical geometries at horizon intersections and mergers*, *JHEP* **1110** (2011) 064 [hep-th/1109.1983].

[161] Ó. J. C. Dias, J. E. Santos and B. Way, *Localised and nonuniform thermal states of super-Yang-Mills on a circle*, *JHEP* **06** (2017) 029 [hep-th/1702.07718].

[162] J. M. Maldacena, *The Large N Limit of Superconformal Field Theories and Supergravity*, *Adv. Theor. Math. Phys.* **2** (1998) 231 [hep-th/9711200].

[163] E. Witten, *Anti-de Sitter space and holography*, *Adv. Theor. Math. Phys.* **2** (1998) 253 [hep-th/9802150].

[164] E. Witten, *Anti-de Sitter space, thermal phase transition, and confinement in gauge theories*, *Adv. Theor. Math. Phys.* **2** (1998) 505 [hep-th/9803131].

[165] S. Gubser, I. R. Klebanov, and A. M. Polyakov, *Gauge theory correlators from non-critical string theory*, *Phys. Lett. B* **428** (1998) 105 [hep-th/9802109].

[166] O. Aharony, S. S. Gubser, J. M. Maldacena, H. Ooguri and Y. Oz, *Large N Field Theories, String Theory and Gravity*, *Phys. Rept.* **323** (2000) 183 [hep-th/9905111].

[167] R. Grimm, M. Sohnius and J. Wess, *Extended supersymmetry and gauge theories*, *Nucl. Phys. B* **133** (1978) 275.

[168] R. Bousso, *The holographic principle*, *Rev. Mod. Phys.* **74** (2002) 825 [hep-th/0203101].

[169] G. 't Hooft, *Dimensional reduction in quantum gravity*, (1993) [gr-qc/9310026].

[170] L. Susskind, *The World as a Hologram*, *J. Math. Phys.* **36** (1995) 6377 [hep-th/9409089].

[171] G. 't Hooft, *A planar diagram theory for strong interactions*, *Nucl. Phys. B* **72** (1974) 461.

[172] J. Casalderrey-Solana, H. Liu, D. Mateos, K. Rajagopal and U. A. Wiedemann, *Gauge/String Duality, Hot QCD and Heavy Ion Collisions*, (2011) [hep-th/1101.0618].

[173] Y. V. Kovchegov, *AdS/CFT applications to relativistic heavy ion collisions: a brief review*, *Rept. Prog. Phys.* **75** (2012) 124301 [hep-ph/1112.5403].

[174] S. S. Gubser, *The gauge-string duality and heavy ion collisions*, *Found. Phys.* **43** (2013) 140 [hep-th/1103.3636].

[175] O. DeWolfe, S. S. Gubser, C. Rosen and D. Teaney, *Heavy ions and string theory*, *Prog. Part. Nucl. Phys.* **75** (2014) 86 [hep-th/1304.7794].

[176] G. Policastro, D. T. Son and A. O. Starinets, *The shear viscosity of strongly coupled $\mathcal{N} = 4$ supersymmetric Yang-Mills plasma*, *Phys. Rev. Lett.* **87** (2001) 081601 [hep-th/0104066].

[177] P. Kovtun, D. T. Son and A. O. Starinets, *Viscosity in strongly interacting quantum field theories from black hole physics*, *Phys. Rev. Lett.* **94** (2005) 111601 [hep-th/0405231].

[178] D. T. Son and A. O. Starinets, *Viscosity, Black Holes, and Quantum Field Theory*, *Ann. Rev. Nucl. Part. Sci.* **57** (2007) 95 [hep-th/0704.0240].

[179] R. Baier, P. Romatschke, D. T. Son, A. O. Starinets, and M. A. Stephanov, *Relativistic viscous hydrodynamics, conformal invariance, and holography*, *JHEP* **0804** (2008) 100 [hep-th/0712.2451].

[180] S. Bhattacharyya, V. E. Hubeny, S. Minwalla and M. Rangamani, *Nonlinear Fluid Dynamics from Gravity*, *JHEP* **0802** (2008) 045 [hep-th/0712.2456].

[181] S. Bhattacharyya, S. Lahiri, R. Loganayagam and S. Minwalla, *Large rotating AdS black holes from fluid mechanics*, *JHEP* **0809** (2008) 054 [hep-th/0708.1770].

[182] S. Kachru, X. Liu and M. Mulligan, *Gravity Duals of Lifshitz-like Fixed Points*, *Phys. Rev. D* **78** (2008) 106005 [hep-th/0808.1725].

[183] S. A. Hartnoll, *Lectures on holographic methods for condensed matter physics*, *Class. Quant. Grav.* **26** (2009) 224002 [hep-th/0903.3246].

[184] C. P. Herzog, *Lectures on Holographic Superfluidity and Superconductivity*, *J. Phys. A* **42** (2009) 343001 [hep-th/0904.1975].

[185] J. McGreevy, *Holographic duality with a view toward many-body physics*, *Adv. High Energy Phys.* **2010** (2010) 723105 [hep-th/0909.0518].

[186] S. Sachdev, *Condensed Matter and AdS/CFT*, *Lect. Notes Phys.* **828** (2011) 273 [hep-th/1002.2947].

[187] E. D'Hoker and D. Z. Freedman, *Supersymmetric Gauge Theories and the AdS/CFT Correspondence*, (2002) [hep-th/0201253].

[188] G. T. Horowitz and J. Polchinski, *Gauge/gravity duality*, (2006) [gr-qc/0602037].

[189] H. Nastase, *Introduction to AdS-CFT*, (2007) [hep-th/0712.0689].

[190] G. T. Horowitz and A. Strominger, *Black strings and P-branes*, *Nucl. Phys. B* **360** (1991) 197.

[191] S. de Haro, K. Skenderis and S.N. Solodukhin, *Holographic Reconstruction of Spacetime and Renormalization in the AdS/CFT Correspondence*, *Comm. Math. Phys* **217** (2001) 595 [hep-th/0002230].

[192] M. Bianchi, D.Z. Freedman, K. Skenderis, *How to go with an RG Flow*, *JHEP* **08** (2001) 041 [hep-th/0105276].

[193] M. Bianchi, D.Z. Freedman, K. Skenderis, *Holographic Renormalization*, *Nucl. Phys. B* **631** (2002) 159 [hep-th/0112119].

[194] C. P. Burgess, N. R. Constable and R. C. Myers, *The Free Energy of $\mathcal{N} = 4$ Super-Yang-Mills and the AdS/CFT Correspondence*, *JHEP* **08** (1999) 017 [hep-th/9907188].

[195] S. W. Hawking and D. N. Page, *Thermodynamics of Black Holes in anti-De Sitter Space*, *Comm. Math. Phys.* **87** (1983) 577.

[196] V. A. Belinsky and V. E. Zakharov, *Integration of the Einstein Equations by the Inverse Scattering Problem Technique and the Calculation of the Exact Soliton Solutions*, *Sov. Phys. JETP* **48** (1978) 985.

[197] V. A. Belinsky and V. E. Sakharov, *Stationary Gravitational Solitons with Axial Symmetry*, *Sov. Phys. JETP* **50** (1979) 1.

[198] T. Harmark, *Small black holes on cylinders*, *Phys. Rev. D* **69** (2004) 104015 [hep-th/0310259].

[199] D. Gorbonos and B. Kol, *A dialogue of multipoles: Matched asymptotic expansion for caged black holes*, *JHEP* **0406** (2004) 053 [hep-th/0406002].

[200] D. Karasik, C. Sahabandu, P. Suranyi and L. C. R. Wijewardhana, *Analytic approximation to 5 dimensional black holes with one compact dimension*, *Phys. Rev. D* **71** (2005) 024024 [hep-th/0410078].

[201] D. Gorbonos and B. Kol, *Matched asymptotic expansion for caged black holes: Regularization of the post-Newtonian order*, *Class. Quant. Grav.* **22** (2005) 3935 [hep-th/0505009].

[202] R. Emparan, T. Harmark, V. Niarchos and N. A. Obers, *World-Volume Effective Theory for Higher-Dimensional Black Holes*, *Phys. Rev. Lett.* **102** (2009) 191301 [hep-th/0902.0427].

[203] R. Emparan, T. Harmark, V. Niarchos and N. A. Obers, *Essentials of Blackfold Dynamics*, *JHEP* **1003** (2010) 063 [hep-th/0910.1601].

[204] R. Emparan, R. Suzuki and K. Tanabe, *The large D limit of General Relativity*, *JHEP* **06** (2013) 009 [hep-th/1302.6382].

[205] R. Emparan, T. Shiromizu, R. Suzuki, K. Tanabe and T. Tanaka, *Effective theory of Black Holes in the 1/D expansion*, *JHEP* **06** (2015) 159 [hep-th/1504.06489].

[206] Ó. J. C. Dias, J. E. Santos and B. Way, *Numerical Methods for Finding Stationary Gravitational Solutions*, *Class. Quant. Grav.* **33** (2016) 133001 [hep-th/1510.02804].

[207] M. Shibata and T. Nakamura, *Evolution of three-dimensional gravitational waves: Harmonic slicing case*, *Phys. Rev. D* **52** (1995) 5428.

[208] T. W. Baumgarte and S. L. Shapiro, *On the numerical integration of Einstein's field equations*, *Phys. Rev. D* **59** (1999) 024007 [gr-qc/9810065].

[209] C. Bona, T. Ledvinka, C. Palenzuela and M. Zacek, *General covariant evolution formalism for numerical relativity*, *Phys. Rev. D* **67** (2003) 104005 [gr-qc/0302083].

[210] D. Alic, C. Bona-Casas, C. Bona, L. Rezzolla and C. Palenzuela, *Conformal and covariant formulation of the Z4 system with constraint-violation damping*, *Phys. Rev. D* **85** (2012) 064040 [gr-qc/1106.2254].

[211] H. Kudoh and T. Wiseman, *Connecting black holes and black strings*, *Phys. Rev. Lett.* **94** (2005) 161102 [hep-th/0409111].

[212] B. Kleihaus and J. Kunz, *Rotating Boson Stars and Q-Balls*, *Phys. Rev. D* **72** (2005) 064002 [gr-qc/0505143].

[213] O. Aharony, S. Minwalla and T. Wiseman, *Plasma-balls in large N gauge theories and localized black holes*, *Class. Quant. Grav.* **23** (2006) 2171 [hep-th/0507219].

[214] M. Headrick, S. Kitchen and T. Wiseman, *A new approach to static numerical relativity, and its application to Kaluza-Klein black holes*, *Class. Quant. Grav.* **27** (2010) 035002 [gr-qc/0905.1822].

[215] A. Adam, S. Kitchen and T. Wiseman, *A numerical approach to finding general stationary vacuum black holes* , *Class. Quant. Grav.* **29** (2012) 165002 [gr-qc/1105.6347].

[216] D. M. DeTurck, *Deforming metrics in the direction of their Ricci tensors*, *J. Differ. Geom.* **18** (1983) 157.

[217] H. Friedrich, *On the hyperbolicity of Einsteins and other gauge field equations*, *Comm. Math. Phys.* **100** (1985) 525.

[218] D. Garfinkle, *Harmonic coordinate method for simulating generic singularities*, *Phys. Rev. D* **65** (2002) 044029 [gr-qc/0110013].

[219] Ó. J. C. Dias, J. E. Santos and B. Way, *Black holes with a single Killing vector field: black resonators*, *JHEP* **12** (2015) 171 [hep-th/1505.04793].

[220] G. T. Horowitz and J. E. Santos, *Geons and the Instability of Anti-de Sitter Spacetime*, (2014) [gr-qc/1408.5906].

[221] P. Figueras and T. Wiseman, *Stationary holographic plasma quenches and numerical methods for non-Killing horizons*, *Phys. Rev. Lett.* **110** (2013) 171602 [hep-th/1212.4498].

[222] S. Fischetti, D. Marolf and J. E. Santos, *AdS flowing black funnels: Stationary AdS black holes with non-Killing horizons and heat transport in the dual CFT*, *Class. Quant. Grav.* **30** (2013) 075001 [hep-th/1212.4820].

[223] M. Rozali, J. B. Stang and M. van Raamsdonk, *Holographic Baryons from Oblate Instantons*, *JHEP* **02** (2014) 044 [hep-th/1309.7037].

[224] P. Figueras, J. Lucietti and T. Wiseman, *Ricci solitons, Ricci flow, and strongly coupled CFT in the Schwarzschild Unruh or Boulware vacua*, *Class. Quant. Grav.* **28** (2011) 215018 [hep-th/1104.4489].

[225] P. Figueras and T. Wiseman, *On the existence of stationary Ricci solitons*, *Class. Quant. Grav.* **34** (2017) 145007 [gr-qc/1610.06178].

[226] R. S. Hamilton, *Three-manifolds with positive Ricci curvature*, *J. Diff. Geom.* **17** (1982) 255.

[227] P. Grandclement and J. Novak, *Spectral methods for numerical relativity*, *Liv. Rev. Rel.* **12** (2009) 1 [gr-qc/0706.2286].

[228] R. P. Macedo and M. Ansorg, *Axisymmetric fully spectral code for hyperbolic equations*, *J. Comput. Phys.* **276** (2014) 357 [physics.comp-ph/1402.7343].

[229] E. Sorkin, *Non-uniform black strings in various dimensions*, *Phys. Rev. D* **74** (2006) 104027 [gr-qc/0608115].

[230] B. Kleihaus, J. Kunz and E. Radu, *New nonuniform black string solutions*, *JHEP* **06** (2006) 016 [hep-th/0603119].

[231] P. Figueras, K. Murata and H. S. Reall, *Stable non-uniform black strings below the critical dimension*, *JHEP* **11** (2012) 071 [gr-qc/1209.1981].

[232] M. Kalisch and M. Ansorg, *Highly Deformed Non-uniform Black Strings in Six Dimensions*, in *Proceedings, 14th Marcel Grossmann Meeting on Recent Developments in Theoretical and Experimental General Relativity, Astrophysics, and Relativistic Field Theories (MG14) (In 4 Volumes): Rome, Italy, July 12-18, 2015*, vol. 2, pp. 1799 (2017) [hep-th/1509.03083].

[233] R. Emparan, R. Luna, M. Martínez, R. Suzuki and K. Tanabe, *Phases and Stability of Non-Uniform Black Strings*, *JHEP* **05** (2018) 104 [hep-th/1802.08191].

[234] E. Sorkin, *A Critical dimension in the black string phase transition*, *Phys. Rev. Lett.* **93** (2004) 031601 [hep-th/0402216].

[235] R. Suzuki and K. Tanabe, *Non-uniform black strings and the critical dimension in the $1/D$ expansion*, *JHEP* **10** (2015) 107 [hep-th/1506.01890].

[236] Y.-Z. Chu, W. D. Goldberger and I. Z. Rothstein, *Asymptotics of d-dimensional Kaluza-Klein black holes: Beyond the newtonian approximation*, *JHEP* **03** (2006) 013 [hep-th/0602016].

[237] B. Kol and M. Smolkin, *Classical Effective Field Theory and Caged Black Holes*, *Phys. Rev. D* **77** (2008) 064033 [hep-th/0712.2822].

[238] B. Kol and T. Wiseman, *Evidence that highly non-uniform black strings have a conical waist*, *Class. Quant. Grav.* **20** (2003) 3493 [hep-th/0304070].

[239] N. Itzhaki, J. M. Maldacena, J. Sonnenschein and S. Yankielowicz, *Supergravity and the large N limit of theories with sixteen supercharges*, *Phys. Rev. D* **58** (1998) 046004 [hep-th/9802042].

[240] T. Harmark and N. A. Obers, *Black holes on cylinders*, *JHEP* **0205** (2002) 032 [hep-th/0204047].

[241] T. Harmark and N. A. Obers, *New phases of near-extremal branes on a circle*, *JHEP* **09** (2004) 022 [hep-th/0407094].

[242] O. Aharony, J. Marsano, S. Minwalla and T. Wiseman, *Black hole-black string phase transitions in thermal 1+1 dimensional supersymmetric Yang-Mills theory on a circle*, *Class. Quant. Grav.* **21** (2004) 5169 [hep-th/0406210].

[243] M. Hanada, J. Nishimura and S. Takeuchi, *Non-lattice simulation for supersymmetric gauge theories in one dimension*, *Phys. Rev. Lett.* **99** (2007) 161602 [hep-lat/0706.1647].

[244] S. Catterall and T. Wiseman, *Towards lattice simulation of the gauge theory duals to black holes and hot strings*, *JHEP* **12** (2007) 104 [hep-lat/0706.3518].

[245] K. N. Anagnostopoulos, M. Hanada, J. Nishimura and S. Takeuchi, *Monte Carlo studies of supersymmetric matrix quantum mechanics with sixteen supercharges at finite temperature*, *Phys. Rev. Lett.* **100** (2008) 021601 [hep-th/0707.4454].

[246] S. Catterall and T. Wiseman, *Black hole thermodynamics from simulations of lattice Yang-Mills theory*, *Phys. Rev. D* **78** (2008) 041502 [hep-th/0803.4273].

[247] M. Hanada, A. Miwa, J. Nishimura and S. Takeuchi, *Schwarzschild radius from Monte Carlo calculation of the Wilson loop in supersymmetric matrix quantum mechanics*, *Phys. Rev. Lett.* **102** (2009) 181602 [hep-th/0811.2081].

[248] M. Hanada, Y. Hyakutake, J. Nishimura and S. Takeuchi, *Higher derivative corrections to black hole thermodynamics from supersymmetric matrix quantum mechanics*, *Phys. Rev. Lett.* **102** (2009) 191602 [hep-th/0811.3102].

[249] D. Kadoh and S. Kamata, *Gauge/gravity duality and lattice simulations of one dimensional SYM with sixteen supercharges*, (2015) [hep-lat/1503.08499].

[250] V. G. Filev and D. O'Connor, *The BFSS model on the lattice*, *JHEP* **05** (2016) 167 [hep-th/1506.01366].

[251] V. G. Filev and D. O'Connor, *A Computer Test of Holographic Flavour Dynamics*, *JHEP* **05** (2016) 122 [hep-th/1512.02536].

[252] M. Hanada, Y. Hyakutake, G. Ishiki and J. Nishimura, *Numerical tests of the gauge/gravity duality conjecture for D0-branes at finite temperature and finite N*, *Phys. Rev. D* **94** (2016) 086010 [hep-th/1603.00538].

[253] E. Berkowitz, E. Rinaldi, M. Hanada, G. Ishiki, S. Shimasaki and P. Vranas, *Supergravity from D0-brane Quantum Mechanics*, (2016) [hep-th/1606.04948].

[254] E. Berkowitz, E. Rinaldi, M. Hanada, G. Ishiki, S. Shimasaki and P. Vranas, *Precision lattice test of the gauge/gravity duality at large-N*, *Phys. Rev. D* **94** (2016) 094501 [hep-lat/1606.04951].

[255] Y. Asano, V. G. Filev, S. Kováčik and D. O'Connor, *The flavoured BFSS model at high temperature*, *JHEP* **01** (2017) 113 [hep-th/1605.05597].

[256] E. Rinaldi, E. Berkowitz, M. Hanada, J. Maltz and P. Vranas, *Toward Holographic Reconstruction of Bulk Geometry from Lattice Simulations*, *JHEP* **02** (2018) 042 [hep-th/1709.01932].

[257] T. Harmark and N. A. Obers, *New Phase Diagram for Black Holes and Strings on Cylinders*, *Class. Quant. Grav.* **21** (2004) 1709 [hep-th/0309116].

[258] T. Harmark and N. A. Obers, *Phase Structure of Black Holes and Strings on Cylinders*, *Nucl. Phys. B* **684** (2004) 183 [hep-th/0309230].

[259] T. Harmark and N. A. Obers, *Phases of Kaluza-Klein black holes: A Brief review*, (2005) [hep-th/0503020].

[260] J. Traschen, *A Positivity Theorem for Gravitational Tension in Brane Spacetimes*, *Class. Quant. Grav.* **21** (2004) 1343 [hep-hp/0308173].

[261] T. Shiromizu, D. Ida, S. Tomizawa, *Kinematical bound in asymptotically translationally invariant spacetimes*, *Phys. Rev. D* **69** (2004) 027503 [gr-qc/0309061].

[262] B. Kol, *The phase transition between caged black holes and black strings: A review*, *Phys. Rept.* **422** (2006) 119 [hep-th/0411240].

[263] B. Kol, *Choptuik scaling and the merger transition*, *JHEP* **10** (2006) 017 [hep-th/0502033].

[264] V. Asnin, B. Kol, and M. Smolkin., *Analytic Evidence for Continuous Self Similarity of the Critical Merger Solution*, *Class. Quant. Grav.* **23** (2006) 6805 [hep-th/0607129].

[265] M. Hanada, Y. Hyakutake, G. Ishiki and J. Nishimura, *Holographic description of quantum black hole on a computer*, *Science* **344** (2014) 882 [hep-th/1311.5607].

[266] D. Marolf, M. Rangamani and T. Wiseman, *Holographic thermal field theory on curved spacetimes*, *Class. Quant. Grav.* **31** (2014) 063001 [hep-th/1312.0612].

[267] T. Banks, M.R. Douglas, G.T. Horowitz and E. Martinec, *AdS Dynamics from Conformal Field Theory*, (1998) [hep-th/9808016].

[268] A.W. Peet and S.F. Ross, *Microcanonical Phases of String Theory on $AdS_m \times S^n$*, *JHEP* **12** (1998) 020 [hep-th/9810200].

[269] T. Prestidge, *Dynamic and thermodynamic stability and negative modes in Schwarzschild-anti-de Sitter*, *Phys. Rev.* **D61** (2000) 084002 [hep-th/9907163].

[270] K. Skenderis and M. Taylor, *Kaluza-Klein Holography*, *JHEP* **05** (2006) 057 [hep-th/0603016].

[271] O. Aharony, O. Bergman, D.L. Jafferis and J. Maldacena, *$\mathcal{N} = 6$ superconformal Chern-Simons-matter theories, M2-branes and their gravity duals*, *JHEP* **10** (2008) 091 [hep-th/0806.1218].

[272] V. Balasubramanian and P. Kraus, *A Stress tensor for Anti-de Sitter gravity*, *Commun. Math. Phys.* **208** (1999) 413 [hep-th/9902121].

[273] L. G. Yaffe, *Large N phase transitions and the fate of small Schwarzschild-AdS black holes*, *Phys. Rev. D* **97** (2018) 026010 [hep-th/1710.06455].

[274] G. Arcioni and E. Lozano-Tellechea, *Stability and Critical Phenomena of Black Holes and Black Rings*, *Phys. Rev. D* **72** (2005) 104021 [hep-th/0412118].

[275] D. Jang, Y. Kim, O.K. Kwon and D.D. Tolla, *Exact Holography of the Mass-deformed M2-brane Theory*, *Eur. Phys. J. C* **77** (2017) 342 [hep-th/1610.01490]; *Mass-deformed ABJM Theory and LLM Geometries: Exact Holography*, *JHEP* **04** (2017) 104 [hep-th/1612.05066].

[276] D. Jang, Y. Kim, O.K. Kwon and D.D. Tolla, *Holography of Massive M2-brane Theory: Non-linear Extension*, (2018) [hep-th/1803.10660]; *Gravity from Entanglement and RG Flow in a Top-down Approach*, (2018) [hep-th/1712.09101].

[277] K. Skenderis and M. Taylor, *Holographic Coulomb branch vevs*, *JHEP* **08** (2006) 001 [hep-th/0604169].

[278] K. Skenderis and M. Taylor, *Anatomy of bubbling solutions*, *JHEP* **09** (2007) 019 [hep-th/0706.0216].

[279] H.J. Kim, L.J. Romans, and P. van Nieuwenhuizen, *Mass spectrum of chiral ten-dimensional $\mathcal{N} = 2$ supergravity on S^5*, *Phys. Rev. D* **32** (1985) 389.

[280] S. Lee, S. Minwalla, M. Rangamani and N. Seiberg, *Three-Point Functions of Chiral Operators in $D = 4$, $\mathcal{N} = 4$ SYM at Large N*, *Adv. Theor. Math. Phys.* **2** (1998) 697 [hep-th/9806074].

[281] G. Arutyunov and S. Frolov, *Some Cubic Couplings in Type IIB Supergravity on $AdS_5 \times S^5$ and Three-point Functions in SYM_4 at Large N*, *Phys. Rev. D* **61** (2000) 064009 [hep-th/9907085].

[282] S.Lee, *AdS_5/CFT_4 Four-point Functions of Chiral Primary Operators: Cubic Vertices*, *Nucl. Phys. B* **563** (1999) 349 [hep-th/9907108].

[283] C. W. Misner, K. Thorne and J. A. Wheeler, "Gravitation," *Princeton University Press* (1973).

[284] R. M. Wald, "General relativity," *University of Chicago Press* (1984).

[285] S. W. Hawking and G. Ellis, "The Large Scale Structure of Space-Time," *Cambridge University Press* (1973).

[286] D. Oriti, "Approaches to Quantum Gravity: Toward a New Understanding of Space, Time and Matter," *Cambridge University Press* (2009).

[287] M. B. Green, J. H. Schwarz and E. Witten, "Superstring Theory: Volume 1, Introduction"; "Superstring Theory: Volume 2, Loop Amplitudes, Anomalies and Phenomenology," *Cambridge University Press* (1987).

[288] J. Polchinski, "String Theory: Volume 1, An Introduction to the Bosonic String"; "String Theory: Volume 2, Superstring Theory and Beyond," *Cambridge University Press* (1998).

[289] K. Becker, M. Becker and J. H. Schwarz, "String theory and M-theory: A modern introduction," *Cambridge University Press* (2007).

[290] G. T. Horowitz (ed.), "Black holes in Higher Dimensions," *Cambridge University Press* (2012).

[291] M. Ammon and J. Erdmenger, "Gauge/Gravity Duality: Foundations and Applications," *Cambridge University Press* (2015).

[292] M. Alcubierre, "Introduction to 3+1 Numerical Relativity," *Oxford Science Publications* (2008).

[293] T. W. Baumgarte and S. L. Shapiro, "Numerical Relativity: Solving Einstein's Equations on the Compute," *Cambridge University Press* (2010).

[294] M. E. Taylor, "Partial differential equations I: Basic theory," (2nd Ed.) *Springer* (2010).

[295] A. D. Rendall, "Partial Differential Equations in General Relativity," *Oxford Graduate Texts in Mathematics* (2008).

[296] W. H. Press, S. A. Teukolsky and W. T. Vetterling, "Numerical Recipes: The Art of Scientific Computing," (3rd Ed.) *Oxford Graduate Texts in Mathematics* (2007).

[297] L. N. Trefethen, "Spectral Methods in MATLAB," *SIAM, Philadelphia* (2000).

[298] J. P. Boyd, "Chebyshev and Fourier Spectral Methods," *Dover Books on Mathematics* (2001).

[299] C. Canuto, M. Y. Hussaini, A. Quarteroni and T. A. Zang, "Spectral Methods," *Springer-Verlag* (2006).

[300] M. Farrashkhalvat and J. P. Miles, "Basic Structured Grid Generation: With an Introduction to Unstructured Grid Generation," *Butterworth-Heinemann* (2003).

[301] D. A. Kopriva, "Implementing Spectral Methods for Partial Differential Equations: Algorithms for Scientists and Engineers," *Springer* (2009).